# Relativistic hydrodynamics and transport in strongly correlated systems

Dissertation
zur Erlangung des Doktorgrades
der Naturwissenschaften

vorgelegt beim Fachbereich Physik
der Johann Wolfgang Goethe-Universität
in Frankfurt am Main

von
Arus Harutyunyan
aus Yerevan, Armenien

Frankfurt am Main 2017
(D 30)

vom Fachbereich Physik der Johann Wolfgang Goethe-Universität
in Frankfurt am Main als Dissertation angenommen

| | |
|---|---|
| Dekan: | Prof. Dr. Owe Philipsen |
| Gutachter: | Prof. Dr. Armen Sedrakian,<br>Prof. Dr. Luciano Rezzolla |
| Datum der Disputation: | 9 April, 2018 |

# Übersicht

Diese Arbeit untersucht im Allgemeinen die relativistische Hydrodynamik und die Transportkoeffizienten von stark korrelierten Systemen. Wir konzentrieren uns auf zwei Arten von Systemen. Erstens untersuchen wir die Eigenschaften der Materie in Schwerionenkollisionen, wenn die Quarks und Mesone die relevante Freiheitsgrade der Materie sind. Zweitens untersuchen wir stark korreliertes Elektron-Ion-Plasma, das in kompakten dichten Sternen bei starken Magnetfeldern und endlichen Temperaturen vorkommt.

Kapitel 1 liefert eine kurze Einführung in das Forschungsgebiet dieser Arbeit, insbesondere in die relativistische Hydrodynamik und den Transport in heißen und dichten Medien, die bei Schwerionenkollisionen und bei warmer dichter stellarer Materie auftreten.

Kapitel 2 ist der Formulierung der allgemeinen Struktur der dissipativen Hydrodynamik für relativistische Quantensysteme gewidmet. Dazu verwenden wir die von Zubarev entwickelte Methode des statistischen Operators im Nichtgleichgewicht. Das Hauptziel dieser Untersuchung ist eine Erweiterung der Hydrodynamik, die alle Terme zweiter Ordnung in Abweichungen vom Nichtgleichgewicht enthält. Dafür lösen wir zuerst die Quanten-Liouville-Gleichung mit einem infinitesimalen Quellterm, um einen statistischen Operator im Nichtgleichgewicht zu konstruieren. Danach wird der statistische Operator bis zur zweiten Ordnung in hydrodynamischen Gradienten entwickelt. Dieses liefert uns dann die Transportgleichungen für den Scherspannungstensor, den Volumenviskositätsdruck und die Diffusionsströme.

Wir stellen fest, dass Korrekturen zweiter Ordnung zu den dissipativen Flüssen aus den quadratischen Termen der Taylorentwicklung des statistischen Operators und aus den linearen Termen entstehen, die aber nicht lokal in der Raumzeit sind. Diese nicht lokalen Korrekturen erzeugen endliche Relaxationszeitskalen in der Evolution der dissipativen Flüssen. Wir erhalten dann die allgemeinste Form der Transportgleichungen, die sowohl Gradienten der dissipativen Flüsse als auch Produkte von zwei Größen erster Ordnung enthalten. Weiterhin werden die Transportkoeffizienten erster und zweiter Ordnung, die in diesen Gleichungen auftreten, durch Zwei- und Dreipunkt-Korrelationsfunktionen ausgedrückt. Schließlich drücken wir die Relaxationszeiten für die dissipativen Flüsse durch die Frequenzableitungen der entsprechenden Transportkoeffizienten erster Ordnung aus.

In Kapitel 3 berechnen wir die Transportkoeffizienten von stark gekoppelter Quarkmaterie im Rahmen des Nambu–Jona-Lasinio (NJL) Modells. Dabei werden nur die zwei leichtesten Flavors von Quarks einbezogen. Wir wenden den Kubo-Formalismus an, um die Wärmeleitfhigkeit ($\kappa$) und Elektrische Leitfähigkeit ($\sigma$), ebenso wie die Scher- ($\eta$) und die Volumen- ($\zeta$) viskositäten zu berechnen. Die entsprechenden Zweipunktkorrelationsfunktionen werden in führender Ordnung in der $1/N_c$ Entwicklung ausgewertet. In dieser Näherung werden die Leitfähigkeiten und die Scherviskosität durch einschleifen (one-loop) Diagramme mit vollen (gekleideten) Quarkpropagatoren gegeben. Dagegen wird die Volumenviskosität durch eine Summation einer unendlichen geometrischen Reihe von mehrschleifen (multi-loop) Diagrammen berechnet. Die dispersiven Effekte, die zu endlichen Werten von Transportkoeffizienten führen, ergeben sich aus Quark-Meson-Fluktuationen oberhalb der Mott-Übergangstemperatur $T_{\mathrm{M}}$. In diesem Temperaturbereich ist der Mesonenzerfall in zwei Quarks, die auf der Massenschale liegen, kinematisch möglich.

Wir finden, dass die Leitfähigkeiten und die Scherviskosität abnehmende Funktionen der Temper-

atur und der Dichte sind. Wir zeigen weiterhin, dass das Wiedemann-Franz-Gesetz für das Verhältnis $\sigma/\kappa$ verletzt wird. Das Verhältnis der Scherviskosität zur Entropiedichte $\eta/s$ ist größer als Eins in der Nähe der Mott-Temperatur, jedoch nähert es sich der AdS/CFT (KSS) Grenze von $1/4\pi$ bei höheren Temperaturen. Wir vermuten auf der Grundlage der Unschärferelation, dass das Verhältniss $\kappa T/c_V$, wobei $c_V$ die Wärmekapazität pro Volumeneinheit ist, von unten durch $1/18$ begrenzt ist.

Der Fall der Volumenviskosität ist komplizierter, da die Mehrschleifendiagramme in den Korrelationsfunktionen in der Nähe der Mott-Linie dominieren, jedoch nur, wenn die chirale Symmetrie explizit gebrochen ist. Wir finden, dass in diesem Fall nur bei hohen Temperaturen die Einschleifendiagramme dominant sind. Die resultierende Volumenviskosität übersteigt die Scherviskosität in der Nähe der Mott-Temperatur um Faktoren $5 \div 20$, angenommen das die Mehrschleifendiagramme berücksichtigt sind. Im Hochtemperaturbereich wird die Volumenviskosität im Vergleich zur Scherviskosität vernachlässigbar. Für praktische Anwendungen bieten wir einfache, aber genaue Fit-Formeln an die Transportkoeffizienten, die die Umsetzung unserer Ergebnisse in numerischen Simulationen von Schwerionenkollisionen im Rahmen der relativistischen Hydrodynamik erlauben.

In Kapitel 4 berechnen wir die elektrische Leitfähigkeit der Elektron-Ion-Plasma die z.B. in der Kruste eines kompakten Sternes vorhanden ist. Unsere Rechnungen basieren auf der Boltzmann Gleichung bei endlichen Temperaturen und unter Berücksichtigung von Magnetfeldern. Dabei erweitern wir die bisherige Untersuchungen bei niedrigen Temperaturen bis auf Temperaturen von 10 MeV. Solche Temperaturen sind relevant für die Beschreibung von Supernovaexplosionen, Verschmelzungen von Neutronensternen oder Akkretionsprozessen in Röntgendoppelsternen.

Wir konzentrieren uns auf den Temperaturbereich, in dem Plasma in einem flüssigen Zustand ist. Folglich wird die elektrische Widerstandsfähigkeit von der Elektronenstreuung an korrelierten Atomkernen verursacht. Die dynamische Abschirmung der Elektronen-Ionen Wechselwirkung erfolgt mittels des QED-Polarisationstensors, der in der Näherung von harten-thermischen-Schleifen (hard-thermal-loop) berechnet wird. Die Korrelationen unter den Ionen werden durch einen Strukturfaktor, der von Monte-Carlo-Simulationen von Einkomponenten-Plasma abgeleitet wird, berücksichtigt. Die entsprechende Boltzmannsche Transportgleichung wird dann in der Relaxationszeit-Näherung unter Berücksichtigung des Magnetfeldes, der zu Anisotropie des Transportkoeffizienten führt, gelöst. Der elektrische Leitfähigkeitstensor wird numerisch als Funktion der Temperatur, der Dichte, des Magnetfeldes und der Krustenzusammensetzung in einem breiten Parameterraum untersucht.

Wir finden, dass die Leitfähigkeit als Funktion der Temperatur ein Minimum aufweist. Dieses Minimum befindet sich bei einer Temperatur an den Elektronen vom entarteten zum nichtentarteten Zustandsübergang. Um unsere Ergebnisse leicht zugänglich zu machen, haben wir auch einfache Fit-Formeln für die drei Komponenten des Leitfähigkeitstensors aufgestellt. Des Weiteren liefern wir genaue Tabellen unserer numerischen Ergebnisse, die in dissipativen magnetohydrodynamischen (MHD) Simulationen von warmen kompakten Sternen verwendet werden können.

Wir fassen unsere Ergebnisse zusammen und diskutieren die Perspektiven in Kapitel 5.

# Zusammenfassung

## Einführung und Motivation

Die Hydrodynamik hat ein breites Anwendungsspektrum in der Physik. Es ist eine universelle effektive Theorie, die für die Erforschung von niederfrequenten und langwelligen kollektiven Phänomenen in statistischen Systemen sehr gut geeignet ist.

Die jüngsten Beobachtungen von anisotropen hydrodynamischen Strömungen bei Schwerionenkollisionen in Experimenten am Relativistic Heavy Ion Collider (RHIC) und Large Hadron Collider (LHC) weisen darauf hin, dass die in diesen Kollisionen entstandene Materie ein nahezu perfektes Quark-Gluon-Plasma (QGP) mit äußerst geringer Scherviskosität ist [1–12]. Diese Beobachtungen motivierten zahlreichen Untersuchungen der relativistischen, dissipativen Hydrodynamik sowie den Transportkoeffizienten des stark wechselwirkenden QGP [13–26]. Insbesondere sind diese Untersuchungen im Bereich von chiralen Phasenübergang für die modernen Experimente relevant.

Die ersten Formulierungen der relativistischen Navier-Stokes–Theorie (d.h., der Hydrodynamik erster Ordnung) wurden von Eckart [27] und Landau [28] ausgearbeitet. Es wurde bald nachgewiesen, dass diese Theorie zu sofortigen Signalausbreitungen führt und daher instabil ist [29–33].

Das Problem der Kausalität wurde in der Theorie zweiter Ordnung gelöst [34–36]. Diese Theorie führt charakteristische Relaxationszeitskalen ein, um die Verzögerung der Reaktion des Systems auf thermodynamische Störungen zu berücksichtigen. Die Theorie zweiter Ordnung kann aus der relativistischen kinetischen Theorie abgeleitet werden [2, 36–56]. Die Entwicklung der Nichtgleichgewichtsstatistik in den letzten Jahrzehnten [57–66] in Kombination mit den feldtheoretischen Methoden bietet einen alternativen Zugang zur Formulierung der relativistischen, dissipativen Hydrodynamik stark korrelierter Systeme [67–70].

Die Transportkoeffizienten eines dissipativen Systems beschreiben, wie das System auf thermodynamische Störungen reagiert, um seinen thermischen Gleichgewichtszustand zu erreichen. Für die Berechnung der Transportkoeffizienten ist die Kenntnis der mikroskopischen Wechselwirkungstheorie innerhalb des Systems erforderlich. Es gibt zwei Haupttechniken für die Berechnung von Transportkoeffizienten: (i) die Boltzmannsche Transporttheorie [71] und (ii) Kubos Methode der Korrelationsfunktionen [58, 59, 72]. Die Boltzmannsche Theorie beruht auf dem Konzept von Quasiteilchen und ist daher für schwach gekoppelte Systeme anwendbar. Beispiele dafür sind das quantenelektrodynamische (QED) Plasma und die Fermi-Flüssigkeiten bei niedrigen Temperaturen. Der Kubo-Formalismus bringt die Transportkoeffizienten in Beziehung mit bestimmten Gleichgewichts-Korrelationsfunktionen, deren Berechnung die Vielteilchen-Methoden von Quantenfeldtheorie erfordert. Dieser Zugang ist grundsätzlich für stark gekoppelten Systeme verwendbar und eignet sich daher für Untersuchungen von Transporteigenschaften von nichtstörungstheoretischen Feldtheorien. Ein derartiges Beispiel hierfür ist das heiße und dichte QGP in der Nähe des chiralen Phasenübergangs.

Gleichermassen interessant sind die magnetohydrodynamische (MHD) Untersuchungen von Verschmelzungen von kompakten Sternen, wobei die dissipativen Prozesse im Plasma von Neutronensternen wichtig sind [73–76]. Diese motivierten unsere Untersuchung von Transportkoeffizienten, insbesondere von elektrischer Leitfähigkeit von heißer und dichter Materie in hohen Magnetfeldern $B \leq 10^{14}$ G. Magnetfelder dieser Größenordnung können in kompakten stellaren Objekten auftreten.

## Relativistische Hydrodynamik zweiter Ordnung von Formalismus des statistischen Operators im Nichtgleichgewicht

Die Hydrodynamik stellt eine wirksame und effektive Methode zur dynamischen Beschreibung von Flüssigkeiten dar. Sie findet zahlreiche Anwendungen in der relativistischen Astrophysik [77], der Kernphysik [16, 17, 22–24] und der Kosmologie [78]. Es ist wohl bekannt, dass die relativistische Hydrodynamik erster Ordnung nicht kausal ist, und für die hydrodynamische Stabilität des Systems eine Zweite-Ordnung-Theorie erforderlich ist [29–32, 34–36].

In Kapitel 2 leiten wir die relativistischen Transportgleichungen zweiter Ordnung für ein allgemeines Quantensystem ab und erhalten Kubo-Formeln für Transportkoeffizienten unter Verwendung der Methode des statistischen Operators im Nichtgleichgewicht [79]. Diese Methode wurde hauptsächlich von Zubarev entwickelt [65, 66]. Ein wichtiges Merkmal dieser Methode ist, dass sie grundsätzlich für beliebig stark wechselwirkende Systeme anwendbar ist. Die hydrodynamischen Gleichungen sind in den Erhaltungssätzen des Energie-Impuls-Tensors und der erhaltenden Stromdichten enthalten

$$\partial_\mu T^{\mu\nu} = 0, \qquad \partial_\mu N_a^\mu = 0, \tag{1}$$

wobei der Index $a$ die Ladungsorte (z.B., elektrische, baryonische, usw.) bezeichnet. Verschiedene dissipative Prozesse können durch Zerlegungen des Energie-Impuls-Tensors und der Stromdichten in ihren Gleichgewichts- und Nichtgleichgewichts-Komponenten getrennt werden

$$T^{\mu\nu} = \epsilon u^\mu u^\nu - (p + \Pi)\Delta^{\mu\nu} + q^\mu u^\nu + q^\nu u^\mu + \pi^{\mu\nu}, \tag{2}$$

$$N_a^\mu = n_a u^\mu + j_a^\mu. \tag{3}$$

Hierhin $\epsilon$, $p$ und $n_a$ sind bzw. die Energiedichte, der Druck und die Ladungsdichten; $u^\mu$ ist die 4-Geschwindigkeit der Flüssigkeit, $\Delta^{\mu\nu} = g^{\mu\nu} - u^\mu u^\nu$ ist der Projektor orthogonal zu $u^\mu$ und $g^{\mu\nu}$ ist die Minkowski-Metriktensor. Die dissipativen Größen $j_a^\mu$, $q^\mu$, $\pi^{\mu\nu}$ und $\Pi$ in Gleichungen (2) und (3) repräsentieren Ladungsdiffusionsflüsse, Energiediffusionsfluss, Scherspannungstensor und Volumenviskosendruck. Um das System der Gleichungen (1) zu schließen, benötigt man noch eine Zustandsgleichung $p = p(\epsilon, n_a)$ und zusätzliche Transportgleichungen für die dissipativen Größen.

Um diese Transportgleichungen abzuleiten, folgen wir zuerst Zubarev, um einen retardierten statistischen Operator (Dichtematrix) im Nichtgleichgewicht aus der Quanten-Liouville-Gleichung zu konstruieren. Die Lösung der Liouville-Gleichung hat die folgende Form [66, 68, 70]

$$\hat{\rho} = Q^{-1} e^{-\hat{A}+\hat{B}}, \qquad Q = \mathrm{Tr} e^{-\hat{A}+\hat{B}}, \tag{4}$$

wobei der Operator $\hat{A}$ der lokale Gleichgewichtsanteil des statistischen Operators ist, während der Operator $\hat{B}$ die Gradienten der Temperatur $\beta^{-1}$, der chemischen Potentiale $\mu_a$ und des Geschwindigkeitsfeldes $u^\mu$ enthält. Der Operator $\hat{B}$ kann daher mit dem Nichtgleichgewichtansteil des Operators $\hat{\rho}$ identifiziert werden. Wenn wir den Operator $\hat{B}$ als Störung behandeln, können wir den vollen statistischen Operator $\hat{\rho}$ in der Taylorreihe in lokalen hydrodynamischen Gradienten enwickeln. Die dissipativen Größen werden dann durch Mittelung der entsprechenden Quantenoperatoren über den statistischen Operator (4) erhalten. Behalten wir nur die linearen Terme in Gradienten, erhalten wir die relativistische Navier-Stokes–Theorie mit

$$\Pi = -\zeta\theta, \qquad \pi^{\mu\nu} = 2\eta\sigma^{\mu\nu}, \qquad \mathscr{J}_a^\mu = \sum_b \chi_{ab}\nabla^\mu\alpha_b, \tag{5}$$

wobei $\eta$ ist die Scherviskosität, $\zeta$ ist die Volumenviskosität, $\chi_{ab}$ ist die Matrix der Diffusionskoeffizienten und $\alpha_a = \beta\mu_a$. Weiterhin definierten wir die folgenden Größen: $\theta = \partial_\mu u^\mu$, $\nabla^\mu = \Delta^{\mu\nu}\partial_\nu$ und

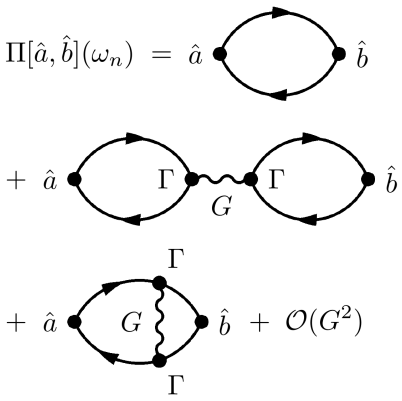


Abbildung 1: Beiträge zu den Zweipunkt-Korrelationsfunktionen aus den $\mathcal{O}(N_c^1)$ (erste und zweite Zeilen) und $\mathcal{O}(N_c^0)$ (die Dritte Zeile) Diagrammen, die bis zu eine einzelne Wechselwirkungslinie $G$ enthalten.

$\sigma^{\mu\nu} = \partial^{<\mu} u^{\nu>}$, wobei die Klammern den symmetrischen, spurlosen und räumlichen Teil eines Tensors auswählen. Schließlich haben wir die Ladungsdiffusionsströme wie folgt definiert

$$\mathscr{J}_a^\mu = j_a^\mu - \frac{n_a}{h} q^\mu, \tag{6}$$

wobei $h$ die Dichte der Enthalpie ist. Wenn wir auch die Terme zweiter Ordnung in $\hat{\rho}$ beibehalten, erhalten wir die folgenden Evolutionsgleichungen für die dissipativen Größen

$$\begin{aligned}
\tau_\pi \dot{\pi}_{\mu\nu} + \pi_{\mu\nu} &= 2\eta\sigma_{\mu\nu} + \tilde{\lambda}_\pi \theta \pi_{\mu\nu} + \lambda \theta \sigma_{\mu\nu} + \lambda_\pi \sigma_{\rho<\mu}\sigma^\rho_{\nu>} + \sum_{ab} \lambda^{ab}_{\pi\mathscr{J}} \nabla_{<\mu}\alpha_a \nabla_{\nu>}\alpha_b, && (7)\\
\tau_\Pi \dot{\Pi} + \Pi &= -\zeta\theta + \tilde{\lambda}_\Pi \theta\Pi + \varsigma\theta^2 + \zeta_\beta(\sigma_{\mu\nu}\pi^{\mu\nu} - \theta\Pi) - \lambda_{\Pi\pi}\sigma_{\mu\nu}\sigma^{\mu\nu} + \sum_a \zeta_{\alpha_a}\partial_\mu \mathscr{J}_a^\mu \\
&\quad -\tilde{\zeta}_\beta \partial_\mu q^\mu + q^\mu \Big[\zeta_\beta \dot{u}_\mu + \sum_a \zeta_{\alpha_a} \nabla_\mu (n_a h^{-1})\Big] + T \sum_{ab} \zeta^{ab}_\Pi \nabla^\mu \alpha_a \nabla_\mu \alpha_b, && (8)\\
\sum_b \tau^{ab}_{\mathscr{J}} \dot{\mathscr{J}}_{b\mu} + \mathscr{J}_{a\mu} &= \sum_b \Big[\chi_{ab}\nabla_\mu\alpha_b + \tilde{\lambda}^{ab}_{\mathscr{J}} \theta \mathscr{J}_{b\mu} + \chi^*_{ab}\theta\nabla_\mu\alpha_b - \lambda^{ab}_{\mathscr{J}}\sigma_{\mu\nu}\nabla^\nu\alpha_b\Big] \\
&\quad +\chi_{aq}\beta h^{-1}\big(-\nabla_\mu\Pi + \Pi\dot{u}_\mu + \dot{q}_\mu + q^\nu\partial_\nu u_\mu + q_\mu\theta + \Delta_{\mu\sigma}\partial_\nu\pi^{\nu\sigma}\big), && (9)
\end{aligned}$$

wobei der Punkt die kovariante Zeitableitung bezeichnet, d.h.,

$$\dot{\Pi} = D\Pi, \quad \dot{\pi}_{\mu\nu} = \Delta_{\mu\nu\rho\sigma} D\pi^{\rho\sigma}, \quad \dot{u}_\mu = Du_\mu, \quad \dot{q}_\mu = \Delta_{\mu\nu} Dq^\nu, \quad \dot{\mathscr{J}}_{a\mu} = \Delta_{\mu\nu} D\mathscr{J}_a^\nu, \tag{10}$$

und $D = u^\mu\partial_\mu$. Die Transportkoeffizienten, die in Gleichungen (7)–(9) auftreten, sind mit bestimmten Zwei- und Dreipunkt-Korrelationsfunktionen im Gleichgewicht verbunden. Die Relaxationszeiten $\tau_\pi$, $\tau_\Pi$ und $\tau^{ab}_{\mathscr{J}}$, die die Kausalität der Theorie wiederherstellen, werden durch die Frequenzableitungen der entsprechenden Transportkoeffizienten erster Ordnung (bzw. $\eta$, $\zeta$ und $\chi$) ausgedrückt.

## Transportkoeffizienten von Quarkmaterie aus dem Kubo-Formalismus

Die Transportkoeffizienten von QGP sind die wichtigsten Parameter in der hydrodynamischen Beschreibung der Schwerionen-Kollisionen in dem Energiebereich vom RHIC bis zum LHC. Die Untersuchung der elliptischen Strömungen in Schwerionenkollisionen weisen auf ein niedriges Verhältnis der Scherviskosität $\eta$ zur Entropiedichte $s$ hin [2–12]. Der Wert des Verhältnisses $\eta/s$ ist nahe an der unteren Grenze $1/4\pi$, die auf der Grundlage der Unschärferelation festgestellt ist [80] sowie aus der

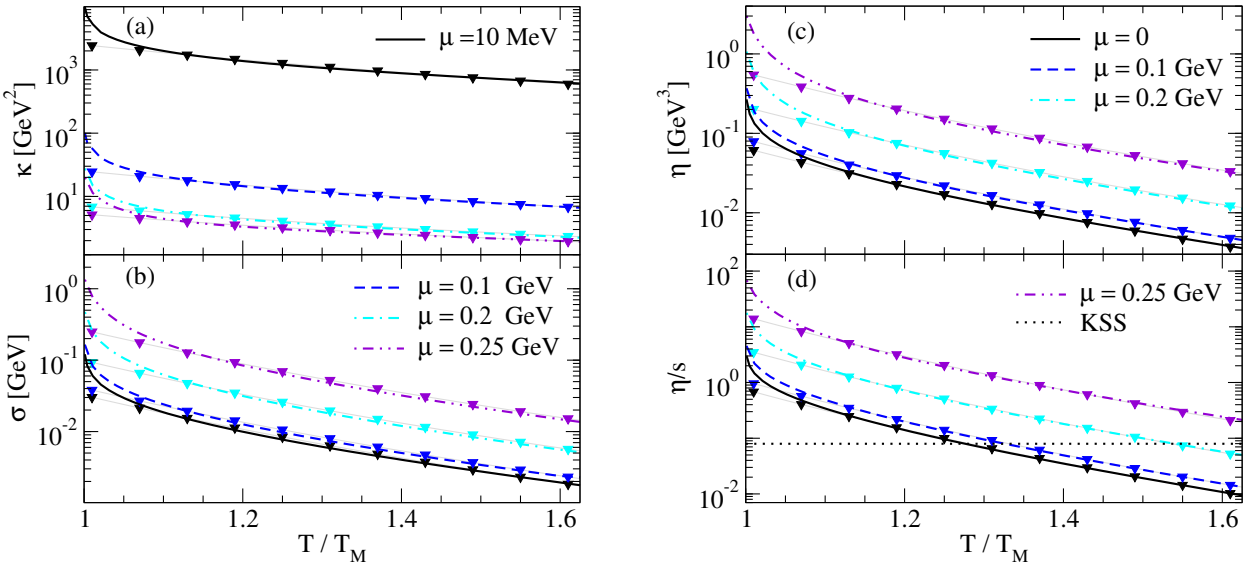


Abbildung 2: Die Wärme- (a) und elektrische (b) Leitfähigkeiten, die Scherviskosität (c) und das Verhältnis $\eta/s$ (d) als Funktionen der skalierten Temperatur $T/T_{\rm M}$ für einige Werte des chemischen Potentials. Die Punktlinie im Teilabbildung (d) ist die KSS Grenze $1/4\pi$ [81]. Die Dreiecke stellen die Ergebnisse unserer Fit-Formeln dar.

AdS/CFT-Korrespondenz vermutet wird [81].

In Kapitel 3 wenden wir den Kubo-Formalismus an [58, 59], um die Wärme- ($\kappa$) und die elektrische ($\sigma$) Leitfähigkeiten, sowie die Scher- ($\eta$) und die Volumenviskositäten ($\zeta$) von Quarkmaterie bei starker Kopplung zu berechnen [82, 83]. Dafür verwenden wir das Nambu–Jona-Lasinio (NJL) Modell mit zwei Quark Flavors [84–89]. Die Wechselwirkung in unserem Modell enthält einen skalaren und einen pseudoskalaren (isovector) Anteil. Die benötigten Zweipunkt-Korrelationsfunktionen werden in führender Ordnung in der $1/N_c$ Entwicklung [90], wobei $N_c$ die Farbenanzahl ist, ausgerechnet. In dieser Näherung wird jede dieser Korrelationsfunktionen durch eine unendliche Reihe von Schleifendiagrammen gegeben, wobei alle Vertexkorrekturen parametrisch unterdrückt sind, siehe Abbildung 1.

Aus der genaueren Untersuchung der Dirac-Struktur der Korrelationsfunktionen folgt, dass die unendliche Reihe der Feynman-Diagramme in den Fällen der Leitfähigkeiten und der Scherviskosität zu einem Einschleifendiagramm mit vollen (gekleideten) Quark-Propagatoren reduziert werden kann. Die Berechnung der Korrelationsfunktionen erfolgt im Rahmen des Matsubara Formalismus, unter der Anwendung von Propagatoren, die in imaginärer Zeit definiert sind. Die Streuungsprozesse, die zu dispersiven Effekten und damit zu endlichen Werten von Transportkoeffizienten führen, sind die Quark-Meson-Fluktuationen oberhalb der Mott-Übergangstemperatur $T_{\rm M}$, wo der Mesonenzerfall in zwei on-shell Quarks kinematisch erlaubt ist [91].

Unsere numerischen Untersuchungen konzentrieren sich auf den Temperatur-Dichte-Bereich der für Schwerionenkollisionen relevant ist. Wir finden, dass oberhalb der Mott-Temperatur die Wärme- und die elektrische Leitfähigkeiten sowie die Scherviskosität abnehmende Funktionen der Temperatur und der Baryonendichte sind. Der Grund dieser Abnahme ist der zunehmende Unterschied zwischen den Quark- und Mesonenmassen mit der Temperatur. Diese Koeffizienten weisen eine universelle Abhängigkeit von der skalierten Temperatur $T/T_{\rm M}$ für verschiedene Baryonendichten auf, d.h., die Ergebnisse unterscheiden sich durch nur eine Konstante die durch das chemische Potential bestimmt wird, siehe Abbildung 2.

Weiterhin zeigen wir, dass das Wiedemann-Franz-Gesetz für das Verhältnis $\sigma/\kappa$ verletzt wird. Im Limes $\mu \to 0$ finden wir, dass die Wärmeleitfähigkeit divergiert als $\kappa \propto \mu^{-2}$, was mit dem Fehlen des wohldefinierten Teilchen-Ruhesystems (sogenannten Eckart-Systems) bei verschwindendem chemis-

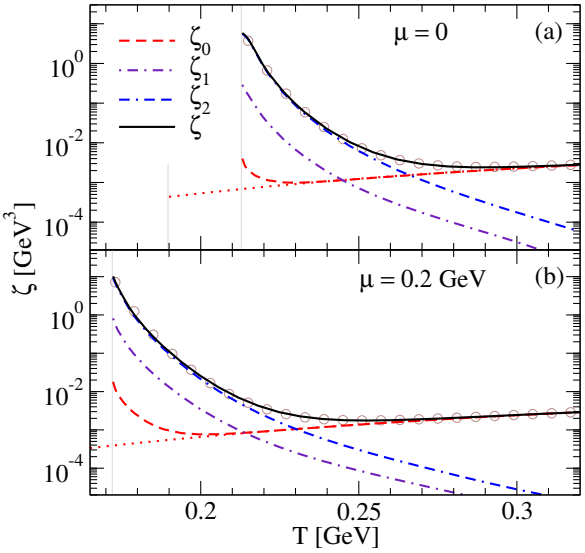


Abbildung 3: Die Beiträge der Ein- ($\zeta_0$) und Mehrschleifendiagramme ($\zeta_1$, $\zeta_2$) zur Volumenviskosität, sowie die Summe $\zeta = \zeta_0+\zeta_1+\zeta_2$ als Funktionen der Temperatur. Die Punktlinie stellt den chiralen Grenzfall dar. Die Kreise beziehen sich auf die Fit-Formeln.

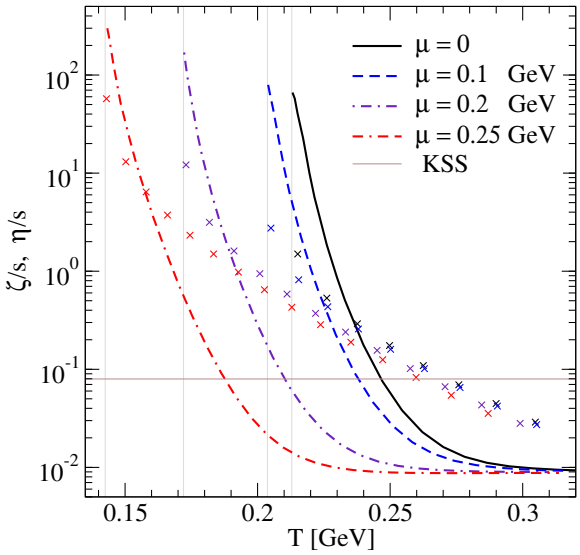


Abbildung 4: Das Verhältnis $\zeta/s$ als Funktion der Temperatur für einige Werte des chemischen Potentials. Das Verhältnis $\eta/s$ ist zum Vergleich durch Kreuze dargestellt. Die durchgezogene waagerechte Linie bezieht sich auf die KSS Grenze für $\eta/s$ [81].

chen Potential zusammenhängt [80].

Eine wichtige Größe neben den Transportkoeffizienten stellt das Verhältnis $\eta/s$. In unserem Modell $\eta/s \geq 1$ bei Temperaturen in der Nähe der Mott-Temperatur. Bei höheren Temperaturen $\eta/s$ nähert sich das sogenannte KSS Minimum, was $1/4\pi$ beträgt [81].

Bei sehr hohen Temperaturen fällt $\eta/s$ unterhalb der KSS Grenze. Wir vermuten, dass der Grund dafür die Abwesenheit von gluonischen Freiheitsgraden im NJL-Modell ist. Der Gluonen-Beitrag bei hohen Temperaturen wird immer wichtiger und kann schließlich zu einer zunehmenden Scherviskosität führen [92–95]. Wir vermuten auch, dass das Verhältnis $\kappa T/c_V$, wobei $c_V$ die Wärmekapazität pro Volumeneinheit ist, auf Grund der Unschärferelation von unten begrenzt ist. Der Grenzwert in natürlichen Einheiten ist durch $\kappa T/c_V = 1/18$ gegeben. Unsere numerischen Rechnungen zeigen, dass bei hohen Temperaturen diese Grenze genauso wie im Falle des Verhältnisses $\eta/s$ verletzt wird.

Der Fall von Volumenviskosität unterscheidet sich von den anderen Transportkoeffizienten, denn um die Volumenviskosität in führender Ordnung zu erhalten, muss man eine unendliche Reihe von Schleifendiagrammen summieren, siehe Abbildung 1, Zeilen 1 und 2. In der Nähe der Mott-Linie sind die Beiträge der unendlich summierten Schleifendiagramme $\zeta_1$ und $\zeta_2$ größer als der Beitrag von einzelnen Schleifendiagramme $\zeta_0$, siehe Abbildung 3. Im Gegensatz dazu wird bei höheren Temperaturen $\zeta_0$ dominant. Die rasche, exponentielle Abnahme der Volumenviskosität in der Nähe der Mott-Linie wird von einer kubischen Zunahme im Hochtemperaturbereich gefolgt. Dieses führt dazu, dass die Volumenviskosität als Funktion der Temperatur ein Minimum aufweist.

Die Volumenviskosität die aus voller Summation folgt, überschreitet die Scherviskosität um Faktoren $5 \div 20$ in der Nähe der Mott-Temperatur. Im Hochtemperaturbereich dagegen wird die Volumenviskosität im Vergleich zur Scherviskosität vernachlässigbar, siehe Abbildung 4. Die Situation unterscheidet sich im Grenzfall der chiral-symmetrische Materie. In diesem Fall ist der erste Term der Reihe in Abbildung 1 der einzige (d.h., die Terme höherer Ordnung verschwinden automatisch). Daher ist im chiralen Limes die Volumenviskosität im Vergleich zur Scherviskosität immer vernachlässigbar.

Für hydrodynamische Anwendungen unserer Ergebnisse haben wir einfache Fit-Formeln für die Transportkoeffizienten mit einer guten relativen Genauigkeit aufgestellt, siehe Abbildungen 2 und 3.

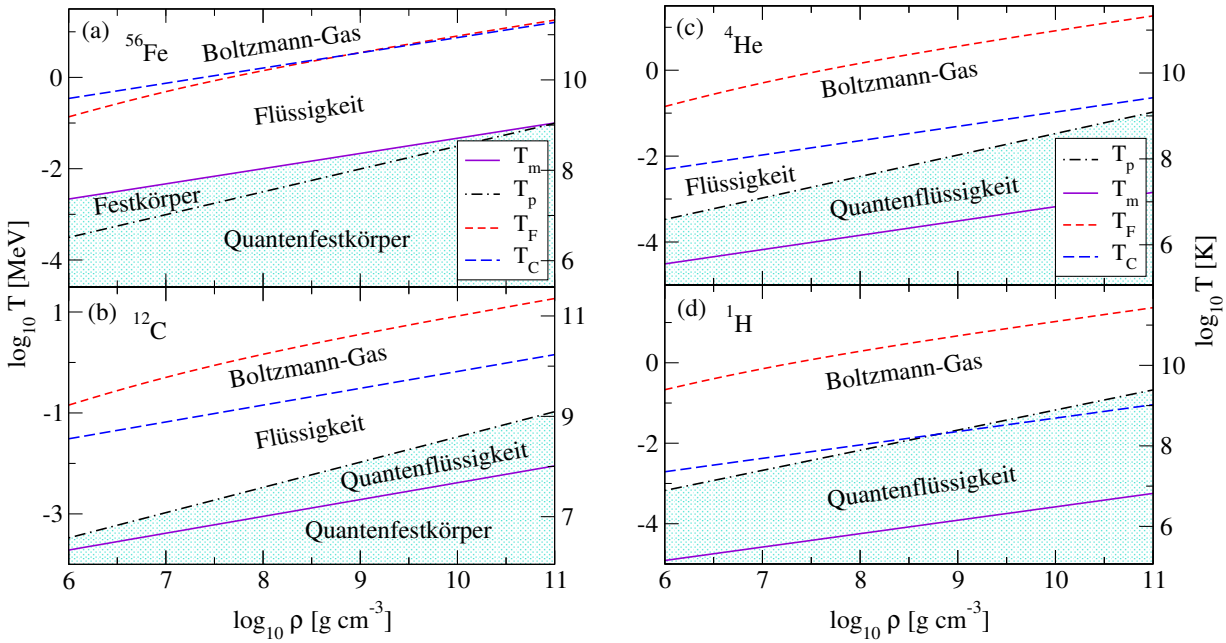


Abbildung 5: Das Phasendiagramm in der Temperatur-Dichte Ebene für QED-Plasma, das sich aus Eisen $^{56}$Fe (a), Kohlenstoff $^{12}$C (b), Helium $^{4}$He (c) und Wasserstoff $^{1}$H (d) zusammensetzt. Die Entartung der Elektronen setzt unterhalb der Fermi-Temperatur $T_F$ ein. Die Ionenkomponente verfestigt sich unterhalb der Schmelztemperatur $T_m$, während Quanteneffekte unterhalb der Plasmatemperatur $T_p$ wichtig werden. Für Temperaturen über $T_C$ bildet die ionische Komponente ein Boltzmann-Gas. Diese Arbeit beschäftigt sich nicht mit dem schattierten Teil des Phasendiagramms.

## Elektrische Leitfähigkeit der warmen, magnetisierten Kruste eines Neutronensternes

Neutronensterne sind dichte kompakte stellare Objekte, die auf verschiedene Weisen, z.B., als Pulsare oder Röntgendoppelsterne beobachtet werden können. Die Transportkoeffizienten sind wichtig für die MHD-Beschreibung der Neutronensterne. Das Spektrum der Phänomene, bei denen die elektrische Leitfähigkeit eine zentrale Rolle spielt, ist sehr breit. Wichtige Beispiele sind die Evolution der Magnetfelder in Neutronensternen [96–101] oder die Dissipation von MHD-Wellen [102–105].

Die Transportkoeffizienten des dichten QED-Plasmas wurden sehr ausführlich im Bereich der niedrigen Temperaturen untersucht [103, 106–130]. Im Falle von Neutronensternen wird der Temperaturbereich unterhalb $T \simeq 1$ MeV meist untersucht. Es entspricht deren inneren Temperaturen von Neutronensterne einigen Minuten bis Stunden nach der Entstehung in einer Supernovaexplosion.

In der letzten Zeit ist Materie bei höheren Temperaturen $T \simeq 10$ MeV in den Fokus der MHD untersuchungen gerückt. Solch eine heiße Materie tritt bei verschiedenen astrophysikalische Szenarien auf, wie z.B., bei Supernovaexplosionen, binären Neutronenstern-Verschmelzungen, sowie bei der Erwärmung der Kruste eines Neutronensternes durch Akkretion von Materie in Doppelsternsystemen.

In Kapitel 4 berechnen wir den elektrischen Leitfähigkeitstensor in der stark magnetisierten Kruste eines Neutronensternes bei nicht-verschwindenden Temperaturen [131,132]. Unsere Berechnungen entsprechen dem Temperatur-Dichte-Bereich, in welchem das Krustenplasma eine klassische Flüssigkeit bildet, siehe Abbildung 5. Die elektrische Leitfähigkeit wird dann durch die Elektronenstreuung von korrelierten Kernen bedingt. Die Korrelationen innerhalb der stark gekoppelten Ionenkomponente werden durch einen Zweipunkt-Strukturfaktor, der aus Monte-Carlo-Simulationen von Einkomponenten-Plasma [133] abgeleitet ist, berücksichtigt. Die thermische Verteilung der Ionen wird durch die klassische Maxwell-Boltzmann-Verteilungsfunktion gegeben. Ein neuer Effekt, der in der Elektronen-

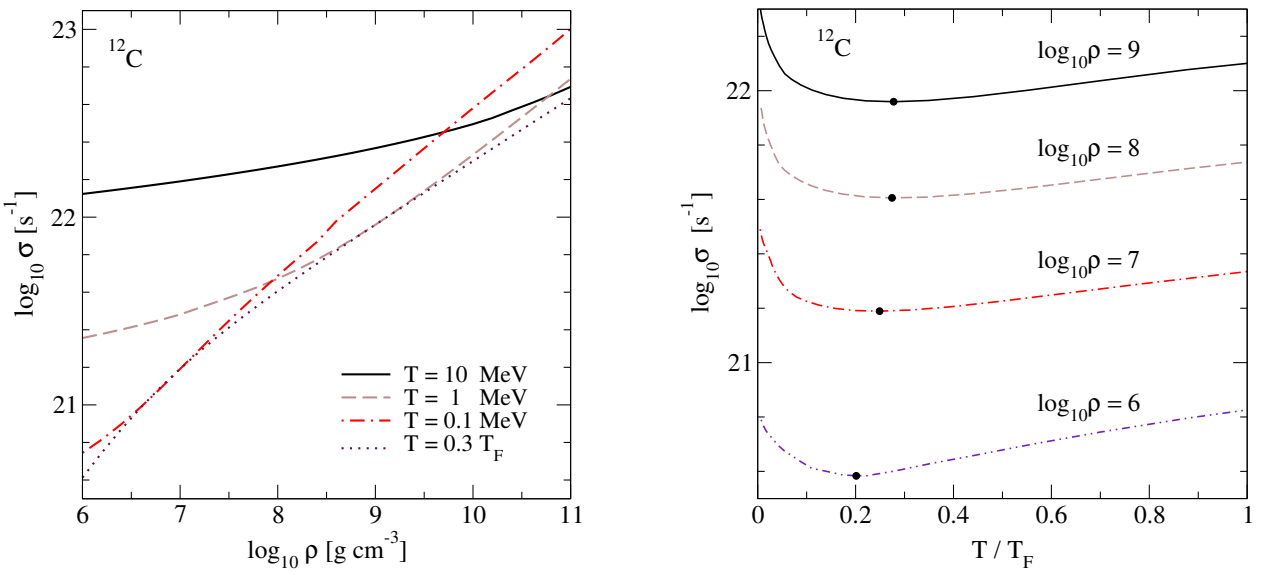


Abbildung 6: Die longitudinale Leitfähigkeit als Funktion der Dichte (linkerseits) und der Temperatur (rechterseits) für Atomkerne von Kohlenstoff $^{12}$C. Die Leitfähigkeit erreicht ein Minimum bei $T \simeq (0.2 \div 0.3)T_F$.

Ionen-Wechselwirkung einbezogen ist, ist die dynamische Abschirmung. Diese wird durch einen Polarisationstensor gegeben, der in der Näherung von harten-thermischen-Schleifen (hard-thermal-loop) berechnet wird. Wir haben die Boltzmannsche kinetische Gleichung in der Relaxationszeit-Näherung under Berücksichtigung von Magnetfeldern $B \leq 10^{14}$ G gelöst. Die obere Grenze des Magnetfeldes wird durch den Übergang zu quantisierten elektronischen Zuständen bestimmt [128], d.h., diese Quantisierung wird in unseren Rechnungen vernachlässigt. Aufgrund der vom Magnetfeld verursachten Anisotropie besitzt der Leitfähigkeitstensor eine longitudinale und zwei transversale Komponenten. Diese Komponenten sind Funktionen der Dichte, der Temperatur, des Magnetfeldes sowie der Zusammensetzung der Materie.

Die drei Komponenten des Leitfähigkeitstensors wurden numerisch als Funktionen von Temperatur, Dichte und Magnetfeldes untersucht. Zuerst betrachten wir den Fall der Materie in der Kruste von Neutronensternen, die aus einer einzigen Sorte von Atomkernen ($^{56}$Fe, $^{12}$C, $^{4}$He und $^{1}$H) besteht. Dann erweitern wir unsere Erforschung für die dichteabhängige Zusammensetzung der Kernmaterie im schwachen $\beta$-Gleichgewicht mit den Elektronen. Die Ergebnisse in diesem Fall sind nahe (sowohl qualitativ als auch quantitativ) an denen, die für die Eisenkerne erhalten worden sind. Wir untersuchen auch das Verhalten der Leitfähigkeit in der Nähe der Übergangstemperatur von der entarteten zur nicht entarteten Materie. Wir finden, dass die longitudinale Leitfähigkeit immer eine zunehmende Funktion der Dichte ist, aber sie besitzt ein Minimum als Funktion der Temperatur bei $T \simeq (0.2 \div 0.3)T_F$, wobei $T_F$ die Fermi-Temperatur der Elektronen ist, siehe Abbildung 6. Weiterhin wird die Abhängigkeit des Leitfähigkeitstensors vom Magnetfeld untersucht. Wir stellen fest, dass die Kruste bei genügend geringer Dichte und hoher Temperatur stark anisotrop ist, d.h., die transversalen Komponenten des Leitfähigkeitstensors im Vergleich zur longitudinalen Komponente stark unterdrückt sind. Der Unterdrückungsfaktor hängt von der Magnetfeldsstärke ab und bei Temperaturen von 10 MeV kann bis zu 12 Größenordnungen betragen. Dieses Ergebnis unterstreicht die Wichtigkeit der Einbeziehung der Anisotropie des Transports in MHD Untersuchungen von heißer und dünner magnetisierter Sternenmaterie auch bei relativ niedrigen Magnetfeldern. Wir stellen auch genaue Fit-Formeln zu unseren numerischen Ergebnissen auf, die in resistiven MHD Simulationen leicht und praktisch umgesetzt werden können.

## Schlussfolgerungen und Perspektiven

Diese Arbeit untersucht die relativistische Hydrodynamik sowie die wichtigsten Transportkoeffiziente von stark korrelierten Systemen. In Kapitel 2 formulieren wir die kausale Hydrodynamik unter Verwendung von Zubarevs Methode des statistischen Operators im Nichtgleichgewicht. Wir betrachten ein allgemeines Quantensystem, dessen Dynamik durch die Operatoren des Energie-Impuls-Tensors und der erhaltenen Ladeströme beschrieben wird. Unter Verwendung der Taylorentwicklung des statistischen Operators in den Gradienten der Temperatur, der chemischen Potentiale und des Geschwindigkeitsfeldes leiten wir Transportgleichungen zweiter Ordnung für die disspativen Anteile des Spannungstensors und der Ladeströme ab. Die entsprechenden Transportkoeffizienten stehen in Beziehung zu bestimmten retardierten Zwei- und Dreipunkt-Korrelationsfunktionen im Gleichgewicht. Diese können unter Anwendung von Standardmethoden der Quantenfeldtheorie berechnet werden.

Die Forschung, die in Kapitel 2 dargestellt wurde, kann erweitert werden auf die physikalischen Situationen, wo starke elektromagnetische und Gravitationsfelder auftreten. Diese sind von großem Interesse für die relativistische Astrophysik und die Kosmologie. Unsere Untersuchungen können auch erweitert werden, um Quantenanomalien einzubeziehen.

In Kapitel 3 berechnen wir die vier wichtigsten Transportkoeffizienten, d.h., die elektrische und Wärmeleit-fähigkeiten, die Scher- und Volumenviskositäten, von stark gekoppeltem Quark-Plasma. Wir benutzen dabei das zwei-Flavor NJL-Modell. Zuerst werden die Kubo-Formeln für diese Transportkoeffizienten hergeleitet. Weiterhin werden die entsprechenden Zweipunkt-Korrelationsfunktionen im Parameterraum, in dem die dispersiven Effekte aus Quark-Meson-Streuungsprozessen entstehen, berechnet. Es wird festgestellt, dass die Leitfähigkeiten und die Scherviskosität abnehmende Funktionen der Temperatur und des baryonischen chemischen Potentials sind, während die Volumenviskosität als Funktion der Temperatur ein Minimum besitzt. Wir finden, dass das Wiedemann-Franz-Gesetz in diesem Parameterraum verletzt wird. Ausgehend von Unschärferelation argumentieren wir weiter, dass eine untere Grenze für das Verhältnis $\kappa T/c_V > 1/18$ existiert. Diese wird im NJL-Modell bei hohen Temperaturen wiederum verletzt. Wir zeigen auch, dass nahe der Mott-Temperatur die Volumenviskosität die Scherviskosität um eine Größenordnung überschreitet.

Unsere Untersuchungen der Transportkoeffizienten von Quarkmaterie können durch Verbesserungen des NJL Lagrangians erweitert werden. Diese können z.B., durch Einbeziehung von Vektor-Wechselwirkungen und/oder Polyakov-Schleife erreicht werden. Eine andere Art von Erweiterung dieser Studien ist die Untersuchung der Drei-Flavor Quarkmaterie, sowie die isospin-asymmetrische Quarkmaterie in der Gegenwart von Leptonen (die für die Quarkkerne kompakter Sterne relevant sind). Eine weitere Herausforderung wäre die Berechnung der Transportkoeffizienten zweiter Ordnung, die für die kausale hydrodynamische Beschreibung von Schwerionenkollisionen notwendig sind.

In Kapitel 4 berechnen wir den elektrischen Leitfähigkeitstensor des warmen QED-Plasmas bei Temperaturen $10^9 \leq T \leq 10^{11}$ K und Dichten, die den äußeren Krusten von Neutronensternen und Innenräumen von weißen Zwergen entsprechen. Wir lösen die Boltzmannsche Transportgleichung in der Relaxationszeit-Näherung. Im Stoßintegral berücksichtigen wir inelastische Elektronen-Ionen-Streuungsprozesse. Wir finden, dass die longitudinale Leitfähigkeit ein Minimum bei der Temperatur $T \simeq (0.2 \div 0.3)T_F$ besitzt, wobei $T_F$ die Fermi Temperatur der Elektronen ist. Wir erhalten die drei Komponenten des Leitfähigkeitstensors in einem breiten Parameterbereich unter Berücksichtigung von Magnetfeldern. Wir zeigen, dass die transversalen Komponenten bei niedrigen Dichten und hohen Temperaturen stark unterdrückt sind.

Die Untersuchungen von Kapitel 4 können auf verschiedene Weisen weitergeführt werden. Zum Beispiel, kann die Zusammensetzung der Materie verbessert werden, in dem das mehrkomponentige Plasma anstatt des einkomponentigen Plasmas untersucht wird. Dabei kann die Zusammensetzung in einer selbstkonsistenten und temperaturabhängigen Art berechnet werden. Eine Reihe astrophysikalischer Probleme motiviert die Untersuchungen anderer Transportkoeffizienten (z.B., Wärmeleitfähigkeit, Viskositäten) bei hohen Temperaturen und in starken Magnetfeldern.

# Abstract

This thesis investigates second-order relativistic hydrodynamics and transport coefficients in strongly correlated systems. Our focus is mainly on the physical conditions relevant to heavy-ion collisions, as well as compact dense stellar objects at nonzero temperatures and in strong magnetic fields.

Chapter 1 provides a brief introduction to the area of research covered by this thesis, specifically relativistic hydrodynamics and transport in hot and dense media, which occur in heavy-ion collisions and heated stellar matter.

In Chapter 2 we give a new formulation of second-order dissipative hydrodynamics for relativistic systems using Zubarev's non-equilibrium statistical operator approach. We first solve the quantum Liouville equation with an infinitesimal source term to construct a non-equilibrium statistical operator which is a non-local functional of the thermodynamic parameters and their space-time gradients. Exploiting then the gradient expansion of the statistical operator we derive transport equations for the shear stress tensor, the bulk viscous pressure and the flavour diffusion currents up to the second-order in hydrodynamic gradients.

We show that the second-order corrections to the dissipative fluxes arise from (i) the quadratic terms of the Taylor expansion of the statistical operator; and (ii) the linear terms which are non-local in space and time. These non-local corrections generate finite relaxation time scales in the evolution of the dissipative quantities. We derive the most generic form of the transport equations which involve gradients of the dissipative fluxes, as well as products of two first-order quantities (*i.e.*, either thermodynamic forces or dissipative fluxes). We then go on to express the first- and the second-order transport coefficients, which appear in these equations, via certain two- and three-point equilibrium correlation functions. Finally, we express the relaxation times for the dissipative fluxes via the frequency-derivatives of the corresponding first-order transport coefficients.

In Chapter 3 we compute the transport coefficients of quark matter in the strong coupling regime within the two-flavor Nambu–Jona-Lasinio model. We apply the Kubo-Zubarev formalism to obtain the thermal ($\kappa$) and the electrical ($\sigma$) conductivities as well as the shear ($\eta$) and the bulk viscosities ($\zeta$) by evaluating the corresponding equilibrium two-point correlation functions at the leading order in the $1/N_c$ expansion. In this approximation the conductivities and the shear viscosity are given by single-loop skeleton diagrams, whereas the bulk viscosity includes an infinite geometrical series of multi-loop diagrams. The dispersive effects that lead to nonzero transport coefficients arise from quark-meson fluctuations above the Mott transition temperature $T_{\rm M}$, where meson decay into two on-mass-shell quarks is kinematically allowed.

We find that the conductivities and the shear viscosity are decreasing functions of temperature and density above $T_{\rm M}$. We also show that the Wiedemann-Franz law for the ratio $\sigma/\kappa$ does not hold. The ratio of the shear viscosity to the entropy density is larger than unity close to the Mott temperature and approaches the AdS/CFT bound $1/4\pi$ at higher temperatures. We conjecture on the basis of the uncertainty principle that the ratio $\kappa T/c_V$, where $c_V$ is the heat capacity per unit volume, is bounded from below by $1/18$.

The case of the bulk viscosity turns out to be special, because the multi-loop contributions dominate the single-loop contribution close to the Mott line in the case where the chiral symmetry is explicitly broken. We find that in this case only at high temperatures the one-loop contribution becomes

dominant. The resulting bulk viscosity exceeds the shear viscosity close to the Mott temperature by factors $5 \div 20$ when multi-loop contributions are included. In the high-temperature domain the bulk viscosity is negligible compared to the shear viscosity. For practical applications we provide simple, but accurate fits to the transport coefficients, which can facilitate the implementation of our results in hydrodynamics codes.

In Chapter 4 we compute the electrical conductivity of finite-temperature, strongly magnetized crust of a compact star which may be formed in the aftermath of a supernova explosion, binary neutron star merger, or during accretion processes in X-ray binaries. We focus on the temperature-density regime where plasma is in the liquid state and, therefore, the conductivity is dominated by the electron scattering off correlated nuclei. The dynamical screening of electron-ion interaction is implemented in terms of the polarization tensor computed in the hard-thermal-loop (HTL) effective field theory of QED plasma. The correlations of the background ionic component are accounted for via a structure factor derived from Monte Carlo simulations of one-component plasma.

With this input we solve the Boltzmann kinetic equation in relaxation time approximation taking into account the anisotropy of transport due to the magnetic field. The electrical conductivity tensor is studied numerically as a function of temperature, density, magnetic field and the crust composition in a broad parameter range. We find that the conductivity as a function of temperature attains a minimum at the transition from the degenerate to the nondegenerate regime of electrons. We also provide accurate fit formulas to our numerical results for three components of the conductivity tensor. In addition, we provide supplemental tables which can be used in dissipative magneto-hydrodynamics (MHD) simulations of warm compact stars.

We summarize our results and discuss the perspectives in Chapter 5.

# Acknowledgements

I would like to express my gratitude to all those people who have supported me in the last three years during which I was working on this thesis.

First and foremost, I would like to thank my supervisor Prof. Armen Sedrakian for providing me with the opportunity to do my graduate studies at Frankfurt University. I express my deepest gratitude for his scientific guidance and useful advice, which helped me to develop also the scope of my own scientific interests. I appreciate the academic and computational skills as well as the teaching experience I obtained under his supervision. Especially, I am grateful for his constant concern and efforts he has made for my future scientific career.

Next, I would like to thank my second supervisor Prof. Luciano Rezzolla for motivating me by suggesting some interesting astrophysical problems. I acknowledge him also for two useful lecture courses on relativistic hydrodynamics and advanced general relativity, from which I learned a lot of new material.

I express my gratitude to my mentor Prof. Dirk H. Rischke for his collaboration, many fruitful discussions, and his constant interest in my research progress.

I am also thankful to Prof. Owe Philipsen for providing an interesting lecture course on QCD and for answering a lot of my questions.

Next, I would like to express my gratitude to Prof. Mark Alford for his interest in my research and for fruitful discussions during his visits to Frankfurt.

I am grateful to the HGS-HIRe graduate program at Frankfurt University for organizing a number of excellent scientific and social events, as well as for encouraging my participation in many international workshops and conferences. In particular, I am thankful to Dr. Gerhard Burau for his permanent support and for answers to my questions on many occasions.

I would like to acknowledge also all my friends and colleagues at Frankfurt University, with whom I had a lot of joyful time in Germany. I express my deepest thanks to my family for the infinite support and encouragement they gave me during all my stay in Germany.

# Contents

# List of Figures

# List of Tables

# Chapter 1

# Introduction

Investigation of strongly interacting hot and dense matter remains one of the most exciting challenges of high-energy physics [134–136]. One of the main goals of today's nuclear research is the creation and exploration of strongly excited form of nuclear matter, so-called quark-gluon plasma (QGP), under controlled experimental conditions. In particular, of great interest are the thermodynamic and transport properties of QGP, which are very important for our understanding of strong interactions and its various manifestations [19, 22, 134].

In this chapter we provide a brief introduction to the area of research covered by this thesis. We start by presenting the current understanding of the QCD phase diagram and describe briefly the phenomenology of heavy-ion collisions. We discuss then the applications of relativistic hydrodynamics in heavy-ion collisions, as well as in astrophysics of compact stellar objects. We provide also a brief summary of the basic properties of neutron stars.

## 1.1 QCD phase diagram

Quantum chromodynamics (QCD) is the fundamental theory of strong interactions [137]. It is a non-abelian gauge field theory described by the symmetry group $SU(3)$. The building blocks of strongly interacting matter within this theory are the elementary particles called quarks [138]. The interaction between quarks is realized via exchange of gauge bosons, called gluons. The relevant gauge charge of quarks which is responsible for their strong interaction is called color charge or simply color. Quarks have three colors, which are conventionally taken to be red, green and blue. Due to the non-abelian nature and strong coupling of QCD, strong interactions exhibit several features which are fundamentally different from those of abelian gauge theories like quantum electrodynamics (QED):

- The non-abelian nature of QCD implies that gluons are color charged particles. Consequently, unlike photons, they are self-interacting. There are eight different types of gluons, which realize the interactions between three colors of quarks.

- In contrast to QED, the running coupling of which increases with increasing energy of interacting particles, QCD exhibits a running coupling which drops and tends to zero at energies higher than 1 GeV. This situation is typical to any $SU(N)$ non-abelian gauge theory and is called asymptotic freedom [139, 140]. Thus, QCD becomes weakly coupled at high energies, where it can be explored by perturbative methods.

- The running coupling of QCD becomes large at low energies, which makes the theory non-perturbative in the most interesting regimes of temperature and density. The strong coupling leads to the effect of confinement: color charged particles, *i.e.*, quarks and gluons, do not appear in nature as free particles, but are bound in color-singlet states which are called hadrons.

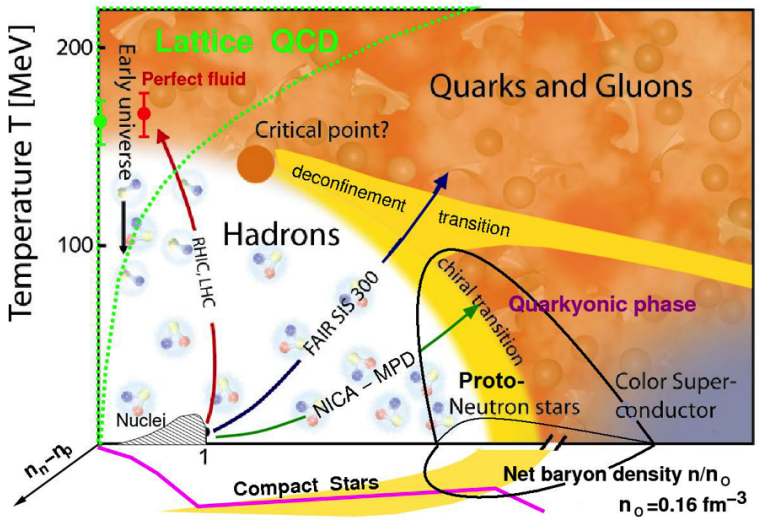


Figure 1.1: The QCD phase diagram in the space of temperature, net baryon density and net isospin density (adopted from Ref. [141]). The net baryon density is given in the units of nuclear density $n_0$.

As a consequence of the color confinement, the relevant degrees of freedom of QCD at low energies are hadrons, which are singlet representations of the color symmetry group $SU(3)$. Nuclear matter in this regime consists typically of two types of hadrons: (i) quark-antiquark bound states, called mesons; and (ii) bound states of three quarks, which are fully antisymmetric in the color space and are called baryons. This hadronic phase of QCD matter corresponds to the low-temperature and low-density domain of the QCD phase diagram, shown schematically in Fig. 1.1.

The figure illustrates the possible phases of quark matter, which are expected to be realized in various regions of the space of temperature, net baryon density and net isospin density. The net baryon density on the phase diagram is given in the units of the normal nuclear density. Below this density hadrons are bound in atomic nuclei at sufficiently low temperatures $T \lesssim 17$ MeV. At higher temperatures and/or densities hadrons are evaporated from nuclei due to the nuclear liquid-gas phase transition [134, 142].

At very high energies the elementary constituents of strongly interacting matter - quarks and gluons, become weakly interacting quasiparticles due to the asymptotic freedom. Therefore, it is natural to expect that at sufficiently high temperatures and densities they become the relevant degrees of freedom of QCD matter [143,144]. The phase of matter where quarks are deconfined from hadrons is called QGP. At very high temperatures and/or densities QGP can be described by means of perturbative QCD (pQCD).

High-temperature and low-density QGP is believed to have existed in the Early Universe. Due to the rapid expansion and cooling of the Universe quarks and gluons should have been confined into hadrons a few milliseconds after the Big Bang.

The deconfined quark matter is still expected to exist in the cores of massive compact stars, which correspond to the high-density and low-temperature domain of the phase diagram 1.1. In this regime quark matter is strongly degenerate and possibly in the color superconducting phase [136, 145, 146]. It is worthy to note, that the charge neutrality of $\beta$-equilibrated matter in compact stars implies non-vanishing net isospin density, *i.e.*, symmetry breaking between neutron and proton number densities, which corresponds to the third axis (perpendicular to the plain of the figure) in Fig. 1.1.

The confined and deconfined phases of quark matter described above are separated by a confinement-deconfinement phase transition line. The transition is expected to occur at temperatures $T_c \approx 160 \div 170$ MeV at vanishing baryon density. At vanishing temperature, the transition line ends at baryon densities a few times larger than the nuclear density. In the same parameter range, the chiral phase

transition is also expected, above which the (approximate) chiral symmetry of QCD is restored.

The deconfinement phase transition is of the first order at sufficiently high densities and low temperatures [147, 148]. At low densities it is most probably a crossover, as anticipated from lattice simulations [149–153]. These two regimes of phase transitions are separated by a critical point, see Fig. 1.1. The position of the critical point has drawn a lot of attention recently and is under intense investigations [154, 155].

Because of the non-perturbative nature of QCD, it is not possible to explore the whole phase structure of QCD matter within a single theoretical framework. Therefore, different approaches (and approximations) should be applied to investigate different portions of the phase diagram. The low-energy sector of hadronic phase, where the chiral symmetry is spontaneously broken, can be investigated by so-called chiral perturbation theory [156–160].

At very high temperatures and baryon densities QGP can be described by perturbative methods. However, pQCD fails already at temperatures and densities several times above the (expected) deconfinement transition line. The non-perturbative dynamics of QCD matter can be accurately described by the discretized version of QCD, called lattice QCD. The latter gives reliable results for phase transitions at zero baryon density, but fails at high densities because of so-called sign problem [161, 162]. Only recently some progress has been made in lattice computations at finite, but sufficiently small ($\mu_B \lesssim T$) baryon chemical potentials, see Refs. [162–164] for recent reviews.

In the non-perturbative regime effective models that capture some aspects of QCD relevant to the problem offer an alternative framework to explore the properties of moderately hot and dense quark matter. An example is the Nambu–Jona-Lasinio (NJL) model [84–89], which incorporates quark-quark scattering via four-fermion contact interactions without gluonic degrees of freedom. This model features all global symmetries, as well as the chiral symmetry breaking of QCD, but fails to incorporate the effect of confinement.

An alternative effective model is the MIT-bag model, which was suggested as a microscopic model of hadrons [165–167]. This model incorporates the effect of confinement, but fails to reproduce the symmetries of QCD.

For completeness we mention also, that some properties of strongly interacting matter can be extracted from the AdS/CFT correspondence, based on Maldacena's gauge/gravity duality conjecture [168]. A detailed description of this approach can be found in Refs. [169–171].

## 1.2 Relativistic heavy-ion collisions

The rapid development of experimental technique during the last decades opens new doors for creation and exploration of various phases of QCD matter in laboratory conditions. In particular, it is expected that QGP can be formed in relativistic heavy-ion collisions.

The heavy-ion collision experiments at Relativistic Heavy Ion Collider (RHIC) at Brookhaven National Laboratory and Large Hadron Collider (LHC) at CERN offer the opportunity to explore the high-temperature and low-density domain of the QCD phase diagram shown in Fig. 1.1. The forthcoming experiments at the Facility for Anti-proton and Ion Research (FAIR) at GSI [172] and Nuclotron-based Ion Collider fAcility (NICA) at JINR [173] are expected to achieve relatively high densities and low temperatures, see Fig. 1.1. These experiments are targeted especially at the creation and investigation of thermally equilibrated QGP.

The collective behavior of QCD matter created in heavy-ion collision experiments can be described by relativistic fluid dynamics. The analysis of the anisotropic hydrodynamical flows detected in the experiments at RHIC and LHC predict a very low value of the shear viscosity [2–12], which is close to the lower bound placed by the uncertainty principle [80] and conjectured from AdS/CFT duality arguments [81, 174]. Such a small value of the shear viscosity is an indication of the formation of strongly correlated matter, which is probably QGP [1, 175].

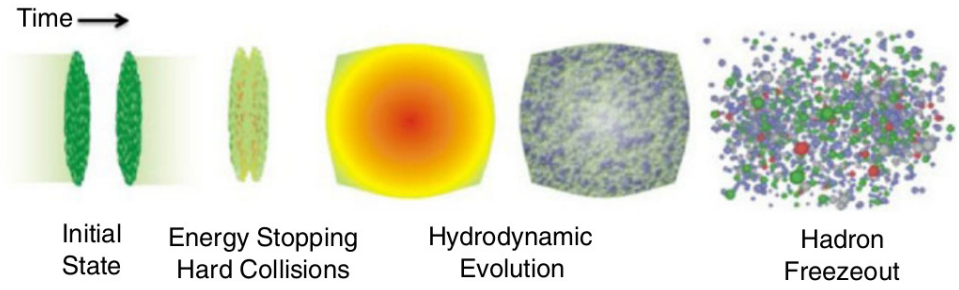


Figure 1.2: Sketch of various stages of a central ultrarelativistic heavy-ion collision in the center-of-mass frame (adopted from Ref. [176]).

Figure 1.2 shows the dynamical stages of a central ultrarelativistic collision between two heavy nuclei (*i.e.*, nuclei heavier than carbon nucleus) in their center-of-mass frame. (The collisions are called ultrarelativistic, if the center-of-mass energy of nuclei is much larger than their rest mass. For example, the typical energy of Au+Au collisions at RHIC is 200 GeV per nucleon, which exceeds the rest mass of the nucleons by two orders of magnitude.) Because of strong Lorentz-contraction of nuclei in the direction of motion the collision in the laboratory frame takes place effectively between two "pancakes" moving (almost) at the speed of light. After the collision a fireball of highly energetic nuclear matter is produced, which expands rapidly in all directions. If the energy density in the fireball is above the deconfinement transition, then QGP is formed. The evolution of the expanding fireball can be divided into the following dynamical stages [15, 21, 22, 25]:

- Pre-equilibrium

  At very short (proper) times $\tau \lesssim 1$ fm (1 fm $\simeq 3.3 \cdot 10^{-24}$ s) after the collision the constituents of matter in the fireball move almost freely away from the center of the collision with high velocities. In this stage the velocities of the particles are not distributed thermally, and, therefore, this stage is called pre-equilibrium.

- Thermalization and hydrodynamic flow

  After a typical time scale $\tau_0 \simeq 1$ fm the correlations between the constituents become sufficiently strong, and a local thermal equilibrium is achieved. Soon after thermalization the collective dynamics of the system emerges. During the time interval $\tau_0 \leq \tau \leq 4\tau_0$ the expansion of the fireball can be described by relativistic dissipative hydrodynamics.

- Hadronization and freeze-out

  When the temperature of expanding fireball has sufficiently decreased, the QGP undergoes a transition to the confined hadronic phase. After hadronization the interactions between particles become gradually weaker, and the system goes out of thermal equilibrium. In this stage hydrodynamic description breaks down and the dynamics of particles which flow to the detectors should be described by kinetic theory. This final stage of collisions is called freeze-out.

In the case of non-central collisions the distribution of particle momenta in the fireball is anisotropic, which leads to detected elliptic flows. This anisotropy motivates the modelling of heavy-ion collisions in the framework of viscous hydrodynamics [13–25]. The transport coefficients and the equation of state of QCD matter are key inputs in the hydrodynamic description of heavy-ion collisions and can be extracted then from the analysis of the particle spectra [19, 20, 26].

Thus, the relativistic heavy-ion collisions are very useful for exploration of fundamental properties of strongly interacting QCD matter. Apart from that, these experiments offer an opportunity also to test and verify the theory of relativistic dissipative hydrodynamics. In order to implement viscous

hydrodynamics in studies of nuclear collisions, one needs first to choose an appropriate theory. In the following section we give an overview on relativistic hydrodynamics.

## 1.3 Relativistic hydrodynamics

Hydrodynamics (fluid dynamics) is a powerful effective theory for the dynamical description of low-frequency and long-wave-length collective phenomena in many-particle systems. It finds numerous applications in relativistic astrophysics [77], nuclear physics [16, 17, 22–24] and cosmology [78].

Hydrodynamics relies on the possibility of the *reduced description* of many-particle systems, the idea of which was proposed by Bogolyubov [177]. In such description the state of the system is determined by means of the local fields of a few macroscopic quantities. For relativistic systems these are the energy-momentum tensor and the currents of conserved (or approximately conserved) charges.

The validity of hydrodynamics is limited to systems, which are close to local thermal equilibrium. The latter implies that each small, but still macroscopic fluid element can be described by means of local values of fluid velocity, temperature and chemical potentials, which vary slowly in space and time. In this context "slowly" means that the characteristic *macroscopic* scales in which the hydrodynamic quantities change in space and time should be much larger compared to the characteristic *microscopic* scales of the system. The ratio of the microscopic to macroscopic scales, referred to as Knudsen number, is the effective (small) expansion parameter in hydrodynamics.

In dilute systems with well-defined quasiparticles there are three typical time scales governing the dynamical evolution of the system [66, 178]. The shortest time scale is the mean collision time $\tau_0 = r_0/\bar{v}$, where $r_0$ is the interaction length, and $\bar{v}$ is the mean velocity of the particles. The second time scale is the time between two subsequent collisions $\tau_{\rm mfp} = l_{\rm mfp}/\bar{v}$, with $l_{\rm mfp}$ being the mean free path of the particles. Apart from these two *microscopic* time scales, there exists also the third *macroscopic* time scale $\tau_{\rm loc}$, which is the characteristic time for the establishment of local thermal equilibrium in separate subsystems, each of which is macroscopically small, but still contains a huge number of particles. This time scale can be associated with a characteristic length scale $l_{\rm loc}$, which determines the minimal size of a fluid element in which local equilibration can take place. Finally, one can introduce also a characteristic time $\tau_{\rm eq}$ for the establishment of complete (global) thermal equilibrium. (This time scale depends on the size of the system and does not depend on the details of microphysics [60].) Thus, we have a hierarchy of several relaxation times which satisfy the inequalities

$$\tau_0 \ll \tau_{\rm mfp} \ll \tau_{\rm loc} \ll \tau_{\rm eq}. \tag{1.1}$$

In strongly coupled systems the concepts of the collisional time scale and the mean-free-path are not well-defined, and there is a single microscopic interaction time scale $\tau_{\rm m}$ with $\tau_{\rm m} \ll \tau_{\rm loc} \ll \tau_{\rm eq}$. Due to the hierarchy of these relaxation times the dynamical evolution of the system can be divided into the following stages. At short time scales $\tau_0 \leq t \leq \tau_{\rm loc}$ (or $\tau_{\rm m} \leq t \leq \tau_{\rm loc}$) the system is said to be in the *kinetic stage* and should be described by means of the statistical distribution function. At sufficiently larger time scales $\tau_{\rm loc} \leq t \leq \tau_{\rm eq}$ the system achieves thermodynamic equilibrium locally, and local values of a few macroscopic quantities (*e.g.*, local densities of energy, momentum and particle number) are sufficient to describe the system. This *reduced description* of the system corresponds to the *hydrodynamic stage*. In this stage further equilibration processes occur via a macroscopic energy-momentum exchange between neighboring subsystems of the size $l \gtrsim l_{\rm loc}$.

The local equilibrium in each fluid element is achieved due to the microscopic interactions. Consequently, the *local* equilibration time scale $\tau_{\rm loc}$ is smaller for systems with stronger interactions. In contrast to this, the *global* equilibration time $\Delta\tau \simeq \tau_{\rm eq} - \tau_{\rm loc}$ is larger for stronger interacting systems (for a given size of the system, and, therefore, for a given value of $\tau_{\rm eq}$). This implies, that equilibration processes in the *hydrodynamic regime* occur slower in systems with stronger interactions. The result is that stronger interacting fluids are less dissipative than the ones with weaker interactions.

The irreversible processes in the hydrodynamic regime are described via macroscopic dissipative fluxes. These fluxes arise as a response of the system to local non-uniformities in thermodynamic parameters (thermodynamic forces), and drive the system towards its global thermal equilibrium. For small departures from global equilibrium these dissipative fluxes can be treated as linear functions of the thermodynamic forces.

Relativistic formulation of dissipative hydrodynamics based on the linear response theory was given by Eckart [27] and Landau-Lifshitz [28]. However, these formulations of relativistic fluid dynamics, also referred to as first-order theories, are incompatible with fundamental concepts of the special relativity. The linear relations between the dissipative fluxes and the thermodynamic forces lead to a parabolic set of equations, which contains as a solution collective modes propagating with arbitrarily large speeds [29, 31, 34, 35]. Apart from suffering from acausality, the first-order theory is also numerically unstable [29–33].

The acausal behavior of the first-order theory is easy to demonstrate on the example of the classical Fourier law for the heat flux $\boldsymbol{q} = -\kappa\nabla T$, where $T$ is the temperature, and $\kappa$ is the thermal conductivity [28]. Fourier law leads to the following heat diffusion equation [28]

$$\frac{\partial T}{\partial t} = \frac{\kappa}{c}\Delta T, \tag{1.2}$$

where $c$ is the heat capacity per unit volume. Equation (1.2) is parabolic and leads to instantaneous heat propagation. This problem can be solved by adding a relaxation term to the Fourier law [179]

$$\tau\frac{\partial \boldsymbol{q}}{\partial t} + \boldsymbol{q} = -\kappa\nabla T. \tag{1.3}$$

The heat relaxation term in Eq. (1.3) implies an exponential decay $\boldsymbol{q} \propto \exp(-t/\tau)$ of the heat flux to its Fourier value in short time scales $t \lesssim \tau$. The modified Fourier law (1.3) leads to the equation

$$\tau\frac{\partial^2 T}{\partial t^2} + \frac{\partial T}{\partial t} = \frac{\kappa}{c}\Delta T, \tag{1.4}$$

which is already hyperbolic and implies finite speed of heat propagation $v_T = \sqrt{\kappa/c\tau}$. Kinetic theory shows that $v_T$ is of the order of speed of sound [34, 36]. Thus, the acausal behavior of the first-order theory can be removed by introducing characteristic relaxation time scales, which incorporate the retardation of the response of the system to thermodynamic perturbations. This argument implies, that the causal theory of relativistic dissipative fluids should be at least of the second order in the Knudsen number (see, for example, the discussion in Ref. [41]).

The first phenomenological theory of causal fluid dynamics was proposed by Müller [34] for nonrelativistic fluids. For relativistic fluids an analogous theory was developed by Israel and Stewart [35, 36]. In these theories the dissipative fluxes are treated as independent state variables and satisfy evolution equations with characteristic relaxation time scales.

In contrast to the first-order fluid dynamics, there are many candidates for the second-order theory, and the final form of the equations of the causal fluid dynamics is not yet established. The equations of the second-order fluid dynamics and the relevant transport coefficients can be derived from the relativistic kinetic theory [2, 36–56]. The equations of hydrodynamics, in this case, emerge as a result of the second-order expansion of quasiparticle distribution function with respect to the Knudsen and/or inverse Reynolds numbers (see, *e.g.*, Refs. [41, 46]).

The development of non-equilibrium statistical methods during the last decades [57–66] in combination with field-theoretical formalism offers an alternative framework for the derivation of equations of dissipative hydrodynamics and computation of transport coefficients for strongly correlated systems [67–70]. The transport equations in this approach are obtained from the quantum Liouville equation for the non-equilibrium statistical operator (density matrix).

The main problem of the non-equilibrium statistical mechanics is the derivation of *time-irreversible* transport equations from the originally *time-reversible* Liouville equation. In order to incorporate the irreversibility in the solution of the Liouville equation, an additional assumption should be made to choose an appropriate initial condition. In this thesis we follow the method of the non-equilibrium statistical operator developed by Zubarev [65,66]. The key idea of this approach is the assumption that at sufficiently large time scales the details of the initial state become unimportant for the evolution of the system, and the number of parameters which are necessary to describe the state of the system is sufficiently reduced. As a result, the system loses information about its preceding states, and, therefore, the evolution becomes irreversible.

Important ingredients of the hydrodynamic description of many-particle systems are various transport coefficients. These describe how the system reacts to thermodynamic perturbations to achieve its thermal equilibrium state. Computation of transport coefficients requires proper knowledge of the underlying microscopic theory of interactions within the system.

There are two main techniques for computation of transport coefficients: (i) kinetic theory based on the Boltzmann equation [71]; and (ii) Kubo's method of correlation functions [58, 59, 72]. The standard kinetic theory relies on the quasiparticle picture and incorporates the interactions between quasiparticles via local binary collisions. Consequently, this approach is applicable for weakly coupled systems, *e.g.*, QED plasma relevant to a wide class of astrophysical problems, or Fermi liquids at low temperatures.

The Kubo formalism is an alternative to the kinetic theory. It relates the transport coefficients to certain equilibrium correlation functions, computation of which can be performed by applying standard many-body methods of the quantum field theory [180–183]. The advantage of Kubo's method as compared to the kinetic theory is that it does not make any assumption about the weakness of interactions within the system, and thereby provides a rigorous theoretical framework for the investigation of transport properties in non-perturbative field theories. A typical example is hot and dense quark matter in the vicinity of the chiral phase transition. However, because of its non-perturbative nature, Kubo's method requires a resummation of an infinite series of Feynman diagrams even for weakly interacting systems.

## 1.4 Neutron stars

Neutron stars (NS) are the densest stellar objects in the Universe. They are natural laboratories which allow us to study the properties of nuclear matter under extreme physical conditions. The density of matter in NS cores exceeds several times the normal nuclear density. These extremely dense objects may contain the most exotic forms of matter, *e.g.*, hypernuclear or deconfined quark matter in their interiors.

Neutron stars have masses up to $2M_\odot$, where $M_\odot$ is the solar mass. The typical radius of a NS is of the order of 10 km, which is only a few times larger than the corresponding Schwarzschild radius. As a result of such high compactness, NSs carry very strong gravitational fields. The latters play an important role in the phenomenology of these stars. Precise measurements of NS mass-radius relations and orbital parameters, as well as the detection of gravitational waves from compact star binaries offer an opportunity for testing various aspects of the general theory of relativity.

Neutron stars have also superstrong magnetic fields. Typical values of magnetic fields on NS surface vary in the range $10^{10} - 10^{13}$ G. A special class of NSs, called magnetars, have even stronger magnetic fields up to $10^{16}$ G on the surface and up to $10^{18}$ G inside the core. These are most probably the highest magnetic fields in the Universe.

Because of extremely high compactness, NSs have very short rotational periods. Their values vary from milliseconds to several tens of seconds. Due to the rapid rotation and strong magnetic fields, many NSs are observable as radio pulsars, which emit electromagnetic rays in a narrow beam. Many NSs are visible also in other parts of the electromagnetic spectrum, *e.g.*, in optical, X-ray or $\gamma$-ray

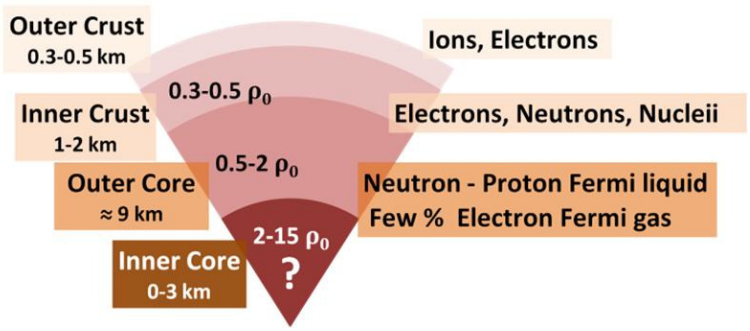


Figure 1.3: Schematic picture of the inner structure of a neutron star (adopted from Ref. [184]).

spectrum. In addition, NSs can be detected also as X-ray binaries, which radiate due to the accretion of matter from the companion.

It is now widely accepted that NSs are formed after supernova explosions of massive stars with $M \geq 8M_\odot$. Once the thermonuclear fuel in the core of a main-sequence star is exhausted, the core undergoes a gravitational collapse producing a dense, compact object, known also as a NS. In a NS the gravity is balanced purely by the degeneracy pressure of the matter.

Figure 1.3 shows the schematic picture of the inner structure of a NS. A typical NS consists of a crust and a core. The crust at low densities $10^4 \lesssim \rho \lesssim 4 \cdot 10^{11}$ g cm$^{-3}$ consists of fully ionized, strongly correlated nuclei embedded in a relativistic gas of degenerate electrons. This part of the crust is called the outer crust, see also Fig. 1.4. At low densities $\rho \leq 10^4$ g cm$^{-3}$ the outer crust is covered by a thin envelope of iron nuclei.

The nuclei in the outer crust become increasingly neutron-rich with increasing density. Above the so-called neutron-drip density $\rho_{\rm nd} \simeq 4 \cdot 10^{11}$ g cm$^{-3}$ the number density of neutrons becomes so large that some amount of neutrons is liberated from nuclei to form a degenerate, superfluid gas, see Fig. 1.4. This phase of matter constitutes the inner crust of the star and exists up to the density $\rho \simeq 0.5\rho_0$, where $\rho_0 = 2.8 \cdot 10^{14}$ g cm$^{-3}$ is the nuclear density. In the high-density region of the crust the nuclei may have non-spherical shapes, *i.e.*, the matter may form the so-called pasta phase just before the transition to the homogeneous core [185]. The thickness of the crust is of order of 1 km.

Above the density $\rho \simeq 0.5\rho_0$ nuclei cannot exist anymore: they dissolve to form a continuum fluid of neutrons, which contains a small percentage of protons and electrons in $\beta$-equilibrium, see Fig. 1.3. This phase of matter may contain also some amount of muons and is called $npe\mu$ phase. It constitutes the outer core of the NS and extends up to the densities $(2 \div 3)\rho_0$.

The composition of matter in the inner core of NSs, *i.e.*, at densities $\rho \gtrsim (2 \div 3)\rho_0$, is still unclear. The matter may contain heavier hadrons, like $\Lambda$ and $\Sigma$ hyperons, as well as condensates of $\pi$ and $K$ mesons. An alternative possibility is the transition to the deconfined phase with $u, d$, and, possibly, heavier $s$ quarks. These exotic phases can exist only in massive NSs, in which the central density is larger than several times the nuclear density.

A broad spectrum of astrophysical processes relevant to NSs can be modelled in the framework of relativistic magnetohydrodynamics (MHD). In the MHD description of NSs the transport coefficients of stellar matter play important role in the description of various phenomena. For example, the thermal conductivity is crucial for the modelling of thermal evolution and cooling of NSs [186–188]. The phenomena where the electrical conductivity plays a central role include magnetic field evolution [96–101], dissipation of MHD waves [102–105], etc. The shear and the bulk viscosities are important for the description of damping non-uniform rotation and various unstable oscillation modes of NSs [189, 190].

Because of their astrophysical importance, the transport coefficients of dense stellar matter have been studied extensively during the last decades [103, 106–130]. These computations are relevant to the interiors of NSs in the cold regime, *i.e.*, for temperatures $T \leq 1$ MeV.

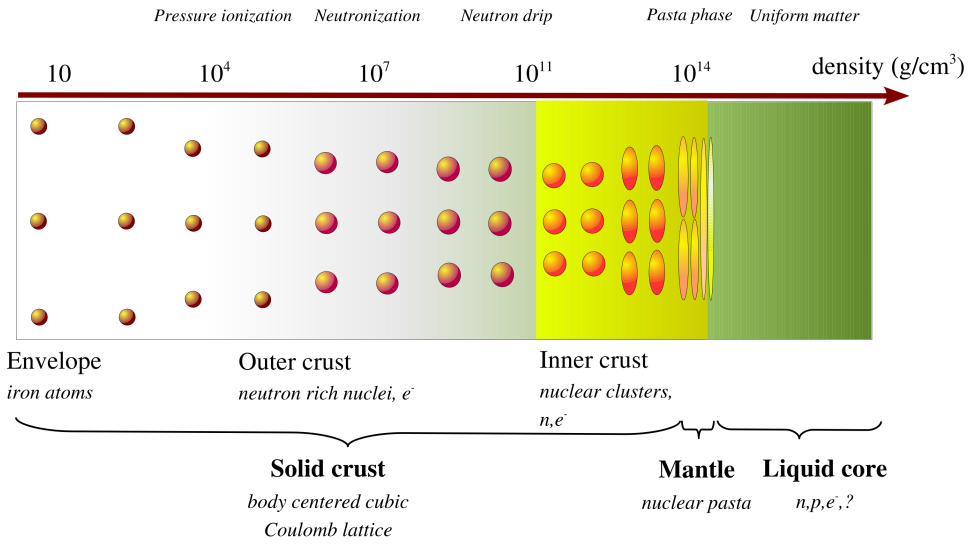


Figure 1.4: The structure of the neutron star crust (adopted from Ref. [185]).

Recent advances in resistive MHD simulations of NSs [73–76] motivate the investigation of transport coefficients, in particular, the electrical conductivity of hot and dense stellar matter including the effects of high magnetic fields. The formation of hot crustal matter in compact stars is anticipated by various astrophysical scenarios, such as supernova explosions, binary NS mergers, as well as heating of NS crusts in accreting binaries.

## 1.5 Structure of the thesis

The area of research covered by this thesis includes second-order relativistic hydrodynamics and transport in strongly correlated systems. The thesis is organized in the following manner.

In Chapter 2 we formulate the second-order dissipative hydrodynamics for relativistic quantum systems using Zubarev's non-equilibrium statistical operator approach [79]. We start the chapter with a brief review of the phenomenological theories of relativistic fluid dynamics as well as the non-equilibrium statistical method developed by Zubarev [65, 66]. This is then followed by a derivation of the evolution equations for dissipative fluxes, where we keep all second-order corrections which arise from the gradient expansion of the statistical operator. We establish the Green-Kubo relations between the relevant transport coefficients and certain equilibrium correlation functions.

In Chapter 3 we compute the transport coefficients of quark matter in the strong coupling regime. We adopt the two-flavor NJL model and the Kubo-Zubarev formalism to obtain formulas for the transport coefficients in terms of the quark spectral function. We review also the main features of the NJL model, including the dynamical generation of quark and meson masses. Our main results concern the electrical and the thermal conductivities [82] and the bulk viscosity [83] in the temperature-density range close to the chiral phase transition line.

In Chapter 4 we employ the Boltzmann kinetic equation in the relaxation time approximation to compute the electrical conductivity tensor of finite-temperature, strongly magnetized dense QED plasma, relevant to the crusts of neutron stars and the interiors of white dwarfs. Our results cover the transition from the degenerate to the nondegenerate regime of matter, as well as the transition from the isotropic to the anisotropic conduction. This chapter is based on Refs. [131, 132].

We give a short summary of our results and discuss the perspectives in Chapter 5.

Throughout this thesis we use the natural (Gaussian) units with $\hbar = c = k_B = k_e = 1$ and the metric signature $(+,-,-,-)$. Greek and Latin indices are utilized to label 4-space and 3-space tensor quantities, respectively. Further conventions used in separate chapters are specified below.

# Chapter 2

# Second-order relativistic hydrodynamics from a non-equilibrium statistical operator

## 2.1 Introduction

Hydrodynamics (fluid dynamics) is an effective theory for the dynamical description of low-frequency and long-wavelength collective phenomena in many-particle systems. Recently, relativistic hydrodynamics has been successfully used to describe the heavy-ion collision processes at RHIC and LHC. The matter created in these experiments exhibits a very small ratio of the shear viscosity to the entropy density [1–12]. Thus, the models of heavy-ion collisions based on relativistic dissipative hydrodynamics, which include shear stresses, allow us to gain insight into the dynamics of strongly interacting matter [13–26].

The hydrodynamic description is adequate for fluids which are close to local thermal equilibrium. The hydrodynamic state of a relativistic fluid is described by means of its energy-momentum tensor and currents of conserved charges, which in the low-frequency and long-wavelength limit allow a Taylor expansion around their equilibrium values in thermodynamic gradients (so-called thermodynamic forces). The validity of such gradient expansion is guaranteed due to the clear separation between the typical microscopic and macroscopic scales of the system. The zeroth-order term in this expansion corresponds to the limit of the ideal hydrodynamics.

The truncation of the gradient expansion at the first order leads to the relativistic Navier-Stokes (NS) theory, which was worked out by Eckart [27] and Landau-Lifshitz [28]. It is known that the solutions of the relativistic NS equations are acausal and unstable [29–32]. The reason of the acausality is the parabolic structure of NS equations, originated from the linear constitutive relations between the dissipative fluxes and the thermodynamic forces.

The problem of acausality can be solved in the second-order theory, where additional terms appear that contain higher (second) order derivatives in thermodynamic quantities. For nonrelativistic fluids the second-order theory was proposed by Müller [34], and then rediscovered and extended to relativistic systems by Israel and Stewart [35,36]. In these theories the dissipative fluxes are treated as independent state variables and satisfy relaxation-type equations which can be derived from the entropy principle. The relaxation terms which appear in these equations recover the causality of the theory in a certain parameter domain [32, 33].

The equations of relativistic hydrodynamics can be derived from the underlying microscopic theory in the relevant (for hydrodynamics) low-frequency and long-wavelength limit. Unlike the first-order hydrodynamics, where the equations of motion have a unique form, the equations of the second-order hydrodynamics are not well established so far. The form of the transport equations for the dissipative fluxes obtained from different methods do not coincide. Furthermore, the transport coefficients

obtained within different methods do not agree always among each other.

For weakly interacting systems the second-order transport equations and the relevant transport coefficients have been extensively studied in the framework of the relativistic kinetic theory [2,36–56], by employing mainly Grad's 14-moment approximation [36, 37, 39, 41–48] and the Chapman-Enskog expansion method [49, 50, 52–54]. In the first approach the non-equilibrium quasiparticle distribution function is expanded in powers of four-momenta up to the second-order around its local equilibrium form [36,191]. The Chapman-Enskog method uses the expansion in the Knudsen number, which is the ratio of the characteristic microscopic and macroscopic scales [192,193]. The transport equations and the relevant transport coefficients can be derived also from the renormalization group method [38,55] and from the fluid/gravity correspondence [39,194–196]. Different approaches to the derivation of the second-order transport equations are reviewed and compared to each other in Refs. [21,25,51].

Recently several groups identified all second-order gradient terms in the shear viscous tensor [39, 194, 197] and made estimates of their relative importance with respect to the shear viscosity that appears in the first-order theory [39,40,194,196,198,199]. In the case of conformally invariant theories, like QCD at high temperatures, Baier *et al.* identified five distinct second-order coefficients, with only four relevant to the flat space [39]. These coefficients have been evaluated in a number of simple models and compared to the shear viscosity. Specifically Baier *et al.* [39] and Bhattacharyya *et al.* [194] estimated these coefficients in the case of strongly coupled supersymmetric Yang-Mills theory. York and Moore estimated them to the leading order in the weakly coupled QCD as well as for QED and scalar $\lambda\phi^4$ theory [40]. They found that the typical ratios of the second-order coefficients to the shear viscosity $\eta$ are given by $\tau_\pi/\eta \simeq 6h^{-1}$, $\lambda_1/\eta^2 \simeq 5h^{-1}$, $\lambda_2/\eta = -2\tau_\pi$, and $\lambda_3/\eta = 0$, where $h$ is the enthalpy density. Thus, there are in fact only two independent second-order coefficients $\eta\tau_\pi$ and $\lambda_1$. Furthermore, numerically, these two coefficients are found to be close, *i.e.*, $\lambda_1 \simeq \eta\tau_\pi$ [39–41]. A comparison of the second-order transport coefficients computed within different formalisms is carried out in Refs. [40,196,197].

As mentioned above, kinetic theory based on the Boltzmann equation is applicable for weakly interacting systems with well-defined quasiparticles. For strongly interacting systems the transport equations should be derived from the Liouville equation for the non-equilibrium density matrix (statistical operator) of the statistical ensemble. Quantum-statistical approach to transport phenomena based on the Liouville equation was systematically developed during the last decades [57–66]. This formalism relates the transport coefficients to certain equilibrium correlation functions via the Kubo formulas [58,59,72], which are applicable in principle for strongly interacting systems.

In the non-equilibrium statistical mechanics one faces the problem to derive the *time-irreversible* transport equations starting from the *time-reversible* Liouville equation. In this thesis we follow the method of the non-equilibrium statistical operator developed mainly by Zubarev [65, 66]. This formalism is based on the key assumption that at sufficiently large time scales the details of the initial state become unimportant for the evolution of the system, and the number of state variables is sufficiently reduced. From this postulate one can construct a non-equilibrium statistical operator [65, 66], which is the generalization of the Gibbs canonical ensemble for non-equilibrium states and is a non-local functional of the thermodynamic parameters and their space-time derivatives. If the deviations of the system from the local equilibrium are sufficiently small, the statistical operator can be expanded into Taylor series in thermodynamic gradients to the required order. The transport equations for the dissipative fluxes are obtained then by statistical averaging of the relevant quantum operators.

This formalism was employed to derive the relativistic transport equations in a generic nonlinear form in Ref. [67]. The Kubo formulas for the relevant first-order transport coefficients for isotropic media were derived in Ref. [68], and then were extended for systems in the presence of strong magnetic fields in Ref. [70].

The aim of the present work is the extension of the above mentioned studies up to the second-order in thermodynamic forces. Because the approach of the non-equilibrium statistical operator is based on the concepts of the relativistic quantum field theory, it is expected to be intrinsically causal. The

causality is incorporated in terms of memory effects in the statistical operator, which is the retarded solution of the Liouville equation. As shown in Refs. [64,178,200,201], the memory effects are naturally incorporated into causal fluid dynamics.

We exploit the gradient expansion of the statistical operator to derive complete second-order transport equations for dissipative fluxes of a relativistic quantum system. In particular, we extend the previous treatments of Refs. [67, 68, 70, 202] to include second-order corrections originating from non-local effects. The terms which are non-local in time encapsulate the memory effects and introduce nonzero relaxation times in the relevant equations. We find that the characteristic relaxation times of the dissipative fluxes are related to the frequency-derivatives of the corresponding first-order transport coefficients taken in the zero-frequency limit. We obtain formulas also for all second-order transport coefficients in terms of certain two- and three-point equilibrium correlation functions.

This chapter is structured as follows. Section 2.2 reviews the phenomenological theories of relativistic hydrodynamics, including ideal and dissipative cases. In Sec. 2.3 we describe Zubarev's formalism of the non-equilibrium statistical operator and provide the details of the derivation of the statistical operator from the quantum Liouville equation. Section 2.4 is devoted to the derivation of the first-order transport equations and the relevant Kubo formulas using the statistical operator obtained in Sec. 2.3. We go on then to derive all second-order corrections to the dissipative fluxes in Sec. 2.5 and obtain formulas for the second-order transport coefficients in terms of two- and three-point correlation functions. We discuss our results and compare them with those of previous studies in Sec. 2.6. Appendix A.1 provides the details of the derivation of the Kubo formulas. Some properties of non-local correlation functions are discussed in Appendix A.2. This chapter is based on the preprint [79].

## 2.2 Phenomenological theory of relativistic hydrodynamics

Relativistic hydrodynamics describes the state of the fluid by means of its energy-momentum tensor $T^{\mu\nu}$ and currents of conserved charges $N_a^\mu$, such as the baryonic, electric, etc.; here we consider the general case of a multicomponent system with $l$ independent flavors of conserved charges, which are labeled by the index $a$. The equations of relativistic hydrodynamics are contained in the conservation laws for the energy-momentum tensor and the charge currents

$$\partial_\mu T^{\mu\nu} = 0, \qquad \partial_\mu N_a^\mu = 0, \quad a = 1, 2, ..., l. \tag{2.1}$$

In the dissipative hydrodynamics also the entropy principle $\partial_\mu S^\mu \geq 0$ should be applied to close the system (2.1), where $S^\mu$ is the entropy 4-current.

### 2.2.1 Relativistic ideal hydrodynamics

Ideal hydrodynamics corresponds to the zeroth-order expansion of the energy-momentum tensor and charge currents with respect to the thermodynamic forces. In this case each fluid element is considered to maintain local thermal equilibrium during its evolution [28, 78]. The macroscopic state of the fluid is therefore fully described by means of the fields of the energy density $\epsilon(x)$, the charge densities $n_a(x)$, and the fluid 4-velocity defined as

$$u^\mu(x) = \frac{dx^\mu}{d\tau} = \big(\gamma(x), \gamma v^i(x)\big)\,, \tag{2.2}$$

where $x^\mu$ is the displacement 4-vector of a fluid element, $d\tau = \sqrt{g_{\mu\nu}dx^\mu dx^\nu}$ is the infinitesimal change in the proper time, $\boldsymbol{v}(x)$ is the fluid 3-velocity and $\gamma(x) = (1 - \boldsymbol{v}^2)^{-1/2}$ is the relevant Lorentz-factor. The 4-velocity given by Eq. (2.2) is normalized by the condition $u^\mu(x)u_\mu(x) = 1$ and has only three independent components.

Because the thermal equilibrium is maintained locally, each fluid element can be assigned well-

defined local values of the temperature $T(x)$, chemical potentials $\mu_a(x)$ [conjugate to charge densities $n_a(x)$], entropy density $s(x)$ and pressure $p(x)$. These quantities are related to the local energy and charge densities via an equation of state $p = p(\epsilon, n_a)$ and the standard thermodynamic relations

$$Tds = d\epsilon - \sum_a \mu_a dn_a, \qquad \text{(first law)} \tag{2.3}$$

$$dp = sdT + \sum_a n_a d\mu_a, \qquad \text{(Gibbs} - \text{Duhem relation)} \tag{2.4}$$

$$h = \epsilon + p = Ts + \sum_a \mu_a n_a, \tag{2.5}$$

where $h$ is the enthalpy density.

The fluid 4-velocity is defined in such a way that in the fluid rest frame the energy and charge flows vanish: $N^i = 0$ and $T^{0i} = 0$, if $u^i = 0$. These conditions together with the spatial isotropy imply the following form for the energy-momentum tensor and charge currents [28, 78]

$$T_0^{\mu\nu} = \epsilon u^\mu u^\nu - p\Delta^{\mu\nu}, \qquad N_{a0}^\mu = n_a u^\mu, \tag{2.6}$$

where the index 0 labels the quantities in ideal hydrodynamics; $\Delta^{\mu\nu} = g^{\mu\nu} - u^\mu u^\nu$ is the projection operator onto the 3-space orthogonal to $u_\mu$ and has the properties

$$u_\mu \Delta^{\mu\nu} = \Delta^{\mu\nu} u_\nu = 0, \qquad \Delta^{\mu\nu}\Delta_{\nu\lambda} = \Delta^\mu_\lambda, \qquad \Delta^\mu_\mu = 3. \tag{2.7}$$

Note that written in the form (2.6), the energy-momentum tensor is symmetric.

From Eqs. (2.6) and (2.7) we obtain

$$\epsilon = u_\mu u_\nu T_0^{\mu\nu}, \qquad p = -\frac{1}{3}\Delta_{\mu\nu} T_0^{\mu\nu}, \qquad n_a = u_\mu N_{a0}^\mu. \tag{2.8}$$

In the fluid rest frame $u^\mu = (1, 0, 0, 0)$, therefore $\Delta^{\mu\nu} = \mathrm{diag}(0, -1, -1, -1)$ and $\Delta^{ij} = \Delta_{ij} = -\delta_{ij}$. In this case Eq. (2.8) simplifies to

$$\epsilon = T_0^{00}, \qquad p = \frac{1}{3} T_0^{ii}, \qquad n_a = N_{a0}^0. \tag{2.9}$$

We introduce also the energy 4-current or momentum density by the formula

$$P_0^\mu = u_\nu T_0^{\mu\nu} + pu^\mu = hu^\mu, \tag{2.10}$$

which is the relativistic generalization of the 3-momentum density (mass current). As seen from Eqs. (2.6) and (2.10), all charge currents are parallel to each other and to the energy flow, which is due to the possibility of a unique definition of the velocity field for ideal fluids.

The equations of ideal hydrodynamics are obtained by substituting the expressions (2.6) into the conservation laws (2.1)

$$\partial_\mu N_{a0}^\mu = \partial_\mu (n_a u^\mu) = 0, \qquad \partial_\mu T_0^{\mu\nu} = \partial_\mu (hu^\mu u^\nu - pg^{\mu\nu}) = 0. \tag{2.11}$$

Contracting the second equation in (2.11) once with $u_\nu$ and then with the projector $\Delta_{\alpha\nu}$ and taking into account Eq. (2.7) and the condition $u_\nu \partial_\mu u^\nu = 0$ we obtain

$$Dn_a + n_a\theta = 0, \qquad D\epsilon + h\theta = 0, \qquad hDu_\alpha = \nabla_\alpha p, \tag{2.12}$$

where we introduced the covariant time-derivative, covariant spatial derivative and velocity 4-divergence via $D = u^\mu \partial_\mu$, $\nabla_\alpha = \Delta_{\alpha\beta}\partial^\beta$ and $\theta = \partial_\mu u^\mu$, respectively. The velocity 4-divergence $\theta$ quantifies how

fast the fluid is expanding ($\theta > 0$) or contracting ($\theta < 0$); it is called the *fluid expansion rate*. In the case of an incompressible flow of the fluid we have $\theta = 0$.

The first and the second equations in Eq. (2.12) are the covariant forms of the charge and the energy conservation laws, respectively. The third equation is the relativistic analogue of the Euler equation of nonrelativistic hydrodynamics. We see that the rest mass density is replaced here by the enthalpy density $h$, which therefore is the appropriate measure of inertia for relativistic fluids. This fact makes clear the meaning of the quantity (2.10) as the relativistic analogue of the momentum flow.

The system (2.12) contains $l + 4$ equations for $l + 5$ variables $\epsilon$, $p$, $n_a$ and $u^\mu$. To close the system one still needs to specify an equation of state $p = p(\epsilon, n_a)$ which relates the pressure to the conserved thermodynamic variables.

It is easy to show that the equations of ideal hydrodynamics lead automatically to the entropy conservation. The entropy flux can be written as

$$S_0^\mu = s u^\mu, \tag{2.13}$$

Using the thermodynamic relations (2.3)–(2.5) and the equations of motion (2.12) we obtain

$$T\partial_\mu S_0^\mu = Ds + s\theta = D\epsilon + h\theta - \sum_a \mu_a (n_a\theta + Dn_a) = 0, \tag{2.14}$$

which is the second law of thermodynamics for a non-dissipative system. Using Eqs. (2.5), (2.6), (2.10) and (2.13) we can rewrite the entropy current as

$$S_0^\mu = \beta P_0^\mu - \sum_a \alpha_a N_{a0}^\mu = p\beta^\mu + \beta_\nu T_0^{\mu\nu} - \sum_a \alpha_a N_{a0}^\mu, \tag{2.15}$$

where we defined

$$\beta = T^{-1}, \qquad \beta^\nu = \beta u^\nu, \qquad \alpha_a = \beta\mu_a. \tag{2.16}$$

The expression (2.15) is the covariant form of the relation (2.5). To proceed further it is convenient to modify Eqs. (2.3) and (2.4) using the definitions (2.16). We obtain for Eq. (2.4)

$$dp = -\beta^{-1} h d\beta + \beta^{-1} \sum_a n_a d\alpha_a, \tag{2.17}$$

where we used Eq. (2.5) in the second step. Now the first law of thermodynamics and Gibbs-Duhem relation can be written in an alternative form

$$ds = \beta d\epsilon - \sum_a \alpha_a dn_a, \qquad \beta dp = -h d\beta + \sum_a n_a d\alpha_a. \tag{2.18}$$

With the aid of Eqs. (2.6) and (2.15) these relations can be cast into a covariant form

$$dS_0^\mu = \beta_\nu dT_0^{\mu\nu} - \sum_a \alpha_a dN_{a0}^\mu, \tag{2.19}$$

$$d(p\beta^\mu) = -T_0^{\mu\nu} d\beta_\nu + \sum_a N_{a0}^\mu d\alpha_a. \tag{2.20}$$

where we used the second relation in Eq. (2.18). One should note that, despite of their vector form, these equations do not contain more information than the scalar thermodynamic relations [contraction of Eqs. (2.19) and (2.20) with the projector $\Delta_{\mu\nu}$ leads to identities].

### 2.2.2 Dissipative fluids: matching conditions

Ideal hydrodynamics relies on the strong assumption of local thermodynamic equilibrium of each fluid element. However, the local equilibrium cannot be maintained permanently, since all real systems react to the non-uniformities of the fluid on finite time scales by generating irreversible (dissipative) fluxes. These fluxes tend to eliminate the local gradients in order to drive the system towards global thermal equilibrium, leading thereby to energy dissipation and entropy increase.

As in the case of ideal hydrodynamics, the equations of relativistic dissipative hydrodynamics can be obtained from the conservation laws given by Eq. (2.1). The expressions (2.6) then need to be generalized by taking into account all possible effects of dissipation. The energy-momentum tensor obtains an anisotropic contribution because of irreversible momentum exchange between different fluid elements, as well as heat transfer due to relative motion of energy and charge currents. The diffusion processes between different charge species in their turn introduce dissipative terms in the charge currents $N_a^\mu$. As a result, the energy-momentum tensor and the charge currents for a dissipative fluid can be written in the following form

$$T^{\mu\nu} = T_0^{\mu\nu} + \tau^{\mu\nu} = \epsilon u^\mu u^\nu - p\Delta^{\mu\nu} + \tau^{\mu\nu}, \tag{2.21}$$

$$N_a^\mu = N_{a0}^\mu + j_a^\mu = n_a u^\mu + j_a^\mu, \tag{2.22}$$

where $j_a^\mu$ and $\tau^{\mu\nu}$ are dissipative terms, and the tensor $\tau^{\mu\nu}$ is symmetric. Note that since the system is out of thermodynamic equilibrium, the thermodynamic parameters are not well-defined anymore, and one needs to impose additional conditions to specify what should be exactly understood under $\epsilon$, $n_a$ and $p$ in Eqs. (2.21) and (2.22). The thermodynamic variables in non-equilibrium states can be defined only by means of a *fictitious equilibrium state*, which should be constructed in such a way to satisfy the thermodynamic relations (2.3)–(2.5) [36]. In order to construct such an equilibrium state for the given values of $T^{\mu\nu}$ and $N_a^\mu$, we define first the energy and charge densities via the so-called matching (fitting) conditions

$$\epsilon(u) = u_\mu u_\nu T^{\mu\nu}, \qquad n_a(u) = u_\mu N_a^\mu. \tag{2.23}$$

Equations (2.23) imply simply that $\epsilon$ and $n_a$ are the time-like eigenvalues of the energy-momentum tensor and the charge currents, respectively, measured by a local observer comoving with the fluid element. We remark that the quantities $\epsilon$ and $n_a$ depend in general on the choice of $u^\mu$, which is the consequence of the ambiguity of the definition of the velocity field for dissipative fluids (see Sec. 2.2.4 for details).

We define in the next step an equilibrium entropy density via an equation of state $s = s(\epsilon, n_a)$, which is chosen to be *the same function* of the parameters $\epsilon$ and $n_a$, as it would be in full thermodynamic equilibrium [29,35,36,203]. The rest of local thermodynamic quantities can be defined then by means of standard thermodynamic relations (2.3)–(2.5), *i.e.*,

$$\beta = \left(\frac{\partial s}{\partial \epsilon}\right)_{n_a}, \qquad \mu_a = -T\left(\frac{\partial s}{\partial n_a}\right)_{\epsilon, n_b \neq n_a}, \qquad p = Ts + \sum_a \mu_a n_a - \epsilon, \tag{2.24}$$

which imply that all thermodynamic parameters are defined in non-equilibrium states via the *same functions* of $\epsilon$ and $n_a$ as their equilibrium counterparts.

The thermodynamic parameters defined above form a fictitious equilibrium state for which the *reversible* thermodynamic relations are formally valid. However, it is worthwhile to stress, that only the energy and charge densities can be ascribed a definite physical meaning, whereas the quantities $s$, $p$, $T$, and $\mu_a$ do not retain their usual physical meaning when the system is out of thermal equilibrium. Anyhow, these quantities are mathematically convenient to use, since they have the approximate physical meaning of their equilibrium counterparts for small departures from local equilibrium [35,36].

For instance, the quantity $p$ is not the *actual thermodynamic pressure* (*i.e.*, the work done by a unit change of the fluid volume), but differs from the latter by an additional non-equilibrium term, which is of the first order in velocity gradients [28,36]. Similarly, the quantity $s$ is not the *actual non-equilibrium entropy density*, since it is defined by means of reversible thermodynamic relations. In other words, $s$ is not the proper quantity which *should increase* in non-equilibrium processes according to the second law of thermodynamics. However, the first non-equilibrium correction in this case appears only at the second order in gradients, and, therefore, can be ignored in the first-order theory [28, 35, 36]. Indeed, the correction to $s$ should be negatively defined, since the entropy attains its maximum in equilibrium. The only scalar quantity which might contribute to the entropy density at the first order in gradients is the velocity 4-divergence $\theta$, therefore the non-equilibrium entropy density should be $s' = s(\epsilon, n_a) - a\theta$, with some thermodynamic coefficient $a$. Since $\theta$ can be of both signs, we conclude that $a = 0$.

### 2.2.3 Decomposition in different dissipative processes

In order to identify different dissipative processes it is convenient to separate scalar, vector and traceless parts of the tensor $\tau^{\mu\nu}$. We first note that the matching conditions (2.23) together with Eqs. (2.21) and (2.22) impose the following orthogonality conditions on the dissipative terms

$$u_\mu u_\nu \tau^{\mu\nu} = 0, \qquad u_\mu j_a^\mu = 0. \tag{2.25}$$

The tensor $\tau^{\mu\nu}$ can be further decomposed into its irreducible components parallel and orthogonal to the fluid 4-velocity $u^\mu$. For that purpose, it is useful to introduce a forth-rank traceless projector orthogonal to $u^\mu$ via

$$\Delta_{\mu\nu\rho\sigma} = \frac{1}{2}\left(\Delta_{\mu\rho}\Delta_{\nu\sigma} + \Delta_{\mu\sigma}\Delta_{\nu\rho}\right) - \frac{1}{3}\Delta_{\mu\nu}\Delta_{\rho\sigma}, \tag{2.26}$$

which has the properties

$$\begin{gathered}\Delta_{\mu\nu\rho\sigma} = \Delta_{\nu\mu\rho\sigma} = \Delta_{\rho\sigma\mu\nu}, \quad u^\mu \Delta_{\mu\nu\rho\sigma} = 0, \quad \Delta^\mu_\alpha \Delta_{\mu\nu\rho\sigma} = \Delta_{\alpha\nu\rho\sigma}, \\ \Delta_\mu{}^\mu{}_{\rho\sigma} = 0, \quad \Delta_{\nu\mu}{}^\mu{}_\sigma = \frac{5}{3}\Delta_{\nu\sigma}, \quad \Delta_{\mu\nu}{}^{\mu\nu} = 5, \quad \Delta_{\mu\nu\rho\sigma}\Delta^{\rho\sigma}_{\alpha\beta} = \Delta_{\mu\nu\alpha\beta}.\end{gathered} \tag{2.27}$$

The most general tensor decomposition of $\tau^{\mu\nu}$ consistent with the orthogonality condition (2.25) can be now written as

$$\tau^{\mu\nu} = -\Pi\Delta^{\mu\nu} + q^\mu u^\nu + q^\nu u^\mu + \pi^{\mu\nu}, \tag{2.28}$$

where we defined new dissipative quantities via

$$\Pi = -\frac{1}{3}\Delta_{\mu\nu}\tau^{\mu\nu} = -\frac{1}{3}\tau^\mu_\mu, \qquad q^\mu = u_\alpha \Delta^\mu_\beta \tau^{\alpha\beta}, \qquad \pi^{\mu\nu} = \Delta^{\mu\nu}_{\alpha\beta}\tau^{\alpha\beta}, \tag{2.29}$$

and used the properties (2.7). From Eqs. (2.21), (2.22) and (2.28) we obtain the most general decompositions of the energy-momentum tensor and the charge currents into their irreducible components

$$T^{\mu\nu} = \epsilon u^\mu u^\nu - (p + \Pi)\Delta^{\mu\nu} + q^\mu u^\nu + q^\nu u^\mu + \pi^{\mu\nu}, \tag{2.30}$$

$$N^\mu_a = n_a u^\mu + j^\mu_a. \tag{2.31}$$

The energy flow defined in Eq. (2.10) can be generalized for dissipative fluids as

$$P^\mu = u_\nu T^{\mu\nu} + p u^\mu = h u^\mu + q^\mu. \tag{2.32}$$

The dissipative terms $j^\mu_a$, $q^\mu$, $\pi^{\mu\nu}$ and $\Pi$ in Eqs. (2.30) and (2.31) are called charge diffusion fluxes,

energy diffusion flux, shear stress tensor and bulk viscous pressure, respectively. The shear stress tensor is the traceless spatial part of the energy-momentum tensor and describes the dissipation by anisotropic momentum flow, whereas the bulk viscous pressure is the non-equilibrium part of the pressure and is responsible for dissipation during isotropic expansion or compression. The dissipative currents satisfy the following conditions

$$u_\nu q^\nu = 0, \qquad u_\nu j_a^\nu = 0, \qquad u_\nu \pi^{\mu\nu} = 0; \qquad \pi^\mu_\mu = 0, \tag{2.33}$$

the first three of which reflect the fact that the dissipation in the fluid should be spatial.

Finally, all quantities on the right-hand sides of Eqs. (2.21) and (2.22) can be obtained by the relevant projections of $T^{\mu\nu}$ and $N_a^\mu$

$$\epsilon = u_\mu u_\nu T^{\mu\nu}, \qquad n_a = u_\mu N_a^\mu, \qquad p + \Pi = -\frac{1}{3}\Delta_{\mu\nu} T^{\mu\nu}, \tag{2.34}$$

$$\pi^{\mu\nu} = \Delta^{\mu\nu}_{\alpha\beta} T^{\alpha\beta}, \qquad q^\mu = u_\alpha \Delta^\mu_\beta T^{\alpha\beta}, \qquad j_a^\nu = \Delta^\nu_\mu N_a^\mu, \tag{2.35}$$

as follows from Eqs. (2.21)–(2.23), (2.29) and the properties (2.7), (2.27). In the fluid rest frame we have

$$\epsilon = T^{00}, \qquad n_a = N_a^0, \qquad p + \Pi = -\frac{1}{3} T^k_k, \tag{2.36}$$

$$\pi_{kl} = \left(\delta_{ki}\delta_{lj} - \frac{1}{3}\delta_{kl}\delta_{ij}\right) T_{ij}, \qquad q^i = T^{0i}, \qquad j_a^i = N_a^i. \tag{2.37}$$

We see from these expressions that all dissipative quantities are purely spatial in the fluid rest frame, as expected. Each of the vectors $q^\mu$ and $j_a^\mu$ has therefore 3 independent components, and the shear stress tensor $\pi^{\mu\nu}$ has 5 independent components because of its tracelessness. Thus, the total number of independent quantities in Eqs. (2.36) and (2.37) is $4l + 10$, which is equal to the degrees of freedom of the energy-momentum tensor and the charge currents (recall that $p$ is fixed by an equation of state). As to the fluid velocity $u^\mu$, it should not be treated as an independent variable itself, but should be connected to one of the physical currents. We devote the next subsection to the discussion of the possible definitions of the velocity field.

### 2.2.4 Definition of the fluid velocity

Another important issue in dissipative fluid dynamics is the proper definition of the fluid velocity. In ideal hydrodynamics the energy and the charge flows are always parallel, and the fluid rest frame is defined as the frame where all these currents vanish. The simultaneous presence of energy and particle diffusion fluxes in the case of dissipative fluids makes the definition of the fluid velocity and the fluid rest frame ambiguous. There are two natural ways to define the fluid rest frame, which we will discuss in this subsection.

#### Landau frame

One of the natural choices of the fluid rest frame is the frame where the net energy flow is zero (Landau frame or L-frame) [28]. In this case $u^\mu$ is chosen to be the time-like eigenvector of $T^{\mu\nu}$

$$u_L^\mu = \frac{u_{L\nu} T^{\mu\nu}}{\sqrt{u_{L\nu} T^{\mu\nu} u_L^\lambda T_{\mu\lambda}}}, \tag{2.38}$$

which together with Eqs. (2.23), (2.30) and (2.33) implies

$$\epsilon_L = \sqrt{u_{L\nu} T^{\mu\nu} u_L^\lambda T_{\mu\lambda}}, \qquad u_{L\nu} T^{\mu\nu} = \epsilon_L u_L^\mu, \qquad q_L^\mu = 0, \tag{2.39}$$

where the index $L$ labels the quantities evaluated according to the Landau definition of $u^\mu$. Thus, with this choice of the velocity field the energy diffusion flux vanishes, and the heat transport phenomena are expressed via the particle diffusion fluxes $j^\mu_{La}$. The energy flow (2.32) in the L-frame is parallel to the fluid velocity, which allows one to write Eq. (2.38) in an alternative way

$$u^\mu_L = \frac{P^\mu}{\sqrt{P^\mu P_\mu}}. \tag{2.40}$$

In order to find the relation between $u^\mu_L$ and a generic velocity $u^\mu$ we note that in a generic fluid rest frame the current (2.32) reads $P^\mu = (h, q^i)$, therefore the boost velocity from an arbitrarily defined rest frame ($u^i = 0$) to the Landau rest frame ($u^i_L = 0$) is $v^i_L = q^i/h = \mathcal{O}_1$; following Refs. [35, 36], we introduced here the symbol $\mathcal{O}_n$ to denote the quantities of $n$th order in deviation from equilibrium. Transformation of the charge currents into the L-frame then reads

$$N'^i_a = N^i_a - v^i_L N^0_a + \mathcal{O}_2. \tag{2.41}$$

Substituting here $N^i_a = j^i_a$, $N'^i_a = j^i_{La}$, and $N^0_a = n_a$, we obtain the charge diffusion fluxes measured in the Landau rest frame

$$j^i_{La} = j^i_a - \frac{n_a}{h} q^i + \mathcal{O}_2. \tag{2.42}$$

Note that the transformed current $j^i_{La}$ is evaluated at transformed coordinate $x'$, but the difference $j^i_{La}(x') - j^i_{La}(x) \simeq (x' - x)\partial j^i_{La} \propto v_L \partial j^i_{La}$ is already of the third order in gradients and can be ignored. Taking into account that in the fluid rest frame $j^0_{La} = j^0_a = q^0 = 0$, we can last Eq. (2.42) into a covariant form

$$j^\mu_{La} = j^\mu_a - \frac{n_a}{h} q^\mu + \mathcal{O}_2, \tag{2.43}$$

which is valid already for an arbitrary frame, *i.e.*, not only in the fluid rest frame. The 4-currents

$$\mathscr{J}^\mu_a = j^\mu_a - \frac{n_a}{h} q^\mu \equiv N^\mu_a - \frac{n_a}{h} P^\mu \tag{2.44}$$

are the charge diffusion fluxes with respect to the energy flow, *i.e.*, the charge currents in the case where the energy flow is absent. Although the energy diffusion flux $q^\mu$ and the charge diffusion fluxes $j^\mu_a$ depend on the choice of the velocity field, the combinations (2.44) remain invariant under first-order changes in $u^\mu$. As we will see in Sec. 2.2.6, these currents are the proper quantities which are responsible for the energy dissipation in irreversible processes.

The rest of thermodynamic variables entering Eqs. (2.30) and (2.31) change only in the second order in thermodynamic gradients under the change of $u^\mu$ [35, 36]. We obtain then the following relation between $u$ and $u_L$

$$u^\mu_L = u^\mu + \frac{q^\mu}{h} + \mathcal{O}_2, \tag{2.45}$$

which follows immediately from a comparison of Eqs. (2.32) and (2.40).

### Eckart frame

According to the Eckart definition the velocity field is chosen to be parallel to one of the conserved currents $N^\mu_a$ (E-frame). In the case where there is only one sort of conserved charge (*e.g.*, the net

particle number), we have $N^\mu = nu^\mu + j^\mu$, and the 4-velocity is defined as [27]

$$u_E^\mu = \frac{N^\mu}{\sqrt{N^\mu N_\mu}}, \tag{2.46}$$

which gives together with Eqs. (2.23) and (2.31)

$$n_E = \sqrt{N^\mu N_\mu}, \qquad N^\mu = n_E u_E^\mu, \qquad j_E^\mu = 0, \tag{2.47}$$

*i.e.*, the particle diffusion flux is absent in this case. The index $E$ in Eqs. (2.46) and (2.47) labels the E-frame.

The boost velocity from a generic rest frame to the Eckart rest frame is $v_E^i = j^i/n$, and the velocities $u^\mu$ and $u_E^\mu$ are related via

$$u_E^\mu = u^\mu + \frac{j^\mu}{n} + \mathcal{O}_2. \tag{2.48}$$

Transforming the energy flux into the Eckart rest frame we obtain

$$P'^i = P^i - \frac{j^i}{n} P^0 + \mathcal{O}_2, \tag{2.49}$$

therefore the energy diffusion flux in the E-frame reads

$$q_E^\mu = q^\mu - \frac{h}{n} j^\mu + \mathcal{O}_2. \tag{2.50}$$

The quantity

$$h^\mu = q^\mu - \frac{h}{n} j^\mu = -\frac{h}{n} \mathscr{J}^\mu \tag{2.51}$$

is the energy flow with respect to the particle flow, and, therefore, it is natural to call it heat flux. The relation (2.51) shows that *heat conduction and particle diffusion are the same phenomena observed from different reference frames*, in the case where only the first-order deviations from equilibrium are taken into account. From Eqs. (2.45) and (2.48) we find the relation between the L-frame and the E-frame to the order $\mathcal{O}_1$

$$u_L^\mu - u_E^\mu = \frac{h^\mu}{h} = -\frac{\mathscr{J}^\mu}{n}. \tag{2.52}$$

The generalization to the case of multiple conserved charges is straightforward. We can connect a reference frame to each of these species via the definition

$$u_a^\mu = \frac{N_a^\mu}{\sqrt{N_a^\mu N_{a\mu}}}, \tag{2.53}$$

which implies that the corresponding diffusion flux vanishes, *i.e.*, $j_a^\mu = 0$.

In the rest of this chapter we will keep the fluid velocity generic (if not stated otherwise) without specifying any particular reference frame.

### 2.2.5 Equations of relativistic dissipative hydrodynamics

Equations of relativistic dissipative hydrodynamics are obtained by substituting the decompositions (2.30) and (2.31) into the conservation laws (2.1). Using the same technique as in Sec. 2.2.1 and

recalling the properties (2.33) we obtain

$$Dn_a + n_a\theta + \partial_\mu j_a^\mu = 0, \tag{2.54}$$
$$D\epsilon + (h+\Pi)\theta + \partial_\mu q^\mu - q^\mu Du_\mu - \pi^{\mu\nu}\sigma_{\mu\nu} = 0, \tag{2.55}$$
$$(h+\Pi)Du_\alpha - \nabla_\alpha(p+\Pi) + \Delta_{\alpha\mu}Dq^\mu + q^\mu\partial_\mu u_\alpha + q_\alpha\theta + \Delta_{\alpha\nu}\partial_\mu\pi^{\mu\nu} = 0, \tag{2.56}$$

where we introduced the velocity stress tensor as $\sigma_{\mu\nu} = \Delta^{\alpha\beta}_{\mu\nu}\partial_\alpha u_\beta$.

The system of Eqs. (2.54)–(2.56) contains $l+4$ equations, as it was in the case of ideal hydrodynamics, whereas the number of independent variables is now $4l+10$. The additional unknown quantities here are $3l$ components of the diffusion fluxes, 5 components of the shear stress tensor and the bulk viscous pressure (recall that the equilibrium pressure is given by the equation of state, and one of the diffusion fluxes can always be eliminated). Thus, in order to close the system of Eqs. (2.54)–(2.56), we still need additional $3l+6$ equations for these dissipative quantities. These relations are established in the phenomenological theory via the second law of thermodynamics (the entropy principle).

### 2.2.6 Relativistic Navier-Stokes (first-order) theory

The entropy conservation law (2.14) derived in the framework of ideal fluid dynamics is no longer valid for dissipative fluids. In this case it should be replaced by the second law of thermodynamics, which implies that the entropy production rate of an isolated system must be always non-negative

$$\partial_\mu S^\mu \geq 0, \tag{2.57}$$

where the equality holds only for reversible processes. By analogy with the decomposition of the charge currents (2.31), we can decompose $S^\mu$ into contributions parallel and orthogonal to $u^\mu$

$$S^\mu = su^\mu + j_s^\mu, \tag{2.58}$$

where $s$ is identified with the equilibrium entropy density (which is sufficient for the first-order accuracy, as explained in Sec. 2.2.2), and the vector $j_s^\mu$ satisfies the condition $u_\mu j_s^\mu = 0$. For small departures from equilibrium it is natural to assume that $j_s^\mu$ is a linear combination of the energy and charge diffusion fluxes

$$j_s^\mu = \tilde{\beta}q^\mu - \sum_a \tilde{\alpha}_a j_a^\mu, \tag{2.59}$$

where $\tilde{\beta}$ and $\tilde{\alpha}_a$ are functions of thermodynamic variables and should be determined from the condition (2.57). This formulation of relativistic dissipative fluid dynamics was proposed by Eckart [27] and Landau, Lifshitz [28], and leads to the relativistic version of the NS theory. Inserting Eq. (2.59) into Eq. (2.58) and introducing the dissipation function via $R \equiv T\partial_\mu S^\mu$ we obtain

$$\begin{aligned} R = -\Pi\theta + \pi^{\mu\nu}\sigma_{\mu\nu} + q^\mu(T\partial_\mu\tilde{\beta} + Du_\mu) - T\sum_a j_a^\mu\partial_\mu\tilde{\alpha}_a \\ +(T\tilde{\beta}-1)\partial_\mu q^\mu + \sum_a(\mu_a - T\tilde{\alpha}_a)\partial_\mu j_a^\mu, \end{aligned} \tag{2.60}$$

where we employed the relations (2.3) and (2.5) and eliminated the terms $D\epsilon$ and $Dn_a$ using Eqs. (2.54) and (2.55). Requiring $R \geq 0$, we identify from Eq. (2.60) $\tilde{\beta} = \beta$, $\tilde{\alpha}_a = \alpha_a$. In the third and the forth terms we can replace $\partial_\mu \to \nabla_\mu$ due to the orthogonality conditions (2.33). Then we have

$$R = -\Pi\theta + \pi^{\mu\nu}\sigma_{\mu\nu} + q^\mu(T\nabla_\mu\beta + Du_\mu) - T\sum_a j_a^\mu\nabla_\mu\alpha_a. \tag{2.61}$$

We can further simplify the third term by approximating $Du_\mu = h^{-1}\nabla_\mu p$ from Eq. (2.12), since $q^\mu$ is already of the order $\mathcal{O}_1$. Using Eq. (2.18) we obtain

$$T\nabla_\mu\beta + Du_\mu = T\sum_a \frac{n_a}{h}\nabla_\mu\alpha_a. \tag{2.62}$$

Substituting this result into Eq. (2.61) and recalling the definition (2.44) we obtain finally

$$R = -\Pi\theta + \pi^{\mu\nu}\sigma_{\mu\nu} - T\sum_a \mathscr{J}_a^\mu\nabla_\mu\alpha_a. \tag{2.63}$$

The second law of thermodynamics implies $R \geq 0$, which requires the right-hand side of Eq. (2.63) to be a quadratic form of thermodynamic forces $\theta$, $\pi^{\mu\nu}$ and $\nabla_\mu\alpha_a$. Assuming linear dependence of the dissipative fluxes on the thermodynamic forces we obtain the constitutive relations

$$\Pi = -\zeta\theta, \qquad \pi^{\mu\nu} = 2\eta\sigma^{\mu\nu}, \qquad \mathscr{J}_a^\mu = \sum_b \chi_{ab}\nabla^\mu\alpha_b, \tag{2.64}$$

where $\eta$ and $\zeta$ are called the shear and the bulk viscosities, respectively, and $\chi_{ab}$ is the matrix of the diffusion coefficients. These relations together with Eqs. (2.54)–(2.56) constitute a closed system of equations, which are known as relativistic NS equations.

From Eqs. (2.63) and (2.64) we obtain for the dissipation function

$$\begin{aligned} R &= \zeta\theta^2 + 2\eta\sigma^{\mu\nu}\sigma_{\mu\nu} - T\sum_{ab}\chi_{ab}\nabla^\mu\alpha_a\nabla_\mu\alpha_b \\ &= \frac{1}{\zeta}\Pi^2 + \frac{1}{2\eta}\pi^{\mu\nu}\pi_{\mu\nu} - T\sum_{ab}(\chi^{-1})_{ab}\mathscr{J}_a^\mu\mathscr{J}_{b\mu}. \end{aligned} \tag{2.65}$$

The positivity of this expression is guaranteed by the positivity of the viscosity coefficients and the eigenvalues of the matrix $\chi_{ab}$ (recall that the diffusion fluxes $\mathscr{J}_a^\mu$ are spatial). We see from Eq. (2.65) that the contribution of diffusion processes to the function $R$ depends only on the relative diffusion currents $\mathscr{J}_a^\mu$, but not on the currents $j_a^\mu$ and $q^\mu$ separately. This result obtained in the framework of the relativistic NS (first-order) theory is the direct consequence of the Lorentz invariance and indicates that the dissipation in the fluid is independent of the choice of the fluid velocity field, as expected.

The entropy current given by Eqs. (2.58) and (2.59) can now be written as

$$S^\mu = su^\mu + \beta q^\mu - \sum_a \alpha_a j_a^\mu = \frac{s}{h}P^\mu - \sum_a \alpha_a \mathscr{J}_a^\mu, \tag{2.66}$$

where we used Eqs. (2.5), (2.16), (2.32) and (2.44) to obtain the second relation. One can give a simple interpretation to the second expression in Eq. (2.66). Recalling that $P^\mu/h = u_L^\mu$ is the fluid velocity measured in the L-frame [see Eq. (2.32)], we observe that the first term on the right-hand side of Eq. (2.66) is the entropy current that is convected together with the energy. The second term arises as a result of the relative flow between the energy and the charges and, therefore, should be identified with the irreversible part of the entropy flow. Using Eqs. (2.5), (2.16), (2.32) and (2.44) we can rewrite Eq. (2.66) also in the following form

$$S^\mu = \beta P^\mu - \sum_a \alpha_a N_a^\mu = p\beta^\mu + \beta_\nu T^{\mu\nu} - \sum_a \alpha_a N_a^\mu, \tag{2.67}$$

which formally coincides with its counterpart of ideal hydrodynamics (2.15).

If we have only one sort of conserved charges ($l = 1$), then instead of the third relation in Eq. (2.64)

we have simply

$$\mathscr{J}^{\mu} = \chi \nabla^{\mu}\alpha, \qquad h^{\mu} = -\kappa \frac{nT^2}{h} \nabla^{\mu}\alpha, \tag{2.68}$$

where we used the definition of the heat current given by Eq. (2.51) and introduced the coefficient of thermal conductivity via

$$\kappa = \left(\frac{h}{nT}\right)^2 \chi. \tag{2.69}$$

Equation (2.69) establishes the relation between the thermal conductivity and the diffusion coefficient $\chi$. Thus, there are only three independent transport coefficients in the first-order theory which relate the irreversible fluxes to the corresponding thermodynamics forces. Employing Eq. (2.62) we can write the heat flux (2.68) in the following way

$$h^{\mu} = \kappa \left(\nabla^{\mu} T - \frac{T}{h} \nabla^{\mu} p\right), \tag{2.70}$$

which in the fluid rest frame reads

$$h^{i} = -\kappa \left(\partial_i T - \frac{T}{h} \partial_i p\right). \tag{2.71}$$

Equation (2.71) is the relativistic generalization of the well-known Fourier law $h^i = -\kappa \partial_i T$ of the nonrelativistic hydrodynamics [28].

The expressions (2.65)–(2.67) in the case of $l = 1$ reduce to

$$R = \zeta \theta^2 + 2\eta \sigma^{\mu\nu}\sigma_{\mu\nu} - T\chi \left(\nabla^{\mu}\alpha\right)^2 = \frac{1}{\zeta}\Pi^2 + \frac{1}{2\eta}\pi^{\mu\nu}\pi_{\mu\nu} - \frac{1}{\kappa T} h^{\mu} h_{\mu}, \tag{2.72}$$

and

$$S^{\mu} = s u^{\mu} + \beta q^{\mu} - \alpha j^{\mu} = \frac{s}{n} N^{\mu} + \beta h^{\mu}. \tag{2.73}$$

The last relation in Eq. (2.73) is the decomposition of the entropy flow into its reversible and irreversible components observed from the E-frame.

Note that in the case where there are no conserved charges, *i.e.*, when $l = 0$, the heat conduction and/or diffusion phenomena are absent [80].

### 2.2.7 Israel-Stewart (second-order) theory

The first-order theory described in the previous section turns out to be acausal, and, therefore, can not be regarded as a consistent theory of relativistic dissipative fluids. The origin of acausality lies in the constitutive relations (2.64), which imply that the thermodynamic forces generate dissipative fluxes instantaneously [29, 31, 34, 35]. In addition, this theory suffers also form instability, which is a consequence of acausality [29–33].

It turns out that in order to recover the causality the entropy current $S^{\mu}$ is required to be at least a quadratic function of the dissipative fluxes. This idea of an extension of the entropy current up to the second order was first proposed by Müller [34] for nonrelativistic fluids. For relativistic fluids a similar second-order theory was developed by Israel and Stewart [35, 36]. In this subsection we review briefly the Israel-Stewart (IS) formulation of causal hydrodynamics, following mainly Ref. [35].

As a starting point the entropy current given by Eqs. (2.66) and (2.67) is extended up to the second order in dissipative quantities $j_a^{\mu}$, $q^{\mu}$, $\pi^{\mu\nu}$ and $\Pi$. It is worth stressing that, despite the

frame-dependence of these quantities, the entropy current $S^\mu$ along with the energy-momentum tensor $T^{\mu\nu}$ and the charge currents $N_a^\mu$ should be regarded as a *primary variable* and should be therefore frame-independent up to the second order [35, 36] [we note that the expressions (2.66) and (2.67) are frame-independent only at the first order in deviations from equilibrium].

We write now the entropy current in the following form

$$S^\mu = \bar{S}^\mu - \bar{R}^\mu - R^\mu, \tag{2.74}$$

where $\bar{S}^\mu$ is the first-order contribution given by Eqs. (2.66) and (2.67), and the terms $\bar{R}^\mu$ and $R^\mu$ collect all possible second-order corrections.

The most general form of the vectors $R^\mu$ and $\bar{R}^\mu$ in a generic frame is [35]

$$\begin{aligned} R^\mu &= \frac{\beta u^\mu}{2}\left(\beta_\Pi \Pi^2 + \beta_\pi \pi^{\alpha\beta}\pi_{\alpha\beta} - \sum_{ab}\beta_{\mathscr{J}}^{ab}\mathscr{J}_a^\alpha \mathscr{J}_{b\alpha}\right) \\ &\quad + \beta\Pi\sum_a \alpha_\Pi^a \mathscr{J}_a^\mu + \beta\pi_\nu^\mu \sum_a \alpha_\pi^a \mathscr{J}_a^\nu, \end{aligned} \tag{2.75}$$

$$\bar{R}^\mu = \beta h^{-1}\left(\Pi q^\mu - \pi^{\mu\nu}q_\nu - \frac{1}{2}u^\mu q^\nu q_\nu\right), \tag{2.76}$$

where the new coefficients $\beta_\Pi$, $\beta_\pi$, $\beta_{\mathscr{J}}^{ab} = \beta_{\mathscr{J}}^{ba}$, $\alpha_\Pi^a$ and $\alpha_\pi^a$ are unknown functions of $\epsilon$ and $n_a$. The vector $R^\mu$ is frame-independent up to the second order, and $\bar{R}^\mu$ collects the second-order contributions to $S^\mu$ which are not frame-independent to the order $\mathcal{O}_2$ (note that we use different metric signature from Ref. [35]). Because the contribution $\bar{S}^\mu$ is frame-independent only to the first order, the term $\bar{R}^\mu$ is necessary to provide the frame-independence of the total entropy current (2.74) [35].

The terms in Eqs. (2.75) and (2.76) which are proportional to $u^\mu$ are responsible for the second-order corrections to the equilibrium entropy density $s$. Indeed, the non-equilibrium entropy density is identified with $S = S^\mu u_\mu$, which can be found from Eqs. (2.74)–(2.76)

$$S = s - \frac{\beta}{2}\left(\beta_\Pi \Pi^2 + \beta_\pi \pi^{\alpha\beta}\pi_{\alpha\beta} - \sum_{ab}\beta_{\mathscr{J}}^{ab}\mathscr{J}_a^\alpha \mathscr{J}_{b\alpha} - h^{-1}q^\alpha q_\alpha\right) \leq s, \tag{2.77}$$

where we used Eqs. (2.66). The last inequality in Eq. (2.77) requires the entropy density in non-equilibrium states to be smaller than its equilibrium value $s$. From here we conclude that $\beta_\Pi \geq 0$, $\beta_\pi \geq 0$, and the matrix $\beta_{\mathscr{J}}^{ab}$ is positive-semidefinite. The term in Eq. (2.77) which is proportional to $q^\mu q_\mu$ represents the shift in the entropy density because of the change of the reference frame and is automatically negative. Those terms in Eqs. (2.75) and (2.76) which are orthogonal to $u^\mu$ represent the irreversible entropy flux arising from couplings between the diffusion and viscous fluxes.

The phenomenological equations for the dissipative fluxes should be found again from the positivity condition of the dissipative function

$$R = T\partial_\mu S^\mu = T\partial_\mu \bar{S}^\mu - T\partial_\mu \bar{R}^\mu - T\partial_\mu R^\mu \geq 0. \tag{2.78}$$

The first term in Eq. (2.78) was already computed in Eq. (2.61)

$$T\partial_\mu \bar{S}^\mu = -\Pi\theta + \pi^{\mu\nu}\sigma_{\mu\nu} + q^\mu(T\nabla_\mu\beta + Du_\mu) - T\sum_a j_a^\mu \nabla_\mu \alpha_a. \tag{2.79}$$

Now we use Eq. (2.56) to eliminate the accelaration term in Eq. (2.79)

$$\begin{aligned} hDu_\mu = \nabla_\mu p + \nabla_\mu\Pi - \Pi Du_\mu - \Delta_{\mu\nu}Dq^\nu - q^\nu\partial_\nu u_\mu - q_\mu\theta - \Delta_{\mu\nu}\partial_\alpha\pi^{\alpha\nu} = -hT\nabla_\mu\beta \\ + T\sum_a n_a\nabla_\mu\alpha_a + \nabla_\mu\Pi - \Pi Du_\mu - \Delta_{\mu\nu}Dq^\nu - q^\nu\partial_\nu u_\mu - q_\mu\theta - \Delta_{\mu\nu}\partial_\alpha\pi^{\alpha\nu}, \end{aligned} \tag{2.80}$$

where we used the second relation of Eq. (2.18) to modify the pressure gradient in Eq. (2.80). Equation (2.80) differs from Eq. (2.62) by additional third-order terms, which now cannot be neglected. Substituting Eq. (2.80) in the third term of Eq. (2.79) and recalling the definitions (2.44) we obtain

$$\begin{aligned} T\partial_\mu \bar{S}^\mu &= -\Pi\theta + \pi^{\mu\nu}\sigma_{\mu\nu} - T\sum_a \mathscr{J}_a^\mu \nabla_\mu \alpha_a + h^{-1}\big(q^\mu \partial_\mu \Pi \\ &\quad -\Pi q^\mu Du_\mu - q_\mu Dq^\mu - q^\mu q^\nu \partial_\nu u_\mu - q^\mu q_\mu \theta - q_\nu \partial_\mu \pi^{\mu\nu}\big), \end{aligned} \tag{2.81}$$

where we used the notation $\nabla_\mu = \Delta_{\mu\nu}\partial^\nu$. Using Eqs. (2.76) and (2.81) we obtain

$$\begin{aligned} T\partial_\mu \bar{S}^\mu - T\partial_\mu \bar{R}^\mu &= -\Pi\Big[\theta + h^{-1}\partial_\mu q^\mu + \bar{\gamma}_\Pi h^{-1} q^\mu Du_\mu + \tilde{\gamma}_\Pi T q^\mu \partial_\mu(\beta h^{-1})\Big] \\ &+ \pi^{\mu\nu}\Big[\sigma_{\mu\nu} + h^{-1}\partial_\mu q_\nu + \bar{\gamma}_\pi T q_\nu \partial_\mu(\beta h^{-1})\Big] - T\sum_a \mathscr{J}_a^\mu \nabla_\mu \alpha_a \\ &- q^\mu\Big[h^{-1}q^\nu\partial_\nu u_\mu + \frac{1}{2}h^{-1}q_\mu\theta - \frac{1}{2}Tq_\mu D(\beta h^{-1}) + (1-\bar{\gamma}_\Pi)h^{-1}\Pi Du_\mu \\ &+ (1-\tilde{\gamma}_\Pi)T\Pi\partial_\mu(\beta h^{-1}) - (1-\bar{\gamma}_\pi)T\pi_\mu^\nu\partial_\nu(\beta h^{-1})\Big]. \end{aligned} \tag{2.82}$$

Here we introduced three additional coefficients $\bar{\gamma}_\Pi$, $\tilde{\gamma}_\Pi$ and $\bar{\gamma}_\pi$ because there is an ambiguity in "sharing" the terms involving $\Pi q^\mu$ and $\pi_\nu^\mu q^\nu$ between the diffusion and viscous fluxes [29].

Now we take the divergence of Eq. (2.75)

$$\begin{aligned} \partial_\mu R^\mu &= \beta\Pi\Big[\beta_\Pi D\Pi + \frac{1}{2}T\Pi\partial_\mu(\beta\beta_\Pi u^\mu) + \sum_a \alpha_\Pi^a \partial_\mu \mathscr{J}_a^\mu + \gamma_\Pi T\sum_a \mathscr{J}_a^\mu \partial_\mu(\beta\alpha_\Pi^a)\Big] \\ &+ \beta\pi^{\mu\nu}\Big[\beta_\pi D\pi_{\mu\nu} + \frac{1}{2}T\pi_{\mu\nu}\partial_\lambda(\beta\beta_\pi u^\lambda) + \sum_a \alpha_\pi^a \partial_\mu \mathscr{J}_{a\nu} + \gamma_\pi T\sum_a \mathscr{J}_{a\nu}\partial_\mu(\beta\alpha_\pi^a)\Big] \\ &- \beta\sum_a \mathscr{J}_a^\mu\Big[\sum_b \beta_\mathscr{J}^{ab} D\mathscr{J}_{b\mu} + \frac{1}{2}T\sum_b \mathscr{J}_{b\mu}\partial_\nu(\beta\beta_\mathscr{J}^{ab}u^\nu) - \alpha_\Pi^a\partial_\mu\Pi - \alpha_\pi^a\partial_\nu\pi_\mu^\nu \\ &- (1-\gamma_\Pi)T\Pi\partial_\mu(\beta\alpha_\Pi^a) - (1-\gamma_\pi)T\pi_\mu^\nu\partial_\nu(\beta\alpha_\pi^a)\Big], \end{aligned} \tag{2.83}$$

where we introduced again two additional coefficients $\gamma_\Pi$ and $\gamma_\pi$ to "share" the terms containing $\Pi\mathscr{J}_a^\mu$ and $\pi_\nu^\mu\mathscr{J}_a^\nu$ between the diffusion and viscous fluxes [29].

Combining Eqs. (2.82) and (2.83), and fixing for simplicity the L-frame $q^\mu = 0$, we obtain for the dissipative function (2.78)

$$\begin{aligned} R &= -\Pi\Big[\theta + \beta_\Pi\dot{\Pi} + \sum_a \alpha_\Pi^a\partial_\mu\mathscr{J}_a^\mu + \gamma_\Pi T\sum_a \mathscr{J}_a^\mu\partial_\mu(\beta\alpha_\Pi^a) + \frac{1}{2}T\Pi\partial_\mu(\beta\beta_\Pi u^\mu)\Big] \\ &+ \pi^{\mu\nu}\Big[\sigma_{\mu\nu} - \beta_\pi\dot{\pi}_{\mu\nu} - \sum_a \alpha_\pi^a\nabla_{<\mu}\mathscr{J}_{a\nu>} - \gamma_\pi T\sum_a \mathscr{J}_{a<\nu}\nabla_{\mu>}(\beta\alpha_\pi^a) - \frac{1}{2}T\pi_{\mu\nu}\partial_\lambda(\beta\beta_\pi u^\lambda)\Big] \\ &- \sum_a \mathscr{J}_a^\mu\Big[T\nabla_\mu\alpha_a - \sum_b \beta_\mathscr{J}^{ab}\dot{\mathscr{J}}_{b\mu} - \frac{1}{2}T\sum_b \mathscr{J}_{b\mu}\partial_\nu(\beta\beta_\mathscr{J}^{ab}u^\nu) + \alpha_\Pi^a\nabla_\mu\Pi + \alpha_\pi^a\Delta_{\alpha\mu}\partial_\nu\pi^{\nu\alpha} \\ &\qquad + (1-\gamma_\Pi)T\Pi\nabla_\mu(\beta\alpha_\Pi^a) + (1-\gamma_\pi)T\pi_\mu^\nu\partial_\nu(\beta\alpha_\pi^a)\Big], \end{aligned} \tag{2.84}$$

where we introduced the shorthand notations

$$\dot{\Pi} = D\Pi, \qquad \dot{\pi}_{\mu\nu} = \Delta_{\mu\nu\rho\sigma}D\pi^{\rho\sigma}, \qquad \dot{\mathscr{J}}_{a\mu} = \Delta_{\mu\nu}D\mathscr{J}_a^\nu, \tag{2.85}$$

$$A_{<\mu\nu>} = \Delta_{\mu\nu}^{\alpha\beta}A_{\alpha\beta}. \tag{2.86}$$

The expressions in the square brackets in Eq. (2.84) are called *generalized or extended thermodynamic forces*. Requiring $R \geq 0$ and assuming linear relations between these forces and the dissipative fluxes we obtain the following evolution equations

$$\Pi = -\zeta\left[\theta + \beta_\Pi\dot{\Pi} + \sum_a \alpha^a_\Pi \partial_\mu \mathscr{J}^\mu_a + \gamma_\Pi T\sum_a \mathscr{J}^\mu_a \partial_\mu(\beta\alpha^a_\Pi) + \frac{1}{2}T\Pi\partial_\mu(\beta\beta_\Pi u^\mu)\right], \tag{2.87}$$

$$\pi_{\mu\nu} = 2\eta\left[\sigma_{\mu\nu} - \beta_\pi\dot{\pi}_{\mu\nu} - \sum_a \alpha^a_\pi \nabla_{<\mu}\mathscr{J}_{a\nu>} - \gamma_\pi T\sum_a \mathscr{J}_{a<\nu}\nabla_{\mu>}(\beta\alpha^a_\pi) - \frac{1}{2}T\pi_{\mu\nu}\partial_\lambda(\beta\beta_\pi u^\lambda)\right], \tag{2.88}$$

$$\begin{aligned}\mathscr{J}_{a\mu} = \sum_b \chi_{ab}\Bigg[&\nabla_\mu\alpha_b - \beta\sum_c \beta^{bc}_{\mathscr{J}}\dot{\mathscr{J}}_{c\mu} - \frac{1}{2}\sum_c \mathscr{J}_{c\mu}\partial_\nu(\beta\beta^{bc}_{\mathscr{J}}u^\nu) + \beta\alpha^b_\Pi\nabla_\mu\Pi \\ &+\beta\alpha^b_\pi\Delta_{\mu\alpha}\partial_\nu\pi^{\nu\alpha} + (1-\gamma_\Pi)\Pi\nabla_\mu(\beta\alpha^b_\Pi) + (1-\gamma_\pi)\pi^\nu_\mu\partial_\nu(\beta\alpha^b_\pi)\Bigg].\end{aligned} \tag{2.89}$$

Equations (2.87)–(2.89) in this form for one type of conserved charges were derived in Ref. [29] (written in the E-frame), while in the original papers of Israel and Stewart [35,36,204] the terms which are nonlinear in thermodynamic forces and dissipative fluxes were dropped.

With the aid of Eqs. (2.87)–(2.89) the dissipative function (2.84) obtains the form

$$R = \frac{1}{\zeta}\Pi^2 + \frac{1}{2\eta}\pi^{\mu\nu}\pi_{\mu\nu} - T\sum_{ab}\mathscr{J}^\mu_a(\chi^{-1})_{ab}\mathscr{J}_{b\mu}, \tag{2.90}$$

which formally coincides with Eq. (2.65). Defining relaxation times according to

$$\tau_\Pi = \zeta\beta_\Pi, \qquad \tau_\pi = 2\eta\beta_\pi, \qquad \tau^{ac}_{\mathscr{J}} = \beta\sum_b \chi_{ab}\beta^{bc}_{\mathscr{J}}, \tag{2.91}$$

we can write Eqs. (2.87)–(2.89) in the following form

$$\tau_\Pi\dot{\Pi} + \Pi = -\zeta\theta - \zeta\left[\sum_a \alpha^a_\Pi\partial_\mu\mathscr{J}^\mu_a + \gamma_\Pi T\sum_a \mathscr{J}^\mu_a\partial_\mu(\beta\alpha^a_\Pi) + \frac{1}{2}T\Pi\partial_\mu(\beta\beta_\Pi u^\mu)\right], \tag{2.92}$$

$$\begin{aligned}\tau_\pi\dot{\pi}_{\mu\nu} + \pi_{\mu\nu} = 2\eta\sigma_{\mu\nu} - 2\eta\Bigg[&\sum_a \alpha^a_\pi\nabla_{<\mu}\mathscr{J}_{a\nu>} + \gamma_\pi T\sum_a \mathscr{J}_{a<\nu}\nabla_{\mu>}(\beta\alpha^a_\pi) \\ &+\frac{1}{2}T\pi_{\mu\nu}\partial_\lambda(\beta\beta_\pi u^\lambda)\Bigg],\end{aligned} \tag{2.93}$$

$$\begin{aligned}\sum_c \tau^{ac}_{\mathscr{J}}\dot{\mathscr{J}}_{c\mu} + \mathscr{J}_{a\mu} = \sum_b \chi_{ab}\nabla_\mu\alpha_b + \sum_b \chi_{ab}\Bigg[&-\frac{1}{2}\sum_c \mathscr{J}_{c\mu}\partial_\nu(\beta\beta^{bc}_{\mathscr{J}}u^\nu) + \beta\alpha^b_\Pi\nabla_\mu\Pi \\ &+\beta\alpha^b_\pi\Delta_{\mu\alpha}\partial_\nu\pi^{\nu\alpha} + (1-\gamma_\Pi)\Pi\nabla_\mu(\beta\alpha^b_\Pi) + (1-\gamma_\pi)\pi^\nu_\mu\partial_\nu(\beta\alpha^b_\pi)\Bigg].\end{aligned} \tag{2.94}$$

The first terms on the right-hand sides of these equations represent the corresponding NS contributions to the dissipative fluxes, see Eq. (2.64). The first terms on the left-hand sides incorporate the relaxation of the dissipative fluxes to their NS values on finite time scales given by Eq. (2.91). Thus, these relaxation terms imply a delay in the response of the dissipative fluxes to thermodynamic forces and recover the causality of the theory [32,33]. The rest of the terms in Eqs. (2.92)–(2.94) are responsible for spatial inhomogeneities in the dissipative fluxes as well as nonlinear couplings between different dissipative processes.

We note that the derivation of the second-order hydrodynamics from kinetic theory produces additional terms which are not obtained within the phenomenological theory [36]. The derivation of complete IS equations from kinetic theory is discussed in Refs. [41,44–46,51].

## 2.3 The non-equilibrium statistical operator formalism

In this section we describe Zubarev's non-equilibrium statistical operator formalism for a generic quantum system which is in the hydrodynamic regime [65–67]. The starting point are again the conservation laws for the energy-momentum tensor and the charge currents written in the operator form

$$\partial_\mu \hat{T}^{\mu\nu} = 0, \qquad \partial_\mu \hat{N}^\mu_a = 0. \tag{2.95}$$

The hydrodynamic quantities $T^{\mu\nu}$ and $N^\mu_a$ discussed in Sec. 2.2 correspond to the statistical averages of the operators $\hat{T}^{\mu\nu}$ and $\hat{N}^\mu_a$ over the full non-equilibrium statistical operator. This operator should be found from the quantum Liouville equation with an infinitesimal source term [65–67] and can be expanded then into a series with respect to thermodynamic forces at the required order. Statistical averaging of the dissipative currents leads then to the transport equations and provides explicit expressions for the transport coefficients via certain equilibrium correlation functions of the system.

### 2.3.1 Local equilibrium statistical operator

As well known, the thermodynamic state of a macroscopic quantum system is described by means of the statistical operator $\hat{\rho}(t)$. It obeys the Liouville equation which in the Schrödinger representation reads [205]

$$\frac{\partial \hat{\rho}_s(t)}{\partial t} + i[\hat{H}, \hat{\rho}_s(t)] = 0, \tag{2.96}$$

with $\hat{H}$ being the Hamiltonian of the system. In this representation the operators acting on the quantum states of the system are independent of time, therefore the explicit time-dependence in $\hat{\rho}_s(t)$ arises from the time-dependence of thermodynamic parameters. In the Heisenberg picture, which we will adopt in this work, the time-evolution is moved onto the operators, whereas the density matrix is independent of time

$$\frac{d\hat{\rho}_H(t)}{dt} = 0. \tag{2.97}$$

In this case the differentiation in Eq. (2.97) with respect to time acts simultaneously on the operators and the thermodynamic parameters. The two representations are related via $\hat{\rho}_H(t) = e^{i\hat{H}t}\hat{\rho}_s(t)e^{-i\hat{H}t}$. From now on we will omit the index $H$, writing simply $\hat{\rho}(t)$. In addition to the equation of motion (2.97), the statistical operator should satisfy also the normalization condition $\mathrm{Tr}\hat{\rho}(t) = 1$. Knowledge of the statistical operator allows one to compute the thermal expectation value of any quantum operator $\hat{F}(t)$ via the formula

$$\langle \hat{F}(t) \rangle = \mathrm{Tr}[\hat{\rho}\hat{F}(t)]. \tag{2.98}$$

In full thermal equilibrium the statistical operator depends only on the integrals of motion. For a system which is in contact with a thermostat with given temperature $T = \beta^{-1}$ and chemical potentials $\mu_a$ (corresponding to conserved charges $\hat{N}_a$) the equilibrium density matrix is given by the grand canonical (Gibbs) distribution

$$\hat{\rho}_{\mathrm{eq}} = \exp\left[\Omega - \beta\Big(\hat{H} - \sum_a \mu_a \hat{\mathcal{N}}_a\Big)\right], \tag{2.99}$$

$$e^{-\Omega} = \mathrm{Tr}\exp\left[-\beta\Big(\hat{H} - \sum_a \mu_a \hat{\mathcal{N}}_a\Big)\right], \tag{2.100}$$

where $\hat{\mathcal{N}}_a$, where $a = 1, 2, \ldots, l$, are the operators of conserved charges. In this case both the Heisen-

berg and Schrödinger representations for $\hat{\rho}$ coincide. Note that the distribution (2.99) is written in the frame where the system as a whole is at rest. We can generalize the equilibrium distribution for an arbitrary reference frame via a Lorentz transformation $\hat{H} \to \hat{\mathcal{P}}_\nu U^\nu$, where $U^\nu$ is the 4-velocity of the system in the chosen frame, $\hat{\mathcal{P}}_\nu$ is the operator of 4-momentum and $\hat{H} \equiv \hat{\mathcal{P}}_0$ in the fluid rest frame. The operators $\hat{\mathcal{P}}_\nu$ and $\hat{\mathcal{N}}_a$ in terms of the energy-momentum tensor and the charge currents are given by

$$\hat{\mathcal{P}}_\nu = \int d^3x \hat{T}_{0\nu}(\boldsymbol{x}, t), \qquad \hat{\mathcal{N}}_a = \int d^3x \hat{N}_{a0}(\boldsymbol{x}, t). \tag{2.101}$$

Substituting Eq. (2.101) into Eqs. (2.99) and (2.100) we obtain the Lorentz-covariant form of the Gibbs distribution

$$\hat{\rho}_{\rm eq} = \exp\left\{\Omega - \int d^3x \beta\Big[U^\nu \hat{T}_{0\nu}(\boldsymbol{x}, t) - \sum_a \mu_a \hat{N}_{a0}(\boldsymbol{x}, t)\Big]\right\}, \tag{2.102}$$

$$e^{-\Omega} = {\rm Tr}\exp\left\{-\int d^3x \beta\Big[U^\nu \hat{T}_{0\nu}(\boldsymbol{x}, t) - \sum_a \mu_a \hat{N}_{a0}(\boldsymbol{x}, t)\Big]\right\}. \tag{2.103}$$

Now we consider a system which is out of full thermodynamic equilibrium, but each small (but still macroscopic) portion of the system has reached its local equilibrium state. This situation corresponds to the *hydrodynamic stage* of the dynamical evolution of the system. The local equilibrium implies that each small element of the fluid can be ascribed local values of hydrodynamic parameters such as temperature $\beta^{-1}(\boldsymbol{x}, t)$, chemical potentials $\mu_a(\boldsymbol{x}, t)$ and macroscopic 4-velocities $u^\nu(\boldsymbol{x}, t)$, which vary slowly in space and time. In this case the global equilibrium distribution given by Eqs. (2.102) and (2.103) is replaced by a local equilibrium statistical operator via [65–70]

$$\hat{\rho}_l(t) = \exp\left\{\Omega_l(t) - \int d^3x \Big[\beta^\nu(\boldsymbol{x}, t)\hat{T}_{0\nu}(\boldsymbol{x}, t) - \sum_a \alpha_a(\boldsymbol{x}, t)\hat{N}^0_a(\boldsymbol{x}, t)\Big]\right\}, \tag{2.104}$$

$$e^{-\Omega_l(t)} = {\rm Tr}\exp\left\{-\int d^3x \Big[\beta^\nu(\boldsymbol{x}, t)\hat{T}_{0\nu}(\boldsymbol{x}, t) - \sum_a \alpha_a(\boldsymbol{x}, t)\hat{N}^0_a(\boldsymbol{x}, t)\Big]\right\}, \tag{2.105}$$

where

$$\beta^\nu(\boldsymbol{x}, t) = \beta(\boldsymbol{x}, t)u^\nu(\boldsymbol{x}, t), \qquad \alpha_a(\boldsymbol{x}, t) = \beta(\boldsymbol{x}, t)\mu_a(\boldsymbol{x}, t). \tag{2.106}$$

Here the fluid 4-velocity $u^\nu$ can be defined for the given average values of $\langle\hat{T}^{\mu\nu}\rangle$ and $\langle\hat{N}^\mu_a\rangle$ according to either Landau or Eckart definition, see Sec. 2.2.4. The local equilibrium distribution (2.104) is referred also to as *relevant statistical operator* [65, 66].

Next we define the operators of the energy and charge densities in the comoving frame via $\hat{\epsilon} = u_\mu u_\nu \hat{T}^{\mu\nu}$ and $\hat{n}_a = u_\mu \hat{N}^\mu_a$, by analogy with Eq. (2.23). The local values of the Lorentz-invariant thermodynamic parameters $\beta$ and $\alpha_a$ are fixed then by given average values of the operators $\hat{\epsilon}$ and $\hat{n}_a$ via the following matching conditions [60, 65–67, 69, 70]

$$\langle\hat{\epsilon}(\boldsymbol{x}, t)\rangle = \langle\hat{\epsilon}(\boldsymbol{x}, t)\rangle_l, \tag{2.107}$$

$$\langle\hat{n}_a(\boldsymbol{x}, t)\rangle = \langle\hat{n}_a(\boldsymbol{x}, t)\rangle_l, \tag{2.108}$$

where we introduced the notation

$$\langle\hat{F}(\boldsymbol{x}, t)\rangle_l = {\rm Tr}\big[\hat{\rho}_l(t)\hat{F}(\boldsymbol{x}, t)\big]. \tag{2.109}$$

Note that the conditions (2.107) and (2.108) define the temperature and the chemical potentials in general as *non-local functionals* of $\langle\hat{\epsilon}(\boldsymbol{x}, t)\rangle$ and $\langle\hat{n}_a(\boldsymbol{x}, t)\rangle$ [64]. However, in the hydrodynamic description of the fluid one needs to define thermodynamic parameters as *local* functions of the energy

and charge densities, as it is the case for full thermal equilibrium. This can be done if one assumes that all fluid elements where the local equilibrium is already established are stastically independent of each other [60]. In other words, the local equilibrium values $\langle\hat{\epsilon}\rangle_l$ and $\langle\hat{n}_a\rangle_l$ in Eqs. (2.107) and (2.108) should be evaluated at *constant values* of $\beta$ and $\mu_a$, which are identified then by matching $\langle\hat{\epsilon}\rangle_l$ and $\langle\hat{n}_a\rangle_l$ to the real values of these quantities $\langle\hat{\epsilon}\rangle$ and $\langle\hat{n}_a\rangle$ at the given point $(\boldsymbol{x},t)$. In this way we construct a *fictitious local equilibrium state* for any given point, such that it reproduces the local values of the energy and charge densities. In addition, the relevant distribution fixes also the local values of the 3-momentum or one of the charge currents, when adopting the Landau or the Eckart definition of the fluid velocity, respectively. Using Eq. (2.39) we can write the matching conditions in the L-frame as follows

$$u_\mu\langle\hat{T}^{\mu\nu}\rangle = u_\mu\langle\hat{T}^{\mu\nu}\rangle_l, \tag{2.110}$$
$$u_\mu\langle\hat{N}^\mu_a\rangle = u_\mu\langle\hat{N}^\mu_a\rangle_l. \tag{2.111}$$

In the E-frame connected to the current $\hat{N}^\mu_a$ we have instead [see Eq. (2.53)]

$$u_\mu u_\nu\langle\hat{T}^{\mu\nu}\rangle = u_\mu u_\nu\langle\hat{T}^{\mu\nu}\rangle_l, \tag{2.112}$$
$$u_\mu\langle\hat{N}^\mu_b\rangle = u_\mu\langle\hat{N}^\mu_b\rangle_l, \quad b\neq a, \tag{2.113}$$
$$\langle\hat{N}^\mu_a\rangle = \langle\hat{N}^\mu_a\rangle_l. \tag{2.114}$$

We keep in mind that all local equilibrium averages in Eqs. (2.110)–(2.114) should be evaluated formally at constant values of $\beta$, $\mu_a$ and $u^\mu$, as explained above.

It is useful to write the relevant distribution also in a Lorentz-covariant form. In the fluid rest frame (note that the rest frame is defined only locally for each fluid element) Eqs. (2.104) and (2.105) can be written in the following form

$$\begin{aligned}\hat{\rho}_l(t) &= \exp\left\{\Omega_l(t)-\int d^3\tilde{x}\beta(\boldsymbol{x},t)\Big[\hat{T}_{00}(\boldsymbol{x},t)-\sum_a\mu_a(\boldsymbol{x},t)\hat{N}^0_a(\boldsymbol{x},t)\Big]\Big|_{\text{rest}}\right\}\\ &= \exp\left\{\Omega_l(t)-\int d^3\tilde{x}\beta(\boldsymbol{x},t)\Big[\hat{\epsilon}(\boldsymbol{x},t)-\sum_a\mu_a(\boldsymbol{x},t)\hat{n}_a(\boldsymbol{x},t)\Big]\right\},\end{aligned} \tag{2.115}$$
$$e^{-\Omega_l(t)} = \mathrm{Tr}\exp\left\{-\int d^3\tilde{x}\beta(\boldsymbol{x},t)\Big[\hat{\epsilon}(\boldsymbol{x},t)-\sum_a\mu_a(\boldsymbol{x},t)\hat{n}_a(\boldsymbol{x},t)\Big]\right\}, \tag{2.116}$$

where $d^3\tilde{x}=\gamma(\boldsymbol{x},t)d^3x$ is the proper volume of a fluid element with $\gamma(\boldsymbol{x},t)\equiv u^0(\boldsymbol{x},t)$ being the relevant Lorentz factor.

### 2.3.2 Deriving the thermodynamic relations

In this section we derive the thermodynamic relations for local thermodynamic parameters starting from the relevant distribution (2.104) or (2.115). Following Zubarev we define first the entropy operator as [66, 67]

$$\begin{aligned}\hat{S}(t) &= -\ln\hat{\rho}_l(t) = -\Omega_l(t)+\int d^3x\Big[\beta^\nu(\boldsymbol{x},t)\hat{T}_{0\nu}(\boldsymbol{x},t)-\sum_a\alpha_a(\boldsymbol{x},t)\hat{N}^0_a(\boldsymbol{x},t)\Big]\\ &= -\Omega_l(t)+\int d^3\tilde{x}\beta(\boldsymbol{x},t)\Big[\hat{\epsilon}(\boldsymbol{x},t)-\sum_a\mu_a(\boldsymbol{x},t)\hat{n}_a(\boldsymbol{x},t)\Big],\end{aligned} \tag{2.117}$$

which allows one to write the relevant statistical operator as

$$\hat{\rho}_l(t)=e^{-\hat{S}(t)}. \tag{2.118}$$

The thermodynamic entropy in local equilibrium is defined as the statistical average of the entropy operator

$$S(t) = \langle \hat{S}(t) \rangle_l = -\Omega_l(t) + \int d^3\tilde{x}\beta(\boldsymbol{x},t)\Big[\epsilon(\boldsymbol{x},t) - \sum_a \mu_a(\boldsymbol{x},t)n_a(\boldsymbol{x},t)\Big] \equiv \langle \hat{S}(t) \rangle, \tag{2.119}$$

where we used the matching conditions (2.107) and (2.108) and denoted the local values of the energy and charge densities by $\epsilon(\boldsymbol{x},t)$ and $n_a(\boldsymbol{x},t)$.

We can now derive the thermodynamic relations using Eq. (2.116). For that purpose we consider small variations $\delta\epsilon(\boldsymbol{x},t)$ and $\delta n_a(\boldsymbol{x},t)$ in the local energy and charge densities. These variations induce small changes in the thermodynamic parameters which we will denote by $\delta\beta(\boldsymbol{x},t)$ and $\delta\mu_a(\boldsymbol{x},t)$. The change in $\Omega_l(t)$ will be

$$\delta\Omega_l(t) = \int d^3\tilde{x}\left[\frac{\delta\Omega_l(t)}{\delta\beta(\boldsymbol{x},t)}\delta\beta(\boldsymbol{x},t) + \sum_a \frac{\delta\Omega_l(t)}{\delta\mu_a(\boldsymbol{x},t)}\delta\mu_a(\boldsymbol{x},t)\right], \tag{2.120}$$

where the derivatives in the square brackets are the corresponding Lorentz-invariant functional derivatives of $\Omega_l(t)$. Taking the functional derivative of Eq. (2.116) with respect to $\beta(\boldsymbol{x},t)$ we obtain

$$\frac{\delta\Omega_l(t)}{\delta\beta(\boldsymbol{x},t)} = \mathrm{Tr}\Big\{\hat{\rho}_l(t)\Big[\hat{\epsilon}(\boldsymbol{x},t) - \sum_a \mu_a(\boldsymbol{x},t)\hat{n}_a(\boldsymbol{x},t)\Big]\Big\} \equiv \epsilon(\boldsymbol{x},t) - \sum_a \mu_a(\boldsymbol{x},t)n_a(\boldsymbol{x},t), \tag{2.121}$$

where we used Eqs. (2.109) and (2.115). In the same way we obtain

$$\frac{\delta\Omega_l(t)}{\delta\mu_a(\boldsymbol{x},t)} = -\beta(\boldsymbol{x},t)n_a(\boldsymbol{x},t). \tag{2.122}$$

The infinitesimal change in the entropy can be then found from Eq. (2.119)

$$\delta S(t) = -\delta\Omega_l(t) + \int d^3\tilde{x}\Big[\delta\beta(\epsilon - \sum_a \mu_a n_a) + \beta(\delta\epsilon - \sum_a \mu_a \delta n_a) - \beta\sum_a \delta\mu_a n_a\Big], \tag{2.123}$$

where we suppressed the arguments $(\boldsymbol{x},t)$ for brevity. Substituting here Eqs. (2.120)–(2.122) we obtain

$$\delta S(t) = \int d^3\tilde{x}\beta(\delta\epsilon - \sum_a \mu_a \delta n_a). \tag{2.124}$$

We define in the next step invariant entropy density via

$$S(t) = \int d^3\tilde{x}s(\boldsymbol{x},t), \tag{2.125}$$

which gives together with Eq. (2.124)

$$\int d^3\tilde{x}\Big[\beta(\delta\epsilon - \sum_a \mu_a\delta n_a) - \delta s\Big] = 0. \tag{2.126}$$

Because $\delta\varepsilon$ and $\delta n_a$ are arbitrary changes and the entropy density $s$ is assumed to be a *local function* of $\varepsilon$ and $n_a$, we derive from Eq. (2.126) the relation

$$T\delta s = \delta\epsilon - \sum_a \mu_a \delta n_a, \tag{2.127}$$

which is the first law of thermodynamics for local variables, see Eq. (2.3).

To obtain other thermodynamic relations we recall that the grand thermodynamic ponential $\Omega_l$ is

equal to $-\beta pV$ in full thermal equilibrium, with $p$ and $V$ being the pressure and the volume of the system. In local equilibrium $\Omega_l(t)$ given by Eq. (2.116) is a functional of $\epsilon(\boldsymbol{x},t)$ and $n_a(\boldsymbol{x},t)$, therefore we can define a scalar function $p = p(\epsilon, n_a) = p(\boldsymbol{x},t)$, such that

$$\Omega_l(t) = -\int d^3\tilde{x}\beta(\boldsymbol{x},t)p(\boldsymbol{x},t). \tag{2.128}$$

The form of the function $p = p(\epsilon, n_a)$ should be established from Eqs. (2.116) and (2.128) and the matching conditions (2.107) and (2.108) (which determine the temperature and the chemical potentials); it is called the *equation of state*.

Using Eq. (2.128) we can write Eq. (2.119) also as

$$S(t) = \int d^3\tilde{x}\beta(\boldsymbol{x},t)\Big[\epsilon(\boldsymbol{x},t) + p(\boldsymbol{x},t) - \sum_a \mu_a(\boldsymbol{x},t)n_a(\boldsymbol{x},t)\Big], \tag{2.129}$$

which in combination with Eq. (2.125) leads to the well-known thermodynamic relation

$$s = \beta(\epsilon + p) - \sum_a \alpha_a n_a, \tag{2.130}$$

in accordance with Eq. (2.5). From Eqs. (2.127) and (2.130) we obtain the Gibbs-Duhem relation

$$\delta p = s\delta T + \sum_a n_a \delta\mu_a, \tag{2.131}$$

which is identical to Eq. (2.4).

Thus, using the relevant statistical operator, we constructed a full set of thermodynamic variables (*i.e.*, a fictitious equilibrium state) for the given fields of the energy-momentum tensor and charge current densities, as it was required for the hydrodynamic description of the system (see Sec. 2.2.2).

### 2.3.3 Deriving the non-equilibrium statistical operator

Due to the matching conditions discussed in Sec. 2.3.1 the relevant statistical operator reproduces the local values of macroscopic observables, *i.e.*, the energy and charge densities at an arbitrary point of the space-time. However, the relevant distribution does not satisfy the Liouville equation (2.97) and, consequently, it cannot describe the irreversible dynamics of the system. On the other hand, the Liouville equation is time-reversible, therefore an irreversible solution can be obtained only via an appropriate choice of initial condition. In order to construct a statistical operator which satisfies the Liouville equation and at the same time is able to describe irreversible processes we follow the method proposed in Ref. [66]. For our purposes it is more convenient to start from the Liouville equation written for the logarithm of the statistical operator. Defining $\hat{\sigma}(t) = -\ln\hat{\rho}(t)$, we find from Eq. (2.97)

$$\frac{d\hat{\sigma}(t)}{dt} = 0. \tag{2.132}$$

Now we make an assumption that at some initial moment of time $t'$ the statistical distribution function coincides with the local equilibrium distribution: $\hat{\sigma}(t') = \hat{S}(t')$ [62,63,65,66,206,207]. Because $\hat{\sigma}$ is independent of time according to Eq. (2.132), it remains unchanged for all subsequent moments of time, *i.e.*,

$$\hat{\sigma}(t) = \hat{S}(t'), \quad t \geq t'. \tag{2.133}$$

Our next step is to modify the expression (2.133) in such a way that it can incorporate the irreversibility of the thermodynamic evolution of the system. The irreversibility of processes actually

implies that the system "forgets" the details of the initial state after some characteristic (microscopic) time scale $\tau$ [65, 66]. This statement is consistent with the empirical fact that the thermodynamic evolution of a macroscopic system ends always with the establishment of complete thermostatic equilibrium *independent* of the initial conditions. Therefore, fixing a remote instant of time $t_0$ in the past, one can postulate that all initial states given by the relevant distribution in the time interval $t_0 \leq t' \leq t - \tau$ are *equally probable*, *i.e.*, they all can be used to construct the non-equilibrium state at the moment $t$. This statement implies that the required solution for $\hat{\sigma}(t)$ can be obtained by averaging the right-hand side of Eq. (2.133) over $t'$ in the interval $t_0 \leq t' \leq t - \tau$ [65, 66]

$$\hat{\sigma}(t) = \frac{1}{t - t_0 - \tau} \int_{t_0}^{t-\tau} dt' \hat{S}(t') = \frac{1}{t - t_0 - \tau} \int_{-(t-t_0-\tau)}^{0} dt' \hat{S}(t' + t - \tau). \tag{2.134}$$

The value of $t_0$ was arbitrary so far, and it is natural to take the limit $t_0 \to -\infty$. We will use Abel's theorem

$$\lim_{T\to\infty} \frac{1}{T} \int_{-T}^{0} dt' f(t') = \lim_{\varepsilon\to+0} \varepsilon \int_{-\infty}^{0} dt' e^{\varepsilon t'} f(t'), \tag{2.135}$$

which is valid if the function $f(t)$ is sufficiently smooth and at least one of the above limits exists. Then we obtain for Eq. (2.134)

$$\hat{\sigma}(t) = \lim_{\varepsilon\to 0} \varepsilon \int_{-\infty}^{0} dt' e^{\varepsilon t'} \hat{S}(t' + t - \tau) = \lim_{\varepsilon\to 0} \varepsilon \int_{-\infty}^{t} dt' e^{\varepsilon(t'-t)} \hat{S}(t' - \tau). \tag{2.136}$$

It is easy to show that this operator satisfies the Liouville equation (2.132). Indeed,

$$\frac{d\hat{\sigma}(t)}{dt} = \varepsilon \hat{S}(t - \tau) - \varepsilon^2 \int_{-\infty}^{t} dt' e^{\varepsilon(t'-t)} \hat{S}(t' - \tau) = -\varepsilon[\hat{\sigma}(t) - \hat{S}(t - \tau)], \tag{2.137}$$

where we omitted the limit $\varepsilon \to 0$ for brevity. Since the deviation of the distribution function from its local equilibrium form is assumed to be finite, the right-hand side of Eq. (2.137) vanishes in the limit $\varepsilon \to 0$. Note also, that in this limit the Liouville equation is satisfied independent of the characteristic time scale $\tau$, which we can therefore set to zero. According to Eqs. (2.136) and (2.137) the statistical operator

$$\hat{\rho}_\varepsilon(t) = \exp\left[-\varepsilon \int_{-\infty}^{t} dt' e^{\varepsilon(t'-t)} \hat{S}(t')\right] \tag{2.138}$$

prior to taking the limit $\varepsilon \to 0$ satisfies the Liouville equation with an infinitesimal source term. The latter breaks the reversibility of the Liouville equation by choosing its retarded solution. This is clearly seen from the expression (2.138), where the time-integration incorporates the retardation of the response of the system to thermodynamic perturbations due to memory effects of the past. Hence we draw an important conclusion that the limit $\varepsilon \to +0$ should be performed only after the thermodynamic limit is taken. Due to this procedure one maintains irreversibility in the evolution of the system untill the end of the calculations. Thus, the statistical average of any operator $\hat{F}(t)$ should be computed according to the following rule [66]

$$\langle \hat{F}(t) \rangle = \lim_{\varepsilon\to+0} \lim_{V\to\infty} \mathrm{Tr}[\hat{\rho}_\varepsilon(t) \hat{F}(t)], \tag{2.139}$$

where $V$ is the volume of the system. Furthermore, because the statistical operator (2.138) incorporates memory effects, the transport equations obtained from Eq. (2.138) are expected to involve finite relaxation time scales, and, therefore, respect causality [64, 178, 200, 201]. Thus, we constructed a causal non-equilibrium statistical operator starting from the relevant distribution.

Now we substitute the explicit expression for $\hat{S}(t)$ given by Eq. (2.117) into Eq. (2.138) to obtain (omitting the index $\varepsilon$ for brevity)

$$\hat{\rho}(t) = Q^{-1}(t) \exp\left\{-\int d^3x \hat{Z}(\boldsymbol{x},t)\right\}, \qquad Q(t) = \mathrm{Tr} \exp\left\{-\int d^3x \hat{Z}(\boldsymbol{x},t)\right\}, \tag{2.140}$$

where

$$\hat{Z}(\boldsymbol{x},t) = \varepsilon \int_{-\infty}^{t} dt_1 e^{\varepsilon(t_1-t)} \Big[\beta^\nu(\boldsymbol{x},t_1)\hat{T}_{0\nu}(\boldsymbol{x},t_1) - \sum_a \alpha_a(\boldsymbol{x},t_1)\hat{N}^0_a(\boldsymbol{x},t_1)\Big]. \tag{2.141}$$

In the case of one type of conserved charge ($l = 1$) Eqs. (2.140) and (2.141) coincides with Eqs. (42)–(44) in Ref. [70], and in the case of $l = 0$ we recover Eqs. (2.4) and (2.8) in Ref. [68].

We can separate the local equilibrium contribution from Eq. (2.141) by integrating it by parts:

$$\begin{aligned}\hat{Z}(\boldsymbol{x},t) &= \beta^\nu(\boldsymbol{x},t)\hat{T}_{0\nu}(\boldsymbol{x},t) - \sum_a \alpha_a(\boldsymbol{x},t)\hat{N}^0_a(\boldsymbol{x},t) \\ &- \int_{-\infty}^{t} dt_1 e^{\varepsilon(t_1-t)} \frac{d}{dt_1}\Big[\beta^\nu(\boldsymbol{x},t_1)\hat{T}_{0\nu}(\boldsymbol{x},t_1) - \sum_a \alpha_a(\boldsymbol{x},t_1)\hat{N}^0_a(\boldsymbol{x},t_1)\Big],\end{aligned} \tag{2.142}$$

where we assumed that the exponential factor $e^{\varepsilon(t_1-t)}$ guarantees the limiting behavior

$$\lim_{t_1\to-\infty} e^{\varepsilon(t_1-t)}\hat{F}(t_1) = 0. \tag{2.143}$$

Conservation laws (2.95) imply the relations $\partial^\mu \hat{T}_{\mu\nu} = \partial^0\hat{T}_{0\nu} + \partial^i\hat{T}_{i\nu} = 0$ and $\partial^\mu \hat{N}_{a\mu} = \partial^0\hat{N}_{a0} + \partial^i\hat{N}_{ai} = 0$, which give for the integrand of the second term in Eq. (2.142)

$$\partial^0\Big(\beta^\nu\hat{T}_{0\nu} - \sum_a \alpha_a\hat{N}^0_a\Big) = \hat{T}_{\mu\nu}\partial^\mu\beta^\nu - \sum_a \hat{N}^\mu_a\partial_\mu\alpha_a - \partial^i(\beta^\nu\hat{T}_{i\nu} - \sum_a \alpha_a\hat{N}_{ai}). \tag{2.144}$$

The surface term in Eq. (2.144) vanishes after integration in Eq. (2.142) and we are left with

$$\begin{aligned}\int d^3x\hat{Z}(\boldsymbol{x},t) &= \int d^3x\Big[\beta^\nu(\boldsymbol{x},t)\hat{T}_{0\nu}(\boldsymbol{x},t) - \sum_a \alpha_a(\boldsymbol{x},t)\hat{N}^0_a(\boldsymbol{x},t)\Big] \\ &- \int d^3x \int_{-\infty}^{t} dt_1 e^{\varepsilon(t_1-t)}\Big[\hat{T}_{\mu\nu}(\boldsymbol{x},t_1)\partial^\mu\beta^\nu(\boldsymbol{x},t_1) - \sum_a \hat{N}^\mu_a(\boldsymbol{x},t_1)\partial_\mu\alpha_a(\boldsymbol{x},t_1)\Big].\end{aligned} \tag{2.145}$$

The first term of this expression corresponds to the local equilibrium part of the statistical operator. The integrand of the second term is a thermodynamic "force" as it involves gradients of temperature, chemical potentials and velocity field. Naturally, the second term in Eq. (2.145) is identified then with the non-equilibrium part of the statistical operator. Using Eqs. (2.140) and (2.145) we can write the full statistical operator as [68, 70]

$$\hat{\rho}(t) = Q^{-1}e^{-\hat{A}+\hat{B}}, \qquad Q = \mathrm{Tr}e^{-\hat{A}+\hat{B}}, \tag{2.146}$$

with

$$\hat{A}(t) = \int d^3x\Big[\beta^\nu(\boldsymbol{x},t)\hat{T}_{0\nu}(\boldsymbol{x},t) - \sum_a \alpha_a(\boldsymbol{x},t)\hat{N}^0_a(\boldsymbol{x},t)\Big], \tag{2.147}$$

$$\hat{B}(t) = \int d^3x \int_{-\infty}^{t} dt_1 e^{\varepsilon(t_1-t)}\hat{C}(\boldsymbol{x},t_1), \tag{2.148}$$

$$\hat{C}(\boldsymbol{x},t) = \hat{T}_{\mu\nu}(\boldsymbol{x},t)\partial^\mu\beta^\nu(\boldsymbol{x},t) - \sum_a \hat{N}^\mu_a(\boldsymbol{x},t)\partial_\mu\alpha_a(\boldsymbol{x},t). \tag{2.149}$$

The statistical operator given by Eq. (2.146) can now be used to derive the transport equations for dissipative currents. For this purpose we will treat the non-equilibrium part (2.148) as a perturbation keeping only the first- and the second-order terms in the Taylor expansion of $\hat{\rho}(t)$ with respect to the operator $\hat{B}(t)$.

### 2.3.4 Second-order expansion of the statistical operator

We start from the following formula for arbitrary two operators

$$e^{-A+B}e^{A} = 1 + \int_0^1 d\tau e^{\tau(-A+B)} B e^{\tau A}, \tag{2.150}$$

which can be obtained by integrating the identity

$$\frac{d}{d\tau} e^{\tau(-A+B)} e^{\tau A} = e^{\tau(-A+B)} B e^{\tau A} \tag{2.151}$$

over $\tau$ variable from 0 to 1. We omitted here the operator signs of $\hat{A}$ and $\hat{B}$ for the sake of simplicity of formulas. Keeping only the linear term in $B$ we obtain from Eq. (2.150)

$$e^{-A+B} = e^{-A} + \int_0^1 d\lambda e^{-\lambda A} B e^{\lambda A} e^{-A} + \mathcal{O}(B^2). \tag{2.152}$$

Our next task is the second-order expansion of the non-equilibrium statistical operator given by Eq. (2.146) with respect to the operator $B$. We start with the nominator and expand the identity (2.150) up to the second order. The integrand in Eq. (2.150) is already of the order of $\mathcal{O}(B)$, therefore it is sufficient to evaluate the operator $e^{\tau(-A+B)}$ using the first-order expansion (2.152). Replacing $A \to \tau A$, $B \to \tau B$ in Eq. (2.152) and inserting the result into Eq. (2.150) we find

$$e^{-A+B} = (1 + \hat{\alpha}_1 + \hat{\alpha}_2) e^{-A}, \tag{2.153}$$

with

$$\hat{\alpha}_1 = \int_0^1 d\tau \hat{B}_\tau, \qquad \hat{\alpha}_2 = \frac{1}{2} \int_0^1 d\tau \int_0^1 d\lambda \tilde{T}\{\hat{B}_\lambda \hat{B}_\tau\}, \tag{2.154}$$

where we introduced a shorthand notation for any operator $\hat{X}$

$$\hat{X}_\tau = e^{-\tau A} \hat{X} e^{\tau A}, \tag{2.155}$$

where $\tilde{T}$ is the anti-chronological operator for $\tau$ variable.

Next we need the second-order expansion of the trace $Q$ in Eq. (2.146). We use the expansion formula $(1+x)^{-1} = 1 - x + x^2 + O(x^3)$ to obtain

$$\frac{1}{\mathrm{Tr} e^{-A+B}} = \frac{1}{\mathrm{Tr} e^{-A}} \left[1 - \langle \hat{\alpha}_1 \rangle_l - \langle \hat{\alpha}_2 \rangle_l + \langle \hat{\alpha}_1 \rangle_l^2\right], \tag{2.156}$$

where we used the notation (2.109). Substituting now Eqs. (2.153) and (2.156) into Eq. (2.146) and dropping again higher-order terms we obtain

$$\hat{\rho} = \hat{\rho}_l + \hat{\rho}_1 + \hat{\rho}_2, \tag{2.157}$$

with

$$\hat{\rho}_1 = \big(\hat{\alpha}_1 - \langle \hat{\alpha}_1 \rangle_l\big)\hat{\rho}_l, \qquad \hat{\rho}_2 = -\langle \hat{\alpha}_1 \rangle_l \hat{\rho}_1 + \big(\hat{\alpha}_2 - \langle \hat{\alpha}_2 \rangle_l\big)\hat{\rho}_l. \tag{2.158}$$

From Eqs. (2.154) and (2.158) we obtain

$$\hat{\rho}_1 = \int_0^1 d\tau \left(\hat{B}_\tau - \langle \hat{B}_\tau \rangle_l\right) \hat{\rho}_l, \tag{2.159}$$

$$\hat{\rho}_2 = \frac{1}{2}\int_0^1 d\tau \int_0^1 d\lambda \left(\tilde{T}\{\hat{B}_\lambda \hat{B}_\tau\} - \langle \tilde{T}\{\hat{B}_\lambda \hat{B}_\tau\}\rangle_l - \hat{B}_\tau \langle \hat{B}_\lambda\rangle_l - \hat{B}_\lambda \langle \hat{B}_\tau\rangle_l + 2\langle \hat{B}_\tau\rangle_l \langle \hat{B}_\lambda\rangle_l\right) \hat{\rho}_l. \tag{2.160}$$

Equation (2.159) coincides with the result given in Ref. [70].

In the last step we substitute the explicit expression for the operator $\hat{B}$ from Eq. (2.148), which gives for the first-order correction

$$\hat{\rho}_1(t) = \int d^4x_1 \int_0^1 d\tau \left[\hat{C}_\tau(x_1) - \langle \hat{C}_\tau(x_1)\rangle_l\right] \hat{\rho}_l, \tag{2.161}$$

and for the second-order correction

$$\begin{aligned}\hat{\rho}_2(t) = \frac{1}{2}\int d^4x_1 d^4x_2 \int_0^1 d\tau \int_0^1 d\lambda \Big[&\tilde{T}\{\hat{C}_\lambda(x_1)\hat{C}_\tau(x_2)\} - \langle \tilde{T}\{\hat{C}_\lambda(x_1)\hat{C}_\tau(x_2)\}\rangle_l \\ &- \langle \hat{C}_\lambda(x_1)\rangle_l \hat{C}_\tau(x_2) - \hat{C}_\lambda(x_1)\langle \hat{C}_\tau(x_2)\rangle_l + 2\langle \hat{C}_\lambda(x_1)\rangle_l \langle \hat{C}_\tau(x_2)\rangle_l\Big]\hat{\rho}_l,\end{aligned} \tag{2.162}$$

where we compressed the arguments $x \equiv (\boldsymbol{x}, t)$ and introduced the shorthand notation

$$\int d^4x_1 = \int d^3x_1 \int_{-\infty}^{t} dt_1 e^{\varepsilon(t_1 - t)}. \tag{2.163}$$

Now for the statistical average of an arbitrary operator $\hat{X}(x)$ we can write according to Eqs. (2.98), (2.157), (2.161) and (2.162)

$$\langle \hat{X}(x)\rangle = \langle \hat{X}(x)\rangle_l + \langle \hat{X}(x)\rangle_1' + \langle \hat{X}(x)\rangle_2', \tag{2.164}$$

with

$$\langle \hat{X}(x)\rangle_1' = \int d^4x_1 \Big(\hat{X}(x), \hat{C}(x_1)\Big), \tag{2.165}$$

where we defined a two-point correlation function via

$$\Big(\hat{X}(x), \hat{Y}(x_1)\Big) = \int_0^1 d\tau \langle \hat{X}(x) \left[\hat{Y}_\tau(x_1) - \langle \hat{Y}_\tau(x_1)\rangle_l\right]\rangle_l. \tag{2.166}$$

The second-order correction with respect to the operator $\hat{C}$ reads

$$\langle \hat{X}(x)\rangle_2' = \int d^4x_1 d^4x_2 \Big(\hat{X}(x), \hat{C}(x_1), \hat{C}(x_2)\Big), \tag{2.167}$$

where the three-point correlation function between three *arbitrary* operators $\hat{X}$, $\hat{Y}$ and $\hat{Z}$ is defined as

$$\begin{aligned}\Big(\hat{X}(x), \hat{Y}(x_1), \hat{Z}(x_2)\Big) \;=\; &\frac{1}{2}\int_0^1 d\tau \int_0^1 d\lambda \langle \tilde{T}\hat{X}(x)\Big[\hat{Y}_\lambda(x_1)\hat{Z}_\tau(x_2) - \langle \tilde{T}\hat{Y}_\lambda(x_1)\hat{Z}_\tau(x_2)\rangle_l \\ &- \langle \hat{Y}_\lambda(x_1)\rangle_l \hat{Z}_\tau(x_2) - \hat{Y}_\lambda(x_1)\langle \hat{Z}_\tau(x_2)\rangle_l + 2\langle \hat{Y}_\lambda(x_1)\rangle_l \langle \hat{Z}_\tau(x_2)\rangle_l\Big]\rangle_l.\end{aligned} \tag{2.168}$$

From Eq. (2.168) it is straightforward to find the symmetry relation

$$\int d^4x_1 d^4x_2 \Big(\hat{X}(x), \hat{Y}(x_1), \hat{Z}(x_2)\Big) = \int d^4x_1 d^4x_2 \Big(\hat{X}(x), \hat{Z}(x_1), \hat{Y}(x_2)\Big), \tag{2.169}$$

which we will utilize below.

The averages in Eqs. (2.165) and (2.167) are primed to stress that these are the first- and the second-order corrections only with respect to the operator $\hat{C}$. As we will show below in Sec. 2.5, there are second-order gradient terms arising from the two-point correlators (2.165) as well.

### 2.3.5 Operator decomposition of energy-momentum tensor and charge currents

To separate the dissipative processes related to the viscous and diffusion fluxes we need to decompose the energy-momentum tensor and the charge currents into their equilibrium and dissipative parts. The most general decompositions were already given by Eqs. (2.30) and (2.31), which we write now in an equivalent operator form

$$\hat{T}^{\mu\nu} = \hat{\epsilon} u^\mu u^\nu - \hat{p}\Delta^{\mu\nu} + \hat{Q}^\mu u^\nu + \hat{Q}^\nu u^\mu + \hat{\pi}^{\mu\nu}, \tag{2.170}$$

$$\hat{N}^\mu_a = \hat{n}_a u^\mu + \hat{J}^\mu_a, \tag{2.171}$$

where the dissipative operators $\hat{\pi}^{\mu\nu}$, $\hat{Q}^\mu$ and $\hat{J}^\mu_a$ are orthogonal to $u_\mu$, and $\hat{\pi}^{\mu\nu}$ is traceless:

$$u_\nu \hat{Q}^\nu = 0, \qquad u_\nu \hat{J}^\nu_a = 0, \qquad u_\nu \hat{\pi}^{\mu\nu} = 0; \qquad \hat{\pi}^\mu_\mu = 0. \tag{2.172}$$

Note that we did not separate here the equilibrium part of the pressure from the bulk viscous pressure as it was done in Eq. (2.30). The statistical average of the operator $\hat{p}$ gives the actual thermodynamic (non-equilibrium) pressure, which differs in general from the equilibrium pressure $p = p(\epsilon, n_a)$ introduced in Sec. 2.3.2. The latter is obtained from the operator $\hat{p}$ by averaging it over the local equilibrium distribution (evaluated formally at constant values of thermodynamic parameters). The bulk viscous pressure is defined as the difference of these two averages; see Sec. 2.4.2 for details.

The operators on the right-hand sides of Eqs. (2.170) and (2.171) are given by the relevant projections of $\hat{T}^{\mu\nu}$ and $\hat{N}^\mu_a$, by analogy with Eqs. (2.34) and (2.35)

$$\hat{\epsilon} = u_\mu u_\nu \hat{T}^{\mu\nu}, \qquad \hat{n}_a = u_\mu \hat{N}^\mu_a, \qquad \hat{p} = -\frac{1}{3}\Delta_{\mu\nu}\hat{T}^{\mu\nu}, \tag{2.173}$$

$$\hat{\pi}^{\mu\nu} = \Delta^{\mu\nu}_{\alpha\beta}\hat{T}^{\alpha\beta}, \qquad \hat{Q}^\mu = u_\alpha \Delta^\mu_\beta \hat{T}^{\alpha\beta}, \qquad \hat{J}^\nu_a = \Delta^\nu_\mu \hat{N}^\mu_a, \tag{2.174}$$

which in the local rest frame read [see Eqs. (2.36) and (2.37)]

$$\hat{\epsilon} = \hat{T}^{00}, \qquad \hat{n}_a = \hat{N}^0_a, \qquad \hat{p} = -\frac{1}{3}\hat{T}^k_k, \tag{2.175}$$

$$\hat{\pi}_{kl} = \left(\delta_{ki}\delta_{lj} - \frac{1}{3}\delta_{kl}\delta_{ij}\right)\hat{T}_{ij}, \qquad \hat{Q}^i = \hat{T}^{0i}, \qquad \hat{J}^i_a = \hat{N}^i_a. \tag{2.176}$$

The quantities on the left-hand sides of Eqs. (2.34)–(2.37) are obtained via statistical averaging of the corresponding operators on the left-hand sides of Eqs. (2.173)–(2.176). In this procedure one should take into account that the averages of the dissipative operators over the local equilibrium distribution vanish [67]:

$$\langle \hat{Q}^\mu \rangle_l = 0, \qquad \langle \hat{J}^\mu_a \rangle_l = 0, \qquad \langle \hat{\pi}^{\mu\nu} \rangle_l = 0. \tag{2.177}$$

Indeed, the relevant distribution given by Eqs. (2.115) and (2.116) depends only on the scalar operators $\hat{\epsilon}$ and $\hat{n}_a$, which are not correlated with vector and tensor quantities due to Curie's theorem [67, 68, 208, 209]. As a result, the averaging of Eqs. (2.95), (2.170) and (2.171) over the relevant distribution leads to the equations of ideal hydrodynamics (2.12). In order to include the dissipative phenomena, one needs to take into account the deviation of the statistical operator from its local equilibrium form.

## 2.4 The first-order transport equations

With the non-equiliblium statistical operator obtained in the previous section we are now in a position to derive the transport equations for dissipative quantities. In this section we will keep only the terms which are linear in thermodynamic forces and will derive Kubo formulas for the first-order transport coefficients.

### 2.4.1 Decomposing the thermodynamic force in different dissipative processes

For our further computations it is convenient to decompose the operator $\hat{C}$ given by Eq. (2.149) into different dissipative processes according to Eqs. (2.170) and (2.171). Similar decompositions were performed in Refs. [67, 68, 70]. Recalling the properties (2.7) and (2.172) we obtain

$$\hat{C} = \hat{\epsilon} D\beta - \hat{p}\beta\theta - \sum_a \hat{n}_a D\alpha_a + \hat{Q}_\sigma(\beta Du^\sigma + \partial^\sigma\beta) - \sum_a \hat{J}_a^\sigma \partial_\sigma \alpha_a + \beta\hat{\pi}_{\rho\sigma}\partial^\rho u^\sigma, \tag{2.178}$$

where we used the notations $D = u^\rho\partial_\rho$, $\theta = \partial_\rho u^\rho$ introduced in Sec. 2.2. The first three terms correspond to the scalar, the next two terms - to the vector and the last term - to the tensor dissipative processes. As a first approximation we can expell the terms $D\beta$, $D\alpha_a$ and $Du^\sigma$ using the equations of *ideal* hydrodynamics (2.12). Choosing $\epsilon$ and $n_a$ as independent thermodynamic variables and using the first two equations in (2.12) we can write

$$D\beta = \left(\frac{\partial\beta}{\partial\epsilon}\right)_{n_a} D\epsilon + \sum_a \left(\frac{\partial\beta}{\partial n_a}\right)_{\epsilon, n_b\neq n_a} Dn_a = -h\theta\left(\frac{\partial\beta}{\partial\epsilon}\right)_{n_a} - \sum_a n_a\theta\left(\frac{\partial\beta}{\partial n_a}\right)_{\epsilon, n_b\neq n_a}, \tag{2.179}$$

$$D\alpha_c = \left(\frac{\partial\alpha_c}{\partial\epsilon}\right)_{n_a} D\epsilon + \sum_a \left(\frac{\partial\alpha_c}{\partial n_a}\right)_{\epsilon, n_b\neq n_a} Dn_a = -h\theta\left(\frac{\partial\alpha_c}{\partial\epsilon}\right)_{n_a} - \sum_a n_a\theta\left(\frac{\partial\alpha_c}{\partial n_a}\right)_{\epsilon, n_b\neq n_a}. \tag{2.180}$$

Exploiting the first relation in Eq. (2.18) we obtain

$$\left(\frac{\partial\beta}{\partial n_a}\right)_{\epsilon, n_b\neq n_a} = -\left(\frac{\partial\alpha_a}{\partial\epsilon}\right)_{n_b}, \qquad \left(\frac{\partial\alpha_c}{\partial n_a}\right)_{\epsilon, n_b\neq n_a} = \left(\frac{\partial\alpha_a}{\partial n_c}\right)_{\epsilon, n_b\neq n_c}. \tag{2.181}$$

The second relation in Eq. (2.18) gives

$$h = -\beta\left(\frac{\partial p}{\partial\beta}\right)_{\alpha_a}, \qquad n_a = \beta\left(\frac{\partial p}{\partial\alpha_a}\right)_{\beta, \alpha_b\neq\alpha_a}. \tag{2.182}$$

Substituting Eqs. (2.181) and (2.182) into Eqs. (2.179) and (2.180) we obtain

$$D\beta = \beta\theta\left(\frac{\partial p}{\partial\beta}\right)_{\alpha_a}\left(\frac{\partial\beta}{\partial\epsilon}\right)_{n_a} + \sum_a \beta\theta\left(\frac{\partial p}{\partial\alpha_a}\right)_{\beta, \alpha_b\neq\alpha_a}\left(\frac{\partial\alpha_a}{\partial\epsilon}\right)_{n_b} = \beta\theta\gamma, \tag{2.183}$$

$$D\alpha_c = -\beta\theta\left(\frac{\partial p}{\partial\beta}\right)_{\alpha_a}\left(\frac{\partial\beta}{\partial n_c}\right)_{\epsilon, n_b\neq n_c} - \sum_a \beta\theta\left(\frac{\partial p}{\partial\alpha_a}\right)_{\beta, \alpha_b\neq\alpha_a}\left(\frac{\partial\alpha_a}{\partial n_c}\right)_{\epsilon, n_b\neq n_c} = -\beta\theta\delta_c, \tag{2.184}$$

where

$$\gamma = \left(\frac{\partial p}{\partial\epsilon}\right)_{n_a}, \qquad \delta_a = \left(\frac{\partial p}{\partial n_a}\right)_{\epsilon, n_b\neq n_a}. \tag{2.185}$$

Now the first three terms in Eq. (2.178) can be combined as follows

$$\hat{\epsilon} D\beta - \hat{p}\beta\theta - \sum_a \hat{n}_a D\alpha_a = -\beta\theta\hat{p}^*, \tag{2.186}$$

where

$$\hat{p}^* = \hat{p} - \gamma\hat{\epsilon} - \sum_a \delta_a \hat{n}_a. \tag{2.187}$$

Note that the coefficient $\gamma$ coincides with the square of the speed of sound $c_s$ in the case where conserved charges are absent. However, in a general case $\gamma \neq c_s^2$.

Using Eq. (2.62) and the conditions $\hat{Q}^\sigma \nabla_\sigma = \hat{Q}^\sigma \partial_\sigma$ and $\hat{J}_a^\sigma \nabla_\sigma = \hat{J}_a^\sigma \partial_\sigma$ following from Eq. (2.172), we modify the vector terms in Eq. (2.178) as follows

$$\hat{Q}^\sigma(\beta D u_\sigma + \partial_\sigma \beta) = \sum_a \frac{n_a}{h} \hat{Q}^\sigma \nabla_\sigma \alpha_a, \tag{2.188}$$

$$\hat{J}_a^\sigma \partial_\sigma \alpha_a = \hat{J}_a^\sigma \nabla_\sigma \alpha_a. \tag{2.189}$$

Finally, we can replace $\partial^\rho u^\sigma \to \sigma^{\rho\sigma} = \Delta_{\mu\nu}^{\rho\sigma} \partial^\mu u^\nu$ in the last term in Eq. (2.178) according to the symmetry properties of the shear stress tensor $\hat{\pi}_{\rho\sigma}$. Combining now Eqs. (2.178), (2.186), (2.188) and (2.189) we obtain the final form of the operator $\hat{C}$ at the first order in gradients

$$\hat{C} = -\beta\theta\hat{p}^* + \beta\hat{\pi}_{\rho\sigma}\sigma^{\rho\sigma} - \sum_a \hat{\mathcal{J}}_a^\sigma \nabla_\sigma \alpha_a, \tag{2.190}$$

where the operators

$$\hat{\mathcal{J}}_a^\sigma = \hat{J}_a^\sigma - \frac{n_a}{h}\hat{Q}^\sigma \tag{2.191}$$

correspond to the diffusion currents defined in Eq. (2.44).

We see from Eq. (2.190), that the operator $\hat{C}$ depends linearly on the thermodynamic forces $\theta$, $\sigma^{\rho\sigma}$ and $\nabla_\sigma \alpha_a$, which are identical to those obtained in Sec. 2.2.6 and which correspond to the bulk viscous, the shear viscous and the flavor diffusion effects, respectively. We will show below how to obtain the linear NS relations between these thermodynamic forces and the dissipative fluxes.

### 2.4.2 Computing the dissipative quantities

In this subsection we are going to compute the thermodynamic averages of the dissipative operators over the first-order non-equilibrium statistical operator using Eqs. (2.165) and (2.190). Taking into account Curie's theorem, which states that in isotropic medium the correlations between operators of different rank vanish [208, 209], for the shear stress tensor we obtain

$$\langle \hat{\pi}_{\mu\nu}(x) \rangle_1 = \int d^4x_1 \Big( \hat{\pi}_{\mu\nu}(x), \hat{\pi}_{\rho\sigma}(x_1) \Big) \beta(x_1) \sigma^{\rho\sigma}(x_1). \tag{2.192}$$

To proceed further we note that the integrand in Eq. (2.192) is maily concentrated in the range $|x_1 - x| \lesssim l$, where $l$ is the mean correlation length, which is the characteristic *microscopic* length scale of interactions (the analogue of the quasiparticle mean free path for strongly interacting systems). The hydrodynamic regime implies that the changes of thermodynamic parameters are sufficiently small over these microscopic length scales. As a result, the thermodynamic forces in the integrand of Eq. (2.192) in the first approximation can be factored out from the integral with their values at $x$ [67, 68, 70]. This leads as to a *local* relation between the shear stress tensor and the velocity gradients

$$\langle \hat{\pi}_{\mu\nu}(x) \rangle_1 = \beta\sigma^{\rho\sigma} \int d^4x_1 \Big( \hat{\pi}_{\mu\nu}(x), \hat{\pi}_{\rho\sigma}(x_1) \Big). \tag{2.193}$$

Because $|\sigma^{\rho\sigma}| \simeq |u^\rho|/L$, where $L$ is the typical *macroscopic* length scale of the system, this approximation corrensponds actually to the first-order expansion of the shear stress tensor in the powers of

the Knudsen number $K \equiv l/L$. However, as we will show in the next section, the non-locality of the thermodynamic forces is crucial for derivation of causal transport equations [64, 178, 200, 201].

Now we compute the bulk viscous pressure. By definition, this measures the deviation of the actual thermodynamic pressure from its equilibrium value as a result of the fluid expansion or compression. Therefore, it might seem that the bulk viscous pressure $\Pi$ should be identified with the quantity $\langle\hat{p}\rangle - \langle\hat{p}\rangle_l = \langle\hat{p}\rangle_1$. However, it is easy to see that such a definition for $\Pi$ would be erroneous.

In order to understand the problem we go back to the matching conditions (2.107) and (2.108), which define the local equilibrium state. As it was explained in Sec. 2.3.1, these conditions are satisfied (at a fixed point $x$) only if the relevant distribution function is evaluated formaly at *uniform* thermodynamic parameters, *i.e.*, as if the latters were constant in space and time with the given values $\beta(x)$ and $\mu_a(x)$. Because the relevant distribution (2.104) is actually a functional of *non-uniform* thermodynamic parameters, the average values $\langle\hat{\epsilon}\rangle_l$ and $\langle\hat{n}_a\rangle_l$ in the full computation are shifted from the actual values of $\epsilon$ and $n_a$ by additional gradient terms $\langle\hat{\epsilon}\rangle_1 \equiv \Delta\epsilon$ and $\langle\hat{n}_a\rangle_1 \equiv \Delta n_a$, which were neglected in Eqs. (2.107) and (2.108). These shifts bring in their turn an additional shift in the equilibrium part of the pressure $\langle\hat{p}\rangle_l$, which should not be included in the bulk viscous pressure [210, 211]. Thus, the bulk viscous pressure should be defined as the difference between the actual non-equilibrium pressure $\langle\hat{p}\rangle$ and the equilibrium pressure $p(\epsilon, n_a)$, which is not equal to $\langle\hat{p}\rangle_l$:

$$\Pi \equiv \langle\hat{p}\rangle - p(\epsilon, n_a) = \langle\hat{p}\rangle_l + \langle\hat{p}\rangle_1 - p(\epsilon, n_a). \tag{2.194}$$

At the first order in gradients we have

$$\langle\hat{p}\rangle_l = p(\langle\hat{\epsilon}\rangle_l, \langle\hat{n}_a\rangle_l) = p(\epsilon - \Delta\epsilon, n_a - \Delta n_a) = p(\epsilon, n_a) - \gamma\Delta\epsilon - \sum_a \delta_a \Delta n_a, \tag{2.195}$$

where the coefficients $\gamma$, $\delta_a$ are defined in Eq. (2.185). Then we find for the bulk viscous pressure

$$\Pi = \langle\hat{p} - \gamma\hat{\epsilon} - \sum_a \delta_a \hat{n}_a\rangle_1 = \langle\hat{p}^*\rangle_1, \tag{2.196}$$

where we used the definition of $\hat{p}^*$ given by Eq. (2.187). Now from Eqs. (2.165) and (2.190) we obtain

$$\Pi = \langle\hat{p}^*(x)\rangle_1 = -\beta\theta \int d^4x_1 \Big(\hat{p}^*(x), \hat{p}^*(x_1)\Big). \tag{2.197}$$

Thus, the bulk viscous pressure is expressed automatically by a symmetric correlator.

Next we average the charge diffusion currents

$$\langle\hat{\mathcal{J}}_a^\mu(x)\rangle_1 = -\sum_b \nabla_\sigma \alpha_b \int d^4 \left(\hat{\mathcal{J}}_a^\mu(x), \hat{\mathcal{J}}_b^\sigma(x_1)\right), \tag{2.198}$$

which are expressed through symmetric correlators as well.

Equations (2.193), (2.197) and (2.198) establish the required linear relations between the dissipative fluxes and the thermodynamic forces.

### 2.4.3 Transport coefficients for isotropic medium

The isotropy of the medium together with the conditions (2.172) further implies [68]

$$\Big(\hat{\mathcal{J}}_a^\mu(x), \hat{\mathcal{J}}_b^\nu(x_1)\Big) = \frac{1}{3}\Delta^{\mu\nu}\Big(\hat{\mathcal{J}}_a^\lambda(x), \hat{\mathcal{J}}_{b\lambda}(x_1)\Big), \tag{2.199}$$

$$\Big(\hat{\pi}_{\mu\nu}(x,t), \hat{\pi}_{\rho\sigma}(x_1)\Big) = \frac{1}{5}\Delta_{\mu\nu\rho\sigma}\Big(\hat{\pi}^{\lambda\eta}(x), \hat{\pi}_{\lambda\eta}(x_1)\Big), \tag{2.200}$$

where all projectors are taken at the point $x$. Defining the shear and the bulk viscosities as

$$\eta = \frac{\beta}{10}\int d^4x_1\Big(\hat{\pi}_{\mu\nu}(x),\hat{\pi}^{\mu\nu}(x_1)\Big), \tag{2.201}$$

$$\zeta = \beta\int d^4x_1\Big(\hat{p}^*(x),\hat{p}^*(x_1)\Big), \tag{2.202}$$

we obtain from Eqs. (2.193), (2.197) and (2.200)

$$\pi_{\mu\nu} = 2\eta\sigma_{\mu\nu}, \qquad \Pi = -\zeta\theta. \tag{2.203}$$

The definitions (2.201) and (2.202) imply that the shear and the bulk viscosities are positive quantities, as expected. The two-point correlators in these equations can be evaluated already at constant values of thermodynamic parameters, *i.e.*, as if the system were in *full thermal equilibrium*.

Next using Eqs. (2.198) and (2.199) we obtain for the diffusion currents

$$\mathscr{J}_a^\mu = \sum_b \chi_{ab}\nabla^\mu\alpha_b, \tag{2.204}$$

where we defined the matrix of diffusion coefficients via

$$\chi_{ab} = -\frac{1}{3}\int d^4x_1\left(\hat{\mathcal{J}}_a^\lambda(x),\hat{\mathcal{J}}_{b\lambda}(x_1)\right), \tag{2.205}$$

which is positive-semidefinite in the flavor space due to the fact that all diffusion fluxes are spatial.

In the case of one sort of conserved charge we can define the operator of the heat flux via

$$\hat{H}^\mu = \hat{Q}^\mu - \frac{h}{n}\hat{\jmath}^\mu = -\frac{h}{n}\hat{\mathcal{J}}^\mu. \tag{2.206}$$

Then for the heat flux defined in Eq. (2.51) we obtain

$$h^\mu = -\kappa\frac{nT^2}{h}\nabla^\mu\alpha, \tag{2.207}$$

where the thermal conductivity is defined as

$$\kappa = -\frac{\beta^2}{3}\int d^4x_1\left(\hat{H}^\lambda(x),\hat{H}_\lambda(x_1)\right). \tag{2.208}$$

We see that Eqs. (2.203), (2.204) and (2.207) are fully consistent with their phenomenological counterparts given by Eqs. (2.64) and (2.68). We thus conclude, that the non-equilibrium statistical operator correctly reproduces the NS limit of relativistic dissipative hydrodynamics.

As shown in Appendix A.1, the transport coefficients defined in Eqs. (2.201), (2.202), (2.205) and (2.208) can be expressed via two-point redarded Green's functions as follows

$$\eta = -\frac{1}{10}\frac{d}{d\omega}\mathrm{Im}G^R_{\hat{\pi}_{\mu\nu}\hat{\pi}^{\mu\nu}}(\omega)\Big|_{\omega=0}, \qquad \zeta = -\frac{d}{d\omega}\mathrm{Im}G^R_{\hat{p}^*\hat{p}^*}(\omega)\Big|_{\omega=0}, \tag{2.209}$$

$$\chi_{ab} = \frac{T}{3}\frac{d}{d\omega}\mathrm{Im}G^R_{\hat{\mathcal{J}}_a^\lambda\hat{\mathcal{J}}_{b\lambda}}(\omega)\Big|_{\omega=0}, \qquad \kappa = \frac{1}{3T}\frac{d}{d\omega}\mathrm{Im}G^R_{\hat{H}^\lambda\hat{H}_\lambda}(\omega)\Big|_{\omega=0}, \tag{2.210}$$

where

$$G^R_{\hat{X}\hat{Y}}(\omega) = -i\int_0^\infty dt e^{i\omega t}\int d^3x\langle\big[\hat{X}(\boldsymbol{x},t),\hat{Y}(\mathbf{0},0)\big]\rangle_l \tag{2.211}$$

is the Fourier-transform of the two-point retarded correlator taken in the zero-wavenumber limit,

and the square brackets denote the commutator. Relations (2.209) and (2.210) are known as Kubo formulas [58, 59, 68–70].

### 2.4.4 The entropy generation rate

It is interesting to compute also the entropy production rate using the formalism of the non-equilibrium statistical operator. From Eq. (2.117) we can write

$$\frac{d}{dt}\hat{S}(t) = -\frac{d}{dt}\Omega_l(t) + \int d^3x \frac{d}{dt}\Big[\beta^\nu(\boldsymbol{x},t)\hat{T}_{0\nu}(\boldsymbol{x},t) - \sum_a \alpha_a(\boldsymbol{x},t)\hat{N}^0_a(\boldsymbol{x},t)\Big]. \tag{2.212}$$

The first term can be computed from Eq. (2.105)

$$\frac{d}{dt}\Omega_l(t) = \int d^3x \Big\langle \frac{d}{dt}\Big[\beta^\nu(\boldsymbol{x},t)\hat{T}_{0\nu}(\boldsymbol{x},t) - \sum_a \alpha_a(\boldsymbol{x},t)\hat{N}^0_a(\boldsymbol{x},t)\Big]\Big\rangle_l, \tag{2.213}$$

where we used also Eqs. (2.104) and (2.109). The time-derivative of the integrand in Eqs. (2.212) and (2.213) was already computed in Eq. (2.144), where the surface term can be dropped. Recalling the definition of the thermodynamic force given by Eq. (2.149) we obtain for Eq. (2.212)

$$\frac{d}{dt}\hat{S}(t) = \int d^3x \big[\hat{C}(\boldsymbol{x},t) - \langle \hat{C}(\boldsymbol{x},t)\rangle_l\big]. \tag{2.214}$$

Upon using Eqs. (2.164), (2.165) and (2.167), we can write Eq. (2.214) in the flollowing form

$$\frac{d}{dt}\hat{S}(t) = \int d^3x d^4x_1 \Big(\hat{C}(x), \hat{C}(x_1)\Big) + \int d^3x d^4x_1 d^4x_2 \Big(\hat{C}(x), \hat{C}(x_1), \hat{C}(x_2)\Big) + \ldots, \tag{2.215}$$

where the dots stand for higher-order terms.

Thus, the entropy generation rate can be computed in principle at *any order* by means of *equilibrium* correlators between several opeators $\hat{C}(x)$. We see from Eq. (2.214) that the source of the irreversible entropy production is given by the deviation of the operator $\hat{C}$ from its local equilibrium average. The physical meaning of this result is intuitively clear: entropy can be produced only if the system deviates from its local thermal equilibrium.

In the first-order approximation we can substitute the expression (2.190) into Eq. (2.214)

$$\begin{aligned}\frac{d}{dt}S(t) &= \int d^3x \langle -\beta\theta\hat{p}^* + \beta\hat{\pi}_{\rho\sigma}\sigma^{\rho\sigma} - \sum_a \hat{\mathcal{J}}^\sigma_a \nabla_\sigma \alpha_a\rangle_1 \\ &= \int d^3x \Big( - \beta\theta\Pi + \beta\pi_{\rho\sigma}\sigma^{\rho\sigma} - \sum_a \mathscr{J}^\sigma_a \nabla_\sigma\alpha_a\Big),\end{aligned} \tag{2.216}$$

which is consistent with Eq. (2.63), where $R = T\partial_\mu S^\mu$. Indeed, multiplying Eq. (2.63) by $\beta$ and integrating over the 3-volume we obtain

$$\int d^3x \beta R = \int d^3x \left(\partial_0 S^0 + \partial_i S^i\right) = \frac{d}{dt}\int d^3x S^0(\boldsymbol{x},t) = \frac{d}{dt}S(t), \tag{2.217}$$

where we dropped the surface term.

Substituting the transport equations (2.203) and (2.204) in Eq. (2.216) we obtain

$$\frac{d}{dt}S(t) = \int d^3x \Big(\zeta\beta\theta^2 + 2\eta\beta\sigma_{\mu\nu}\sigma^{\mu\nu} - \sum_{ab}\chi_{ab}\nabla_\mu\alpha_a\nabla^\mu\alpha_b\Big), \tag{2.218}$$

in agreement with the phenomenological expression (2.65).

## 2.5 The second-order transport equations

In this section we compute systematically all second-order corrections to the dissipative fluxes. These fluxes along with the thermodynamic forces are regarded as *first-order* quantities in deviations from equilibrium. The second-order terms are those, which involve either space-time derivatives or products of the first-order terms. It is easy to see that second-order contributions arise not only from the three-point correlators (2.167) which are quadratic in the operator $\hat{C}$, but also from the two-point correlators (2.165), where one should take into account the second-order corrections to the operator $\hat{C}$ which were neglected while deriving Eq. (2.190). Apart from that, additional second-order gradient terms arise from the non-locality of the thermodynamic forces in Eq. (2.165), *i.e.*, when the difference between the space-time arguments $x$ and $x_1$ respectively in the dissipative fluxes and the thermodynamic forces is taken into account. As we will show below in Secs. 2.5.3–2.5.5, these non-local effects generate relaxation terms in the transport equations which are required for the causality.

### 2.5.1 Decomposing the thermodynamic force up to the second order

In this subsection we repeat the decomposition of the operator $\hat{C}$ keeping all second-order corrections that were neglected in Sec. 2.4.1. Our starting point is Eq. (2.178), which we write now in the following form

$$\hat{C} = \hat{\epsilon} D\beta - \hat{p}\beta\theta - \sum_a \hat{n}_a D\alpha_a + \hat{Q}_\sigma(\beta Du^\sigma + \nabla^\sigma\beta) - \sum_a \hat{J}^\sigma_a \nabla_\sigma \alpha_a + \beta\hat{\pi}_{\rho\sigma}\sigma^{\rho\sigma}. \tag{2.219}$$

We use now the equations of *dissipative* hydrodynamics (2.54)–(2.56) to eliminate the terms $D\beta$, $D\alpha_a$ and $Du^\sigma$ in Eq. (2.219). Intsead of Eqs. (2.179), (2.180), (2.183) and (2.184) we now have

$$D\beta = \beta\theta\gamma - (\Pi\theta + \partial_\mu q^\mu - q^\mu Du_\mu - \pi^{\mu\nu}\sigma_{\mu\nu})\left(\frac{\partial\beta}{\partial\epsilon}\right)_{n_a} - \sum_a \partial_\mu j^\mu_a \left(\frac{\partial\beta}{\partial n_a}\right)_{\epsilon, n_b\neq n_a}, \tag{2.220}$$

$$D\alpha_c = -\beta\theta\delta_c - (\Pi\theta + \partial_\mu q^\mu - q^\mu Du_\mu - \pi^{\mu\nu}\sigma_{\mu\nu})\left(\frac{\partial\alpha_c}{\partial\epsilon}\right)_{n_a} - \sum_a \partial_\mu j^\mu_a \left(\frac{\partial\alpha_c}{\partial n_a}\right)_{\epsilon, n_b\neq n_a}. \tag{2.221}$$

Now the first three terms in Eq. (2.219) can be combined as follows

$$\hat{\epsilon} D\beta - \hat{p}\beta\theta - \hat{n}_a D\alpha_a = -\beta\theta\hat{p}^* - \hat{\beta}^*(\Pi\theta + \partial_\mu q^\mu - q^\mu Du_\mu - \pi^{\mu\nu}\sigma_{\mu\nu}) + \sum_a \hat{\alpha}^*_a \partial_\mu j^\mu_a, \tag{2.222}$$

where we used Eqs. (2.181) and (2.187) and defined new operators

$$\hat{\beta}^* = \hat{\epsilon}\left(\frac{\partial\beta}{\partial\epsilon}\right)_{n_a} + \sum_a \hat{n}_a \left(\frac{\partial\beta}{\partial n_a}\right)_{\epsilon, n_b\neq n_a}, \tag{2.223}$$

$$\hat{\alpha}^*_a = \hat{\epsilon}\left(\frac{\partial\alpha_a}{\partial\epsilon}\right)_{n_b} + \sum_c \hat{n}_c \left(\frac{\partial\alpha_a}{\partial n_c}\right)_{\epsilon, n_b\neq n_c}. \tag{2.224}$$

Next we use Eq. (2.80) to modify the vector term involving $\hat{Q}_\sigma$ in Eq. (2.219)

$$\hat{Q}^\sigma(\beta Du_\sigma + \nabla_\sigma\beta) = \sum_a \frac{n_a}{h}\hat{Q}^\sigma\nabla_\sigma\alpha_a - \hat{Q}^\sigma\beta h^{-1}\times$$
$$(-\nabla_\sigma\Pi + \Pi Du_\sigma + Dq_\sigma + q^\mu\partial_\mu u_\sigma + q_\sigma\theta + \partial_\mu\pi^\mu_\sigma). \tag{2.225}$$

Combining Eqs. (2.219), (2.222) and (2.225) we obtain

$$\hat{C}(x) = \hat{C}_1(x) + \hat{C}_2(x), \tag{2.226}$$

where $\hat{C}_1$ and $\hat{C}_2$ are the first- and the second-order contributions, respectively:

$$\hat{C}_1(x) = -\beta\theta\hat{p}^* + \beta\hat{\pi}_{\rho\sigma}\sigma^{\rho\sigma} - \sum_a \hat{\mathcal{J}}_a^\sigma \nabla_\sigma \alpha_a, \tag{2.227}$$

$$\begin{aligned}\hat{C}_2(x) &= -\hat{\beta}^*(\Pi\theta + \partial_\mu q^\mu - q^\mu Du_\mu - \pi^{\mu\nu}\sigma_{\mu\nu}) + \sum_a \hat{\alpha}_a^*(\partial_\mu j_a^\mu) \\ &- \hat{Q}^\sigma \beta h^{-1}(-\nabla_\sigma\Pi + \Pi Du_\sigma + Dq_\sigma + q^\mu\partial_\mu u_\sigma + q_\sigma\theta + \partial_\mu\pi_\sigma^\mu).\end{aligned} \tag{2.228}$$

We observe that the operator $\hat{C}_2$ contains only scalar and vector terms, and, therefore, contributes only to the bulk viscous pressure and the diffusion currents. The reason for such structure of $\hat{C}_2$ is that this operator comes from the non-ideality of the hydrodynamics equations (2.54)–(2.56), which have either scalar or vector structure. The expressions contained in the brackets in Eq. (2.228) are natural to call *generalized or extended termodynamic forces*. They involve either space-time derivatives of the dissipative currents, or their products with the "ordinary" thermodynamic forces. (Note that this was the case also in the IS theory.) However, these generalized thermodynamic forces lack the covariant time-derivatives (2.85) of the dissipative currents $\Pi$, $\pi^{\mu\nu}$ and $\mathscr{J}_a^\mu$, which should be present in a causal theory. As we will show below, these terms arise from the *non-locality* of the thermodynamic forces involved in Eq. (2.227). [Note that we have a similar term in Eq. (2.228) only for the energy flow, *i.e.*, $Dq^\mu$. This term, however, is absent in the L-frame. Therefore, we have actually only space-like gradients of the dissipative fluxes in Eq. (2.228).]

Now using Eqs. (2.164), (2.165) and (2.167), for the statistical average of an *arbitrary operator* $\hat{X}(x)$ up to the second order we can write

$$\langle\hat{X}(x)\rangle = \langle\hat{X}(x)\rangle_l + \langle\hat{X}(x)\rangle_1 + \langle\hat{X}(x)\rangle_2. \tag{2.229}$$

The first-order correction is given by

$$\langle\hat{X}(x)\rangle_1 = \int d^4x_1 \Big(\hat{X}(x), \hat{C}_1(x_1)\Big)\Big|_{loc}, \tag{2.230}$$

where the intex *loc* indicates that the thermodynamic parameters in the integrand are approximated by their local values at the point $x$, *i.e.*, the non-local effects are neglected, as explained in Sec. 2.4.2.

The second-order correction $\langle\hat{X}(x)\rangle_2$ can be splitted into three terms

$$\langle\hat{X}(x)\rangle_2 = \langle\hat{X}(x)\rangle_2^1 + \langle\hat{X}(x)\rangle_2^2 + \langle\hat{X}(x)\rangle_2^3, \tag{2.231}$$

with

$$\langle\hat{X}(x)\rangle_2^1 = \int d^4x_1 \Big(\hat{X}(x), \hat{C}_1(x_1)\Big) - \langle\hat{X}(x)\rangle_1, \tag{2.232}$$

$$\langle\hat{X}(x)\rangle_2^2 = \int d^4x_1 \Big(\hat{X}(x), \hat{C}_2(x_1)\Big), \tag{2.233}$$

$$\langle\hat{X}(x)\rangle_2^3 = \int d^4x_1 d^4x_2 \Big(\hat{X}(x), \hat{C}_1(x_1), \hat{C}_1(x_2)\Big). \tag{2.234}$$

The first term in Eq. (2.231) collects those corrections which arise from the non-locality of the thermodynamic parameters involved in the operator $\hat{C}(x_1)$. These corrections are of the second order, because they involve the differences of a thermodynamic force, *e.g.*, $\sigma^{\mu\nu}$, at the points $x_1$ and $x$, as seen from Eqs. (2.227), (2.230) and (2.232). Therefore, we can approximate $\sigma^{\mu\nu}(x_1) - \sigma^{\mu\nu}(x) \simeq \partial_\alpha\sigma^{\mu\nu}(x)(x_1 - x)^\alpha \sim K\sigma^{\mu\nu}(x)$, because $x_1 - x \sim l$ and $\partial \sim L^{-1}$, as mentioned in Sec. 2.4.2. Thus, the corrections of the type (2.232) contain an additional power of the Knudsen number $K$ as compared to the first-order expression (2.230), and, therefore, are at least of the second order in the hydrodynamic expansion.

The second term in Eq. (2.231) includes the corrections from the generalized thermodynamic forces. Finally, the third term stands for the corrections which are nonlinear (quadratic) in the three thermodynamic forces $\theta$, $\sigma_{\rho\sigma}$ and $\nabla_\sigma \alpha_a$ which appear in the NS limit.

In order to derive properly the non-local corrections (2.230) to the dissipative fluxes, we should first generalize the expressions for the two-point correlators given by Eqs. (2.199) and (2.200), which were written initially to provide only the first-order accuracy.

### 2.5.2 Non-local generalization of two-point correlators

The two-point correlators (2.199) and (2.200) can be generalized in a straightforward manner to incorporate the non-locality of the spatial projectors

$$\Big(\hat{\mathcal{J}}_a^\mu(x), \hat{\mathcal{J}}_b^\nu(x_1)\Big) = \frac{1}{3}\Delta^{\mu\nu}(x,x_1)\Big(\hat{\mathcal{J}}_a^\lambda(x), \hat{\mathcal{J}}_{b\lambda}(x_1)\Big), \tag{2.235}$$

$$\Big(\hat{\pi}_{\mu\nu}(x), \hat{\pi}_{\rho\sigma}(x_1)\Big) = \frac{1}{5}\Delta_{\mu\nu\rho\sigma}(x,x_1)\Big(\hat{\pi}^{\lambda\eta}(x), \hat{\pi}_{\lambda\eta}(x_1)\Big). \tag{2.236}$$

Here the new projectors

$$\Delta_{\mu\nu}(x,x_1) = \Delta_{\mu\lambda}(x)\Delta^\lambda_\nu(x_1), \tag{2.237}$$

$$\Delta_{\mu\nu\rho\sigma}(x,x_1) = \Delta_{\mu\nu\alpha\beta}(x)\Delta^{\alpha\beta}_{\rho\sigma}(x_1) \tag{2.238}$$

are the natural non-local generalizations of the second and forth-rank projectors $\Delta_{\mu\nu}(x)$ and $\Delta_{\mu\nu\rho\sigma}(x)$ defined after Eq. (2.6) and in Eqs. (2.26), respectively.

The normalization of the right-hand sides of Eqs. (2.235) and (2.236) is performed at the leading order in velocity gradients, see Appendix A.2 for details. The non-local form of the projectors (2.237) and (2.238) guarantees that the orthogonality conditions (2.172) are satisfied for the correlation functions given by Eqs. (2.235) and (2.236) in both points $x$ and $x_1$.

For our calculations it is enough to keep only the linear terms in the difference $x_1 - x$ of the expansion of the non-local projectors around $x_1 = x$. As shown in Appendix A.2, the first derivative of the forth-rank projector is

$$\frac{\partial}{\partial x_1^\alpha}\Delta_{\mu\nu\rho\sigma}(x,x_1)\Big|_{x_1=x} = -(\Delta_{\mu\nu\rho\beta}u_\sigma + \Delta_{\mu\nu\sigma\beta}u_\rho)\partial_\alpha u^\beta, \tag{2.239}$$

which we will utilize below. In addition, we will assume that Curie's theorem holds also in this approximation, *i.e.*, the two-point correlations between tensors of different rank vanish.

### 2.5.3 Second-order corrections to the shear stress tensor

According to Eq. (2.231)–(2.234), the second-order corrections to the dissipative fluxes arise from three different sources. In this and the following two subsections we compute all these corrections separately for the shear stress tensor, the bulk viscous pressure and the diffusion currents.

#### Non-local corrections from the two-point correlation function

Substituting the decomposition (2.227) into Eq. (2.232) and recalling Curie's theorem we obtain

$$\langle\hat{\pi}_{\mu\nu}(x)\rangle_2^1 = \int d^4x_1\Big(\hat{\pi}_{\mu\nu}(x), \hat{\pi}_{\rho\sigma}(x_1)\Big)(\beta\sigma^{\rho\sigma})_{x_1} - 2\eta\sigma_{\mu\nu}, \tag{2.240}$$

where we used the first-order relation $\langle\hat{\pi}_{\mu\nu}(x)\rangle_1 = 2\eta(x)\sigma_{\mu\nu}(x)$ given by Eq. (2.203). The index $x_1$ in the integrand of Eq. (2.240) labels the space-time argument of the thermodynamic force $\beta\sigma^{\rho\sigma}$, which now cannot be factored out from the integral with its value at $x$, but should be expanded around that

value at the first order with respect to the difference $x_1 - x$. Here we note, that in order to obtain all second-order corrections which have non-local origin, we should take into account also the non-locality of the fluid velocity $u^\lambda$ in the expression $\hat{\pi}^{\lambda\eta}(x_1) = \Delta^{\lambda\eta}_{\gamma\delta}(x_1)\hat{T}^{\gamma\delta}(x_1)$ [see Eq. (2.174)]. In contrast to $\Delta^{\lambda\eta}_{\gamma\delta}(x_1)$, which is a hydrodynamic quantity, the energy-momentum tensor $\hat{T}^{\gamma\delta}(x_1)$ is a microscopic quantity, and, therefore, does not require hydrodynamic expansion.

Now we substitute the two-point correlation function given by Eqs. (2.236) and (2.238) into Eq. (2.240) and use the definition of the shear stress tensor given in Eq. (2.174)

$$\begin{aligned}\langle\hat{\pi}_{\mu\nu}(x)\rangle^1_2 &= \frac{1}{5}\Delta_{\mu\nu\rho\sigma}(x)\int d^4x_1\Big(\hat{\pi}^{\lambda\eta}(x),\hat{\pi}_{\lambda\eta}(x_1)\Big)(\beta\sigma^{\rho\sigma})_{x_1} - 2\eta\sigma_{\mu\nu}\\ &= \frac{1}{5}\Delta_{\mu\nu\rho\sigma}(x)\int d^4x_1\Big(\hat{T}^{\alpha\beta}(x),\hat{T}^{\gamma\delta}(x_1)\Big)\Delta_{\alpha\beta\gamma\delta}(x,x_1)(\beta\sigma^{\rho\sigma})_{x_1} - 2\eta\sigma_{\mu\nu}.\end{aligned} \tag{2.241}$$

In the following step we expand $\Delta_{\alpha\beta\gamma\delta}(x,x_1)(\beta\sigma^{\rho\sigma})_{x_1}$ into series with respect to $x_1$ around $x$ keeping only the linear terms in the difference $x_1 - x$. The zeroth-order term in this expansion is exactly the viscosity term $2\eta\sigma_{\mu\nu}$. Using Eq. (2.239) we obtain

$$\begin{aligned}\langle\hat{\pi}_{\mu\nu}(x)\rangle^1_2 &= \frac{1}{5}\Delta_{\mu\nu\rho\sigma}(x)\int d^4x_1\Big(\hat{T}^{\alpha\beta}(x),\hat{T}^{\gamma\delta}(x_1)\Big)\Big\{(\beta\sigma^{\rho\sigma}\Delta_{\alpha\beta\gamma\delta})_x + (x_1-x)^\tau\\ &\quad\times\Big[\Delta_{\alpha\beta\gamma\delta}\partial_\tau(\beta\sigma^{\rho\sigma}) - \beta\sigma^{\rho\sigma}(\Delta_{\alpha\beta\gamma\lambda}u_\delta + \Delta_{\alpha\beta\delta\lambda}u_\gamma)\partial_\tau u^\lambda\Big]_x\Big\} - 2\eta\sigma_{\mu\nu}\\ &= 2a^\tau\beta^{-1}\Delta_{\mu\nu\rho\sigma}\partial_\tau(\beta\sigma^{\rho\sigma}) - 4b^\tau_\lambda\sigma_{\mu\nu}\partial_\tau u^\lambda,\end{aligned} \tag{2.242}$$

where we used the identity $\Delta_{\mu\nu\rho\sigma}\sigma^{\rho\sigma} = \sigma_{\mu\nu}$ and defined

$$a^\tau = \Delta_{\alpha\beta\gamma\delta}I^{\alpha\beta\gamma\delta,\tau}, \qquad b^\tau_\lambda = \Delta_{\alpha\beta\gamma\lambda}u_\delta I^{\alpha\beta\gamma\delta,\tau}, \tag{2.243}$$

with

$$I^{\alpha\beta\gamma\delta,\tau}(x) = \frac{\beta}{10}\int d^4x_1\Big(\hat{T}^{\alpha\beta}(x),\hat{T}^{\gamma\delta}(x_1)\Big)(x_1-x)^\tau. \tag{2.244}$$

The local value of the shear viscosity according to Eq. (2.242) is defined as

$$\eta(x) = \frac{\beta(x)}{10}\Delta_{\alpha\beta\gamma\delta}(x)\int d^4x_1\Big(\hat{T}^{\alpha\beta}(x),\hat{T}^{\gamma\delta}(x_1)\Big) = \frac{\beta(x)}{10}\int d^4x_1\Big(\hat{\pi}_{ij}(x),\hat{\pi}^{ij}(x_1)\Big), \tag{2.245}$$

where the second relation is written in the fluid rest frame. Indeed, in that frame

$$\Delta_{\alpha\beta\gamma\delta}(x) \to \Delta_{ijkl} = \frac{\delta_{ik}\delta_{jl}+\delta_{il}\delta_{jk}}{2} - \frac{1}{3}\delta_{ij}\delta_{kl}, \tag{2.246}$$

which is independent of $x$, and, therefore, it projects both operators of the energy-momentum tensor in Eq. (2.245) on $\pi_{ij}$; see also Eq. (2.176). The correlators in Eqs. (2.244) and (2.245) are evaluated then in *full thermal equilibrium* with corresponding local values of the thermodynamic parameters. As a result, the shear viscosity defined in Eq. (2.245) is a *local* function of the temperature and the chemical potentials.

Recalling the relations (2.173) and (2.174) we can write the expressions (2.243) and (2.244) in the following form

$$a^\tau = \frac{\beta}{10}\int d^4x_1\Big(\hat{\pi}_{\alpha\beta}(x),\hat{\pi}^{\alpha\beta}(x_1)\Big)(x_1-x)^\tau, \tag{2.247}$$

$$b^\tau_\lambda = \frac{\beta}{10}\int d^4x_1\Big(\hat{\pi}_{\alpha\lambda}(x),\hat{Q}^{\alpha}(x_1)\Big)(x_1-x)^\tau = 0, \tag{2.248}$$

where we approximated $u^\mu(x) \simeq u^\mu(x_1)$, because the quantities (2.247) and (2.248) are multiplied with second-order terms in Eq. (2.242). The tensor $b^\tau_\lambda$ vanishes due to Curie's theorem, and the vector $a^\tau$ can be written in the following form [see Appendix A.1, Eqs. (A.28)–(A.31)]

$$a^\tau = -\eta\tau_\pi u^\tau, \tag{2.249}$$

where we defined

$$\eta\tau_\pi = -i\frac{d}{d\omega}\eta(\omega)\Big|_{\omega=0} = \frac{1}{10}\frac{d^2}{d\omega^2}\mathrm{Re}G^R_{\hat\pi_{ij}\hat\pi^{ij}}(\omega)\Big|_{\omega=0}. \tag{2.250}$$

Here the retarded Green's function is given by Eq. (2.211), and the frequency-dependent shear viscosity $\eta(\omega)$ is defined by analogy with Eq. (A.11). As seen from Eq. (2.250), the new coefficient $\tau_\pi$ has a dimension of time and can be regarded as a relaxation time for the shear stress tensor.

Combining Eqs. (2.242), (2.248) and (2.249) we obtain

$$\langle\hat\pi_{\mu\nu}\rangle^1_2 = -2\eta\tau_\pi\beta^{-1}\Delta_{\mu\nu\rho\sigma}D(\beta\sigma^{\rho\sigma}) = -2\eta\tau_\pi(\Delta_{\mu\nu\rho\sigma}D\sigma^{\rho\sigma} + \gamma\theta\sigma_{\mu\nu}), \tag{2.251}$$

where we used Eq. (2.183) in the second step and omitted the argument of $\hat\pi_{\mu\nu}$ for brevity.

### Corrections from the operator $\hat C_2$

Since the operator $\hat C_2$ given by Eq. (2.228) does not have a tensor part, the correction of $\hat\pi_{\mu\nu}$ from this term vanishes due to Curie's theorem

$$\langle\hat\pi_{\mu\nu}(x)\rangle^2_2 = \int d^4x_1\Big(\hat\pi_{\mu\nu}(x), \hat C_2(x_1)\Big) = 0. \tag{2.252}$$

### Nonlinear corrections from the three-point correlation function

From Eqs. (2.227) and (2.234) we have

$$\langle\hat\pi_{\mu\nu}(x)\rangle^3_2 = \int d^4x_1d^4x_2\Big(\hat\pi_{\mu\nu}(x), \hat C_1(x_1), \hat C_1(x_2)\Big) = \int d^4x_1d^4x_2\Big(\hat\pi_{\mu\nu}(x),$$
$$\big[-\beta\theta\hat p^* + \beta\hat\pi_{\rho\sigma}\sigma^{\rho\sigma} - \sum_a \hat{\mathcal{J}}^\sigma_a\nabla_\sigma\alpha_a\big]_{x_1}, \big[-\beta\theta\hat p^* + \beta\hat\pi_{\alpha\beta}\sigma^{\alpha\beta} - \sum_b \hat{\mathcal{J}}^\alpha_b\nabla_\alpha\alpha_b\big]_{x_2}\Big). \tag{2.253}$$

In contrast to the two-point correlators, where only operators of the same rank are coupled, in the three-point correlators one may have a mixing between operators of different rank. The three-point mixed correlators in Eq. (2.253) which in general do not vanish are [1]

$$(\hat\pi_{\mu\nu}, \hat p^*, \hat\pi_{\alpha\beta}) = \frac{1}{5}\Delta_{\mu\nu\alpha\beta}(\hat\pi_{\gamma\delta}, \hat p^*, \hat\pi^{\gamma\delta}), \qquad (\hat\pi_{\mu\nu}, \hat{\mathcal{J}}_{a\sigma}, \hat{\mathcal{J}}_{b\alpha}) = \frac{1}{5}\Delta_{\mu\nu\sigma\alpha}(\hat\pi_{\gamma\delta}, \hat{\mathcal{J}}^\gamma_a, \hat{\mathcal{J}}^\delta_b), \tag{2.254}$$

where we exploited the symmetries of the relevant operators. Because these correlators stand in front of second-order thermodynamic forces, it is sufficient to evaluate all $\Delta$-projectors at the point $x$.

The most general expression for the correlator between three shear stresses which satisfies the orthogonality condition $u^\mu\hat\pi_{\mu\nu} = 0$ is

$$\begin{aligned}(\hat\pi_{\mu\nu}, \hat\pi_{\rho\sigma}, \hat\pi_{\alpha\beta}) \;=\; & a(\Delta_{\mu\nu}\Delta_{\rho\sigma\alpha\beta} + \Delta_{\rho\sigma}\Delta_{\mu\nu\alpha\beta} + \Delta_{\alpha\beta}\Delta_{\mu\nu\rho\sigma}) + b\Delta_{\mu\nu}\Delta_{\rho\sigma}\Delta_{\alpha\beta}\\ & + c(\Delta_{\mu\rho}\Delta_{\nu\alpha}\Delta_{\sigma\beta} + \Delta_{\mu\rho}\Delta_{\nu\beta}\Delta_{\sigma\alpha} + \Delta_{\mu\sigma}\Delta_{\nu\alpha}\Delta_{\rho\beta} + \Delta_{\mu\sigma}\Delta_{\nu\beta}\Delta_{\rho\alpha}\\ & + \Delta_{\mu\alpha}\Delta_{\nu\rho}\Delta_{\sigma\beta} + \Delta_{\mu\alpha}\Delta_{\nu\sigma}\Delta_{\rho\beta} + \Delta_{\mu\beta}\Delta_{\nu\rho}\Delta_{\sigma\alpha} + \Delta_{\mu\beta}\Delta_{\nu\sigma}\Delta_{\rho\alpha}).\end{aligned} \tag{2.255}$$

[1] For example, the mixed correlator $(\hat\pi_{\mu\nu}, \hat p^*, \hat{\mathcal{J}}_\alpha)$ vanishes because it is not possible to constract a fully space-like tensor of the third rank from the projector $\Delta_{\mu\nu}$, etc.

Here the coefficients $a, b, c$ should be still determined from the condition $\hat{\pi}^{\alpha}_{\alpha} = 0$. Contracting the indices $\alpha$ and $\beta$ in Eq. (2.255) and using the properties (2.7) and (2.27), we obtain

$$\begin{aligned}(\hat{\pi}_{\mu\nu}, \hat{\pi}_{\rho\sigma}, \hat{\pi}^{\alpha}_{\alpha}) &= 3a\Delta_{\mu\nu\rho\sigma} + 3b\Delta_{\mu\nu}\Delta_{\rho\sigma} + 4c(\Delta_{\mu\sigma}\Delta_{\nu\rho} + \Delta_{\mu\rho}\Delta_{\nu\sigma}) \\ &= (3a + 8c)\Delta_{\mu\nu\rho\sigma} + \left(3b + \frac{8c}{3}\right)\Delta_{\mu\nu}\Delta_{\rho\sigma} = 0, \end{aligned} \tag{2.256}$$

from where we find $b = a/3$, $c = -3a/8$. In order to find $a$ we compute the mixed contraction

$$\begin{aligned}(\hat{\pi}_{\mu\nu}, \hat{\pi}^{\nu\alpha}, \hat{\pi}_{\alpha\beta}) &= 3a\Delta_{\mu\ \alpha\beta}^{\ \alpha} + b\Delta_{\mu\beta} + 22c\Delta_{\mu\beta} = -\frac{35}{12}a\Delta_{\mu\beta} \\ &\Rightarrow \quad (\hat{\pi}^{\nu}_{\mu}, \hat{\pi}^{\alpha}_{\nu}, \hat{\pi}^{\mu}_{\alpha}) = -\frac{35}{4}a, \quad a = -\frac{4}{35}(\hat{\pi}^{\nu}_{\mu}, \hat{\pi}^{\alpha}_{\nu}, \hat{\pi}^{\mu}_{\alpha}). \end{aligned} \tag{2.257}$$

Then Eq. (2.255) is cast into the compact form

$$\begin{aligned}(\hat{\pi}_{\mu\nu}, \hat{\pi}_{\rho\sigma}, \hat{\pi}_{\alpha\beta}) &= \frac{1}{35}\Big[3(\Delta_{\rho\alpha}\Delta_{\mu\nu\sigma\beta} + \Delta_{\rho\beta}\Delta_{\mu\nu\sigma\alpha} + \Delta_{\sigma\alpha}\Delta_{\mu\nu\rho\beta} + \Delta_{\sigma\beta}\Delta_{\mu\nu\rho\alpha}) \\ &\qquad -4(\Delta_{\rho\sigma}\Delta_{\mu\nu\alpha\beta} + \Delta_{\alpha\beta}\Delta_{\mu\nu\rho\sigma})\Big](\hat{\pi}^{\delta}_{\gamma}, \hat{\pi}^{\lambda}_{\delta}, \hat{\pi}^{\gamma}_{\lambda}). \end{aligned} \tag{2.258}$$

Substituting the correlation functions given by Eqs. (2.254) and (2.258) back into Eq. (2.253), factoring the thermodynamic forces out from the integral with their values at $x$, taking into account the symmetry property (2.169) and defining a set of coefficients

$$\lambda_{\pi} = \frac{12}{35}\beta^2 \int d^4x_1 d^4x_2 \Big(\hat{\pi}^{\delta}_{\gamma}(x), \hat{\pi}^{\lambda}_{\delta}(x_1), \hat{\pi}^{\gamma}_{\lambda}(x_2)\Big), \tag{2.259}$$

$$\lambda_{\pi\Pi} = -\frac{\beta^2}{5} \int d^4x_1 d^4x_2 \Big(\hat{\pi}_{\gamma\delta}(x), \hat{\pi}^{\gamma\delta}(x_1), \hat{p}^{*}(x_2)\Big), \tag{2.260}$$

$$\lambda^{ab}_{\pi\mathscr{J}} = \frac{1}{5} \int d^4x_1 d^4x_2 \Big(\hat{\pi}_{\gamma\delta}(x), \hat{\mathcal{J}}^{\gamma}_{a}(x_1), \hat{\mathcal{J}}^{\delta}_{b}(x_2)\Big), \tag{2.261}$$

we finally obtain

$$\langle \hat{\pi}_{\mu\nu} \rangle^3_2 = 2\lambda_{\pi\Pi}\theta\sigma_{\mu\nu} + \lambda_{\pi}\sigma_{\alpha<\mu}\sigma^{\alpha}_{\nu>} + \sum_{ab}\lambda^{ab}_{\pi\mathscr{J}}\nabla_{<\mu}\alpha_a\nabla_{\nu>}\alpha_b, \tag{2.262}$$

where we used the notation introduced in Eq. (2.86) and employed the identities $\sigma^{<\alpha\beta>} = \sigma^{\alpha\beta}$, $\sigma^{\alpha\beta}\Delta_{\beta\lambda} = \sigma^{\alpha}_{\lambda}$ and $\sigma^{\alpha}_{\alpha} = 0$.

### Final equation for the shear stress tensor

Combining all corrections from Eqs. (2.203), (2.251), (2.252) and (2.262) and using Eqs. (2.177), (2.229) and (2.231) we obtain the complete second-order expression for the shear stress tensor

$$\begin{aligned}\pi_{\mu\nu} &= 2\eta\sigma_{\mu\nu} - 2\eta\tau_{\pi}(\Delta_{\mu\nu\rho\sigma}D\sigma^{\rho\sigma} + \gamma\theta\sigma_{\mu\nu}) \\ &+ 2\lambda_{\pi\Pi}\theta\sigma_{\mu\nu} + \lambda_{\pi}\sigma_{\alpha<\mu}\sigma^{\alpha}_{\nu>} + \sum_{ab}\lambda^{ab}_{\pi\mathscr{J}}\nabla_{<\mu}\alpha_a\nabla_{\nu>}\alpha_b. \end{aligned} \tag{2.263}$$

Here the second-order terms in the first line represent the non-local corrections, whereas the second line collects the nonlinear corrections from the three-point correlations. The physical interpretation of various terms in Eq. (2.263) is discussed in Sec. 2.6.2.

We can derive a relaxation-type equation for $\pi_{\mu\nu}$ from the expression (2.263). For this purpose we note that we can replace $2\sigma^{\rho\sigma} \to \eta^{-1}\pi^{\rho\sigma}$ in the second term of the right-hand side of Eq. (2.263), as suggested also in Refs. [39, 49, 196]. This substitution is justified because that term is of the second

order in the space-time gradients. We then have

$$-2\eta\tau_\pi\Delta_{\mu\nu\rho\sigma}D\sigma^{\rho\sigma} \simeq -\tau_\pi\dot{\pi}_{\mu\nu} + \tau_\pi\beta\eta^{-1}\Big(\gamma\eta'_\beta - \sum_a \delta_a\eta'_{\alpha_a}\Big)\theta\pi_{\mu\nu}, \tag{2.264}$$

where we used Eqs. (2.85), (2.183) and (2.184). The quantities $\eta'_\beta$, $\eta'_{\alpha_a}$ denote the corresponding partial derivatives of $\eta$, which in general are not small and should not be neglected. Combining Eqs. (2.263) and (2.264) and introducing the coefficients

$$\lambda = 2(\lambda_{\pi\Pi} - \gamma\eta\tau_\pi), \tag{2.265}$$

$$\tilde{\lambda}_\pi = \tau_\pi\beta\eta^{-1}\Big(\gamma\eta'_\beta - \sum_a \delta_a\eta'_{\alpha_a}\Big), \tag{2.266}$$

we obtain finally

$$\pi_{\mu\nu} = 2\eta\sigma_{\mu\nu} - \tau_\pi\dot{\pi}_{\mu\nu} + \tilde{\lambda}_\pi\theta\pi_{\mu\nu} + \lambda\theta\sigma_{\mu\nu} + \lambda_\pi\sigma_{\alpha<\mu}\sigma^\alpha_{\nu>} + \sum_{ab}\lambda^{ab}_\pi\nabla_{<\mu}\alpha_a\nabla_{\nu>}\alpha_b. \tag{2.267}$$

### 2.5.4 Second-order corrections to the bulk viscous pressure

In order to evaluate the bulk viscous pressure in the second order, we should include also the relevant corrections to Eqs. (2.195) and (2.196)

$$\langle\hat{p}\rangle_l = p(\epsilon, n_a) - \gamma\Delta\epsilon - \sum_a \delta_a\Delta n_a + \psi_{\epsilon\epsilon}\Delta\epsilon^2 + 2\sum_a \psi_{\epsilon a}\Delta\epsilon\Delta n_a + \sum_{ab}\psi_{ab}\Delta n_a\Delta n_b, \tag{2.268}$$

where we defined

$$\psi_{\epsilon\epsilon} = \frac{1}{2}\frac{\partial^2 p}{\partial\epsilon^2}, \qquad \psi_{\epsilon a} = \frac{1}{2}\frac{\partial^2 p}{\partial\epsilon\partial n_a}, \qquad \psi_{ab} = \frac{1}{2}\frac{\partial^2 p}{\partial n_a\partial n_b}. \tag{2.269}$$

Then we have for the bulk viscous pressure

$$\Pi = \langle\hat{p}\rangle_l + \langle\hat{p}\rangle_1 + \langle\hat{p}\rangle_2 - p(\epsilon, n_a) = \langle\hat{p}\rangle_1 + \langle\hat{p}\rangle_2 - \gamma\Delta\epsilon - \sum_a \delta_a\Delta n_a$$
$$+\psi_{\epsilon\epsilon}\Delta\epsilon^2 + 2\sum_a \psi_{\epsilon a}\Delta\epsilon\Delta n_a + \sum_{ab}\psi_{ab}\Delta n_a\Delta n_b. \tag{2.270}$$

The quadratic terms in the deviations $\Delta\epsilon$ and $\Delta n_a$ can be approximated by substituting $\Delta\epsilon = \langle\hat{\epsilon}\rangle_1$ and $\Delta n_a = \langle\hat{n}_a\rangle_1$, whereas in the linear terms we should keep also the second-order corrections, *i.e.*, $\Delta\epsilon = \langle\hat{\epsilon}\rangle_1 + \langle\hat{\epsilon}\rangle_2$ and $\Delta n_a = \langle\hat{n}_a\rangle_1 + \langle\hat{n}_a\rangle_2$. We then obtain

$$\Pi = \langle\hat{p}^*\rangle_1 + \langle\hat{p}^*\rangle_2 + \psi_{\epsilon\epsilon}\langle\hat{\epsilon}\rangle_1^2 + 2\sum_a \psi_{\epsilon a}\langle\hat{\epsilon}\rangle_1\langle\hat{n}_a\rangle_1 + \sum_{ab}\psi_{ab}\langle\hat{n}_a\rangle_1\langle\hat{n}_b\rangle_1, \tag{2.271}$$

where we used the definition of $\hat{p}^*$ given by Eq. (2.187).

Upon introducing the coefficients [see Eq. (A.22) in Appendix A.1]

$$\zeta_\epsilon = \beta\int d^4x_1\Big(\hat{\epsilon}(x), \hat{p}^*(x_1)\Big) = -\frac{d}{d\omega}\mathrm{Im}G^R_{\hat{\epsilon}\hat{p}^*}(\omega)\Big|_{\omega=0}, \tag{2.272}$$

$$\zeta_a = \beta\int d^4x_1\Big(\hat{n}_a(x), \hat{p}^*(x_1)\Big) = -\frac{d}{d\omega}\mathrm{Im}G^R_{\hat{n}_a\hat{p}^*}(\omega)\Big|_{\omega=0}, \tag{2.273}$$

the averages $\langle\hat{\epsilon}\rangle_1$ and $\langle\hat{n}_a\rangle_1$ according to Eqs. (2.227) and (2.230) can be written as

$$\langle\hat{\epsilon}\rangle_1 = -\zeta_\epsilon\theta, \qquad \langle\hat{n}_a\rangle_1 = -\zeta_a\theta. \tag{2.274}$$

Then we have from Eqs. (2.203), (2.271) and (2.274)

$$\Pi = -\zeta\theta + \Big(\psi_{\epsilon\epsilon}\zeta_\epsilon^2 + 2\zeta_\epsilon \sum_a \psi_{\epsilon a}\zeta_a + \sum_{ab}\psi_{ab}\zeta_a\zeta_b\Big)\theta^2 + \langle \hat{p}^*\rangle_2. \tag{2.275}$$

**Non-local corrections from the two-point correlation function**

From Eqs. (2.227), (2.232) and (2.203) we have

$$\langle \hat{p}^*(x)\rangle_2^1 = -\int d^4x_1 \Big(\hat{p}^*(x), \hat{p}^*(x_1)\Big)(\beta\theta)_{x_1} + \zeta\theta. \tag{2.276}$$

Now we need to expand all *hydrodynamic* quantities which are evaluated at the point $x_1$ around the point $x$, as explained in Sec. 2.5.3. For this purpose we use Eqs. (2.187) and (2.173) to express the operator $\hat{p}^*$ in terms of the *primary* (*i.e.*, microscopic) operators $\hat{T}^{\mu\nu}$ and $\hat{N}^\mu_a$

$$\hat{p}^*(x_1) = -\frac{1}{3}\Delta_{\mu\nu}(x_1)\hat{T}^{\mu\nu}(x_1) - \gamma(x_1)u_\mu(x_1)u_\nu(x_1)\hat{T}^{\mu\nu}(x_1) - \sum_a \delta_a(x_1)u_\mu(x_1)\hat{N}^\mu_a(x_1). \tag{2.277}$$

Expanding the hydrodynamic quantities, *i.e.*, $u_\mu(x_1)$, $\gamma(x_1)$ and $\delta_a(x_1)$ in Eq. (2.277) into series around $x_1 = x$ and keeping only the linear terms in this expansion we obtain

$$\hat{p}^*(x_1) = \hat{p}^*(x_1)_x + (x_1 - x)^\tau \partial_\tau \hat{p}^*, \tag{2.278}$$

where $\hat{p}^*(x_1)_x$ is obtained from $\hat{p}^*(x_1)$ via replacing the arguments $x_1$ of all hydrodynamic quantities (but not the primary operators!) with $x$, and

$$\begin{aligned}\partial_\tau \hat{p}^* = \left(\frac{1}{3} - \gamma\right)(\hat{Q}^\nu \partial_\tau u_\nu + \hat{Q}^\mu \partial_\tau u_\mu) - 2\hat{\epsilon}\Big(\psi_{\epsilon\epsilon}\partial_\tau\epsilon + \sum_a \psi_{\epsilon a}\partial_\tau n_a\Big) \\ -2\sum_a \hat{n}_a\Big(\psi_{\epsilon a}\partial_\tau\epsilon + \sum_b \psi_{ab}\partial_\tau n_b\Big) - \sum_a \hat{J}^\mu_a \delta_a \partial_\tau u_\mu,\end{aligned} \tag{2.279}$$

where all operators are evaluated at $x_1$. To obtain Eqs. (2.278) and (2.279) we used Eqs. (2.173), (2.174), (2.185) and (2.269), the relation $u_\mu \partial_\tau u^\mu = 0$ and approximated $u_\mu(x) \approx u_\mu(x_1)$ in the second-order terms.

Substituting Eq. (2.278) into Eq. (2.276) and expanding also the thermodynamic force $\beta\theta$ around $x_1 = x$ we obtain up to the second order in gradients

$$\begin{aligned}\langle \hat{p}^*(x)\rangle_2^1 &= -\int d^4x_1 \Big(\hat{p}^*(x), \hat{p}^*(x_1)_x + \partial_\tau \hat{p}^*(x_1 - x)^\tau\Big)\big[(\beta\theta)_x + \partial_\tau(\beta\theta)(x_1 - x)^\tau\big] + \zeta\theta \\ &= -\partial_\tau(\beta\theta)\int d^4x_1 \Big(\hat{p}^*(x), \hat{p}^*(x_1)_x\Big)(x_1 - x)^\tau - \beta\theta \int d^4x_1 \Big(\hat{p}^*(x), \partial_\tau \hat{p}^*\Big)(x_1 - x)^\tau,\end{aligned} \tag{2.280}$$

where we cancelled the zeroth-order term of the expansion with $\zeta\theta$.

The bulk viscosity according to Eq. (2.280) is defined as

$$\begin{aligned}\zeta = \beta \int d^4x_1 \Big(\hat{p}^*(x), \hat{p}^*(x_1)_x\Big) = \beta \int d^4x_1 \Big(\frac{1}{3}\hat{T}_{ii}(x) - \gamma\hat{T}_{00}(x) - \sum_a \delta_a \hat{N}_{a0}(x), \\ \frac{1}{3}\hat{T}_{jj}(x_1) - \gamma\hat{T}_{00}(x_1) - \sum_a \delta_a \hat{N}_{a0}(x_1)\Big),\end{aligned} \tag{2.281}$$

where the second expression is valid in the fluid rest frame. Here $\beta$, $\gamma$ and $\delta_a$ are evaluated at $x$, and, therefore, $\zeta$ defined in this way is a local function of $\beta$ and $\mu_a$.

Now inserting Eq. (2.279) into Eq. (2.280), taking into account Curie's theorem and using Eqs. (A.28)–

(A.31) in Appendix A.1 we obtain

$$\begin{aligned}\langle\hat{p}^*(x)\rangle_2^1 &= -\partial_\tau(\beta\theta)\int d^4x_1\Big(\hat{p}^*(x),\hat{p}^*(x_1)\Big)(x_1-x)^\tau + 2\theta\Big(\psi_{\epsilon\epsilon}\partial_\tau\epsilon+\sum_a\psi_{\epsilon a}\partial_\tau n_a\Big)\\ &\times\beta\int d^4x_1\Big(\hat{p}^*(x),\hat{\epsilon}(x_1)\Big)(x_1-x)^\tau + 2\theta\sum_a\Big(\psi_{\epsilon a}\partial_\tau\epsilon+\sum_b\psi_{ab}\partial_\tau n_b\Big)\\ &\times\beta\int d^4x_1\Big(\hat{p}^*(x),\hat{n}_a(x_1)\Big)(x_1-x)^\tau = D(\beta\theta)\beta^{-1}\zeta\tau_\Pi\\ &-2\theta\Big(\psi_{\epsilon\epsilon}D\epsilon+\sum_a\psi_{\epsilon a}Dn_a\Big)\zeta_\epsilon\tau_\epsilon - 2\theta\sum_a\Big(\psi_{\epsilon a}D\epsilon+\sum_b\psi_{ab}Dn_b\Big)\zeta_a\tau_a, \qquad (2.282)\end{aligned}$$

where we neglected the difference $\hat{p}^*(x_1)_x-\hat{p}^*(x_1)$ in the first term because this term is already multiplied by a second-order gradient $\partial_\tau(\beta\theta)$. The new coefficients $\tau_\Pi$, $\tau_\epsilon$ and $\tau_a$ introduced in Eq. (2.282) are given by

$$\zeta\tau_\Pi = -i\frac{d}{d\omega}\zeta(\omega)\Big|_{\omega=0} = \frac{d^2}{d\omega^2}\mathrm{Re}G^R_{\hat{p}^*\hat{p}^*}(\omega)\Big|_{\omega=0}, \qquad (2.283)$$

$$\zeta_\epsilon\tau_\epsilon = -i\frac{d}{d\omega}\zeta_\epsilon(\omega)\Big|_{\omega=0} = \frac{d^2}{d\omega^2}\mathrm{Re}G^R_{\hat{p}^*\hat{\epsilon}}(\omega)\Big|_{\omega=0}, \qquad (2.284)$$

$$\zeta_a\tau_a = i\frac{d}{d\omega}\zeta_a(\omega)\Big|_{\omega=0} = \frac{d^2}{d\omega^2}\mathrm{Re}G^R_{\hat{p}^*\hat{n}_a}(\omega)\Big|_{\omega=0}, \qquad (2.285)$$

where $\zeta$, $\zeta_\epsilon$ and $\zeta_a$ in the limit $\omega\to 0$ are defined in Eqs. (2.202), (2.272) and (2.273). In the case of $\omega\neq 0$ the formula (A.11) should be used with the relevant choices of the operators $\hat{X}$ and $\hat{Y}$. [Note that there is no summation on the left-hand side of Eq. (2.285).]

The derivatives $D\beta$, $D\epsilon$ and $Dn_a$ can be eliminated from Eq. (2.282) by employing Eqs. (2.12), (2.183) and (2.184). Denoting

$$\zeta^* = \gamma\zeta\tau_\Pi + 2\zeta_\epsilon\tau_\epsilon\Big(\psi_{\epsilon\epsilon}h+\sum_a n_a\psi_{\epsilon a}\Big) + 2\sum_a\zeta_a\tau_a\Big(\psi_{\epsilon a}h+\sum_b\psi_{ab}n_b\Big), \qquad (2.286)$$

we obtain from Eqs. (2.282)–(2.286)

$$\langle\hat{p}^*\rangle_2^1 = \zeta\tau_\Pi D\theta + \zeta^*\theta^2. \qquad (2.287)$$

**Corrections from the operator $\hat{C}_2$**

Inserting Eq. (2.228) into Eq. (2.233) and taking into account again Curie's theorem we obtain

$$\langle\hat{p}^*(x)\rangle_2^2 = -\zeta_\beta(\Pi\theta+\partial_\mu q^\mu - q^\mu Du_\mu - \pi^{\mu\nu}\sigma_{\mu\nu}) + \sum_a\zeta_{\alpha_a}\partial_\mu j_a^\mu, \qquad (2.288)$$

where we factored out all thermodynamic forces from the integral with their values at $x$ and defined

$$\zeta_\beta = \int d^4x_1\Big(\hat{p}^*(x),\hat{\beta}^*(x_1)\Big) = -\frac{1}{\beta}\frac{d}{d\omega}\mathrm{Im}G^R_{\hat{p}^*\hat{\beta}^*}(\omega)\Big|_{\omega=0}, \qquad (2.289)$$

$$\zeta_{\alpha_a} = \int d^4x_1\Big(\hat{p}^*(x),\hat{\alpha}_a^*(x_1)\Big) = -\frac{1}{\beta}\frac{d}{d\omega}\mathrm{Im}G^R_{\hat{p}^*\hat{\alpha}_a^*}(\omega)\Big|_{\omega=0}. \qquad (2.290)$$

The operators $\hat{\beta}^*$ and $\hat{\alpha}_a^*$ are given by Eqs. (2.223) and (2.224), respectively.

It is convenient to modify the second term in Eq. (2.288) using Eq. (2.44)

$$\partial_\mu j_a^\mu = \partial_\mu\mathscr{J}_a^\mu + n_a h^{-1}\partial_\mu q^\mu + q^\mu\partial_\mu(n_a h^{-1}). \qquad (2.291)$$

Using Eq. (2.291) and defining

$$\tilde{\zeta}_\beta = \zeta_\beta - h^{-1}\sum_a n_a \zeta_{\alpha_a}, \tag{2.292}$$

we obtain for Eq. (2.288)

$$\langle \hat{p}^* \rangle_2^2 = \sum_a \zeta_{\alpha_a} \partial_\mu \mathscr{J}_a^\mu - \zeta_\beta(\Pi\theta - \pi^{\mu\nu}\sigma_{\mu\nu}) - \tilde{\zeta}_\beta \partial_\mu q^\mu + q^\mu \Big[\zeta_\beta D u_\mu + \sum_a \zeta_{\alpha_a} \nabla_\mu (n_a h^{-1})\Big]. \tag{2.293}$$

**Nonlinear corrections from the three-point correlation function**

From Eqs. (2.227) and (2.234) we have

$$\begin{aligned}\langle \hat{p}^*(x) \rangle_2^3 = \int d^4x_1 d^4x_2 \Big(\hat{p}^*(x), \hat{C}_1(x_1), \hat{C}_1(x_2)\Big) = \int d^4x_1 d^4x_2 \Big(\hat{p}^*(x), \\ \big[-\beta\theta\hat{p}^* + \beta\hat{\pi}_{\rho\sigma}\sigma^{\rho\sigma} - \sum_a \hat{\mathcal{J}}_a^\sigma \nabla_\sigma \alpha_a\big]_{x_1}, \big[-\beta\theta\hat{p}^* + \beta\hat{\pi}_{\alpha\beta}\sigma^{\alpha\beta} - \sum_a \hat{\mathcal{J}}_b^\alpha \nabla_\alpha \alpha_b\big]_{x_2}\Big).\end{aligned} \tag{2.294}$$

The non-vanishing correlators in Eq. (2.294) are $(\hat{p}^*, \hat{p}^*, \hat{p}^*)$ and

$$(\hat{p}^*, \hat{\mathcal{J}}_{a\sigma}, \hat{\mathcal{J}}_{b\alpha}) = \frac{1}{3}\Delta_{\sigma\alpha}(\hat{p}^*, \hat{\mathcal{J}}_{a\gamma}, \hat{\mathcal{J}}_b^\gamma), \qquad (\hat{p}^*, \hat{\pi}_{\rho\sigma}, \hat{\pi}_{\alpha\beta}) = \frac{1}{5}\Delta_{\rho\sigma\alpha\beta}(\hat{p}^*, \hat{\pi}_{\gamma\delta}, \hat{\pi}^{\gamma\delta}). \tag{2.295}$$

Inserting these expressions in to Eq. (2.294) we obtain

$$\langle \hat{p}^* \rangle_2^3 = \lambda_\Pi \theta^2 - \lambda_{\Pi\pi}\sigma_{\alpha\beta}\sigma^{\alpha\beta} + T\sum_{ab} \zeta_\Pi^{ab} \nabla^\sigma \alpha_a \nabla_\sigma \alpha_b, \tag{2.296}$$

where we defined the coefficients

$$\lambda_\Pi = \beta^2 \int d^4x_1 d^4x_2 \Big(\hat{p}^*(x), \hat{p}^*(x_1), \hat{p}^*(x_2)\Big), \tag{2.297}$$

$$\lambda_{\Pi\pi} = -\frac{\beta^2}{5} \int d^4x_1 d^4x_2 \Big(\hat{p}^*(x), \hat{\pi}_{\gamma\delta}(x_1), \hat{\pi}^{\gamma\delta}(x_2)\Big), \tag{2.298}$$

$$\zeta_\Pi^{ab} = \frac{\beta}{3} \int d^4x_1 d^4x_2 \Big(\hat{p}^*(x), \hat{\mathcal{J}}_{a\gamma}(x_1), \hat{\mathcal{J}}_b^\gamma(x_2)\Big). \tag{2.299}$$

**Final equation for the bulk viscous pressure**

Combining all pieces from Eqs. (2.287), (2.293) and (2.296) we obtain according to Eq. (2.231)

$$\begin{aligned}\langle \hat{p}^*(x) \rangle_2 &= \zeta\tau_\Pi D\theta - \zeta_\beta(\Pi\theta - \pi^{\mu\nu}\sigma_{\mu\nu}) - \tilde{\zeta}_\beta \partial_\mu q^\mu + (\lambda_\Pi + \zeta^*)\theta^2 - \lambda_{\Pi\pi}\sigma_{\alpha\beta}\sigma^{\alpha\beta} \\ &+ \sum_a \zeta_{\alpha_a} \partial_\mu \mathscr{J}_a^\mu + T\sum_{ab} \zeta_\Pi^{ab} \nabla^\sigma \alpha_a \nabla_\sigma \alpha_b + q^\mu \Big[\zeta_\beta D u_\mu + \sum_a \zeta_{\alpha_a} \nabla_\mu (n_a h^{-1})\Big].\end{aligned} \tag{2.300}$$

A relaxation equation for the bulk viscous pressure can be obtained by approximating in the first term in Eq. (2.300) $\theta \simeq -\zeta^{-1}\Pi$, as we did in the case of the shear stress tensor. We obtain thus ($\dot{\Pi} \equiv D\Pi$)

$$\zeta\tau_\Pi D\theta = -\tau_\Pi \dot{\Pi} + \tau_\Pi \Pi \zeta^{-1} D\zeta = -\tau_\Pi \dot{\Pi} + \tau_\Pi \beta \zeta^{-1} \Big(\gamma\zeta'_\beta - \sum_a \delta_a \zeta'_{\alpha_a}\Big)\theta\Pi, \tag{2.301}$$

where we used Eqs. (2.183) and (2.184). The quantities $\zeta'_\beta$ and $\zeta'_{\alpha_a}$ in Eq. (2.301) are the corresponding partial derivatives of $\zeta$.

Now combining Eqs. (2.275), (2.300) and (2.301), denoting $\dot{u}_\mu = Du_\mu$ and defining

$$\varsigma = \lambda_\Pi + \zeta^* + \psi_{\epsilon\epsilon}\zeta_\epsilon^2 + 2\zeta_\epsilon \sum_a \psi_{\epsilon a}\zeta_a + \sum_{ab}\psi_{ab}\zeta_a\zeta_b, \tag{2.302}$$

$$\tilde{\lambda}_\Pi = \tau_\Pi \beta \zeta^{-1}\Big(\gamma\zeta'_\beta - \sum_a \delta_a \zeta'_{\alpha_a}\Big), \tag{2.303}$$

we obtain the final evolution equation for the bulk viscous pressure

$$\begin{aligned}\Pi &= -\zeta\theta - \tau_\Pi\dot{\Pi} + \tilde{\lambda}_\Pi\theta\Pi + \zeta_\beta(\sigma_{\mu\nu}\pi^{\mu\nu} - \theta\Pi) + \varsigma\theta^2 - \lambda_{\Pi\pi}\sigma_{\mu\nu}\sigma^{\mu\nu} - \tilde{\zeta}_\beta\partial_\mu q^\mu \\ &+ \sum_a \zeta_{\alpha_a}\partial_\mu \mathscr{J}_a^\mu + T\sum_{ab}\zeta_\Pi^{ab}\nabla^\mu\alpha_a\nabla_\mu\alpha_b + q^\mu\Big[\zeta_\beta\dot{u}_\mu + \sum_a \zeta_{\alpha_a}\nabla_\mu(n_a h^{-1})\Big].\end{aligned} \tag{2.304}$$

### 2.5.5 Second-order corrections to the diffusion currents

#### Non-local corrections from the two-point correlation function

Using Eqs. (2.204), (2.227) and (2.232) and applying again Curie's theorem we obtain

$$\langle\hat{\mathcal{J}}_{c\mu}(x)\rangle_2^1 = -\sum_a \int d^4x_1\Big(\hat{\mathcal{J}}_{c\mu}(x), \hat{\mathcal{J}}_{a\sigma}(x_1)\Big)(\nabla^\sigma\alpha_a)_{x_1} - \sum_a \chi_{ca}\nabla_\mu\alpha_a, \tag{2.305}$$

Now we substitute the correlation function given by Eqs. (2.235) and (2.237) into Eq. (2.305)

$$\langle\hat{\mathcal{J}}_{c\mu}(x)\rangle_2^1 = -\frac{1}{3}\sum_a \Delta_{\mu\beta}(x)\int d^4x_1\Big(\hat{\mathcal{J}}_c^\lambda(x), \hat{\mathcal{J}}_{a\lambda}(x_1)\Big)(\nabla^\beta\alpha_a)_{x_1} - \sum_a \chi_{ca}\nabla_\mu\alpha_a. \tag{2.306}$$

Next we use Eqs. (2.191) and (2.174) to express the operators $\hat{\mathcal{J}}_a^\lambda$ in terms of the energy-momentum tensor and the charge currents, as we did also in the case of the bulk viscous pressure

$$\hat{\mathcal{J}}_{a\lambda}(x_1) = \Delta_{\mu\lambda}(x_1)\hat{N}_a^\mu(x_1) - \frac{n_a(x_1)}{h(x_1)}\Delta_{\lambda\mu}(x_1)u_\nu(x_1)\hat{T}^{\mu\nu}(x_1). \tag{2.307}$$

Expanding all hydrodynamic quanities in Eq. (2.307) around their values at $x_1 = x$ at the first order in gradients and using the decompositions (2.170) and (2.171) we obtain

$$\hat{\mathcal{J}}_{a\lambda}(x_1) = \hat{\mathcal{J}}_{a\lambda}(x_1)_x + (x_1 - x)^\tau\partial_\tau\hat{\mathcal{J}}_{a\lambda}, \tag{2.308}$$

with

$$\partial_\tau\hat{\mathcal{J}}_{a\lambda} = -u_\lambda(\partial_\tau u_\mu)\hat{\mathcal{J}}_a^\mu - \partial_\tau(n_a h^{-1})\hat{Q}_\lambda - \hat{n}_a\partial_\tau u_\lambda + n_a h^{-1}\big(\hat{\epsilon}\partial_\tau u_\lambda + \hat{p}\partial_\tau u_\lambda - \hat{\pi}_\lambda^\nu\partial_\tau u_\nu\big), \tag{2.309}$$

where $\hat{\mathcal{J}}_a^\lambda(x_1)_x$ is obtained from $\hat{\mathcal{J}}_a^\lambda(x_1)$ via replacing the arguments $x_1$ of all hydrodynamic quantities with $x$, while the operators are taken at $x_1$. Substituting Eq. (2.308) into Eq. (2.306) and expanding also the thermodynamic force $(\nabla^\beta\alpha_a)_{x_1}$ around $x$ we obtain

$$\begin{aligned}\langle\hat{\mathcal{J}}_{c\mu}(x)\rangle_2^1 &= -\frac{1}{3}\sum_a \Delta_{\mu\beta}(x)\int d^4x_1\Big(\hat{\mathcal{J}}_c^\lambda(x), \hat{\mathcal{J}}_{a\lambda}(x_1)_x + \partial_\tau\hat{\mathcal{J}}_{a\lambda}(x_1 - x)^\tau\Big) \\ &\quad\times\big[\nabla^\beta\alpha_a(x) + \partial_\tau(\nabla^\beta\alpha_a)(x_1 - x)^\tau\big] - \sum_a \chi_{ca}\nabla_\mu\alpha_a \\ &= -\frac{1}{3}\sum_a \Delta_{\mu\beta}\partial_\tau(\nabla^\beta\alpha_a)\int d^4x_1\Big(\hat{\mathcal{J}}_c^\lambda(x), \hat{\mathcal{J}}_{a\lambda}(x_1)_x\Big)(x_1 - x)^\tau \\ &\quad -\frac{1}{3}\sum_a \nabla_\mu\alpha_a\int d^4x_1\Big(\hat{\mathcal{J}}_c^\lambda(x), \partial_\tau\hat{\mathcal{J}}_{a\lambda}\Big)(x_1 - x)^\tau.\end{aligned} \tag{2.310}$$

Here we cancelled the first-order terms. The diffusion coefficients $\chi_{ab}$ are thus given by

$$\begin{aligned}\chi_{ab} &= -\frac{1}{3}\int d^4x_1\Big(\hat{\mathcal{J}}_a^\lambda(x),\hat{\mathcal{J}}_{b\lambda}(x_1)_x\Big)\\ &= \frac{1}{3}\int d^4x_1\Big(\hat{N}_{ai}(x)-\frac{n_a}{h}\hat{T}_{0i}(x),\hat{N}_{bi}(x_1)-\frac{n_b}{h}\hat{T}_{0i}(x_1)\Big),\end{aligned}\tag{2.311}$$

where the second relation is valid in the fluid rest frame. Equation (2.311) involves the quantities $n_a$ and $h$ evaluated at $x$, and, therefore, is a local function of thermodynamic parameters.

Now substituting Eq. (2.309) into (2.310), taking into account Curie's theorem, employing the orthogonality condition $u^\lambda\hat{\mathcal{J}}_{c\lambda}=0$ and using Eqs. (A.28)–(A.31) in Appendix A.1 we obtain

$$\begin{aligned}\langle\hat{\mathcal{J}}_{c\mu}(x)\rangle_2^1 &= -\frac{1}{3}\sum_a\Delta_{\mu\beta}\partial_\tau(\nabla^\beta\alpha_a)\int d^4x_1\Big(\hat{\mathcal{J}}_c^\lambda(x),\hat{\mathcal{J}}_{a\lambda}(x_1)\Big)(x_1-x)^\tau\\ &\quad+\frac{1}{3}\sum_a\partial_\tau(n_ah^{-1})\nabla_\mu\alpha_a\int d^4x_1\Big(\hat{\mathcal{J}}_c^\lambda(x),\hat{Q}_\lambda(x_1)\Big)(x_1-x)^\tau\\ &= \sum_a\tilde{\chi}_{ca}\Delta_{\mu\beta}D(\nabla^\beta\alpha_a)-\tilde{\chi}_{cq}\sum_a D(n_ah^{-1})\nabla_\mu\alpha_a,\end{aligned}\tag{2.312}$$

where

$$\tilde{\chi}_{ac} = i\frac{d}{d\omega}\chi_{ac}(\omega)\Big|_{\omega=0}=\frac{T}{3}\frac{d^2}{d\omega^2}\mathrm{Re}G^R_{\hat{\mathcal{J}}_a^\lambda\hat{\mathcal{J}}_{c\lambda}}(\omega)\Big|_{\omega=0},\tag{2.313}$$

$$\tilde{\chi}_{cq} = i\frac{d}{d\omega}\chi_{cq}(\omega)\Big|_{\omega=0}=\frac{T}{3}\frac{d^2}{d\omega^2}\mathrm{Re}G^R_{\hat{\mathcal{J}}_c^\lambda,\hat{Q}_\lambda}(\omega)\Big|_{\omega=0},\tag{2.314}$$

and $\chi_{cq}$ is defined in the next subsection. Because the expression (2.312) is already of the second order, we can use Eq. (2.12) to modify $D(n_ah^{-1})=-n_ah^{-2}Dp$. From Eqs. (2.12) and (2.185) we find

$$Dp=\gamma D\epsilon+\sum_a\delta_aDn_a=-\Big(\gamma h+\sum_a\delta_an_a\Big)\theta.\tag{2.315}$$

Substituting these results into Eqs. (2.312) we obtain

$$\langle\hat{\mathcal{J}}_{c\mu}\rangle_2^1=\sum_a\tilde{\chi}_{ca}\Delta_{\mu\beta}D(\nabla^\beta\alpha_a)-\tilde{\chi}_{cq}h^{-2}\Big(\gamma h+\sum_b\delta_bn_b\Big)\theta\sum_a n_a\nabla_\mu\alpha_a.\tag{2.316}$$

**Corrections from the operator $\hat{C}_2$**

Using Eqs. (2.233) and (2.228) and taking into account again Curie's theorem we obtain

$$\langle\hat{\mathcal{J}}_{c\mu}(x)\rangle_2^2=\chi_{cq}\beta h^{-1}(-\nabla_\mu\Pi+\Pi Du_\mu+\Delta_{\mu\nu}Dq^\nu+q^\nu\partial_\nu u_\mu+q_\mu\theta+\Delta_{\mu\sigma}\partial_\nu\pi^{\nu\sigma}),\tag{2.317}$$

where we used a relation analogous to the one given by Eq. (2.199)

$$\Big(\hat{\mathcal{J}}_{c\mu}(x),\hat{Q}^\sigma(x_1)\Big)=\frac{1}{3}\Delta_\mu^\sigma\Big(\hat{\mathcal{J}}_{c\alpha}(x),\hat{Q}^\alpha(x_1)\Big)\tag{2.318}$$

and defined a new coefficient via

$$\chi_{cq}=-\frac{1}{3}\int d^4x_1\Big(\hat{\mathcal{J}}_{c\alpha}(x),\hat{Q}^\alpha(x_1)\Big)=\frac{T}{3}\frac{d}{d\omega}\mathrm{Im}G^R_{\hat{\mathcal{J}}_c^\alpha\hat{Q}_\alpha}(\omega)\Big|_{\omega=0}.\tag{2.319}$$

Denoting

$$\dot{u}_\mu = Du_\mu, \qquad \dot{q}_\mu = \Delta_{\mu\nu}Dq^\nu, \tag{2.320}$$

we can write Eq. (2.317) as

$$\langle\hat{\mathcal{J}}_{c\mu}\rangle_2^2 = \chi_{cq}\beta h^{-1}(-\nabla_\mu\Pi + \Pi\dot{u}_\mu + \dot{q}_\mu + q^\nu\partial_\nu u_\mu + q_\mu\theta + \Delta_{\mu\sigma}\partial_\nu\pi^{\nu\sigma}). \tag{2.321}$$

**Nonlinear corrections from the three-point correlation function**

Substituting Eq. (2.227) into Eq. (2.234) we obtain

$$\langle\hat{\mathcal{J}}_{c\mu}(x)\rangle_2^3 = \int d^4x_1d^4x_2\Big(\hat{\mathcal{J}}_{c\mu}(x),\hat{C}_1(x_1),\hat{C}_1(x_2)\Big) = \int d^4x_1d^4x_2\Big(\hat{\mathcal{J}}_{c\mu}(x),$$
$$\big[-\beta\theta\hat{p}^* + \beta\hat{\pi}_{\rho\sigma}\sigma^{\rho\sigma} - \sum_a\hat{\mathcal{J}}_a^\sigma\nabla_\sigma\alpha_a\big](x_1),\big[-\beta\theta\hat{p}^* + \beta\hat{\pi}_{\alpha\beta}\sigma^{\alpha\beta} - \sum_b\hat{\mathcal{J}}_b^\alpha\nabla_\alpha\alpha_b\big](x_2)\Big). \tag{2.322}$$

The non-vanishing correlators in this case are

$$(\hat{\mathcal{J}}_{c\mu},\hat{\mathcal{J}}_{a\sigma},\hat{p}^*) = \frac{1}{3}\Delta_{\mu\sigma}(\hat{\mathcal{J}}_{c\beta},\hat{\mathcal{J}}_a^\beta,\hat{p}^*), \qquad (\hat{\mathcal{J}}_{c\mu},\hat{\mathcal{J}}_{a\sigma},\hat{\pi}_{\alpha\beta}) = \frac{1}{5}\Delta_{\mu\sigma\alpha\beta}(\hat{\mathcal{J}}_c^\gamma,\hat{\mathcal{J}}_a^\delta,\hat{\pi}_{\gamma\delta}). \tag{2.323}$$

We define now the following coefficients

$$\zeta_{\mathscr{J}}^{ca} = \frac{2\beta}{3}\int d^4x_1d^4x_2\Big(\hat{\mathcal{J}}_{c\gamma}(x),\hat{\mathcal{J}}_a^\gamma(x_1),\hat{p}^*(x_2)\Big), \tag{2.324}$$

$$\lambda_{\mathscr{J}}^{ca} = \frac{2\beta}{5}\int d^4x_1d^4x_2\Big(\hat{\mathcal{J}}_c^\gamma(x),\hat{\mathcal{J}}_a^\delta(x_1),\hat{\pi}_{\gamma\delta}(x_2)\Big). \tag{2.325}$$

Then from Eqs. (2.322)–(2.325) and from the symmetry property (2.169) we obtain

$$\langle\hat{\mathcal{J}}_{c\mu}\rangle_2^3 = \sum_a\Big(\zeta_{\mathscr{J}}^{ca}\theta\nabla_\mu\alpha_a - \lambda_{\mathscr{J}}^{ca}\sigma_{\mu\nu}\nabla^\nu\alpha_a\Big). \tag{2.326}$$

**Final equation for the diffusion currents**

Combining Eqs. (2.177), (2.204), (2.229), (2.231), (2.316), (2.321) and (2.326) we obtain the diffusion currents up to the second-order in hydrodynamic gradients

$$\begin{aligned}\mathscr{J}_{c\mu}(x) &= \sum_b\chi_{cb}\nabla_\mu\alpha_b + \sum_a\tilde{\chi}_{ca}\Delta_{\mu\beta}D(\nabla^\beta\alpha_a) - \tilde{\chi}_{cq}h^{-2}\Big(\gamma h + \sum_b\delta_b n_b\Big)\\ &\times\ \theta\sum_a n_a\nabla_\mu\alpha_a + \sum_a\Big(\zeta_{\mathscr{J}}^{ca}\theta\nabla_\mu\alpha_a - \lambda_{\mathscr{J}}^{ca}\sigma_{\mu\nu}\nabla^\nu\alpha_a\Big)\\ &+\ \chi_{cq}\beta h^{-1}(-\nabla_\mu\Pi + \Pi\dot{u}_\mu + \dot{q}_\mu + q^\nu\partial_\nu u_\mu + q_\mu\theta + \Delta_{\mu\sigma}\partial_\nu\pi^{\nu\sigma}).\end{aligned} \tag{2.327}$$

To obtain relaxation equations for the diffusion currents we invert Eq. (2.204) as

$$\nabla^\beta\alpha_a = \sum_b(\chi^{-1})_{ab}\mathscr{J}_b^\beta, \tag{2.328}$$

and use it to modify the second term in Eq. (2.327). Using Eqs. (2.85), (2.183) and (2.184) we obtain

$$\sum_a\tilde{\chi}_{ca}\Delta_{\mu\beta}D(\nabla^\beta\alpha_a) = -\sum_b\tau_{\mathscr{J}}^{cb}\dot{\mathscr{J}}_{b\mu} + \beta\theta\sum_{ab}\tilde{\chi}_{ca}\Big[\gamma(\chi^{-1})'_{ab,\beta} - \sum_d\delta_d(\chi^{-1})'_{ab,\alpha_d}\Big]\mathscr{J}_{b\mu}, \tag{2.329}$$

where we defined a matrix of relaxation times

$$\tau_{\mathscr{J}}^{cb} = -(\tilde{\chi}\chi^{-1})_{cb} = -\sum_a \tilde{\chi}_{ca}(\chi^{-1})_{ab}. \tag{2.330}$$

Introducing also the coefficients

$$\tilde{\lambda}_{\mathscr{J}}^{cb} = \beta\sum_a \tilde{\chi}_{ca}\Big[\gamma(\chi^{-1})'_{ab,\beta} - \sum_d \delta_d(\chi^{-1})'_{ab,\alpha_d}\Big], \tag{2.331}$$

$$\chi^*_{cb} = \zeta_{\mathscr{J}}^{cb} - \tilde{\chi}_{cq}n_b h^{-2}\Big(\gamma h + \sum_d \delta_d n_d\Big), \tag{2.332}$$

we obtain from Eqs. (2.327) and (2.329)

$$\begin{aligned}\mathscr{J}_{a\mu} = \sum_b \Big[\chi_{ab}\nabla_\mu\alpha_b - \tau_{\mathscr{J}}^{ab}\dot{\mathscr{J}}_{b\mu} + \tilde{\lambda}_{\mathscr{J}}^{ab}\theta\,\mathscr{J}_{b\mu} + \chi^*_{ab}\theta\nabla_\mu\alpha_b - \lambda_{\mathscr{J}}^{ab}\sigma_{\mu\nu}\nabla^\nu\alpha_b\Big] \\ +\chi_{aq}\beta h^{-1}\big(-\nabla_\mu\Pi + \Pi\dot{u}_\mu + \dot{q}_\mu + q^\nu\partial_\nu u_\mu + q_\mu\theta + \Delta_{\mu\sigma}\partial_\nu\pi^{\nu\sigma}\big).\end{aligned} \tag{2.333}$$

If we have only one sort of conserved charge, then Eq. (2.333) simplifies to

$$\begin{aligned}\mathscr{J}_\mu &= \chi\nabla_\mu\alpha - \tau_{\mathscr{J}}\dot{\mathscr{J}}_\mu + \tilde{\lambda}_{\mathscr{J}}\theta\,\mathscr{J}_\mu + \chi^*\theta\nabla_\mu\alpha - \lambda_{\mathscr{J}}\sigma_{\mu\nu}\nabla^\nu\alpha \\ &+ \chi_q\beta h^{-1}\big(-\nabla_\mu\Pi + \Pi\dot{u}_\mu + \dot{q}_\mu + q^\nu\partial_\nu u_\mu + q_\mu\theta + \Delta_{\mu\sigma}\partial_\nu\pi^{\nu\sigma}\big),\end{aligned} \tag{2.334}$$

where the current relaxation time is given by [see Eqs. (2.313) and (2.330)]

$$\chi\tau_{\mathscr{J}} = -i\frac{d}{d\omega}\chi(\omega)\Big|_{\omega=0} = -\frac{T}{3}\frac{d^2}{d\omega^2}\mathrm{Re}G^R_{\hat{\mathcal{J}}_\mu\hat{\mathcal{J}}^\mu}(\omega)\Big|_{\omega=0}, \tag{2.335}$$

and

$$\tilde{\lambda}_{\mathscr{J}} = \tau_{\mathscr{J}}\beta\chi^{-1}(\gamma\chi'_\beta - \delta\chi'_\alpha), \tag{2.336}$$

$$\chi^* = \zeta_{\mathscr{J}} - \tilde{\chi}_q n h^{-2}(\gamma h + \delta n). \tag{2.337}$$

Recalling the relation (2.69) between the diffusion coefficient and the thermal conductivity and Eq. (2.206), we can write the relaxation time $\tau_{\mathscr{J}} \equiv \tau_h$ also in the following form

$$\kappa\tau_h = -i\frac{d}{d\omega}\kappa(\omega)\Big|_{\omega=0} = -\frac{\beta}{3}\frac{d^2}{d\omega^2}\mathrm{Re}G^R_{\hat{H}_\mu\hat{H}^\mu}(\omega)\Big|_{\omega=0}. \tag{2.338}$$

The frequency-dependent coefficients $\chi$ and $\kappa$ in Eqs. (2.335) and (2.338) are defined according to the formula (A.11) in Appendix A.1 with the relevant choice of operators.

## 2.6 Discussion and conclusions

In this section we discuss the main results of this chapter and compare them with previous studies.

### 2.6.1 General structure of the transport equations

The complete set of the second-order transport equations for the dissipative quantities obtained in the previous section reads [see Eqs. (2.267), (2.304) and (2.333)]

$$\tau_\pi\dot{\pi}_{\mu\nu}+\pi_{\mu\nu} = 2\eta\sigma_{\mu\nu}+\tilde{\lambda}_\pi\theta\pi_{\mu\nu}+\lambda\theta\sigma_{\mu\nu}+\lambda_\pi\sigma_{\rho<\mu}\sigma^{\rho}_{\nu>}+\sum_{ab}\lambda^{ab}_{\pi\mathscr{J}}\nabla_{<\mu}\alpha_a\nabla_{\nu>}\alpha_b, \tag{2.339}$$

$$\begin{aligned}\tau_\Pi\dot{\Pi}+\Pi &= -\zeta\theta+\tilde{\lambda}_\Pi\theta\Pi+\varsigma\theta^2+\zeta_\beta(\sigma_{\mu\nu}\pi^{\mu\nu}-\theta\Pi)-\lambda_{\Pi\pi}\sigma_{\mu\nu}\sigma^{\mu\nu}+\sum_a\zeta_{\alpha_a}\partial_\mu\mathscr{J}^\mu_a\\ &\quad -\tilde{\zeta}_\beta\partial_\mu q^\mu+q^\mu\Big[\zeta_\beta\dot{u}_\mu+\sum_a\zeta_{\alpha_a}\nabla_\mu(n_a h^{-1})\Big]+T\sum_{ab}\zeta^{ab}_\Pi\nabla^\mu\alpha_a\nabla_\mu\alpha_b,\end{aligned} \tag{2.340}$$

$$\begin{aligned}\sum_b\tau^{ab}_{\mathscr{J}}\dot{\mathscr{J}}_{b\mu}+\mathscr{J}_{a\mu} &= \sum_b\Big[\chi_{ab}\nabla_\mu\alpha_b+\tilde{\lambda}^{ab}_{\mathscr{J}}\theta\mathscr{J}_{b\mu}+\chi^*_{ab}\theta\nabla_\mu\alpha_b-\lambda^{ab}_{\mathscr{J}}\sigma_{\mu\nu}\nabla^\nu\alpha_b\Big]\\ &\quad +\chi_{aq}\beta h^{-1}\big(-\nabla_\mu\Pi+\Pi\dot{u}_\mu+\dot{q}_\mu+q^\nu\partial_\nu u_\mu+q_\mu\theta+\Delta_{\mu\sigma}\partial_\nu\pi^{\nu\sigma}\big),\end{aligned} \tag{2.341}$$

where the dot denotes the covariant time-derivative

$$\dot{\Pi}=D\Pi,\quad \dot{\pi}_{\mu\nu}=\Delta_{\mu\nu\rho\sigma}D\pi^{\rho\sigma},\quad \dot{u}_\mu=Du_\mu,\quad \dot{q}_\mu=\Delta_{\mu\nu}Dq^\nu,\quad \dot{\mathscr{J}}_{a\mu}=\Delta_{\mu\nu}D\mathscr{J}^\nu_a. \tag{2.342}$$

The first terms on the right-hand sides of Eqs. (2.339)–(2.341) represent the corresponding NS contributions. The first-order coefficients $\eta$, $\zeta$ and $\chi_{ab}$ are the shear viscosity, the bulk viscosity and the matrix of diffusion coefficietns, respectively; these coefficients are expressed via two-point retarded correlation functions via the Kubo formulas (2.209)–(2.211).

The first terms on the left-hand sides of Eqs. (2.339)–(2.341) incorporate the relaxation of the dissipative fluxes towards their leading-order (NS) values, if they differ from those at the initial moment of time. The coefficients $\tau_\pi$, $\tau_\Pi$ and $\tau^{ab}_{\mathscr{J}}$ represent the characteristic time scales during which this relaxation occurs. For example, in the case of $\sigma_{\mu\nu}=0$, Eq. (2.339) implies an exponential decay of the shear stress tensor on the time scale given by $\tau_\pi$, *i.e.*, $\pi_{\mu\nu}\propto\exp(-t/\tau_\pi)$ (if we ignore the rest of the second-order terms).

The relaxation times $\tau_\pi$, $\tau_\Pi$ and $\tau^{ab}_{\mathscr{J}}$ are related to the relevant first-order transport coefficients. For example, the shear relaxation time is given by a Kubo-type formula

$$\eta\tau_\pi=-i\frac{d}{d\omega}\eta(\omega)\Big|_{\omega=0}=\frac{1}{10}\frac{d^2}{d\omega^2}\mathrm{Re}G^R_{\hat{\pi}_{\mu\nu}\hat{\pi}^{\mu\nu}}(\omega)\Big|_{\omega=0}, \tag{2.343}$$

where the retarded Green's function is defined in Eq. (2.211). Here $\eta(\omega)$ is the analogue of the shear viscosity for non-vanishing frequencies and is defined via the generalization of Eq. (2.201) according to Eq. (A.11). The positivity of $\tau_\pi$ can be anticipated from Eqs. (2.343) and (A.11), upon taking into account that $(\pi_{\mu\nu}\pi^{\mu\nu})$ correlator which determines the shear viscosity $\eta$ should be positive. Similar to Eq. (2.343) formulas hold also for the bulk and the diffusion relaxation times [see Eqs. (2.283), (2.313), (2.330) and (2.335)].

The physical meaning of the formula (2.343) for $\tau_\pi$ is easy to understand. As we showed in the previous section, the relaxation terms originate from the non-local (memory) effects encoded in the non-equilibrium statistical operator. In the case where these memory effects are neglected, *i.e.*, in the first-order theory, the proportionality between $\pi_{\mu\nu}$ and $\sigma_{\mu\nu}$ is given by the zero-frequency (static) limit of the shear viscosity, as seen from Eqs. (2.203) and (2.209). The effects of finite memory in the dissipation of shear stresses imply actually a dispersion (*i.e.*, frequency-dependence) in the shear viscosity, which at the leading order should be accounted for by the first frequency-derivative of $\eta(\omega)$. This is exactly what Eq. (2.343) tells us. Hence we conclude, that the memory effects naturally generate finite relaxation time scales in the transoprt equations, as shown also in Refs. [64, 200, 201].

The second terms on the right-hand sides of Eqs. (2.339)–(2.341) arise as a consequence of inhomogeneities in the first-order coefficients, because these are functions of the temperature and the chemical potentials, which vary in space and time. The coefficients $\tilde{\lambda}_\pi$, $\tilde{\lambda}_\Pi$ and $\tilde{\lambda}^{ab}_{\mathscr{J}}$ involve the derivatives of the corresponding first-order transport coefficients with respect to the temperature and the chemical

potentials, see Eqs. (2.266), (2.303) and (2.331).

In Eqs. (2.339)–(2.341) we identify three classes of second-order terms which are not of the relaxation-type: (i) terms which contain products of the thermodynamic forces with dissipative fluxes [*e.g.*, the term $\propto \theta\Pi$ in Eq. (2.340)]; (ii) terms which contain space-like derivatives of the dissipative fluxes (*e.g.*, $\partial_\mu \mathscr{J}_a^\mu$); and (iii) terms which include a product of two thermodynamic forces (*e.g.*, $\sigma_{\mu\nu}\sigma^{\mu\nu}$). The terms of the type (i) originate either from the non-local corrections [second terms on the right-hand sides of Eqs. (2.339)–(2.341)], or from the second-order corrections to the operator $\hat{C}$ [see Eq. (2.228)]. The corrections of the type (ii) arise purely from the operator $\hat{C}_2$. As we discussed in Sec. 2.5.1, the operator $\hat{C}_2$ originates form the dissipative terms of hydrodynamics equations (2.54)–(2.56) and can be viewed as an *extended thermodynamic force*. Thus, the coefficients $\zeta_\beta$, $\tilde{\zeta}_\beta$ and $\zeta_{\alpha_a}$ in Eq. (2.340) and $\chi_{aq}$ in Eq. (2.341) represent the mixing of the transport equations with the conservation laws. We note also, that such mixed terms are absent in the evolution equation (2.339) for the shear stress tensor. The transport coefficients in the terms of type (i) and (ii) are related to two-point correlation functions [see Eqs. (2.289), (2.290), (2.292) and (2.319)].

The corrections of the type (iii) contain all possible combinations which are quadratic in the thermodynamic forces $\sigma_{\mu\nu}$, $\theta$ and $\nabla_\mu\alpha_a$. For example, the relevant corrections for the shear stress tensor are given by three terms which are allowed by the symmetries: $\theta\sigma_{\mu\nu}$, $\sigma_{\rho<\mu}\sigma^\rho_{\nu>}$ and $\nabla_{<\mu}\alpha_a\nabla_{\nu>}\alpha_b$. The transport coefficients coupled with these terms include three-point correlation functions which account for nonlinear couplings between different dissipative processes.

We remark, that because of the terms of the type (iii) the transport equations become parabolic, and, therefore, acausal and unstable [46,196]. This problem can be circumvented by modifying some of the nonlinear terms using the NS equations, *e.g.*, $\lambda_\pi\sigma_{\rho<\mu}\sigma^\rho_{\nu>}$ can be replaced by $(\lambda_\pi/2\eta)\pi_{\rho<\mu}\sigma^\rho_{\nu>}$ [46, 196]. In this case we recover most of the terms of the complete IS equations derived in Ref. [44].

We also note that our transport equations (2.339)–(2.341) do not contain the vorticity terms. In order to derive these terms one needs to include initially a non-zero vorticity to modify the energy-momentum tensor in the local equilibrium distribution [212].

### 2.6.2 Comparison with other studies

In this subsection we discuss in more detail the second-order expression for the shear stress tensor and compare it with results of other studies, specifically with those of Baier *et al.* [39] and Romatschke [197].

For the sake of simplicity we will consider a fluid without conserved charges. Equation (2.185) implies then $\gamma \equiv c_s^2$, with $c_s$ being the speed of sound. It is more suitable to use here the expression for the shear stress tensor given by Eq. (2.263)

$$\pi_{\mu\nu} = 2\eta\sigma_{\mu\nu} - 2\eta\tau_\pi(\dot{\sigma}_{\mu\nu} + c_s^2\theta\sigma_{\mu\nu}) + 2\lambda_{\pi\Pi}\theta\sigma_{\mu\nu} + \lambda_\pi\sigma_{\alpha<\mu}\sigma^\alpha_{\nu>}, \tag{2.344}$$

where $\dot{\sigma}_{\mu\nu} \equiv \Delta_{\mu\nu\rho\sigma}D\sigma^{\rho\sigma}$. We recall that the terms in the brackets are those which arise from the non-locality of the thermodynamic parameters in the statistical operator (see Sec. 2.5.3). The next two terms in Eq. (2.344) arise from the quadratic terms of the expansion of the statistical operator in thermodynamic forces. Thus, the second-order corrections to the shear stress tensor in the absence of consereved charges contain three new coefficients: $\tau_\pi$, $\lambda_\pi$ and $\lambda_{\pi\Pi}$.

The second-order terms in the brackets in Eq. (2.344) have a simple physical interpretation. The effects of non-locality generate two distinct terms in the shear stress tensor. The first term in the brackets involves the covariant time-derivative of the thermodynamic force $\sigma_{\mu\nu}$ and incorporates the effect of the acceleration of the fluid on the shear stresses. In other words, this term contains information about the velocity stresses $\sigma_{\mu\nu}$ from the previous moments of time. The relaxation time $\tau_\pi$ measures how long this information remains in the "memory" of the shear stress tensor $\pi_{\mu\nu}$. Thus, the first term in Eq. (2.344) can be associated with the non-locality of the statistical operator *in time*, *i.e.*, it is related to *memory effects*.

We argue that the second term in brackets in Eq. (2.344) accounts for *spatial* non-local effects. Indeed, this term involves the product of the thermodynamic force $\sigma_{\mu\nu}$ with the fluid 4-divergence $\theta = \partial_\mu u^\mu$, which can be regarded as a relevant (scalar) measure of how strong the spatial "non-locality" in the fluid velocity field is. This term describes how the shear stress tensor is distorted by uniform expansion or contraction of the fluid.

Next we discuss the last two terms in Eq. (2.344). These terms are quadratic in the thermodynamic forces $\sigma_{\mu\nu}$ and $\theta$. The relevant second-order transport coefficients are expressed via three-point correlation functions by the formulas

$$\lambda_\pi = \frac{12}{35}\beta^2 \int d^4x_1 d^4x_2 \Big(\hat{\pi}^\delta_\gamma(x), \hat{\pi}^\lambda_\delta(x_1), \hat{\pi}^\gamma_\lambda(x_2)\Big), \tag{2.345}$$

$$\lambda_{\pi\Pi} = -\frac{\beta^2}{5} \int d^4x_1 d^4x_2 \Big(\hat{\pi}_{\gamma\delta}(x), \hat{\pi}^{\gamma\delta}(x_1), \hat{p}^*(x_2)\Big). \tag{2.346}$$

The coefficient $\lambda_\pi$ describes nonlinear effects of two velocity stresses on $\pi_{\mu\nu}$. By analogy with the relevant linear transport coefficient $\eta$, which measures the correlation between two shear stresses, the second-order coefficient $\lambda_\pi$ measures the correlation between three shear stresses. The coefficient $\lambda_{\pi\Pi}$ describes the nonlinear coupling between the shear and the bulk viscous processes. Similarly, this coefficient is given by a three-point correlation function between two shear stresses and the bulk viscous pressure.

We remark that $\lambda_{\pi\Pi}$ term in Eq. (2.344) has the same gradient structure $\theta\sigma_{\mu\nu}$ as the second term in the brackets. However, despite this formal similarity, these two terms have different origin and, therefore, different physical interpretation. As explained above, the relevant term $\propto \tau_\pi$ originates from *non-local* effects in the statistical distribution, whereas the term $\propto \lambda_{\pi\Pi}$ stands purely for *nonlinear* coupling between the bulk and the shear viscous effects. In this sense it is natural to regard as nonlinear only the term $\propto \lambda_{\pi\Pi}$, but not the term $\propto \tau_\pi$. A similar classification of the second-order terms was suggested also in Ref. [198].

It is interesting to compare our expression for the shear stress tensor (2.344) to the one specified by Baier *et al.* [39] for conformal fluids. The most general second-order expression for the shear stress tensor of a conformal fluid in the flat space-time reads [2]

$$\pi^c_{\mu\nu} = 2\eta\sigma_{\mu\nu} - 2\eta\tau_\pi\left(\dot{\sigma}_{\mu\nu} + \frac{1}{3}\theta\sigma_{\mu\nu}\right) + \lambda_1\sigma_{\alpha<\mu}\sigma^\alpha_{\nu>} + \lambda_2\sigma_{\alpha<\mu}\omega^\alpha_{\nu>} + \lambda_3\omega_{\alpha<\mu}\omega^\alpha_{\nu>}, \tag{2.347}$$

where $w_{\alpha\beta} = (\nabla_\alpha u_\beta - \nabla_\beta u_\alpha)/2$ is the vorticity tensor.

In the case of a conformal fluid we have $c_s^2 = 1/3$. Furthermore, because the conformal invariance implies vanishing bulk viscous pressure, it is natural to expect that the correlations involving the relevant operator $\hat{p}^*$ [see Eq. (2.187)] vanish as well, *i.e.*, $\lambda_{\pi\Pi} = 0$ in this case. We then recover from Eq. (2.344) the term involving $\tau_\pi$ in Eq. (2.347). Hence we conclude, that the terms $\propto \tau_\pi$ in Eq. (2.347) given by Baier *et al.* have a non-local origin. For the rest of the terms we identify $\lambda_1 = \lambda_\pi$, $\lambda_2 = \lambda_3 = 0$.

In the case of non-conformal fluids Eq. (2.347) obtains two additional terms (in flat space-time), as shown by Romatschke [197]. One of those terms shares the same structure with the term $-2\eta\tau_\pi\theta\sigma_{\mu\nu}/3$ and can be written, after converting to our notations, as $-2\eta\tau^*_\pi\theta\sigma_{\mu\nu}/3$. Comparing with our expression (2.344), we identify $\tau^*_\pi = \tau_\pi(3c_s^2 - 1) - 3\lambda_{\pi\Pi}/\eta$. Our formula for $\tau^*_\pi$ contains an additional term $\propto \lambda_{\pi\Pi}$ compared to the formula given by Romatschke [197] for a special class of strongly coupled fluids.

[2] Note that Baier *et al.* use metric convention opposite to ours, and their definition of the shear viscosity differs from ours by a factor of 2.

### 2.6.3 Concluding remarks

In this chapter we provided a novel derivation of the second-order relativistic hydrodynamics for strongly correlated systems. We adopted Zubarev's non-equilibrium statistical operator formalism and extended the existing studies of relativistic dissipative hydrodynamics within this formalism up to the second-order in thermodynamic gradients. We considered a multicomponent quantum system in the hydrodynamic regime, where it is described by means of the energy-momentum tensor and the currents of conserved charges.

After a short review on the phenomenological theories of relativistic hydrodynamics, we presented in detail Zubarev's method of construction of a full non-equilibrium statistical operator from the quantum Liouville equation. The *exact* solution of the Liouville equation is constructed in the form of a non-local functional of thermodynamic parameters and their space-time derivatives. A suitable expansion of the statistical operator with respect to the thermodynamic gradients which captures the low-frequency and the long-wavelengh dynamics of the system allows one to derive the transport equations for dissipative quantities in principle at *any order*.

Exploiting the gradient expansion of the statistical operator we derived second-order transport equations for the shear stress tensor, the bulk viscous pressure and the flavor diffusion currents. In particular, we obtained new non-local terms which do not appear in the first-order treatments of Refs. [67, 68, 70, 202]. We classified the second-order terms by observing that they arise from two different sources: (i) the quadratic terms in the Taylor expansion of the statistical operator; (ii) the linear terms of these expansion with proper inclusion of effects of memory and non-locality. The terms of the type (i) generate corrections which are quadratic (nonlinear) in thermodynamic forces. The terms of the type (ii) generate the relaxation terms for the dissipative fluxes, which are required for the causality. Apart from these non-local terms, the corrections from the class (ii) include also additional second-order terms which account for mixing of the transport equations with the conservation laws. These last type of corrections contribute only to the bulk viscous pressure and to the diffusion currents.

We obtained also formal expressions for all second-order transport coefficients in terms of certain two- and three-point equilibrium correlation functions, computation of which can be performed by applying standard thermal field theory methods [180–183]. In particular, we derived Kubo-type formulas for the relaxation times, which are given via the frequency-derivatives of the relevant first-order transport coefficients, taken in the relevant zero-frequency limit.

We found that in the absence of diffusion currents and fluid vorticity the second-order expression for the shear stress tensor contains in general three second-order transport coefficients, among which the shear relaxation time $\tau_\pi$ and two other coefficients which are responsible for nonlinear couplings between shear and bulk viscous effects. We also compared and identified the second-order terms of our expression for the shear stress tensor with those given in Refs. [39, 197].

It would be interesting to compute the second-order transport coefficients derived in this work for strongly interacting QCD matter. Of special importance are the shear and the bulk relaxation times, which are necessary for hydrodynamic simulations of heavy-ion collisions. The studies of this chapter can be extended to include also fluid vorticity terms, which are important for the hydrodynamic description of systems with quantum anomalies.

# Chapter 3

# Transport coefficients of two-flavor quark matter from the Kubo formalism

## 3.1 Introduction

The transport coefficients of strongly interacting matter in the regime where quarks are liberated to form an interacting quark-gluon plasma are of interest in a number of contexts. The high-temperature and low-density regime of the phase diagram of deconfined QCD matter is explored by heavy-ion collision experiments at RHIC and LHC. The collective dynamics of QCD plasma in these experiments is well described by hydrodynamical models with an extremely low value of the shear viscosity [1–12]. The ratio of the shear viscosity to the entropy density is close to the lower bound placed by the uncertainty principle [80] and conjectured from AdS/CFT duality arguments [81, 174].

The high-density and low-temperature regime of the QCD phase diagram is of great interest in the astrophysics of compact stars, where transport coefficients of deconfined QCD matter are an important input in modelling an array of astrophysical phenomena [213–216]. The intermediate regime of moderately dense and cold deconfined QCD matter, which is targeted by the FAIR program at GSI [172] and the NICA facility at JINR [173], provides a further motivation for studies of the transport coefficients in moderately dense QCD matter close to the chiral phase transition line.

The non-perturbative nature of QCD in the phenomenologically interesting regimes mentioned above precludes the computation of the transport coefficients in full QCD, therefore effective models that capture its low-energy dynamics are required. In this work we use the Nambu–Jona-Lasinio (NJL) model [84, 85], which provides a well-tested framework of low-energy QCD for studies of vacuum and in-matter properties of ensembles of quarks [86–89]. Because this model captures the dynamical chiral symmetry-breaking feature of QCD, it is most suited for the studies of transport coefficients in the vicinity of the chiral phase transition, where the elementary processes contributing to the scattering matrix elements are dominated by mesonic fluctuations.

The transport formalism based on the Boltzmann equation for the quark distribution functions can be applied to strongly interacting ensembles in the limit where the quasiparticle concept is applicable; in that case the collision integral is dominated by two-body collisions between quarks moving in a mean-field between collisions. In this work we use the Kubo-Zubarev formalism [58, 59, 66] as an alternative, in which the transport coefficients are computed from equilibrium correlation functions at nonzero temperature and density. It provides a general framework valid for a strongly interacting system, which is characterized by nontrivial spectral functions, but requires a resummation of an infinite series of diagrams in order to obtain the correct scaling of the transport coefficients with the coupling (even in the weak interaction regime).

The understanding of the elliptic flows observed at heavy-ion collision experiments in terms of dissipative hydrodynamics, in particular the description of the elliptic flow by a low shear viscosity-to-entropy density ratio of the deconfined quark phase stimulated extensive studies of the shear viscosity

of strongly interacting matter. Transport coefficients of QCD matter have been investigated using various methods including perturbative QCD [92,93,217–222], equilibrium correlation functions within the Kubo formalism [91, 223–229], transport simulations of the Boltzmann equation [94, 230–232], relaxation-time approximation to the Boltzmann equation [80, 233–235], lattice methods [236–240] and holographic methods [81, 241–245]. The main emphasis of these studies is the low value of the shear viscosity-to-entropy density ratio required by the hydrodynamical modeling of heavy-ion collision experiments [1–12]. The shear viscosity of quark matter was computed within the NJL model using the Kubo formalism by several authors [91, 224, 225, 227–229]. The problem of the resummation of an infinite series of loops required to obtain the finite-temperature correlation functions of quark matter is simplified by applying a $1/N_c$ power-counting scheme [90], where $N_c$ is the number of colors. At the leading order the loop resummation for the conductivities and the shear viscosity then requires keeping only a single-loop diagram with full (dressed) propagators. Close to the chiral phase transition the quark self-energies are dominated by processes involving mesonic fluctuations, which can be obtained within the NJL model consistent with the two-point correlation functions.

The role of the bulk viscosity, which describes the dissipation in the case where pressure falls out of equilibrium on uniform expansion or contraction of a statistical ensemble, is more subtle. As well known, bulk viscosity vanishes in a number of cases, *e.g.*, for ultrarelativistic and nonrelativistic gases interacting weakly with local forces via binary collisions [71, 203].

The bulk viscosity $\zeta$ of QGP is small in the perturbative regime [210, 246–248], but it was found to be large close to the critical temperature of the chiral phase transition. For example, lattice simulations of the pure gluodynamics close the critical temperature predict $\zeta/s \sim 1$ [249], where $s$ is the entropy density. It is expected that $\zeta$ becomes singular at the critical point of the second-order phase transition [250]. Values of $\zeta/s \sim 1$ affect the description of data in heavy-ion collisions [211] and can lead to a breakdown of the fluid description via onset of cavitation [251].

Controlled computations of the bulk viscosity exist in perturbative QCD which are based on the kinetic theory of relativistic quarks [210, 247, 248]. In the strongly coupled regime various approximate methods were applied, including QCD sum rules in combination with the lattice data on the QCD equation state [247, 252, 253], quasiparticle Boltzmann transport [254–257] and Kubo formalism [229, 258]. Some strongly coupled systems can exhibit zero bulk viscosity if the scale or, more generally, the conformal symmetry is intact. This is the case, for example, in atomic Fermi gases in the unitary limit [259–262], but not in the QCD and QCD-inspired theories when the conformal symmetry is broken by the quark mass terms and/or by dimensionful regularization of the ultraviolet divergences. This is indeed the case in the NJL model of low-energy QCD that we will utilize below.

For completeness, we point out that the bulk viscosity of dense and cold QCD was extensively discussed in the context of compact stars and strange stars because it is the dominant dissipation mechanism to damp the unstable Rossby waves (r-modes) [263–270]. In this regime of QCD the bulk viscosity is dominated by the weak interaction process like $\beta$-decays of quarks $d \to u + e + \bar{\nu}$ or nonleptonic weak process in three-flavor quark matter $u + d \to u + s$. The time scales associated with the weak processes are much larger than the collisional time scale. The situation is an analogue of the case of bulk viscosity of fluids undergoing chemical reactions on time scales much larger than the collisional time scale, which may lead to large bulk viscosity, as shown long ago by Mandelstam and Leontovich [271]. This contribution to the bulk viscosity is called "soft-mode" contribution, because it is described by the response of the system to small frequency perturbations [272]. As we are interested here in the hydrodynamical description of heavy-ion collisions, which have characteristic time scales much shorter than the weak time scale, we will not discuss weak processes. Slow "chemical equilibration" processes may play a role in the bulk viscosity in the multicomponent environment in heavy-ion collisions, but are beyond the scope of this work.

In this chapter we compute the transport coefficients of quark matter at nonzero temperature and density within the NJL model and the Kubo-Zubarev formalism. Our main results concern the electrical and thermal conductivities as well as the bulk viscosity of quark matter within the setup

appropriate for relativistic quantum fields [67–70]. These would enter the hydrodynamical description of a dense QGP in the cases where thermal, charge and pressure relaxations play a phenomenological role. We specifically argue that the one-loop result for the correlation function of quarks, which arises at the leading order of $1/N_c$ expansion for conductivities, cannot be applied for the bulk viscosity, and a resummation of infinite series is required. As a consequence, our results for the bulk viscosity are substantially different from those obtained previously from the one-loop computations. We discuss and update for completeness the shear viscosity of quark matter which was already studied in Refs. [91,224, 225,227]. We consider the regime where the quark self-energies are dominated by mesonic fluctuations, *i.e.*, the regime close to the chiral phase transition line, which is relevant for heavy-ion collisions. Although our method and results can be straightforwardly applied to the dense and cold regime of compact stars, a number of factors, such as nonzero isospin, color superconductivity, and the presence of leptons, would require additional effort.

This chapter is organized as follows. Section 3.2 expresses the transport coefficients in terms of the Lorentz components of the quark spectral function starting from the Kubo formulas. In Sec. 3.3 we discuss dynamically generated quark and meson masses as well as the effective quark-meson couplings within the two-flavor NJL model. In Sec. 3.4 we derive the spectral function of quarks taking into account the full Dirac structure of the self-energies in the case where the dispersive effects arise from quark-meson fluctuations. In Sec. 3.5 we discuss the thermodynamics of the model and compute a number of thermodynamic quantities that are required for the evaluation and discussion of the transport coefficients. Numerical results for the conductivities and the shear viscosity are given in Sec. 3.6. Section 3.7 collects our results for the bulk viscosity. Section 3.8 provides a short summary of our results. Appendix B.1 describes the details of the computation of the bulk viscosity beyond the one-loop approximation. Appendix B.2 is devoted to the computation of the quark self-energy due to meson exchange. We use natural (Gaussian) units with $e = \sqrt{4\pi\alpha}$, where $\alpha = 1/137$ is the fine-structure constant. The content of this chapter is based on the papers [82, 83].

## 3.2 Kubo formulas for transport coefficients

The Kubo-Zubarev formalism relates the transport properties of a statistical ensemble to different types of *equilibrium* correlation functions [58,59,65–67], which in turn can be computed using equilibrium many-body techniques [180–183]. We start our discussion with the Lagrangian of the underlying effective model, as it will specify the power counting required for the computation of the two-point correlation functions.

### 3.2.1 Lagrangian of the model

We consider two-flavor quark matter described by the NJL Lagrangian of the form [84]

$$\mathcal{L} = \bar{\psi}(i\partial\!\!\!/ - m_0)\psi + \frac{G}{2}\left[(\bar{\psi}\psi)^2 + (\bar{\psi}i\gamma_5\boldsymbol{\tau}\psi)^2\right], \tag{3.1}$$

where $\psi = (u, d)^T$ is the iso-doublet quark field, $m_0 = 5.5$ MeV is the current quark mass, $G = 10.1$ GeV$^{-2}$ is the effective four-fermion coupling constant, and $\boldsymbol{\tau}$ is the vector of Pauli isospin matrices. This Lagrangian describes four-fermion scalar-isoscalar and pseudoscalar-isovector contact interactions between quarks with the corresponding bare vertices $\Gamma_s^0 = 1$ and $\Gamma_{ps}^0 = i\boldsymbol{\tau}\gamma_5$. The Lagrangian (3.1) has the global symmetries of the two-flavour QCD: $SU(2) \otimes U(1)$, first of which corresponds to the isospin symmetry and the second one - to the baryon conservation. In the chiral limit $m_0 = 0$ the isospin symmetry is applied independently to the right and left fermions: $SU(2) = SU_V(2) \otimes SU_A(2)$, where the axial symmetry is spontaneously broken. The NJL model features $SU_A(2)$ chiral symmetry breaking (approximate if $m_0 \neq 0$) with pions emerging as the Goldstone modes via dynamically generated quark and meson masses (see Sec. 3.3 for details). Note that the gauge (color) symmetry

$SU_c(3)$ in this model is reduced to a global symmetry, *i.e.*, all quark states are degenerate with the factor $N_c = 3$, which is the number of colors. The four-fermion contact interactions make the model nonrenormalizable, therefore a 3-momentum cutoff ($p \leq \Lambda$) should be applied to regularize the ultraviolet divergences. The cutoff parameter $\Lambda$ together with the current quark mass and the four-fermion coupling constant constitutes the full set of free parameters of the model, the values of which are fitted to experimental values of quark and meson masses and pion decay constant [89]. Below we will adopt the value $\Lambda = 0.65$ GeV [91].

The symmetrized energy-momentum tensor of the model is given in the standard fashion by

$$T_{\mu\nu} = \frac{i}{2}(\bar{\psi}\gamma_\mu\partial_\nu\psi + \bar{\psi}\gamma_\nu\partial_\mu\psi) - g_{\mu\nu}\mathcal{L}, \tag{3.2}$$

and the quark number and charge currents are defined as

$$N_\mu = \bar{\psi}\gamma_\mu\psi, \qquad J_\mu = \bar{\psi}\hat{Q}\gamma_\mu\psi, \tag{3.3}$$

where

$$\hat{Q} = e\begin{pmatrix} 2/3 & 0 \\ 0 & -1/3 \end{pmatrix} \tag{3.4}$$

is the charge matrix in the flavor space with $e$ being the elementary charge. Note that the symmetrization of the energy-momentum tensor (3.2) is necessary for its implementation in Kubo formulas.

### 3.2.2 Thermal and electrical conductivities

Within the Kubo-Zubarev approach the thermal and electrical conductivities are given by the formulas [58, 59, 69, 70, 182] (see also Sec. 2.4.3 in Chapter 2)

$$\kappa = -\frac{\beta}{3}\frac{d}{d\omega}\mathrm{Im}\Pi^R_\kappa(\omega)\Big|_{\omega=0}, \tag{3.5}$$

$$\sigma = -\frac{1}{3}\frac{d}{d\omega}\mathrm{Im}\Pi^R_\sigma(\omega)\Big|_{\omega=0}, \tag{3.6}$$

where $\beta = T^{-1}$ is the inverse temperature, and the retarded correlation functions on the right-hand sides are defined as

$$\Pi^R_\kappa(\omega) = i\int_0^\infty dt\; e^{i\omega t}\int d\boldsymbol{r}\langle[q_\mu(\boldsymbol{r},t), q^\mu(0)]\rangle_0, \tag{3.7}$$

$$\Pi^R_\sigma(\omega) = i\int_0^\infty dt\; e^{i\omega t}\int d\boldsymbol{r}\langle\big[j_\mu(\boldsymbol{r},t), j^\mu(0)\big]\rangle_0, \tag{3.8}$$

*i.e.*, they are the statistical averages of commutators (denoted by $[\cdot,\cdot]$) of the heat and electrical current operators defined, respectively, as (here we use slightly different notations from Chapter 2)

$$q_\mu = \Delta_{\mu\alpha}u_\beta T^{\alpha\beta} - h'\Delta_{\mu\alpha}N^\alpha, \tag{3.9}$$

$$j_\mu = \Delta_{\mu\alpha}J^\alpha. \tag{3.10}$$

Here $u_\beta$ is the 4-velocity of the fluid, $\Delta_{\mu\nu} = g_{\mu\nu} - u_\mu u_\nu$ is the projector on the direction transverse to the fluid velocity, $h'$ is the enthalpy per particle, and the energy-momentum tensor $T^{\mu\nu}$ is assumed to be symmetric in its indices. Note that the heat current (3.9) differs from the net energy flow by the particle-convection term $\propto h'$ (see Sec. 2.2.4 in Chapter 2 for details).

Equations (3.5)–(3.8) apply to arbitrary quantum statistical ensembles without restrictions on the strength of the couplings of the underlying theory. In the following we will derive more specific expressions suitable for the NJL model with contact scalar and pseudoscalar couplings among quarks by applying the $1/N_c$ expansion to select the dominant diagrams contributing to the correlation

functions.

It is convenient to evaluate the correlation functions of interest using the thermal equilibrium Green's functions of the imaginary-time Matsubara technique. In the fluid rest frame $u_\mu = (1,0,0,0)$, $\Delta_{\mu\nu} = \mathrm{diag}(0,-1,-1,-1)$, $j_i = J_i$, $q_i = T_{0i} - h' N_i$, and the Matsubara correlation functions read

$$\Pi^M_\kappa(\omega_n) = \Pi^M_{TT}(\omega_n) - 2h'\Pi^M_{TN}(\omega_n) + h'^2\Pi^M_{NN}(\omega_n), \tag{3.11}$$

$$-\frac{1}{3}\Pi^M_{TT}(\omega_n) = \int_0^\beta d\tau e^{i\omega_n\tau}\int d\boldsymbol{r}\langle\mathcal{T}_\tau(T_{01}(\boldsymbol{r},\tau),T_{01}(0))\rangle_0, \tag{3.12}$$

$$-\frac{1}{3}\Pi^M_{TN}(\omega_n) = \int_0^\beta d\tau e^{i\omega_n\tau}\int d\boldsymbol{r}\langle\mathcal{T}_\tau(T_{01}(\boldsymbol{r},\tau),N_1(0))\rangle_0, \tag{3.13}$$

$$-\frac{1}{3}\Pi^M_{NN}(\omega_n) = \int_0^\beta d\tau e^{i\omega_n\tau}\int d\boldsymbol{r}\langle\mathcal{T}_\tau(N_1(\boldsymbol{r},\tau),N_1(0))\rangle_0, \tag{3.14}$$

$$-\frac{1}{3}\Pi^M_{\sigma}(\omega_n) = \int_0^\beta d\tau e^{i\omega_n\tau}\int d\boldsymbol{r}\langle\mathcal{T}_\tau(J_1(\boldsymbol{r},\tau),J_1(0))\rangle_0, \tag{3.15}$$

where $T_{01}(\boldsymbol{r},\tau)$, $N_1(\boldsymbol{r},\tau)$, and $J_1(\boldsymbol{r},\tau)$ are obtained from $T_{01}(\boldsymbol{r},t)$, $N_1(\boldsymbol{r},t)$, and $J_1(\boldsymbol{r},t)$ via Wick rotation $t \to -i\tau$; $\mathcal{T}_\tau$ is the time-ordering operator for the imaginary time $\tau$, and the factor 3 arises from the summation over the directions of isotropic three-dimensional space. In Eq. (3.11) we decomposed the thermal current according to Eq. (3.9) and used the symmetry of the correlation function with respect to its arguments [58, 70], as shown also in Appendix A.1. The required retarded correlation functions (3.7) and (3.8) can be obtained from Eqs. (3.11)–(3.15) by an analytic continuation $i\omega_n \to \omega + i\delta$. Note that the transformation to imaginary time implies a change of the derivative $\partial_0 \to i\partial_\tau$. Because $T_{\mu\nu}$, $N_\mu$ and $J_\mu$ are bosonic operators, the Matsubara frequencies assume even integer values $\omega_n = 2\pi n T$, $n = 0, \pm 1, \ldots$. The $T_{01}$ component of Eq. (3.2) is given by

$$T_{01}(\boldsymbol{r},\tau) = i\bar\psi(\boldsymbol{r},\tau)\frac{\gamma_0}{2}\partial_1\psi(\boldsymbol{r},\tau) + i\bar\psi(\boldsymbol{r},\tau)\frac{\gamma_1}{2}i\partial_\tau\psi(\boldsymbol{r},\tau). \tag{3.16}$$

Substituting $T_{01}(\boldsymbol{r},\tau)$, $N_1(\boldsymbol{r},\tau)$ and $J_1(\boldsymbol{r},\tau)$ into Eqs. (3.11)–(3.15) we obtain

$$-\frac{1}{3}\Pi^M_{TT}(\omega_n) = \sum_{\alpha,\alpha'}\int_0^\beta d\tau\ e^{i\omega_n\tau}\int d\boldsymbol{r}\langle\mathcal{T}_\tau(i\bar\psi\frac{\gamma_\mu}{2}\partial_\alpha\psi\Big|_{(\boldsymbol{r},\tau)}, i\bar\psi\frac{\gamma_{\mu'}}{2}\partial_{\alpha'}\psi\Big|_0)\rangle_0, \tag{3.17}$$

$$-\frac{1}{3}\Pi^M_{TN}(\omega_n) = \sum_{\alpha}\int_0^\beta d\tau\ e^{i\omega_n\tau}\int d\boldsymbol{r}\langle\mathcal{T}_\tau(i\bar\psi\frac{\gamma_\mu}{2}\partial_\alpha\psi\Big|_{(\boldsymbol{r},\tau)}, \bar\psi\gamma_1\psi\Big|_0)\rangle_0, \tag{3.18}$$

$$-\frac{1}{3}\Pi^M_{NN}(\omega_n) = \int_0^\beta d\tau e^{i\omega_n\tau}\int d\boldsymbol{r}\langle\mathcal{T}_\tau(\bar\psi\gamma_1\psi\Big|_{(\boldsymbol{r},\tau)}, \bar\psi\gamma_1\psi\Big|_0)\rangle_0, \tag{3.19}$$

$$-\frac{1}{3}\Pi^M_{\sigma}(\omega_n) = \int_0^\beta d\tau e^{i\omega_n\tau}\int d\boldsymbol{r}\langle\mathcal{T}_\tau(\bar\psi\hat{Q}\gamma_1\psi\Big|_{(\boldsymbol{r},\tau)}, \bar\psi\hat{Q}\gamma_1\psi\Big|_0)\rangle_0, \tag{3.20}$$

where $\alpha, \alpha', \mu, \mu'$ assume values $1, 0$, with $\mu \neq \alpha, \mu' \neq \alpha'$, *i.e.*, the sums in Eqs. (3.17) and (3.18) contain four and two terms, respectively.

To select the relevant diagrams contributing to the correlation functions we apply the $1/N_c$ power-counting scheme, in which each loop contributes a factor of $N_c$ from the trace over the color space [90, 91, 224, 225, 227–229]. Each coupling $G$ (which is associated with a pair of $\Gamma^0_{s/ps}$ matrices) contributes a factor of $1/N_c$. Therefore, for any given number of $\Gamma^0_{s/ps}$ vertices the leading-order diagram in the $1/N_c$ approximation is the one that has the maximum number of loops. Figure 3.1 shows the diagrammatic expansion for the two-point correlation function, which we define in a generic form

$$\Pi^{\alpha\alpha'}_{\mu\mu'}(\omega_n) = \int_0^\beta d\tau e^{i\omega_n\tau}\int d\boldsymbol{r}\langle\mathcal{T}_\tau(i\bar\psi\gamma_\mu\partial^\alpha\psi\Big|_{(\boldsymbol{r},\tau)}, i\bar\psi\gamma_{\mu'}\partial^{\alpha'}\psi\Big|_0)\rangle_0, \tag{3.21}$$

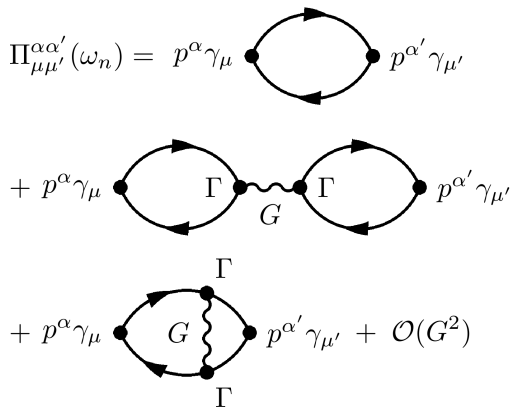


Figure 3.1: Contributions to the two-point correlation functions from $\mathcal{O}(N_c^1)$ (first and second lines) and $\mathcal{O}(N_c^0)$ (the third line) diagrams which contain a single interaction line $G$.

where $\partial_\alpha = (i\partial_\tau, \partial_i)$. The diagrams are arranged according to the $1/N_c$ expansion. The first line contains a loop and no coupling $G$ and is of the order of $N_c$; the second line contains two loops and a coupling, and therefore is again of the order of $N_c$; the third line, which contains a loop and a coupling, is of the order of $N_c^0$. Thus, the correlation function (3.21) at the leading $[\mathcal{O}(N_c^1)]$ order is given by a sum of loop diagrams which contain the single-loop contribution (first line in Fig. 3.1)

$$T\sum_l \int \frac{d\boldsymbol{p}}{(2\pi)^3} p^\alpha p^{\alpha'} \mathrm{Tr}\left[\gamma_\mu G(\boldsymbol{p}, i\omega_l + i\omega_n)\gamma_{\mu'} G(\boldsymbol{p}, i\omega_l)\right], \tag{3.22}$$

plus multi-loop contributions which necessarily contain loop contributions of the type

$$T\sum_l \int \frac{d\boldsymbol{p}}{(2\pi)^3} p^\alpha \mathrm{Tr}\left[\gamma_\mu G(\boldsymbol{p}, i\omega_l + i\omega_n)\Gamma^0_{s/ps} G(\boldsymbol{p}, i\omega_l)\right], \tag{3.23}$$

see the second line in Fig. 3.1. Here $G(\boldsymbol{p}, i\omega_l)$ is the dressed Matsubara Green's function of quarks, the summation goes over fermionic Matsubara frequencies $\omega_l = \pi(2l+1)T - i\mu$, $l = 0, \pm 1, \ldots$, with temperature $T$ and chemical potential $\mu$; (in isospin-symmetric two-flavor quark matter there is a single chemical potential for both $u$ and $d$ quarks). The traces should be taken in the Dirac, color, and flavor space. The Lorentz structure of the Green's function implies that (i) diagrams of type (3.23) with pseudoscalar vertices vanish due to the trace over the Dirac space and (ii) those with scalar vertices vanish if $\alpha \neq \mu$, because the integrand has an odd power of momentum, which implies that the momentum integral vanishes in isotropic momentum space. Thus, the only term contributing to Eq. (3.17) is the one-loop expression (3.22). In the same way one can see that the multi-loop diagrams vanish also for the other three correlation functions (3.18)–(3.20). Thus, for the correlation functions (3.17)–(3.20) we obtain

$$\frac{1}{3}\Pi^M_{TT}(\omega_n) = \frac{T}{4}\sum_l \sum_{\alpha,\alpha'} \int \frac{d\boldsymbol{p}}{(2\pi)^3} p_\alpha p_{\alpha'} \mathrm{Tr}\left[\gamma_\mu G(\boldsymbol{p}, i\omega_l + i\omega_n)\gamma_{\mu'} G(\boldsymbol{p}, i\omega_l)\right], \tag{3.24}$$

$$\frac{1}{3}\Pi^M_{TN}(\omega_n) = \frac{T}{2}\sum_l \sum_{\alpha} \int \frac{d\boldsymbol{p}}{(2\pi)^3} p_\alpha \mathrm{Tr}\left[\gamma_1 G(\boldsymbol{p}, i\omega_l + i\omega_n)\gamma_\mu G(\boldsymbol{p}, i\omega_l)\right], \tag{3.25}$$

$$\frac{1}{3}\Pi^M_{NN}(\omega_n) = T\sum_l \int \frac{d\boldsymbol{p}}{(2\pi)^3} \mathrm{Tr}\left[\gamma_1 G(\boldsymbol{p}, i\omega_l + i\omega_n)\gamma_1 G(\boldsymbol{p}, i\omega_l)\right], \tag{3.26}$$

$$\frac{1}{3}\Pi^M_{\sigma}(\omega_n) = T\sum_l \int \frac{d\boldsymbol{p}}{(2\pi)^3} \mathrm{Tr}\left[\hat{Q}\gamma_1 G(\boldsymbol{p}, i\omega_l + i\omega_n)\hat{Q}\gamma_1 G(\boldsymbol{p}, i\omega_l)\right], \tag{3.27}$$

where $p_\alpha, p_{\alpha'}$ assume values $p_1$ and $p_0 = i\omega_l + i\omega_n/2$. Note that the expressions (3.24)–(3.27) are valid in a wider context, *i.e.*, in any relativistic theory where the single-loop (skeleton) diagram with fully dressed propagators constitutes the leading-order contribution in the power-counting scheme. The Matsubara summations appearing in these expressions can be cast into the general form

$$S_{\mu\nu}\left[f\right](\boldsymbol{p}, i\omega_n) = T\sum_l f(i\omega_l + i\omega_n/2)\mathrm{Tr}\left[\gamma_\mu G(\boldsymbol{p}, i\omega_l + i\omega_n)\gamma_\nu G(\boldsymbol{p}, i\omega_l)\right], \tag{3.28}$$

where $f(z) = z^k$ with $k = 0, 1, 2$. The summation is standard upon introducing the spectral representation of the temperature Green's functions

$$G(\boldsymbol{p}, z) = \int_{-\infty}^{\infty} d\varepsilon \frac{A(\boldsymbol{p}, \varepsilon)}{z - \varepsilon}, \tag{3.29}$$

where the spectral function is given by

$$A(\boldsymbol{p}, \varepsilon) = -\frac{1}{2\pi i}\left[G^R(\boldsymbol{p}, \varepsilon) - G^A(\boldsymbol{p}, \varepsilon)\right], \tag{3.30}$$

and $G^{R/A}$ are the retarded/advanced Green's functions. According to Eq. (3.29), $G(\boldsymbol{p}, z)$ has a branch cut on the real axis, therefore a calculation of the residues gives for Eq. (3.28)

$$S_{\mu\nu}\left[f\right](\boldsymbol{p}, i\omega_n) = -\int_C \frac{dz}{2\pi i}\tilde{n}(z) f(z + i\omega_n/2)\mathrm{Tr}\left[\gamma_\mu G(\boldsymbol{p}, z + i\omega_n)\gamma_\nu G(\boldsymbol{p}, z)\right], \tag{3.31}$$

where $n(z) = [e^{\beta(z-\mu)} + 1]^{-1}$ is the Fermi distribution function, and $\tilde{n}(z) = n(z) - 1/2$. The integration contour $C$ is shown in Fig. 3.2, where the circle should be taken infinitely large in order to include all poles of the function $n(z)$. Note that due to the fact that $\omega_n$ does not coincide with $\omega_l$ for any $n$ and $l$, the poles of $n(z)$ do not lie on the branch cuts of $C$.

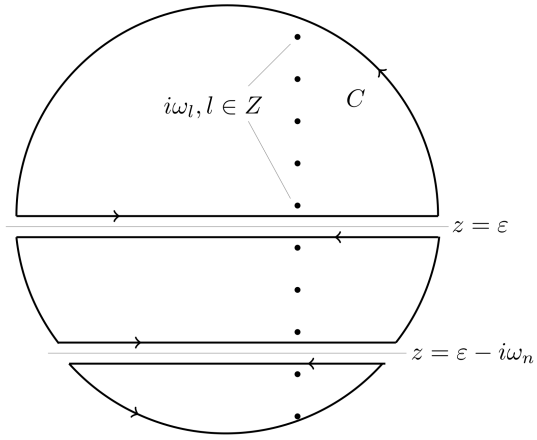


Figure 3.2: The contour of integration in Eq. (3.31). The dots correspond to the fermionic Matsubara frequencies.

We show now that the contribution of the large circle to the integral (3.31) vanishes. Because of the sum rule $\int_{-\infty}^{\infty} d\varepsilon A(\boldsymbol{p}, \varepsilon) = \text{const} \propto \gamma_0$ the quark propagator for large $|z|$ has the scaling $G \propto z^{-1}$. Therefore for large $|z|$ the integrand in Eq. (3.31) scales as $\propto \tilde{n}(z) z^{k-2}$ (recall that $f \propto z^k$). For the Fermi distribution function we have the asymptotics $n(z) \to_{\mathrm{Re}z\to\infty} 0$ and $n(z) \to_{\mathrm{Re}z\to-\infty} 1$.

Substituting $z = Re^{i\phi}, dz = iRe^{i\phi}d\phi, R \to \infty$, for the integral along the circle we can write

$$S_R[f] \propto -\int_{C_R} \frac{dz}{2\pi i} z^{k-2}\tilde{n}(z) = \frac{R^{k-1}}{4\pi}\left[\int_{-\pi/2}^{\pi/2} d\phi e^{i(k-1)\phi} - \int_{\pi/2}^{3\pi/2} d\phi e^{i(k-1)\phi}\right] = \frac{R^{k-1}}{\pi}\begin{cases} \frac{\sin(k-1)\pi/2}{k-1}, & k \neq 1, \\ 0, & k = 1. \end{cases} \tag{3.32}$$

As seen from Eq. (3.32), the integral vanishes in the limit $R \to \infty$ if $k = 0, 1$. If $k = 2$, we have $S \propto R \to \infty$, which is purely real and can be dropped since we need only the imaginary parts of $S[f]$ functions. As a result, we have to keep only the integrals along the two branch cuts shown in Fig. 3.2. Substitution of Eq. (3.30) gives for Eq. (3.31)

$$S_{\mu\nu}[f](\boldsymbol{p}, i\omega_n) = \int_{-\infty}^{\infty} d\varepsilon \tilde{n}(\varepsilon)\Big\{f(\varepsilon - i\omega_n/2)\mathrm{Tr}[\gamma_\mu A(\boldsymbol{p},\varepsilon)\gamma_\nu G(\boldsymbol{p}, \varepsilon - i\omega_n)] + f(\varepsilon + i\omega_n/2)\mathrm{Tr}[\gamma_\mu G(\boldsymbol{p}, \varepsilon + i\omega_n)\gamma_\nu A(\boldsymbol{p},\varepsilon)]\Big\}, \tag{3.33}$$

where we took into account that $n(\varepsilon - i\omega_n) = n(\varepsilon)$. Substituting the spectral representation (3.29) into Eq. (3.33), changing the variables $\varepsilon \leftrightarrow \varepsilon'$ in the first term and analytically continuing via $i\omega_n \to \omega + i\delta$ we find

$$S_{\mu\nu}[f](\boldsymbol{p}, \omega) = \int_{-\infty}^{\infty} d\varepsilon \int_{-\infty}^{\infty} d\varepsilon' \mathrm{Tr}[\gamma_\mu A(\boldsymbol{p}, \varepsilon')\gamma_\nu A(\boldsymbol{p}, \varepsilon)] \frac{\tilde{n}(\varepsilon) f(\varepsilon + \omega/2) - \tilde{n}(\varepsilon') f(\varepsilon' - \omega/2)}{\varepsilon - \varepsilon' + \omega + i\delta}. \tag{3.34}$$

Finally, we separate the real and imaginary parts in Eq. (3.34) via the Dirac identity

$$\frac{1}{x + i\delta} = P\frac{1}{x} - i\pi\delta(x) \tag{3.35}$$

in order to find the required $\omega \to 0$ limit. We find from Eqs. (3.34) and (3.35)

$$\mathrm{Im}S_{\mu\nu}[f](\boldsymbol{p}, \omega) = \pi \int_{-\infty}^{\infty} d\varepsilon [\tilde{n}(\varepsilon + \omega) - \tilde{n}(\varepsilon)] f(\varepsilon + \omega/2)\mathrm{Tr}[\gamma_\mu A(\boldsymbol{p}, \varepsilon + \omega)\gamma_\nu A(\boldsymbol{p}, \varepsilon)], \tag{3.36}$$

and

$$\frac{d}{d\omega}\mathrm{Im}S_{\mu\nu}[f](\boldsymbol{p}, \omega)\Big|_{\omega=0} = \pi \int_{-\infty}^{\infty} d\varepsilon \frac{\partial n(\varepsilon)}{\partial \varepsilon} f(\varepsilon)\mathcal{T}_{\mu\nu}(\boldsymbol{p}, \varepsilon), \tag{3.37}$$

where

$$\mathcal{T}_{\mu\nu}(\boldsymbol{p}, \varepsilon) \equiv \mathrm{Tr}[\gamma_\mu A(\boldsymbol{p}, \varepsilon)\gamma_\nu A(\boldsymbol{p}, \varepsilon)]. \tag{3.38}$$

Substituting Eqs. (3.28) and (3.34) into the correlation functions (3.24)–(3.27) we obtain

$$\frac{1}{3}\Pi_{TT}(\omega) = \frac{1}{4}\int \frac{d\boldsymbol{p}}{(2\pi)^3}\{p_1^2 S_{00}[f = 1] + 2p_1 S_{01}[f = \varepsilon] + S_{11}[f = \varepsilon^2]\}(\boldsymbol{p}, \omega), \tag{3.39}$$

$$\frac{1}{3}\Pi_{TN}(\omega) = \frac{1}{2}\int \frac{d\boldsymbol{p}}{(2\pi)^3}\{p_1 S_{10}[f = 1] + S_{11}[f = \varepsilon]\}(\boldsymbol{p}, \omega), \tag{3.40}$$

$$\frac{1}{3}\Pi_{NN}(\omega) = \int \frac{d\boldsymbol{p}}{(2\pi)^3} S_{11}[f = 1](\boldsymbol{p}, \omega), \tag{3.41}$$

$$\frac{1}{3}\Pi_{\sigma}(\omega) = \frac{1}{3}\Pi_{NN}(\omega) \times \frac{\mathrm{Tr}\hat{Q}^2}{N_f}, \tag{3.42}$$

with $N_f$ being the number of flavors. Substituting Eqs. (3.37)–(3.42) into Eqs. (3.5), (3.6) and (3.11),

we obtain the following expressions for thermal and electrical conductivities

$$\kappa = -\frac{\pi}{4T}\int_{-\infty}^{\infty} d\varepsilon \frac{\partial n(\varepsilon)}{\partial \varepsilon}\int \frac{d\boldsymbol{p}}{(2\pi)^3}\left[p_1^2\mathcal{T}_{00}(\boldsymbol{p},\varepsilon)+2p_1(\varepsilon-2h')\mathcal{T}_{01}(\boldsymbol{p},\varepsilon)+(\varepsilon-2h')^2\mathcal{T}_{11}(\boldsymbol{p},\varepsilon)\right], \quad (3.43)$$

$$\sigma = -\pi\frac{\mathrm{Tr}\hat{Q}^2}{N_f}\int_{-\infty}^{\infty} d\varepsilon \frac{\partial n(\varepsilon)}{\partial \varepsilon}\int \frac{d\boldsymbol{p}}{(2\pi)^3}\mathcal{T}_{11}(\boldsymbol{p},\varepsilon). \quad (3.44)$$

Thus, the problem of computing the transport coefficients reduces to the determination of the spectral function of the quarks followed by computing the components of the trace $\mathcal{T}_{\mu\nu}(\boldsymbol{p},\varepsilon)$.

The quark spectral function in an isotropic medium has a general decomposition in terms of Lorentz components [91, 273]

$$A(\boldsymbol{p},p_0) = -\frac{1}{\pi}(mA_s + p_0\gamma_0 A_0 - \boldsymbol{p}\cdot\boldsymbol{\gamma}A_v), \quad (3.45)$$

where the coefficients $A_s, A_0, A_v$ are expressed in terms of the analogous components of the self-energy in Sec. 3.4. Using Eq. (3.45) and the well-known formulas

$$\mathrm{Tr}[\gamma_\mu\gamma_\nu] = 4g_{\mu\nu}, \qquad \mathrm{Tr}[\gamma_\mu\gamma_\nu\gamma_\alpha\gamma_\beta] = 4(g_{\mu\nu}g_{\alpha\beta} - g_{\mu\alpha}g_{\nu\beta} + g_{\mu\beta}g_{\nu\alpha}), \quad (3.46)$$

we obtain for Eq. (3.38)

$$\begin{aligned}\pi^2\mathcal{T}_{\mu\nu}(\boldsymbol{p},p_0) &= 4(A_s^2m^2 - A_0^2p_0^2 + A_v^2\boldsymbol{p}^2)g_{\mu\nu} + 8\big[A_0^2p_0^2g_{\mu0}g_{\nu0} \\ &\quad + A_v^2p_ip_jg_{\mu i}g_{\nu j} - A_0A_vp_0p_i(g_{\mu i}g_{\nu0}+g_{\mu0}g_{\nu i})\big],\end{aligned} \quad (3.47)$$

and for various components

$$\pi^2\mathcal{T}_{00} = 4(A_s^2m^2 + A_0^2p_0^2 + A_v^2\boldsymbol{p}^2), \qquad \pi^2\mathcal{T}_{01} = 8A_0A_vp_0p_1, \quad (3.48)$$

$$\pi^2\mathcal{T}_{11} = -4(A_s^2m^2 - A_0^2p_0^2 + A_v^2\boldsymbol{p}^2) + 8A_v^2p_1^2, \qquad \pi^2\mathcal{T}_{12} = 8A_v^2p_1p_2. \quad (3.49)$$

Substituting these expressions into Eqs. (3.43) and (3.44) we obtain

$$\begin{aligned}\kappa &= -\frac{N_cN_f}{\pi T}\int_{-\infty}^{\infty} d\varepsilon\frac{\partial n(\varepsilon)}{\partial\varepsilon}\int\frac{d\boldsymbol{p}}{(2\pi)^3}\Big\{p_1^2(A_s^2m^2 + A_0^2\varepsilon^2 + A_v^2\boldsymbol{p}^2) + 4p_1^2\varepsilon(\varepsilon-2h')A_0A_v \\ &\quad -(\varepsilon-2h')^2(A_s^2m^2 - A_0^2\varepsilon^2 + A_v^2\boldsymbol{p}^2 - 2A_v^2p_1^2)\Big\},\end{aligned} \quad (3.50)$$

$$\sigma = -\frac{4N_c}{\pi}\mathrm{Tr}\hat{Q}^2\int_{-\infty}^{\infty} d\varepsilon\frac{\partial n(\varepsilon)}{\partial\varepsilon}\int\frac{d\boldsymbol{p}}{(2\pi)^3}(-A_s^2m^2 + A_0^2\varepsilon^2 - A_v^2\boldsymbol{p}^2 + 2A_v^2p_1^2), \quad (3.51)$$

where we summed over the quark flavor ($N_f$) and color ($N_c$) numbers. Finally, we note that the coefficients $A_s, A_0$ and $A_v$ of the decomposition of the spectral function depend only on $\boldsymbol{p}^2$ and $\varepsilon$ (see below, Sec. 3.4), therefore the angular integration can be done trivially by substituting $p_1^2 \to \boldsymbol{p}^2/3 \equiv p^2/3$, after which we finally obtain

$$\begin{aligned}\kappa &= -\frac{N_cN_f}{6\pi^3T}\int_{-\infty}^{\infty} d\varepsilon\frac{\partial n}{\partial\varepsilon}\int_0^\Lambda dpp^2\Big\{\left[A_s^2(p,\varepsilon)m^2 - A_0^2(p,\varepsilon)\varepsilon^2 + A_v^2(p,\varepsilon)p^2\right] \\ &\quad \times[p^2 - 3(\varepsilon-2h')^2] + 2\big[A_0(p,\varepsilon)\varepsilon + A_v(p,\varepsilon)(\varepsilon-2h')\big]^2p^2\Big\},\end{aligned} \quad (3.52)$$

$$\sigma = \frac{40N_c\alpha}{27\pi^2}\int_{-\infty}^{\infty} d\varepsilon\frac{\partial n}{\partial\varepsilon}\int_0^\Lambda dpp^2\left[3A_s^2(p,\varepsilon)m^2 - 3A_0^2(p,\varepsilon)\varepsilon^2 + A_v^2(p,\varepsilon)p^2\right], \quad (3.53)$$

where we applied a 3-momentum cutoff. In Eq. (3.53) we took into account that $\mathrm{Tr}\hat{Q}^2 = 5e^2/9 = 20\pi\alpha/9$, see Eq. (3.4), with $\alpha$ being the fine structure constant. Given the Lorentz components of the

spectral function we are in a position to compute the thermal and electrical conductivities of two-flavor quark matter using our final expressions (3.52) and (3.53).

### 3.2.3 Shear viscosity

Within the Kubo formalism the shear viscosity is given as [68–70] (see also Sec. 2.4.3 in Chapter 2)

$$\eta = -\frac{1}{10}\frac{d}{d\omega}\mathrm{Im}\Pi^{\mathrm{R}}_{\eta}(\omega)\Big|_{\omega=0}, \tag{3.54}$$

where the relevant retarded correlation function has the form

$$\Pi^{R}_{\eta}(\omega) = -i\int_0^\infty dt\; e^{i\omega t}\int d\boldsymbol{r}\langle[\pi_{\mu\nu}(\boldsymbol{r},t),\pi^{\mu\nu}(0)]\rangle_0, \tag{3.55}$$

with $\pi_{\mu\nu}$ being the shear-viscosity tensor, defined as

$$\pi_{\mu\nu} = \Delta^{\alpha\beta}_{\mu\nu}T_{\alpha\beta}, \tag{3.56}$$

where

$$\Delta^{\alpha\beta}_{\mu\nu} = \frac{\Delta^{\alpha}_{\mu}\Delta^{\beta}_{\nu}+\Delta^{\beta}_{\mu}\Delta^{\alpha}_{\nu}}{2} - \frac{1}{3}\Delta_{\mu\nu}\Delta^{\alpha\beta}. \tag{3.57}$$

It is useful to note that $\Delta^{\alpha\beta}_{\mu\nu}g_{\alpha\beta} = 0$ by definition, therefore the component of the energy-momentum tensor (3.2) containing $g_{\mu\nu}$ does not contribute to Eq. (3.56).

In the fluid rest frame $\Delta^{j}_{i} = \delta_{ij}$, $\Delta^{0}_{0} = \Delta^{j}_{0} = 0$, where $i,j = 1,2,3$, and $\delta_{ij}$ is the Kronecker symbol. In this frame only the spatial components of Eq. (3.56), *i.e.*, $\pi_{ij} = T_{ij} - \delta_{ij}T_{mm}/3$, are nonzero. Then, the two-point correlation function (3.55) takes the form

$$\Pi^{R}_{\eta}(\omega) = -2i\int_0^\infty dt e^{i\omega t}\int d\boldsymbol{r}\langle[T_{11},T_{11}] - [T_{11},T_{22}] + 3[T_{12},T_{12}]\rangle_0, \tag{3.58}$$

where we took into account the isotropy of the medium and for the sake of brevity omitted the arguments of the $T_{ij}$ tensors. The Matsubara counterpart of the function (3.58) is given by

$$\Pi^{M}_{\eta}(\omega_n) = -2\int_0^\beta d\tau e^{i\omega_n\tau}\int d\boldsymbol{r}\langle\mathcal{T}_\tau(T_{11}(\boldsymbol{r},\tau)T_{11}(0) - T_{11}(\boldsymbol{r},\tau)T_{22}(0) + 3T_{12}(\boldsymbol{r},\tau)T_{12}(0))\rangle_0. \tag{3.59}$$

We next compute the components of the energy-momentum tensor contributing to Eq. (3.59), which leads to the expression

$$\Pi^{M}_{\eta}(\omega_n) = -2\Pi^{xx}_{11} + 2\Pi^{xy}_{12} - \frac{3}{2}(\Pi^{yy}_{11} + \Pi^{yx}_{12} + \Pi^{xy}_{21} + \Pi^{xx}_{22}), \tag{3.60}$$

where the lower indices indicate the components of the Dirac matrices, whereas the upper indices indicate the components of the spatial derivative, as defined in Eq. (3.21). The last four terms in Eq. (3.60) obtain contributions only from one-loop diagrams by the same arguments as before, see Eqs. (3.22) and (3.23). For the first two terms in Eq. (3.60) the diagrams containing more than one loop do not vanish. However, the multi-loop contributions cancel each other after integration due to the isotropy. Thus we conclude that only one-loop diagrams are contributing to Eq. (3.60). After carrying out the Matsubara sums and analytical continuation we obtain the retarded correlator, which we write using Eq. (3.34) as

$$\Pi^{R}_{\eta}(\omega) = 2\int\frac{d\boldsymbol{p}}{(2\pi)^3}\left[p_x^2S_{11} - p_xp_yS_{21} + \frac{3}{4}\left(p_y^2S_{11} + p_xp_yS_{21} + p_xp_yS_{12} + p_x^2S_{22}\right)\right], \tag{3.61}$$

where we have suppressed the $(\boldsymbol{p},\omega)$ arguments of the $S_{\mu\nu}[f=1]$ functions. We obtain the shear viscosity from the Kubo-Zubarev formula (3.54) by using the relation (3.37) and the symmetry $p_x \leftrightarrow p_y$

$$\eta = -\frac{\pi}{10}\int_{-\infty}^{\infty} d\varepsilon \frac{\partial n(\varepsilon)}{\partial \varepsilon}\int \frac{d\boldsymbol{p}}{(2\pi)^3}\left[(2p_x^2+3p_y^2)\mathcal{T}_{11}(\boldsymbol{p},\varepsilon)+p_x p_y \mathcal{T}_{12}(\boldsymbol{p},\varepsilon)\right]. \tag{3.62}$$

Substituting Eq. (3.49) into this expression we obtain

$$\eta = -\frac{2N_cN_f}{5\pi}\int_{-\infty}^{\infty} d\varepsilon \frac{\partial n(\varepsilon)}{\partial \varepsilon}\int_0^{\Lambda}\frac{dp}{2\pi^2}p^2\int\frac{d\Omega}{4\pi}\left[5p_x^2(-A_s^2m^2+A_0^2\varepsilon^2-A_v^2p^2)+4A_v^2p_x^4+8A_v^2p_x^2p_y^2\right]. \tag{3.63}$$

Finally, using the formulas for an arbitrary function $f(p)$

$$\int d\Omega p_x^4 f(p) = \frac{4\pi}{5}p^4 f(p), \qquad \int d\Omega p_x^2 p_y^2 f(p) = \frac{4\pi}{15}p^4 f(p), \qquad \int d\Omega p_x^2 f(p) = \frac{4\pi}{3}p^2 f(p), \tag{3.64}$$

we obtain for the shear viscosity

$$\eta = \frac{N_cN_f}{15\pi^3 T}\int_{-\infty}^{\infty} d\varepsilon \frac{\partial n}{\partial \varepsilon}\int_0^{\Lambda} dp\, p^4\left[5A_s^2(p,\varepsilon)m^2-5A_0^2(p,\varepsilon)\varepsilon^2+A_v^2(p,\varepsilon)p^2\right]. \tag{3.65}$$

We conclude that, as in the case of the thermal and electrical conductivities, the knowledge of the Lorentz components of the spectral function completely determines the shear viscosity of quark matter. We note also that the expression (3.58) for the correlation function is consistent with the expressions given in Refs. [91, 224, 225], where only the $[T_{12},T_{12}]$ commutator has been considered, because the spatial isotropy implies the relation $[T_{11},T_{11}]=[T_{11},T_{22}]+2[T_{12},T_{12}]$.

### 3.2.4 Bulk viscosity

The bulk (second) viscosity within the Kubo-Zubarev formalism is given by [69, 70] (see also Sec. 2.4.3 in Chapter 2)

$$\zeta = -\frac{d}{d\omega}\mathrm{Im}\Pi_{\zeta}^{\mathrm{R}}(\omega)\Big|_{\omega=0}, \tag{3.66}$$

where the relevant two-point correlation function is defined as

$$\Pi_{\zeta}^{R}(\omega) = -i\int_0^{\infty} dt\; e^{i\omega t}\int d\boldsymbol{r}\langle[p^*(\boldsymbol{r},t),p^*(0)]\rangle_0, \tag{3.67}$$

with

$$p^*(\boldsymbol{r},t) = p(\boldsymbol{r},t)-\gamma\epsilon(\boldsymbol{r},t)-\delta n(\boldsymbol{r},t) = \frac{1}{3}T_{ii}(\boldsymbol{r},t)-\gamma T_{00}(\boldsymbol{r},t)-\delta N_0(\boldsymbol{r},t). \tag{3.68}$$

Here $p$, $\epsilon$ and $n$ are the operators of the pressure, the energy density and the particle number density, respectively; the second line uses the relations between these quantities and energy-momentum tensor and particle number current in the fluid rest frame; $\gamma$ and $\delta$ are thermodynamic quantities and are given by

$$\gamma = \left(\frac{\partial p}{\partial \epsilon}\right)_n, \qquad \delta = \left(\frac{\partial p}{\partial n}\right)_{\epsilon}. \tag{3.69}$$

In Eq. (3.69) the quantities $p$, $\epsilon$ and $n$ should be understood as the thermal expectation values of the corresponding operators. The last term in Eq. (3.68) is present only at finite chemical potentials, see Sec. 3.5 for details.

Inserting Eqs. (3.68), (3.2) and (3.3) into Eq. (3.67) and switching to the imaginary-time formalism we obtain a set of two-point correlation functions of the generic form

$$\Pi[\hat{a},\hat{b}](\omega_n) = \int_0^\beta d\tau e^{i\omega_n\tau}\int d\boldsymbol{r}\langle\mathcal{T}_\tau(\bar{\psi}\hat{a}\psi\Big|_{(\boldsymbol{r},\tau)},\bar{\psi}\hat{b}\psi\Big|_0)\rangle_0, \tag{3.70}$$

which is the generalization of Eq. (3.21) for arbitrary operators $\hat{a}$ and $\hat{b}$, standing for either a differential operator (contracted with Dirac $\gamma$-matrices) or one of the interaction vertices $\Gamma^0_{s/ps}$ coming from Eqs. (3.1)–(3.3). The procedure of computation of the bulk viscosity is slightly more involved than that of conductivities and shear viscosity [91, 224, 225, 227–229] because the single-loop approximation to Eq. (3.70) does not cover all the relevant diagrams in the $1/N_c$ expansion. Analogous arguments to those given in Sec. 3.2.2 show that the correlation function (3.70) in the leading $[\mathcal{O}(N_c^1)]$ order is given by an infinite sum of bubble diagrams each of which consists of several single-loop diagrams. The latter in the momentum space is given by

$$\Pi_0[\hat{a},\hat{b}](\omega_n) = -T\sum_l\int\frac{d\boldsymbol{p}}{(2\pi)^3}\mathrm{Tr}\left[\hat{a}G(\boldsymbol{p},i\omega_l+i\omega_n)\hat{b}G(\boldsymbol{p},i\omega_l)\right]. \tag{3.71}$$

Here $\hat{a}$ and $\hat{b}$ are the momentum-space counterparts of the same operators appearing in Eq. (3.70). The details of these computations and loop resummation are similar to the computations in Sec. 3.2.2 and are relegated to Appendix B.1.

The bulk viscosity is written then in terms of the components of the spectral function as

$$\zeta = \zeta_0 + \zeta_1 + \zeta_2, \tag{3.72}$$

with the one-loop contribution given by

$$\zeta_0 = -\frac{2N_cN_f}{9\pi^3}\int_{-\infty}^{\infty}d\varepsilon\frac{\partial n}{\partial\varepsilon}\int_0^\Lambda dpp^2\Big[2(ax+by+cz)^2-(x^2-y^2+z^2)(a^2-b^2+c^2)\Big], \tag{3.73}$$

where

$$x = 3(1+\gamma)m_0, \quad y = 3(\delta-\varepsilon), \quad z = (2+3\gamma)p, \tag{3.74}$$

$$a = mA_s, \quad b = \varepsilon A_0, \quad c = pA_v. \tag{3.75}$$

The following two contributions in Eq. (3.72) are given by

$$\zeta_1 = 2(\bar{G}\bar{R})I_1, \qquad \zeta_2 = (\bar{G}\bar{R})^2 I_2, \tag{3.76}$$

where the renormalized coupling $\bar{G}$ arises through resummation of geometrical series as

$$\bar{G} = \frac{G}{1-R_0G}, \tag{3.77}$$

with the polarization loop

$$R_0 = -\frac{2N_cN_f}{\pi^4}\int_{-\infty}^{\infty}d\varepsilon\int_{-\infty}^{\infty}d\varepsilon'\frac{n(\varepsilon)-n(\varepsilon')}{\varepsilon-\varepsilon'}\int_0^\Lambda dpp^2(aa'+bb'-cc'). \tag{3.78}$$

Finally, the three functions appearing in Eq. (3.76) are given by

$$I_1 = -\frac{2N_cN_f}{3\pi^3}\int_{-\infty}^{\infty}d\varepsilon\frac{\partial n}{\partial\varepsilon}\int_0^\Lambda dpp^2\Big[x(a^2+b^2-c^2)+2a(by+cz)\Big], \tag{3.79}$$

$$I_2 = -\frac{2N_cN_f}{\pi^3}\int_{-\infty}^{\infty} d\varepsilon \frac{\partial n}{\partial \varepsilon}\int_0^{\Lambda} dp p^2(a^2+b^2-c^2), \tag{3.80}$$

$$\bar{R} = -\frac{2N_cN_f}{3\pi^4}\int_{-\infty}^{\infty} d\varepsilon \int_{-\infty}^{\infty} d\varepsilon' \int_0^{\Lambda} dp p^2 \frac{1}{\varepsilon-\varepsilon'}\Big\{[n(\varepsilon)-n(\varepsilon')]\big[x(aa'+bb'-cc') + z(a'c+ac')\big] + \Big[yn(\varepsilon)-y'n(\varepsilon')+\frac{3}{2}(\varepsilon-\varepsilon')\Big](a'b+ab')\Big\}. \tag{3.81}$$

Here the functions $a', b', c', y'$ are obtained from $a, b, c, y$ defined in Eqs. (3.74) and (3.75) by the substitution $\varepsilon \to \varepsilon'$. Equations (3.72)–(3.81) express the bulk viscosity of the quark plasma in terms of the components of its spectral function.

It is remarkable that the multi-loop contributions do not vanish if the chiral symmetry is explicitly broken. However, in the chiral limit $m_0 = 0$ they vanish trivially, since quarks become massless above the critical temperature $T_c$ (see the next section). Indeed, from Eqs. (3.74) and (3.75) we find $x = 0$ and $a, a' \propto m = 0$ in this case. Consequently, it follows from Eqs. (3.81) and (3.76) that $\zeta_{1,2} = 0$. Therefore, in this case, the bulk viscosity is given by the single loop contribution $\zeta_0$ which remains finite also in the chiral limit, see also the discussion in Sec. 3.7.3.

## 3.3 Quark and meson masses and coupling constants

In this section we review the calculations of quark and meson masses and effective couplings, as well as discuss the phase structure of matter predicted by this model. The computations in this section are analogous to those given in Refs. [86, 87, 89, 228].

### 3.3.1 Constituent quark mass

At nonzero temperature and density the constituent quark mass $m(T, \mu)$ is found to leading $\mathcal{O}(N_c^0)$ order in the $1/N_c$ expansion from a Dyson-Schwinger equation, where the self-energy is taken in the Hartree approximation, see Fig. 3.3. Analytically it is written as

$$S_0^{-1} = S^{-1} - G\langle\bar{\psi}\psi\rangle, \tag{3.82}$$

where $S_0 = (\not{p} - m_0)^{-1}$ and $S = (\not{p} - m)^{-1}$ are the free and interacting quark propagators, respectively.

The quark condensate $\langle\bar{\psi}\psi\rangle$, represented by the loop diagram in Fig. 3.3, is given by

$$\langle\bar{\psi}\psi\rangle = T\sum_{m\in Z}\int \frac{d\boldsymbol{p}}{(2\pi)^3}\mathrm{Tr}[S(\boldsymbol{p},\omega_m)], \tag{3.83}$$

where the summation is over the fermionic Matsubara frequencies $\omega_m = (2m+1)\pi T - i\mu$. The trace is over the Dirac, color and flavor space and the quark propagator is given by

$$S(\boldsymbol{p},\omega_m) = \frac{\Lambda_p^+\gamma_0}{i\omega_m - E_p} + \frac{\Lambda_p^-\gamma_0}{i\omega_m + E_p}, \tag{3.84}$$

where $\Lambda_p^+$ and $\Lambda_p^-$ are the projection operators onto the positive and negative energy states

$$\Lambda_p^{\pm} = \frac{E_p\gamma_0 \mp \boldsymbol{\gamma}\cdot\boldsymbol{p} \pm m}{2E_p}\gamma_0. \tag{3.85}$$

Substituting Eqs. (3.84) and (3.85) into Eq. (3.83) we obtain

$$\langle\bar{\psi}\psi\rangle = 2N_cN_f m\int \frac{d\boldsymbol{p}}{(2\pi)^3E_p}T\sum_{m\in Z}\left[\frac{1}{i\omega_m - E_p} - \frac{1}{i\omega_m + E_p}\right]. \tag{3.86}$$


Figure 3.3: Dyson-Schwinger equation for the constituent quark mass. The dashed and solid lines are the bare and dressed propagators, respectively, and $\Gamma = 1$.

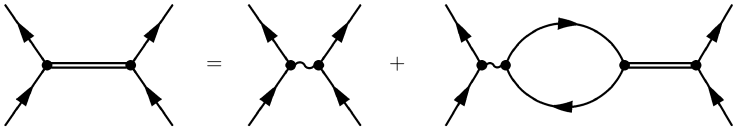

Figure 3.4: The Bethe-Salpeter equation for mesons: the double lines are the dressed meson propagators. The remaining diagrammatic elements are as in Fig. 3.3, except that the vertex assumes the values $\Gamma^0_s = 1$ for $\sigma$-meson and $\Gamma^0_{ps} = i\boldsymbol{\tau}\gamma_5$ for pions.

Next we use the identity

$$T\sum_{m\in Z}\frac{1}{i\omega_m - E_p} = n^+(E_p) - \frac{1}{2}, \tag{3.87}$$

to obtain for Eq. (3.86)

$$\langle\bar{\psi}\psi\rangle = -4N_cN_fmI_1, \tag{3.88}$$

where we defined

$$I_1 = \frac{1}{4\pi^2}\int_0^\Lambda dp\frac{p^2}{E_p}[1 - n^+(E_p) - n^-(E_p)]. \tag{3.89}$$

In Eq. (3.89) the quark/antiquark distribution functions are given by

$$n^\pm(E) = \frac{1}{e^{\beta(E\mp\mu)}+1}. \tag{3.90}$$

From Eqs. (3.82) and (3.88) one finds

$$m = m_0 + 4GN_cN_fmI_1. \tag{3.91}$$

If $m_0 \neq 0$, Eq. (3.91) always has a nontrivial solution $m > m_0$. If $m_0 = 0$, there is a trivial solution $m = 0$, but Eq. (3.91) may have nontrivial solutions satisfying the equation

$$4GN_cN_fI_1 = 1. \tag{3.92}$$

In this case the vacuum energy is minimized by the solution with the largest $m$ [89].

### 3.3.2 Meson masses and quark-meson couplings

The mesonic propagator is obtained from the Bethe-Salpeter equation, shown in Fig. 3.4, which resums contributions from quark-antiquark polarization insertions and analytically reads

$$D_M = G + G\Pi_M D_M = \frac{G}{1 - G\Pi_M}, \tag{3.93}$$

where the quark-antiquark polarizations for the $\sigma$ and $\pi$ mesons $\Pi_M, M = \sigma, \pi$ are given by the formula

$$\Pi_M(\boldsymbol{p},\omega_n) = -T\sum_{m\in Z}\int\frac{d\boldsymbol{q}}{(2\pi)^3}\mathrm{Tr}[\Gamma_M S(\boldsymbol{q}+\boldsymbol{p},\omega_m+\omega_n)\Gamma_M S(\boldsymbol{q},\omega_m)], \tag{3.94}$$

with $\Gamma_\sigma = 1$, $\Gamma_\pi = i\gamma_5\tau_j$, $j = 1,2,3$. From Eq. (3.84) we obtain

$$\Pi_M(\boldsymbol{p},\omega_n) = -\int\frac{d\boldsymbol{q}}{(2\pi)^3}\sum_{\pm\pm}\mathcal{T}_M^{\pm\pm}\mathcal{S}^{\pm\pm}, \tag{3.95}$$

where we defined

$$\mathcal{T}_M^{\pm\pm} = \mathrm{Tr}[\Gamma_M\Lambda_{q+p}^{\pm}\gamma_0\Gamma_M\Lambda_q^{\pm}\gamma_0], \tag{3.96}$$

$$\mathcal{S}^{\pm\pm} = T\sum_m\frac{1}{(i\omega_m+i\omega_n-E_{q+p}^{\pm})(i\omega_m-E_q^{\pm})}, \tag{3.97}$$

with $E_q^{\pm} = \pm E_q$. In Eq. (3.95) the sum runs over all possible combinations of the signs of $E_{q+p}^{\pm}$ and $E_q^{\pm}$. It is enough to calculate only one term of the sum, *e.g.*, the term containing $\mathcal{T}_{\mathcal{M}}^{++}$ and $\mathcal{S}^{++}$, and the others can be obtained by an appropriate choice of signs. Below we skip these signs and recover them in the final expressions. The computation of traces gives

$$\mathcal{T}_M = N_cN_f\frac{P_Mm^2+E_{q+p}E_q-\boldsymbol{q}\cdot(\boldsymbol{q}+\boldsymbol{p})}{E_{q+p}E_q}, \tag{3.98}$$

where $P_\sigma = 1$, and $P_\pi = -1$.

The sum over the Matsubara frequencies gives

$$\mathcal{S} = \frac{n^+(E_q)-n^+(E_{q+p})}{E_q-E_{q+p}+i\omega_n}. \tag{3.99}$$

Using the results (3.98) and (3.99) we find for the polarization tensor (3.95)

$$\begin{aligned}\Pi_M(\boldsymbol{p},\omega_n) &= -N_cN_f\int\frac{d\boldsymbol{q}}{(2\pi)^3}\Bigg\{\frac{P_Mm^2+E_{q+p}E_q-\boldsymbol{q}\cdot(\boldsymbol{q}+\boldsymbol{p})}{E_{q+p}E_q}\Bigg[\frac{n^+(E_q)-n^+(E_{q+p})}{E_-+i\omega_n}\\ &\quad-\frac{n^-(E_q)-n^-(E_{q+p})}{-E_-+i\omega_n}\Bigg]+\frac{P_Mm^2-E_{q+p}E_q-\boldsymbol{q}\cdot(\boldsymbol{q}+\boldsymbol{p})}{E_{q+p}E_q}\\ &\quad\times\Bigg[\frac{n^-(E_q)+n^+(E_{q+p})-1}{-E_++i\omega_n}-\frac{n^+(E_q)+n^-(E_{q+p})-1}{E_++i\omega_n}\Bigg]\Bigg\},\end{aligned} \tag{3.100}$$

with $E_\pm = E_q \pm E_{q+p}$. We now define the shorthand notation $N_M(\boldsymbol{p},\omega_n) = -(\boldsymbol{p}^2+\omega_n^2)-2(1+P_M)m^2$, which gives for the $\pi$- and $\sigma$-modes, respectively, $N_\pi(\boldsymbol{p},\omega_n) = -(\boldsymbol{p}^2+\omega_n^2)$ and $N_\sigma(\boldsymbol{p},\omega_n) = N_\pi(\boldsymbol{p},\omega_n)-4m^2$. From (3.100) we then obtain

$$\begin{aligned}\Pi_M &= N_cN_f\int\frac{d\boldsymbol{q}}{(2\pi)^3}\frac{N_M}{2E_{q+p}E_q}\Bigg\{\frac{(i\omega_n+E_-)[n^-(E_q)-n^-(E_{q+p})]-(i\omega_n-E_-)[n^+(E_q)-n^+(E_{q+p})]}{\omega_n^2+E_-^2}\\ &\quad+\frac{(i\omega_n-E_+)[n^+(E_q)+n^-(E_{q+p})]-(i\omega_n+E_+)[n^-(E_q)+n^+(E_{q+p})]}{\omega_n^2+E_+^2}+\frac{2E_+}{\omega_n^2+E_+^2}\Bigg\}\\ &\quad+N_cN_f\int\frac{d\boldsymbol{q}}{(2\pi)^3}\frac{1}{E_{q+p}E_q}\Big\{E_+-E_{q+p}[n^+(E_q)+n^-(E_q)]-E_q[n^+(E_{q+p}+n^-(E_{q+p})]\Big\}.\end{aligned} \tag{3.101}$$

The second integral in (3.101) is equal to $4I_1$, where $I_1$ is given by Eq. (3.89). In the first integral of

(3.101) we change the variables $\boldsymbol{q} \to \boldsymbol{q} - \boldsymbol{p}$ and define

$$\begin{aligned} I_2(\boldsymbol{p},\omega_n) &= T\sum_{m\in Z}\int\frac{d\boldsymbol{q}}{(2\pi)^3}\frac{1}{[\omega_m^2+E_q^2][(\omega_m-\omega_n)^2+E_{q-p}^2]} = \int\frac{d\boldsymbol{q}}{(2\pi)^3}\frac{1}{4E_qE_{q-p}}\Bigg\{\frac{2E_+}{\omega_n^2+E_+^2} \\ &+ \frac{(i\omega_n-E_+)[n^-(E_q)+n^+(E_{q-p})]-(i\omega_n+E_+)[n^+(E_q)+n^-(E_{q-p})]}{\omega_n^2+E_+^2} \\ &+ \frac{(i\omega_n+E_-)[n^+(E_q)-n^+(E_{q-p})]-(i\omega_n-E_-)[n^-(E_q)-n^-(E_{q-p})]}{\omega_n^2+E_-^2}\Bigg\}, \end{aligned} \tag{3.102}$$

where now we have $E_\pm = E_q \pm E_{q-p}$ because of the shift of the variables above. Then Eq. (3.101) can be written in a compact form

$$\Pi_M(\boldsymbol{p},\omega_n) = 2N_cN_f\big[2I_1 + N_M(\boldsymbol{p},\omega_n)I_2(\boldsymbol{p},\omega_n)\big]. \tag{3.103}$$

Now we can write the meson propagator according to Eqs. (3.93) and (3.103) as

$$D_M^{-1}(\boldsymbol{p},\omega_n) = G^{-1} - 2N_cN_f[2I_1 + N_M(\boldsymbol{p},\omega_n)I_2(\boldsymbol{p},\omega_n)]. \tag{3.104}$$

The momentum-independent meson mass is defined as the pole of the propagator in real spacetime for $\boldsymbol{p}=0$ ($i\omega_n \to m_M + i\delta$)

$$\mathrm{Re}D_M^{-1}[\boldsymbol{0}, -i(m_M+i\delta)] = 0, \tag{3.105}$$

or

$$m_\pi^2 I_2(\boldsymbol{0}, -im_\pi) = \frac{1-4GN_cN_fI_1}{2GN_cN_f}, \tag{3.106}$$

$$(m_\sigma^2-4m^2)I_2(\boldsymbol{0}, -im_\sigma) = \frac{1-4GN_cN_fI_1}{2GN_cN_f}, \tag{3.107}$$

where we took into account that $\mathrm{Re}I_2[\boldsymbol{0}, -i(m_M+i\delta)] = I_2(\boldsymbol{0}, -im_M)$ according to the Dirac identity (3.35). From Eq. (3.102) we have for $\boldsymbol{p}=0$ ($E_-=0$, $E_+=2E_q$)

$$I_2(\boldsymbol{0},\omega_n) = \frac{1}{8\pi^2}\int_0^\Lambda q^2dq\frac{1-n^+(E_q)-n^-(E_q)}{E_q(E_q^2+\omega_n^2/4)}, \tag{3.108}$$

and after analytic continuation $i\omega_n \to \omega + i\delta$ we obtain

$$\mathrm{Re}I_2(\boldsymbol{0},\omega) = I_2(\boldsymbol{0},-i\omega) = \frac{1}{8\pi^2}\int_m^{E_\Lambda} qdE_q\frac{1-n^+(E_q)-n^-(E_q)}{E_q^2-\omega^2/4}, \tag{3.109}$$

where $E_\Lambda = \sqrt{m^2+\Lambda^2}$. For $m < \omega/2$ the integrand of Eq. (3.109) has a single pole, and the integral should be understood in the sense of principal value. For $\omega > 0$ we have

$$\begin{aligned} \mathrm{Im}I_2(\boldsymbol{0},\omega) &= \frac{1}{8\pi^2}\int_m^{E_\Lambda} qdE_q[1-n^+(E_q)-n^-(E_q)]\frac{\pi}{2E_q}\delta(E_q-\omega/2) \\ &= \frac{\sqrt{\omega^2-4m^2}}{16\pi\omega}\frac{\sinh(\beta\omega/2)}{\sinh(\beta\omega/2)+\cosh(\beta\mu)}\theta(\omega-2m)\theta(2E_\Lambda-\omega). \end{aligned} \tag{3.110}$$

As seen from Eq. (3.110), the pion propagator obtains an imaginary part when $\omega > 2m$, therefore the pion becomes unstable to the on-shell decay into a quark-antiquark pair.

From Eqs. (3.89), (3.91), (3.106), (3.107) and (3.109) we obtain the following equation for $m_M$

$$\frac{GN_cN_f}{\pi^2}\int_m^{E_\Lambda} qdE(E^2-\alpha_M m^2)\frac{1-n^+(E)-n^-(E)}{E^2-(m_M/2)^2}=1, \tag{3.111}$$

where $\alpha_\pi=0$, $\alpha_\sigma=1$, and $q=\sqrt{E^2-m^2}$. The solutions of Eq. (3.111) are displayed in Fig. 3.5 and are discussed in the next subsection.

The Mott (critical) temperature $T_{\rm M}$ is defined by the condition $m_\pi(T_{\rm M},\mu)=2m(T_{\rm M},\mu)$, which leads to the following equation

$$\frac{GN_cN_f}{\pi^2}\int_0^{\Lambda} dqE[1-n^+(E)-n^-(E)]=1. \tag{3.112}$$

Now we evaluate the meson propagator using the standard mass-pole approximation (the imaginary part of the pion self-energy is neglected)

$$D_M(\boldsymbol{p},-i\omega)=\frac{-g_M^2}{\omega^2-\boldsymbol{p}^2-m_M^2+i\varepsilon}, \tag{3.113}$$

where the quark-meson coupling is defined as the residue of the full meson propagator at vanishing momentum

$$g_M^{-2}=-\frac{d}{d\omega^2}D_M^{-1}[\mathbf{0},-i\omega]\Big|_{\omega^2=m_M^2}. \tag{3.114}$$

Employing Eqs. (3.104) and (3.108) we obtain for the $\pi$- and $\sigma$-modes

$$g_\pi^{-2} = 2N_cN_f\left[I_2(\mathbf{0},-im_\pi)+m_\pi^2\frac{d}{d\omega^2}I_2(\mathbf{0},-i\omega)\Big|_{\omega^2=m_\pi^2}\right], \tag{3.115}$$

$$g_\sigma^{-2} = 2N_cN_f\left[I_2(\mathbf{0},-im_\sigma+(m_\sigma^2-4m^2)\frac{d}{d\omega^2}I_2(\mathbf{0},-i\omega)\Big|_{\omega^2=m_\sigma^2}\right]. \tag{3.116}$$

To compute the derivatives appearing in Eqs. (3.115)–(3.116) one can formally replace $d/d\omega^2\to-\frac{1}{4}(d/dE_q^2)$ in Eq. (3.109) and integrate by parts to obtain

$$\begin{aligned}\frac{d}{d\omega^2}I_2(\mathbf{0},-i\omega) &= -\frac{1}{64\pi^2}\frac{\Lambda[1-n^+(E_\Lambda)-n^-(E_\Lambda)]}{E_\Lambda(E_\Lambda^2-\omega^2/4)}\\ &+\frac{1}{64\pi^2}\int_m^{E_\Lambda}dE_q\frac{1}{q(E_q^2-\omega^2/4)}\left\{\frac{m^2}{E_q^2}[1-n^+(E_q)-n^-(E_q)]\right.\\ &\left.+\frac{q^2}{E_qT}[n^+(E_q)(1-n^+(E_q))+n^-(E_q)(1-n^-(E_q))]\right\}.\end{aligned} \tag{3.117}$$

### 3.3.3 Numerical results

The behavior of quark and meson masses as functions of density and temperature is shown in Fig. 3.5 in the cases of explicitly broken chiral symmetry $m_0\neq0$ as well as the chiral limit $m_0=0$. As seen from Fig. 3.5, there is always a nontrivial solution for the quark masses with $m>m_0$ if the chiral symmetry is explicitly broken. In the chiral limit, for fixed chemical potential, the quark mass is nonzero below a certain temperature $T\le T_c=T_{\rm M0}$ and is strictly zero for $T\ge T_c$. More generally, at sufficiently high densities and temperatures (for example, $T>T_c\simeq190$ MeV for $\mu=0$ or $\mu>\mu_c\simeq330$ MeV for $T=0$) one finds that the chiral symmetry is restored ($m_0=m=0$).

The meson masses found from the Bethe-Salpeter equation for the meson propagator are also shown

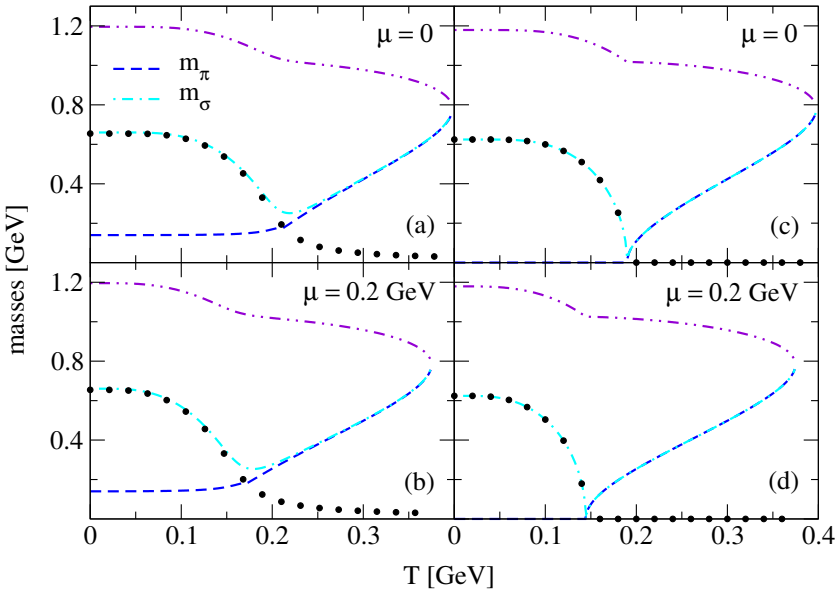


Figure 3.5: Quark and meson masses as functions of temperature at two values of chemical potential. The dots correspond to twice the quark mass, the dashed and dash-dotted lines correspond to the low-mass mesonic solutions, while the dash-double-dotted lines correspond to the high-mass mesonic solution (see the discussion in the text). Left panels: $m_0 > 0$; right panels: $m_0 = 0$.

in Fig. 3.5. At sufficiently low temperatures and densities we find two solutions for the masses of the $\pi$ and $\sigma$ mesons. The two low-mass solutions correspond to the masses of the well-known $\pi$ and $\sigma$ mesons, and they satisfy numerically the relation $m_\sigma^2 = m_\pi^2 + 4m^2$ within 2% precision. The high-mass solutions are approximately the same for the scalar and pseudoscalar modes and may correspond to resonance states. In the chiral limit $m_0 = 0$ the low-mass solutions are given by $m_\pi = 0$ and $m_\sigma = 2m$, below the critical temperature $T_c$ for the chiral phase transition, as seen from Eqs. (3.92), (3.106) and (3.107). Above the critical temperature these solutions become degenerate. As seen from Fig. 3.5, the lower and upper solutions approach each other with increasing temperature and coincide at a temperature $T_{\rm max} \simeq 0.4$ GeV in the case $\mu = 0$. This limiting temperature decreases with increasing chemical potential.

Above $T_{\rm max}$ no solutions are found for the meson masses anymore, *i.e.*, the mesonic modes exist only for $T \leq T_{\rm max}$ within the zero-momentum pole approximation for the meson propagator. The maximal temperature of the existence of mesons $T_{\rm max}$ versus chemical potential is shown in Fig. 3.6. In the limit $T \to 0$ the transition line ends at $\mu_{\rm max} = \Lambda$, which implies $m_M \to 2\Lambda$.

Another important temperature shown in Fig. 3.6 is the Mott temperature $T_{\rm M}$ found from Eq. (3.112) in the cases $m_0 = 0$ and $m_0 \neq 0$. In the region $T \leq T_{\rm M}$ of the phase diagram (Nambu-Goldstone phase) chiral symmetry (approximate) is spontaneously broken with $m_\pi < 2m$. Above the Mott temperature $m_\pi > 2m$ (Wigner-Weyl phase), and the pion can decay into an on-shell quark-antiquark pair. As seen from Figs. 3.5 and 3.6, $T_{\rm M}$ decreases with chemical potential from the value $T_{\rm M} \simeq 213$ MeV at $\mu = 0$ and vanishes at $\mu \approx 345$ MeV. It coincides with the chiral transition temperature in the chiral limit $m_0 = 0$.

Figure 3.7 shows the temperature dependence of the quark-meson couplings given by Eqs. (3.115) and (3.116) at zero and nonzero chemical potentials. Note that the jump in the coupling of the $\pi$-meson arises at the Mott temperature, *i.e.*, $g_\pi \to 0$ at $T \to T_{\rm M}$, which can be verified from Eq. (3.115), where the integral (3.117) diverges for $\omega \to 2m$. The two couplings are almost identical above the Mott temperature. In the chiral limit the overall behavior of the coupling constants remains the same, except for the absence of a discontinuity in the $\pi$-meson coupling at the Mott line.

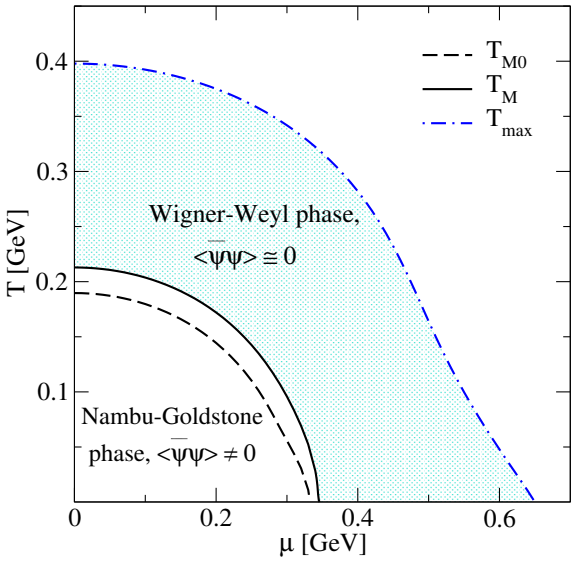


Figure 3.6: The Mott temperature $T_{\rm M}$ and the temperature $T_{\rm max}$ (see the discussion in the text) as functions of the chemical potential. The dashed line is the Mott temperature in the chiral limit $T_{\rm M0} \equiv T_c$. The shaded area shows the portion of the phase diagram where our computations are applicable.

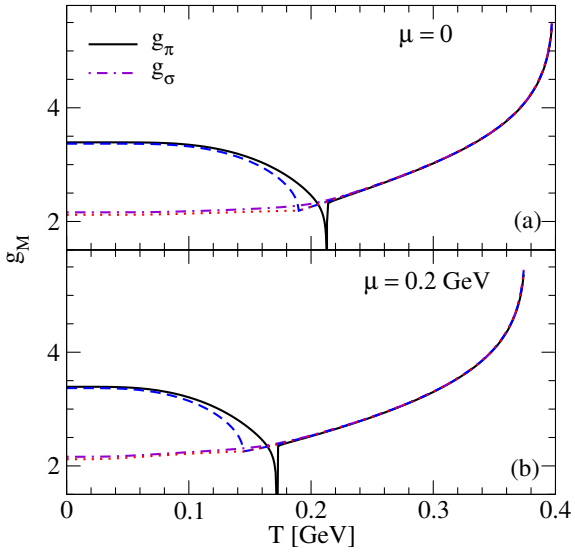


Figure 3.7: Dependence of the couplings $g_\pi$ and $g_\sigma$ on temperature for zero and nonzero chemical potentials. The chiral limit is shown by short-dashed lines for pion and by dotted lines for $\sigma$-meson.

## 3.4 Quark spectral function in the two-flavor NJL model

Equations (3.52), (3.53), (3.63), (3.72)–(3.81) provide the general expressions for the transport coefficients in terms of the Lorentz components of the quark spectral function. Further progress requires the knowledge of the specific form of this spectral function in the regime of physical interest, which is determined by the elementary processes that lead to a nonzero imaginary part of the quark self-energy. We turn now to the derivation of these components within the two-flavor NJL model, mainly following analogous computations in Ref. [91].

### 3.4.1 Calculation of quark self-energy and spectral function

To express the components of the spectral function in terms of the self-energies we write the full quark retarded/advanced Green's function as

$$G^{R/A}(p_0,\boldsymbol{p}) = \frac{1}{\not{p} - m - \Sigma^{R/A}(p_0,\boldsymbol{p})}, \tag{3.118}$$

where $\Sigma^{R/A}$ is the quark-antiquark retarded/advanced self-energy, which in the most general case (due to parity conservation, translational and rotational invariance, as well as time-reversal invariance) can be written in the following form

$$\Sigma^{R(A)} = m\Sigma_s^{(*)} - p_0\gamma_0\Sigma_0^{(*)} + \boldsymbol{p}\cdot\boldsymbol{\gamma}\Sigma_v^{(*)}. \tag{3.119}$$

Substituting the decomposition (3.119) into Eq. (3.118) we obtain

$$\begin{aligned} G^{R(A)}(p_0,\boldsymbol{p}) &= \frac{p_0\gamma_0(1+\Sigma_0^{(*)}) - \boldsymbol{p}\cdot\boldsymbol{\gamma}(1+\Sigma_v^{(*)}) + m(1+\Sigma_s^{(*)})}{p_0^2(1+\Sigma_0^{(*)})^2 - \boldsymbol{p}^2(1+\Sigma_v^{(*)})^2 - m^2(1+\Sigma_s^{(*)})^2} \\ &= \frac{p_0\gamma_0(1+r_0\pm i\varrho_0) - \boldsymbol{p}\cdot\boldsymbol{\gamma}(1+r_v\pm i\varrho_v) + m(1+r_s\pm i\varrho_s)}{n_1 \pm 2in_2}, \end{aligned} \tag{3.120}$$

where we used the shorthand notations $r_i = \mathrm{Re}\Sigma_i$ and $\varrho_i = \mathrm{Im}\Sigma_i$, $i = s, 0, v$, and defined

$$n_1 = p_0^2[(1+r_0)^2 - \varrho_0^2] - \boldsymbol{p}^2[(1+r_v)^2 - \varrho_v^2] - m^2[(1+r_s)^2 - \varrho_s^2], \tag{3.121}$$

$$n_2 = p_0^2\varrho_0(1+r_0) - \boldsymbol{p}^2\varrho_v(1+r_v) - m^2\varrho_s(1+r_s). \tag{3.122}$$

According to the definition of the spectral function (3.30) we find ($p_0 \equiv \varepsilon$)

$$\begin{aligned} A(p_0,\boldsymbol{p}) &= -\frac{1}{2\pi i}\left[\frac{p_0\gamma_0(1+r_0+i\varrho_0) - \boldsymbol{p}\cdot\boldsymbol{\gamma}(1+r_v+i\varrho_v) + m(1+r_s+i\varrho_s)}{n_1+2in_2}\right. \\ &\quad \left. - \frac{p_0\gamma_0(1+r_0-i\varrho_0) - \boldsymbol{p}\cdot\boldsymbol{\gamma}(1+r_v-i\varrho_v) + m(1+r_s-i\varrho_s)}{n_1-2in_2}\right] \\ &= -\frac{1}{\pi}(mA_s + p_0\gamma_0 A_0 - \boldsymbol{p}\cdot\boldsymbol{\gamma}A_v), \end{aligned} \tag{3.123}$$

with

$$A_i = \frac{1}{d}[n_1\varrho_i - 2n_2(1+r_i)], \qquad d = n_1^2 + 4n_2^2. \tag{3.124}$$

From now on we will neglect the irrelevant real parts of the self-energy, which lead to momentum-dependent corrections to the constituent quark mass in the next-to-leading order $\mathcal{O}(N_c^{-1})$.

We now consider the quark self-energy that contributes to the transport phenomena because of a non-vanishing imaginary part, closely following similar computations by Refs. [91,228]. The dominant processes, according to the discussion of the phase structure above, are the meson decays into two quarks and the inverse process above the Mott temperature $T_{\mathrm{M}}$.

The quark self-energy arising from meson exchange is given in the Matsubara space by

$$\Sigma^M(\boldsymbol{p},\omega_n) =$$

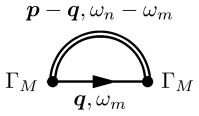


$$= T\sum_m \int \frac{d\boldsymbol{q}}{(2\pi)^3}\left[\Gamma_M S(\boldsymbol{q},\omega_m)\Gamma_M D_M(\boldsymbol{p}-\boldsymbol{q},\omega_n-\omega_m)\right], \tag{3.125}$$

where $S(\boldsymbol{q},\omega_m)$ is the quark propagator with constituent mass, and the index $M=\pi,\sigma$ indicates the meson. Using $\Gamma_\sigma=1$ and $\Gamma_\pi=i\gamma_5\boldsymbol{\tau}$ we find the decomposition

$$\Sigma^M(\boldsymbol{p},\omega_n)=P_M m\Sigma_s^M+i\omega_n\gamma_0\Sigma_0^M-\boldsymbol{p}\cdot\boldsymbol{\gamma}\Sigma_v^M, \tag{3.126}$$

where $P_\sigma=1$, $P_\pi=-1$ and

$$\Sigma_{s,v}^M = g_M^2\int\frac{d\boldsymbol{q}}{(2\pi)^3}\frac{\mathscr{Q}_{s,v}}{4E_qE_M}\left[\frac{i\omega_n\mathscr{C}_3-2E_+\mathscr{C}_1}{E_+^2+\omega_n^2}-\frac{i\omega_n\mathscr{C}_3+2E_-\mathscr{C}_2}{E_-^2+\omega_n^2}\right], \tag{3.127}$$

$$\Sigma_0^M = g_M^2\int\frac{d\boldsymbol{q}}{(2\pi)^3}\frac{\mathscr{Q}_0}{4E_qE_M}\left[\frac{2i\omega_n\mathscr{C}_1-E_+\mathscr{C}_3}{E_+^2+\omega_n^2}+\frac{2i\omega_n\mathscr{C}_2+E_-\mathscr{C}_3}{E_-^2+\omega_n^2}\right], \tag{3.128}$$

with the shorthand notations

$$\begin{aligned}\mathscr{C}_1&=1+n_B(E_M)-\frac{1}{2}[n^+(E_q)+n^-(E_q)],\\ \mathscr{C}_2&=n_B(E_M)+\frac{1}{2}[n^+(E_q)+n^-(E_q)],\\ \mathscr{C}_3&=n^+(E_q)-n^-(E_q),\end{aligned} \tag{3.129}$$

and (see App. B.2 for details)

$$\mathscr{Q}_s=1,\quad \mathscr{Q}_v=\frac{\boldsymbol{q}\cdot\boldsymbol{p}}{p^2},\quad \mathscr{Q}_0=-\frac{E_q}{i\omega_n}. \tag{3.130}$$

The retarded self-energy is now obtained by analytical continuation $i\omega_n\to p_0+i\varepsilon$ and has the same Lorentz structure as its Matsubara counterpart. To obtain the quark self-energy one has to take into account the contributions from three pions and one $\sigma$-meson. The components of this self-energy sum up as follows

$$\Sigma_s=\Sigma_s^\sigma-3\Sigma_s^\pi,\quad \Sigma_{0/v}=-\Sigma_{0/v}^\sigma-3\Sigma_{0/v}^\pi. \tag{3.131}$$

For the imaginary part of the on-shell quark self-energy ($\varrho_j\equiv\mathrm{Im}\Sigma_j$) one finds

$$\varrho_j^M(p)\Big|_{p_0=E_p} = \frac{g_M^2}{16\pi p}\int_{E_{\min}}^{E_{\max}}dE\,\mathscr{T}_j[n_B(E_M)+n^-(E)], \tag{3.132}$$

where $j=s,0,v$, $E_M=E+E_p$, and

$$\mathscr{T}_s=1,\qquad \mathscr{T}_v=\frac{m_M^2-2m^2-2EE_p}{2p^2},\qquad \mathscr{T}_0=-\frac{E}{E_p}. \tag{3.133}$$

In Eq. (3.132) $n_B(E)=(e^{\beta E}-1)^{-1}$ is the Bose distribution function for zero chemical potential. In the same way we find for the antiquark on-shell self-energy ($p_0=-E_p$)

$$\varrho_j^M(p)\Big|_{p_0=-E_p} = -\frac{g_M^2}{16\pi p}\int_{E_{\min}}^{E_{\max}}dE\,\mathscr{T}_j[n_B(E_M)+n^+(E)]. \tag{3.134}$$

The integration limits in Eqs. (3.132) and (3.134) are given by

$$E_{\min,\max}=\frac{1}{2m^2}\left[(m_M^2-2m^2)p_0\pm pm_M\sqrt{m_M^2-4m^2}\right]. \tag{3.135}$$

According to Eq. (3.135) the range of integration is given by

$$E_{\max} - E_{\min} = \frac{p m_M}{m^2}\sqrt{m_M^2 - 4m^2}. \tag{3.136}$$

We note that if $m_M \geq 2m$ the integration range is not empty. The minimum value of $E_{\min}$ is always $m$ and is reached at the momentum

$$p_{\rm m} = \frac{m_M}{2m}\sqrt{m_M^2 - 4m^2}, \tag{3.137}$$

which increases with the temperature and chemical potential. If $m = 0$, we have

$$E_{\min} = \frac{m_M^2}{4p}, \quad E_{\max} \to \infty. \tag{3.138}$$

We stress here that the expressions (3.132)–(3.138) are valid above the Mott temperature (the shaded area in Fig. 3.6), where the dispersive effects of interest, *i.e.*, pion decay into an on-shell $q\bar{q}$ pair and the inverse process are kinematically allowed.

The full quark-antiquark self-energy in the on-shell approximation can be written as

$$\varrho_j(p_0, p) = \theta(p_0)\varrho_j^+(p) + \theta(-p_0)\varrho_j^-(p), \tag{3.139}$$

with $\varrho_j^\pm(p) = \varrho_j(p_0 = \pm E_p, p)$. It is seen from Eqs. (3.132) and (3.134) that $\varrho^+$ and $\varrho^-$ are related by the relation $\varrho_j^-(\mu, p) = -\varrho_j^+(-\mu, p)$, therefore

$$\begin{aligned} \varrho_j(\mu, -p_0, p) &= \theta(-p_0)\varrho_j^+(\mu, p) + \theta(p_0)\varrho_j^-(\mu, p) \\ &= -\theta(-p_0)\varrho_j^-(-\mu, p) - \theta(p_0)\varrho_j^+(-\mu, p) = -\varrho_j(-\mu, p_0, p), \end{aligned} \tag{3.140}$$

where we indicated the $\mu$-dependence of the self-energy explicitly.

Now for a generic transport coefficient $\chi(\mu)$ we can write

$$\chi(\mu) = \int_{-\infty}^{\infty} d\varepsilon n^+(\varepsilon)[1 - n^+(\varepsilon)] \int_0^\Lambda dp \mathscr{F}(p, \varepsilon, \mu), \tag{3.141}$$

where $\mathscr{F}(p, \varepsilon, \mu) \equiv \mathscr{F}(p, \varepsilon, h'(\mu), \gamma(\mu), \delta(\mu), \varrho_j(\mu, \varepsilon, p))$ is an even function of $\varrho_j$ (*i.e.*, does not change under simultaneous changes of the signs of all $\varrho_j$), as seen from Eqs. (3.52), (3.53), (3.63), (3.73), (3.79), (3.80) and (3.121)–(3.124). The function $\mathscr{F}(p, \varepsilon, \mu)$ is invariant under the inversion $\varepsilon \to -\varepsilon$ in the cases of the electrical conductivity and the shear viscosity, and under the simultaneous inversions $\varepsilon \to -\varepsilon$, $h' \to -h'$ and $\varepsilon \to -\varepsilon$, $\delta \to -\delta$ in the cases of the thermal conductivity and the bulk viscosity, respectively. Because $h'$ and $\delta$ are odd, and $\gamma$ - even functions of the chemical potential (see Sec. 3.5), it follows from Eq. (3.140) that

$$\begin{aligned} \mathscr{F}(p, -\varepsilon, \mu) &= \mathscr{F}(p, -\varepsilon, h'(\mu), \gamma(\mu), \delta(\mu), \varrho_j(\mu, -\varepsilon, p)) \\ &= \mathscr{F}(p, \varepsilon, -h'(\mu), \gamma(\mu), -\delta(\mu), -\varrho_j(-\mu, \varepsilon, p)) \\ &= \mathscr{F}(p, \varepsilon, h'(-\mu), \gamma(-\mu), \delta(-\mu), \varrho_j(-\mu, \varepsilon, p)) = \mathscr{F}(p, \varepsilon, -\mu). \end{aligned}$$

Using this property in combination with the relations $n^+(\mu, -\varepsilon) = 1 - n^-(\mu, \varepsilon)$, $n^-(\mu, \varepsilon) = n^+(-\mu, \varepsilon)$, and employing Eq. (3.139) we rewrite Eq. (3.141) as

$$\chi(\mu) = \chi^+(\mu) + \chi^-(\mu), \tag{3.142}$$

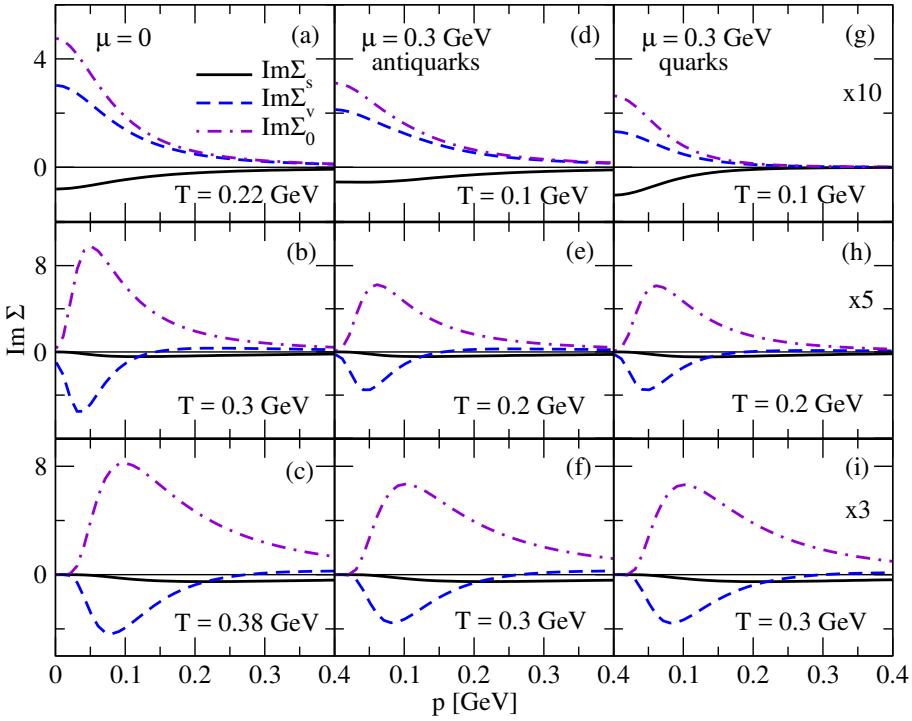


Figure 3.8: The imaginary parts of the three Lorentz components of the quark and antiquark on-shell self-energies as functions of momentum at various values of temperature and chemical potential. The signs of the antiquark self-energies have been inverted.

where we separated the contributions from positive and negative energies

$$\chi^+(\mu) = \int_0^\infty d\varepsilon n^+(\mu,\varepsilon)[1-n^+(\mu,\varepsilon)] \int_0^\Lambda dp \mathscr{F}(p,\varepsilon,...,\varrho_j^+(\mu,p)), \tag{3.143}$$

$$\chi^-(\mu) = \int_{-\infty}^0 d\varepsilon n^+(\mu,\varepsilon)[1-n^+(\mu,\varepsilon)] \int_0^\Lambda dp \mathscr{F}(p,\varepsilon,...,\varrho_j^-(\mu,p)) = \chi^+(-\mu). \tag{3.144}$$

Combining Eqs. (3.143) and (3.144) with Eq. (3.142) we obtain

$$\chi(\mu) = \chi^+(\mu) + \chi^+(-\mu) = \chi(-\mu). \tag{3.145}$$

In a similar manner we can show that the integrals (3.78) and (3.81) are even functions of $\mu$ as well, which with Eq. (3.145) implies that all transport coefficients are even functions of the chemical potential, as expected.

### 3.4.2 Numerical results

The imaginary parts of the quark and antiquark on-shell self-energies, given by Eqs. (3.132) and (3.134), respectively, are shown in Fig. 3.8 as functions of the quark momentum $p$ at fixed values of the temperature and the chemical potential. For each value of $\mu$ the temperature values are chosen to cover the range $T_{\rm M} \leq T \leq T_{\rm max}$, as displayed in Fig. 3.6. Below $T_{\rm M}$, which is defined by the continuum condition $m_\pi = 2m$, the imaginary parts of the on-shell self-energies of quarks are negligible, since the processes of quark scattering with meson exchange are kinematically forbidden in the case of $\pi$-mesons, and are strongly suppressed in the case of $\sigma$-mesons.

The three components of the self-energies differ by the factors $\mathscr{T}_j$. As in the case of the scalar self-energy $\mathscr{T}_s = 1$, we conclude that the differences seen between the components $\varrho_j$ in Fig. 3.8, as for example the different signs of $\varrho_s$ and $\varrho_0$ and more pronounced maxima in $\varrho_0$ and $\varrho_v$ than in

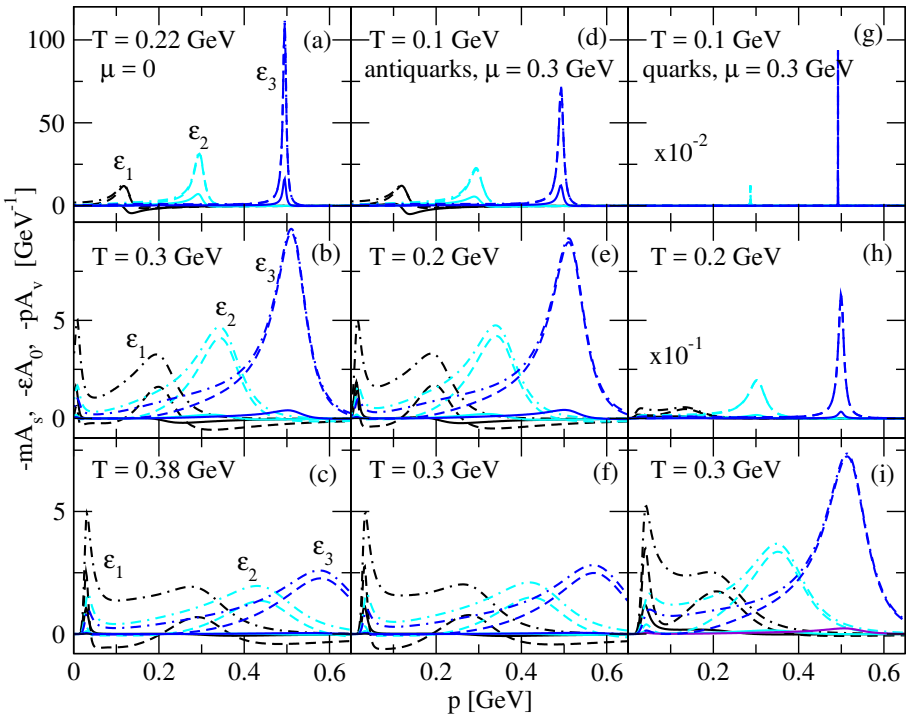


Figure 3.9: Dependence of three Lorentz components of the quark and antiquark spectral functions $-mA_s$ (solid line), $-\varepsilon A_0$ (dash-dotted line) and $-pA_v$ (dashed line) on the momentum. Figures (a)–(c) correspond to $\mu = 0$, (d)–(f) - to antiquarks with $\mu = 0.3$ GeV, and (g)–(i) - to quarks with $\mu = 0.3$ GeV. These spectral functions are shown at three energies $\varepsilon_1 = 0.1$, $\varepsilon_2 = 0.3$, and $\varepsilon_3 = 0.5$ GeV, as indicated in the plot. Note that the vector component of the spectral function changes its sign, whereas the remaining components do not, see the discussion in the text.

$\varrho_s$, originate from the $\mathscr{T}_j$ factors given by Eq. (3.133). To understand the small-$p$ behavior of the self-energies, note first that the explicit $p^{-1}$ divergence in Eqs. (3.132) and (3.134) is cancelled by the linear in $p$ dependence of the integration range, given by Eq. (3.136). Furthermore, when $p \to 0$ the limits of integration tend to $(m_M^2 - 2m^2)/2m$, see Eq. (3.135). If this limiting value is comparable to the temperature, then the quark and antiquark distribution functions are nonzero and contribute to the self-energies for $p \to 0$; this is the case in Figs. 3.8 (a), (d), and (g) (see also Fig. B.3 in App. B.2). In the case where $(m_M^2 - 2m^2)/2m \gg T$, the small-$p$ contributions are suppressed by the vanishingly small distribution functions, see panels (b), (e) and (h), as well as (c), (f) and (i) in Fig. 3.8. However, in the chiral limit $m_0 = 0$ we always find the asymptotic behavior $\mathrm{Im}\Sigma \to 0$, when $p \to 0$, because the lower bound of the integral (3.132) becomes infinitely large as seen from Eq. (3.138).

In the large-$p$ limit the integration range is broad and the asymptotics is controlled by the cutoff of high-momentum contributions by the distribution functions, as well as the factors $\mathscr{T}_j$. Thus the appearance of the maxima in the self-energies [necessarily in the case $(m_M^2 - 2m^2)/2m \gg T$] is the consequence of this asymptotic behavior. The shifts of the maxima to higher momenta with increasing temperature is caused by the shift in energy sampling of the distribution functions.

Next we examine the self-energies at fixed chemical potential, *i.e.*, the vertical columns in Fig. 3.8. Because the difference $m_M - 2m$ increases with temperature as we move away from the Mott line, the integration region increases. At the same time the distribution functions cover phase space with higher energies. In combination this leads to an increase of the imaginary parts of self-energies of quarks and antiquarks with temperature, which is well pronounced for high momenta. This increase is also caused by the additional temperature dependence of the coupling constant $g_M$, see Fig. 3.7.

Consider now the dependence of the self-energies on the chemical potential for fixed temperature by comparing, *e.g.*, panels (a), (e) and (h) with (b), (f) and (i) in Fig. 3.8. We observe two effects:

(i) the contributions to the self-energies from large $p$ domain become larger for $\mu \neq 0$ both for quarks and antiquarks; (ii) the overall magnitude of the quark self-energies (*e.g.*, the maximum) is reduced for $\mu \neq 0$. A nonzero $\mu$ affects quark self-energies stronger than that of antiquarks because of a stronger depletion of the antiquark population at nonzero baryon density, on which the quark self-energy depends. In fact, at any temperature the quark self-energies are by a factor of two smaller than their antiquark counterparts for $\mu = 0.2$ GeV and this difference grows for large $\mu$; *e.g.*, for $\mu = 0.3$ GeV the suppression factor is 10 at $T = 0.1$ GeV. A similar comparison for antiquarks [see panels (a)–(c) and (d)–(f)] shows that the antiquark self-energies at nonzero $\mu$ are comparable to the self-energies for the $\mu = 0$ case.

Next we turn to the three Lorentz components of the spectral function given by Eqs. (3.121)–(3.124), which are shown in Fig. 3.9 as functions of the quark momentum at three values of the quark (off-shell) energy: $\varepsilon_1 = 0.1$, $\varepsilon_2 = 0.3$ and $\varepsilon_3 = 0.5$ GeV. The quasiparticle peak in the spectral functions appears for $p \simeq \varepsilon$, as expected from Eqs. (3.121)–(3.124). An estimate gives $n_1 \approx (p_0^2 - p^2)(1 - \varrho_{0,v}^2)$ and $n_2 \approx (p_0^2 + p^2)\varrho_0$, therefore the denominator $d$ attains its minimum roughly at $p \simeq p_0$. In all cases that the heights of the peaks increase with the quark energy. As expected on physical grounds, the quasiparticle peaks are broadened with increasing temperature and are replaced by more complex structures in the high-temperature regime, see panels (c), (f) and (i) in Fig. 3.9.

A comparison of quark and antiquark spectral functions shows that the quasiparticle peaks of quarks are sharper than that of antiquarks for the same temperature and chemical potential. As indicated in Fig. 3.9, for $\mu = 0.3$ GeV the peak in the spectral function of quarks is by a factor of $10^2$ larger than that of antiquarks at $T = 0.1$ GeV and by a factor of 10 at $T = 0.2$ GeV. Finally, note that the temporal and vector components of the spectral function are of the same order of magnitude and almost coincide at high energies, whereas the scalar component is always suppressed. Thus, we may already conclude that the main contribution to the transport coefficients will originate from the temporal and vector components of the spectral functions. Note that the vector component of the imaginary self-energy changes the sign, consequently the corresponding spectral function changes its sign as well. However, the spectral width of the quasiparticles, which contains contributions from all Lorentz components, remains positive, which guarantees the overall stability of the system [228].

## 3.5 Thermodynamic quantities

In this section we compute several thermodynamic quantities that are necessary for evaluation of the transport coefficients given by Eqs. (3.52), (3.53), (3.65), (3.72)–(3.81).

### 3.5.1 Calculation of quark entropy and enthalpy

The net particle number and entropy densities of quark matter in the leading order of the $1/N_c$ expansion and quasiparticle approximation are given by the formulas [89]

$$n = \frac{N_c N_f}{\pi^2} \int_0^\infty p^2 dp [n^+(E_p) - n^-(E_p)], \tag{3.146}$$

$$s = \frac{N_c N_f}{\pi^2} \int_0^\infty p^2 dp [\beta(E_p - \mu) n^+(E_p) + \beta(E_p + \mu) n^-(E_p) - \log(1 - n^+(E_p)) - \log(1 - n^-(E_p))]. \tag{3.147}$$

The integrals in Eqs. (3.146) and (3.147) should be calculated without momentum cutoff, but for momenta $p > \Lambda$ the quark energy should be evaluated with its bare mass, *i.e.*, $E_p = \sqrt{p^2 + m_0^2}$.

The quark enthalpy density is given by $h = Ts + \mu n$, therefore the enthalpy per particle is

$$h' = \frac{h}{n} = \frac{N_c N_f}{\pi^2 n} \int_0^\infty p^2 dp \left( E_p + \frac{p^2}{3E_p} \right) [n^+(E_p) + n^-(E_p)]. \tag{3.148}$$

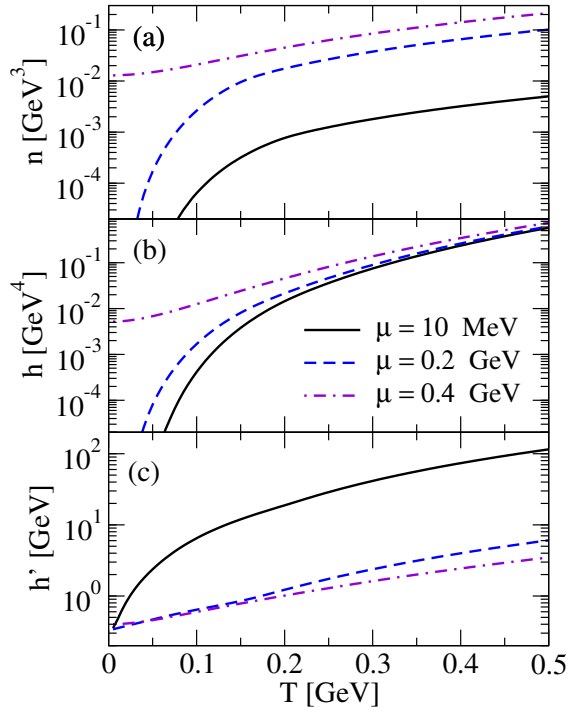


Figure 3.10: Dependence of (a) quark number density, (b) enthalpy density, and (c) the enthalpy per particle on the temperature for several values of the chemical potential.

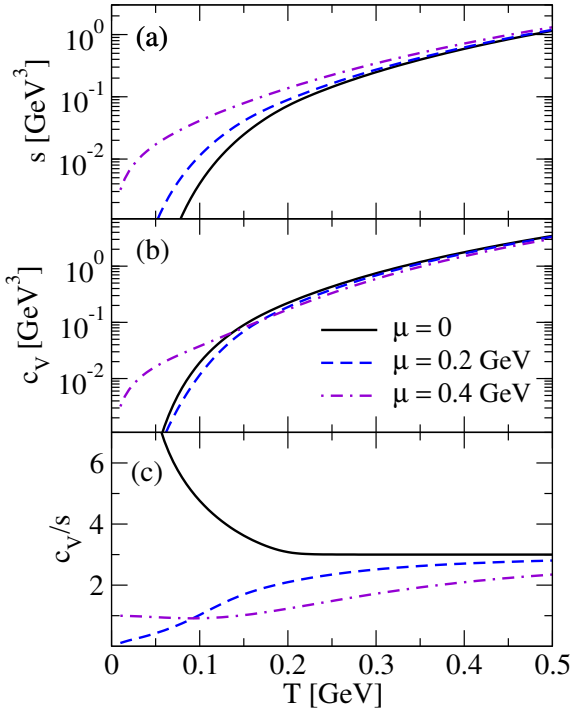


Figure 3.11: Dependence of (a) entropy density, (b) specific heat, and (c) their ratio on the temperature for several values of the chemical potential.

Figure 3.10 shows the quark number density, the enthalpy density and the enthalpy per particle given by Eqs. (3.146) and (3.148). In the nondegenerate regime $T \gg \mu$ we distinguish the following limiting cases: (i) $T \gg m$, *i.e.*, high temperatures where chiral symmetry is (approximately) restored; and (ii) $T \ll m$, *i.e.*, the regime where quarks are nonrelativistic. In the first case $p \simeq \varepsilon \sim T$, therefore we have the scalings $n \propto \mu T^2$, $h \propto T^4$, and $h' \propto T^2/\mu \to \infty$ at $\mu \to 0$. In the second case the integrands of Eqs. (3.146) and (3.148) are exponentially suppressed by the distribution function for energies $\varepsilon - m \gtrsim T$, and we find the scalings $n \propto m\mu(mT)^{1/2}e^{-m/T}$, $h \propto m(mT)^{3/2}e^{-m/T}$, and $h' \simeq mT/\mu \gg m$. Thus, the quark number density and the enthalpy density are exponentially suppressed because of the non-vanishing quark condensate at low temperatures. The enthalpy per particle again diverges as the chemical potential tends to zero. In the opposite, strongly degenerate limit $T \ll \mu$ we consider the cases: (i) $\mu \gg m$ and (ii) $\Delta \gg T$, where $\Delta \equiv m - \mu$. The first case is realized for the chemical potentials $\mu \gtrsim 0.35$ GeV, where we have degenerate matter along with (approximate) chiral symmetry restoration (see Fig. 3.6). In this case all three quantities depend only on the chemical potential: $n \propto \mu^3$, $h \propto \mu^4$, and $h' \to \mu$. The second case is realized for intermediate values of the chemical potential $\mu \lesssim 0.3$ GeV, where the constituent quark mass still exceeds the chemical potential. In this case the quark number density and the enthalpy density vanish exponentially when $T \to 0$ according to the scalings $n \propto (mT)^{3/2}e^{-\Delta/T}$ and $h \propto m(mT)^{3/2}e^{-\Delta/T}$, with $\Delta > 0$, and the enthalpy per particle has a finite limit $h' \to m$, as seen from Fig. 3.10.

### 3.5.2 Calculation of heat capacity

For our discussion of transport coefficients in the next section we need also the heat capacity of quarks, which we compute in this subsection. We use the standard formula for the heat capacity per

unit volume

$$c_V = T\left(\frac{\partial s}{\partial T}\right)_n = -\beta\left(\frac{\partial s}{\partial \beta}\right)_\mu - \beta\left(\frac{\partial s}{\partial \mu}\right)_\beta \left(\frac{\partial \mu}{\partial \beta}\right)_n. \tag{3.149}$$

Using the relations

$$\left(\frac{\partial n^\pm}{\partial \beta}\right)_\mu = -(E_p \mp \mu)n^\pm(1-n^\pm), \qquad \left(\frac{\partial n^\pm}{\partial \mu}\right)_\beta = \pm\beta n^\pm(1-n^\pm), \tag{3.150}$$

we calculate the derivatives of the entropy density given by Eq. (3.147)

$$\left(\frac{\partial s}{\partial \beta}\right)_\mu = -\frac{N_c N_f}{\pi^2 T}\int_0^\infty p^2 dp[(E_p-\mu)^2 n^+(1-n^+) + (E_p+\mu)^2 n^-(1-n^-)], \tag{3.151}$$

$$\left(\frac{\partial s}{\partial \mu}\right)_\beta = \frac{N_c N_f}{\pi^2 T^2}\int_0^\infty p^2 dp[(E_p-\mu) n^+(1-n^+) - (E_p+\mu) n^-(1-n^-)], \tag{3.152}$$

which implies that Eq. (3.149) can be written as

$$c_V = \frac{N_c N_f}{\pi^2 T^2}\int_0^\infty p^2 dp[(E_p-\mu)(E_p-\mu^*) n^+(1-n^+) + (E_p+\mu)(E_p+\mu^*) n^-(1-n^-)], \tag{3.153}$$

where we introduced

$$\mu^*(\beta,\mu) = \mu + \beta\left(\frac{\partial \mu}{\partial \beta}\right)_n. \tag{3.154}$$

Here we neglected the dependence of the constituent quark mass on temperature and chemical potential, as it is of minor importance above the Mott temperature. In order to find $(\partial\mu/\partial\beta)_n$ we take the derivative of Eq. (3.146) with respect to $\beta$ for $n = \text{const}$. As the left-hand side vanishes, we obtain

$$\int_0^\infty p^2 dp\left[-(E_p-\mu)n^+(1-n^+) + (E_p+\mu)n^-(1-n^-)\right] + \beta\left(\frac{\partial \mu}{\partial \beta}\right)_n \int_0^\infty p^2 dp\left[n^+(1-n^+) + n^-(1-n^-)\right] = 0. \tag{3.155}$$

From Eqs. (3.154) and (3.155) it follows that

$$\mu^*(\beta,-\mu) = -\mu^*(\beta,\mu) \tag{3.156}$$

and

$$\int_0^\infty p^2 dp\Big[(E_p-\mu^*)n^+(1-n^+) - (E_p+\mu^*)n^-(1-n^-)\Big] = 0, \tag{3.157}$$

therefore Eq. (3.153) can be written as

$$c_V = \frac{N_c N_f}{\pi^2 T^2}\int_0^\infty p^2 dp E_p[(E_p-\mu^*) n^+(1-n^+) + (E_p+\mu^*) n^-(1-n^-)], \tag{3.158}$$

which is an even function of $\mu$, as expected. From Eq. (3.157) we find for $\mu^*$

$$\mu^*(T,\mu) = \frac{\int_0^\infty p^2 dp E_p\left[n^+(1-n^+) - n^-(1-n^-)\right]}{\int_0^\infty p^2 dp\left[n^+(1-n^+) + n^-(1-n^-)\right]}. \tag{3.159}$$

Figure 3.11 shows the entropy density and the specific heat capacity given by Eqs. (3.147) and

(3.158), respectively, as well as their ratio as functions of the temperature. In the nondegenerate, ultrarelativistic limit $\mu^* \simeq 3\mu \ll T$, $s$ and $c_V$ scale as $T^3$, therefore their ratio tends to its classical limit $c_V/s \to 3$. In the nondegenerate, nonrelativistic limit ($m \gg T \gg \mu$) we find $\mu^* \propto \mu m/T \ll m$ as well as the scalings $s \propto m^2(mT)^{1/2}e^{-m/T}$ and $c_V \propto m^3(m/T)^{1/2}e^{-m/T}$, which demonstrate the exponential suppression of these quantities by the quark condensate. In this case their ratio $c_V/s \simeq m/T$ diverges as $T \to 0$, as seen from the solid line in panel (c). At very high chemical potentials $\mu \gg T, m$ we find $\mu^* \to \mu$ and the scaling $s \simeq c_V \propto \mu^2 T$, which implies therefore $c_V/s \to 1$. In the degenerate regime where $T \ll \Delta$, the scaling is $s \propto m\Delta(mT)^{1/2}e^{-\Delta/T}$. In order to find the leading term contributing to $c_V$, we need to keep the first thermal correction in $\mu^*$, which gives $\mu^* \simeq m + 3T/2$. Then the integral (3.158) can be estimated as $c_V \propto (mT)^{3/2}e^{-\Delta/T}$, and, therefore, the ratio $c_V/s \propto T/\Delta \to 0$ as $T \to 0$ [see the dashed line in panel (c)]. In this limiting case the entropy per particle diverges as $s/n \propto \Delta/T$, and the specific heat per particle tends to its nonrelativistic limit $c_V/n \to 3/2$.

### 3.5.3 Calculation of coefficients $\gamma$, $\delta$

In order to find the derivatives in Eq. (3.69) we use the relation $d\epsilon = Tds + \mu dn$, from which we find

$$\left(\frac{\partial \epsilon}{\partial p}\right)_n = T\left(\frac{\partial s}{\partial p}\right)_n = c_V\left(\frac{\partial T}{\partial p}\right)_n, \tag{3.160}$$

$$\left(\frac{\partial n}{\partial p}\right)_\epsilon = -\frac{T}{\mu}\left(\frac{\partial s}{\partial p}\right)_\epsilon = -\frac{T}{\mu}\left(\frac{\partial s}{\partial \beta}\right)_\epsilon\left(\frac{\partial \beta}{\partial p}\right)_\epsilon, \tag{3.161}$$

therefore

$$\gamma = \left(\frac{\partial p}{\partial \epsilon}\right)_n = \frac{1}{c_V}\left(\frac{\partial p}{\partial T}\right)_n = -\frac{\beta^2}{c_V}\left(\frac{\partial p}{\partial \beta}\right)_n, \tag{3.162}$$

$$\delta = \left(\frac{\partial p}{\partial n}\right)_\epsilon = -\beta\mu\left(\frac{\partial p}{\partial \beta}\right)_\epsilon\left[\left(\frac{\partial s}{\partial \beta}\right)_\epsilon\right]^{-1}, \tag{3.163}$$

where we used Eq. (3.149). Next we will use the relations

$$\left(\frac{\partial s}{\partial \beta}\right)_\epsilon = \left(\frac{\partial s}{\partial \beta}\right)_\mu + \left(\frac{\partial s}{\partial \mu}\right)_\beta\left(\frac{\partial \mu}{\partial \beta}\right)_\epsilon, \tag{3.164}$$

$$\left(\frac{\partial p}{\partial \beta}\right)_n = \left(\frac{\partial p}{\partial \beta}\right)_\mu + \left(\frac{\partial p}{\partial \mu}\right)_\beta\left(\frac{\partial \mu}{\partial \beta}\right)_n, \tag{3.165}$$

$$\left(\frac{\partial p}{\partial \beta}\right)_\epsilon = \left(\frac{\partial p}{\partial \beta}\right)_\mu + \left(\frac{\partial p}{\partial \mu}\right)_\beta\left(\frac{\partial \mu}{\partial \beta}\right)_\epsilon. \tag{3.166}$$

The internal energy density and the pressure at the leading order are given by the formulas [89]

$$\epsilon = \frac{N_c N_f}{\pi^2}\int_0^{\infty,\Lambda} p^2 dp E_p[n^+(E_p) + n^-(E_p) - 1] + \frac{(m-m_0)^2}{2G} - C, \tag{3.167}$$

$$p = \frac{N_c N_f}{\pi^2}\int_0^{\infty,\Lambda} p^2 dp\left\{E_p + [n^+(E_p) + n^-(E_p)]\frac{p^2}{3E_p}\right\} - \frac{(m-m_0)^2}{2G} + C, \tag{3.168}$$

where the cutoff is applied only for divergent parts of the integrals; $C = \text{const}$ and should be fixed by the condition that $p$ and $\epsilon$ vanish in the vacuum, *i.e.*, at $T = \mu = 0$.

Taking the partial derivatives from Eq. (3.168) and employing the relations (3.150) we obtain

$$\left(\frac{\partial p}{\partial \beta}\right)_\mu = -\frac{N_c N_f}{\pi^2}\int_0^\infty p^2 dp\frac{p^2}{3E_p}[(E_p - \mu)n^+(1-n^+) + (E_p + \mu)n^-(1-n^-)], \tag{3.169}$$

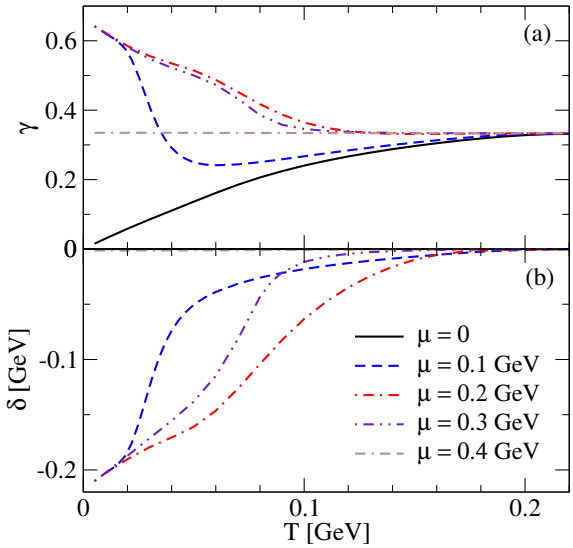


Figure 3.12: The coefficients $\gamma$ (a) and $\delta$ (b) as functions of the temperature for various values of the chemical potential.

$$\left(\frac{\partial p}{\partial \mu}\right)_\beta = \frac{N_c N_f}{\pi^2 T}\int_0^\infty p^2 dp \frac{p^2}{3E_p}[n^+(1-n^+) - n^-(1-n^-)]. \tag{3.170}$$

Introducing

$$\mu^\star(\beta,\mu) = \mu + \beta\left(\frac{\partial \mu}{\partial \beta}\right)_\epsilon, \tag{3.171}$$

from Eqs. (3.151), (3.152), (3.154), (3.164)–(3.166), (3.169)–(3.171) we obtain

$$\left(\frac{\partial s}{\partial \beta}\right)_\epsilon = \mu\frac{N_c N_f}{\pi^2 T}\int_0^\infty p^2 dp[(E_p-\mu^\star)n^+(1-n^+) - (E_p+\mu^\star)n^-(1-n^-)], \tag{3.172}$$

$$\left(\frac{\partial p}{\partial \beta}\right)_n = -\frac{N_c N_f}{\pi^2}\int_0^\infty p^2 dp \frac{p^2}{3E_p}[(E_p-\mu^*)n^+(1-n^+) + (E_p+\mu^*)n^-(1-n^-)], \tag{3.173}$$

$$\left(\frac{\partial p}{\partial \beta}\right)_\epsilon = -\frac{N_c N_f}{\pi^2}\int_0^\infty p^2 dp \frac{p^2}{3E_p}[(E_p-\mu^\star)n^+(1-n^+) + (E_p+\mu^\star)n^-(1-n^-)]. \tag{3.174}$$

In order to compute the derivative $(\partial\mu/\partial\beta)_\epsilon$ we take the $\beta$-derivative of Eq. (3.167) for $\epsilon = \text{const}$. Using Eq. (3.150) we obtain

$$\int_0^\infty p^2 dp E_p\Big[(E_p-\mu)n^+(1-n^+) + (E_p+\mu)n^-(1-n^-)\Big]$$
$$-\beta\left(\frac{\partial \mu}{\partial \beta}\right)_\epsilon \int_0^\infty p^2 dp E_p\left[n^+(1-n^+) - n^-(1-n^-)\right] = 0,$$

which gives in combination with Eq. (3.171)

$$\int_0^\infty p^2 dp E_p\big[(E_p-\mu^\star)n^+(1-n^+) + (E_p+\mu^\star)n^-(1-n^-)\big] = 0. \tag{3.175}$$

The identity (3.175) was already used in deriving Eq. (3.172).

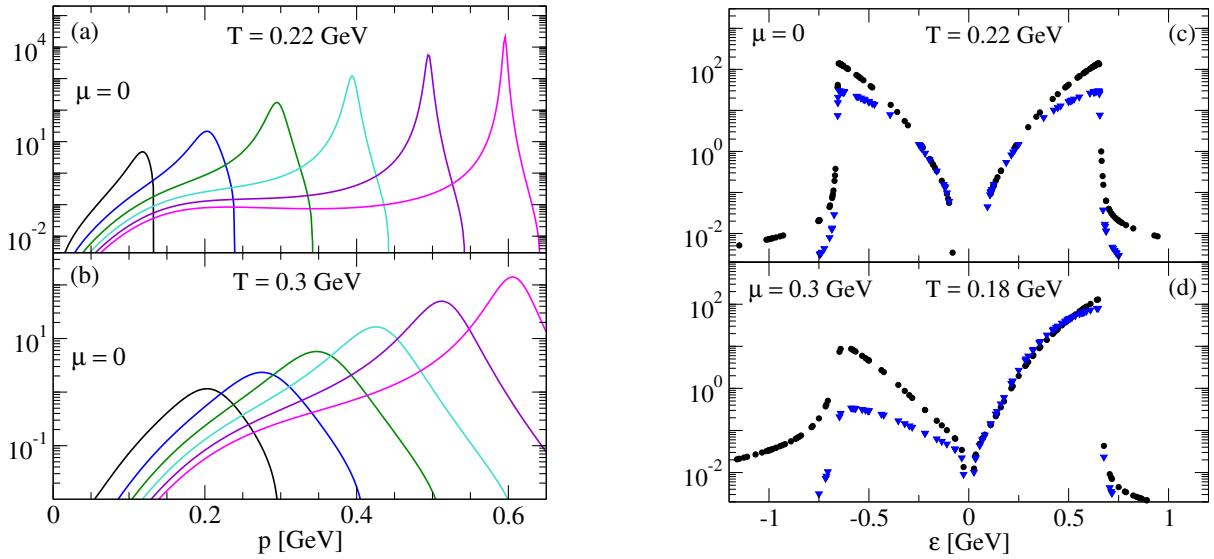


Figure 3.13: The integrands of $\sigma$: (a), (b) - the inner integrand as a function of the quark momentum at various values of the quark (off-shell) energy ($\varepsilon = 0.1$, 0.2, 0.3, 0.4, 0.5 and 0.6 GeV from the left to the right); (c), (d) - the outer integrand as a function of $\varepsilon$ without (black circles, in GeV units) and with (blue triangles) the factor $-\partial n/\partial\varepsilon$ for vanishing (c) and finite (d) chemical potential.

From Eq. (3.175) we find

$$\mu^\star = \frac{\int_0^\infty p^2 dp E_p^2 \left[n^+(1-n^+) + n^-(1-n^-)\right]}{\int_0^\infty p^2 dp E_p \left[n^+(1-n^+) - n^-(1-n^-)\right]}. \tag{3.176}$$

Finally, substituting Eqs. (3.172)–(3.174) and (3.158) into Eqs. (3.162) and (3.163) we obtain

$$\gamma = \frac{\int_0^\infty p^4 dp (3E_p)^{-1}\left[(E_p-\mu^*)n^+(1-n^+) + (E_p+\mu^*)n^-(1-n^-)\right]}{\int_0^\infty p^2 dp E_p\left[(E_p-\mu^*)n^+(1-n^+) + (E_p+\mu^*)n^-(1-n^-)\right]}, \tag{3.177}$$

$$\delta = \frac{\int_0^\infty p^4 dp (3E_p)^{-1}\left[(E_p-\mu^\star)n^+(1-n^+) + (E_p+\mu^\star)n^-(1-n^-)\right]}{\int_0^\infty p^2 dp\left[(E_p-\mu^\star)n^+(1-n^+) - (E_p+\mu^\star)n^-(1-n^-)\right]}. \tag{3.178}$$

Eqs. (3.176)–(3.178) imply that $\mu^\star$ and $\delta$ are odd and $\gamma$ - even functions of the chemical potential. The thermodynamic quantities $\gamma$ and $\delta$ given by Eqs. (3.177) and (3.178) are shown in Fig. 3.12. We find that $\gamma$ tends to a constant value $\gamma = 1/3$ at high temperatures and chemical potentials. In $T \to 0$ limit $\gamma \to 0$ for $\mu = 0$ and $\gamma \to 2/3$ for intermediate values of the chemical potential $T \ll \mu < m(T=0)$. Note that in the limit of vanishing chemical potential $\gamma = s/c_V$ coincides with the sound speed, which makes clear the high-temperature asymptotics of $\gamma$. We find also that $\delta$ is numerically negligible compared to the typical energy scales for the whole temperature-density range of interest. It vanishes asymptotically at high temperatures and densities, but tends to a constant limit $\delta \to -2m(T=0)/3 \simeq 0.22$ GeV at $T \to 0$ if $m(T=0) > \mu \gg T$. In the chiral limit $m = 0$ above the critical temperature $T_c$, and we find from Eqs. (3.175), (3.177) and (3.178) constant values $\gamma = 1/3$ and $\delta = 0$.

## 3.6 Numerical results for conductivities and shear viscosity

### 3.6.1 Thermal and electrical conductivities

We now turn to the evaluation of the thermal and electrical conductivities as given by Eqs. (3.52) and (3.53). Before discussing the numerical results, consider the generic structure of these expressions.

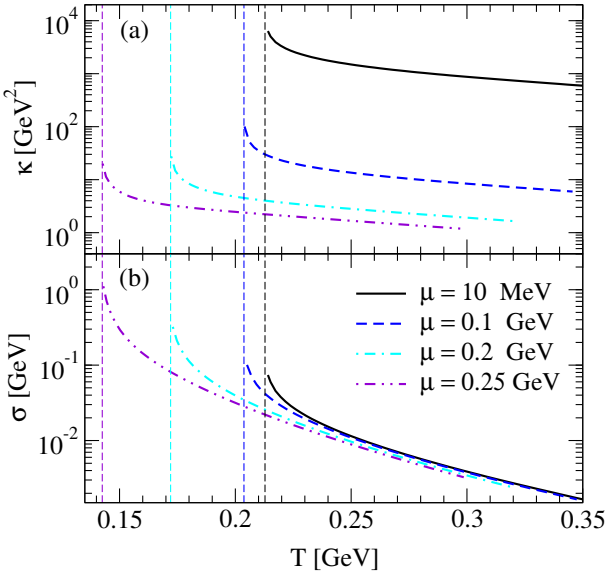


Figure 3.14: Thermal (a) and electrical (b) conductivities as functions of the temperature at various values of the chemical potential. The vertical lines show the Mott temperature at the given value of $\mu$.

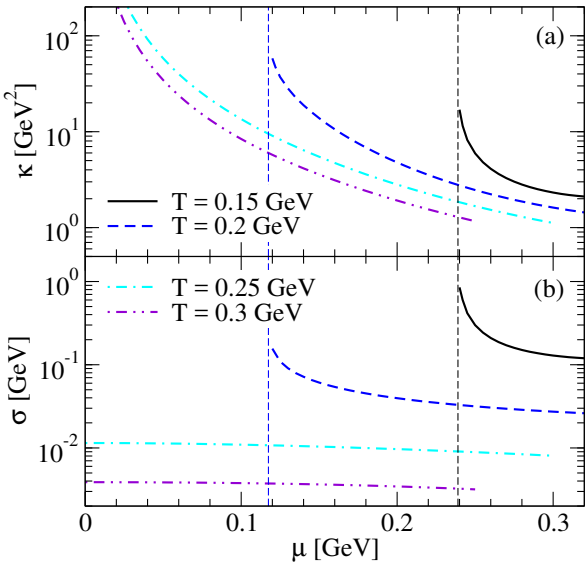


Figure 3.15: Dependence of (a) thermal and (b) electrical conductivities on the chemical potential at various temperatures. The vertical lines show the values of the chemical potential on the Mott line for a given temperature.

For a given value of $\varepsilon$ the inner integrand has a peak structure with a maximum located at $p \simeq \varepsilon$, as implied by the shape of the spectral functions, see Fig. (3.13), panels (a) and (b). The heights of the peaks rapidly increase with $\varepsilon$. As a consequence, the inner (momentum) integrals in Eqs. (3.52) and (3.53) are rapidly increasing functions of $|\varepsilon|$ as long as $|\varepsilon| \leq \Lambda$, see Fig. 3.13, panels (c) and (d). For energies larger than $\Lambda$ the peaks are outside of the integration range (because of the momentum cutoff) and the integral sharply decreases with $\varepsilon$. The outer integration contains the factor $\partial n(\varepsilon)/\partial\varepsilon$ which at low temperatures is strongly peaked at the energy $\varepsilon = \mu$. At high temperatures it transforms into a broad, bell-shaped structure which samples energies far away from $\mu$.

It is evident from Eqs. (3.52) and (3.53) that for $\mu \to 0$ the integrands of the momentum integrals are even functions of $\varepsilon$, as discussed above, and the quark and antiquark contributions originating from positive and negative ranges of the $\varepsilon$-integration are equal. At nonzero chemical potentials the contribution of antiquarks is suppressed by both spectral functions and by the factor $\partial n/\partial\varepsilon$, see Fig. 3.13, panels (c) and (d). We will give explicit numerical examples below.

Figure 3.14 shows the temperature dependence of the thermal and the electrical conductivities for several values of the chemical potential. The conductivities decrease with temperature for all values of the chemical potential. The observed decrease is the result of the broadening of the spectral functions with temperature, which physically corresponds to stronger dispersive effects and shorter relaxation times. This implies smaller conductivities.

Note that at the Mott temperature and below the conductivities become very large because the dispersive effects incorporated in the spectral functions via the imaginary parts of the self-energies vanish for pions and are very small for the $\sigma$-meson. This is the consequence of the on-shell approximation, and can be improved if one incorporates off-shell contributions to the self-energies. This improvement close to (and below) the Mott temperature that incorporates off-shell kinematics is unimportant at temperatures already slightly above the Mott temperature, where the transport coefficients are described by on-shell kinematics quite well. (For a computation of off-shell self-energies see Ref. [91], where their impact on the shear viscosity was found to be small.)

Comparing the overall behavior of the thermal and electrical conductivities we observe two main differences: (i) the electrical conductivity drops faster with temperature than the thermal conductivity,

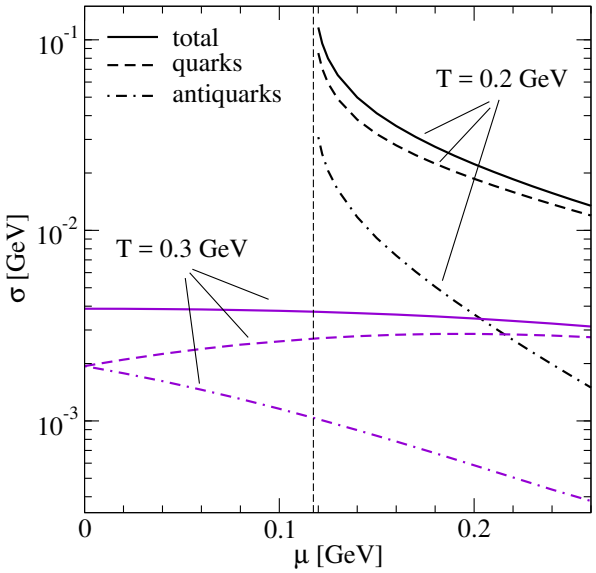


Figure 3.16: The partial contributions of quarks and antiquarks to the electrical conductivity and their sum as functions of the chemical potential at two values of temperatures.

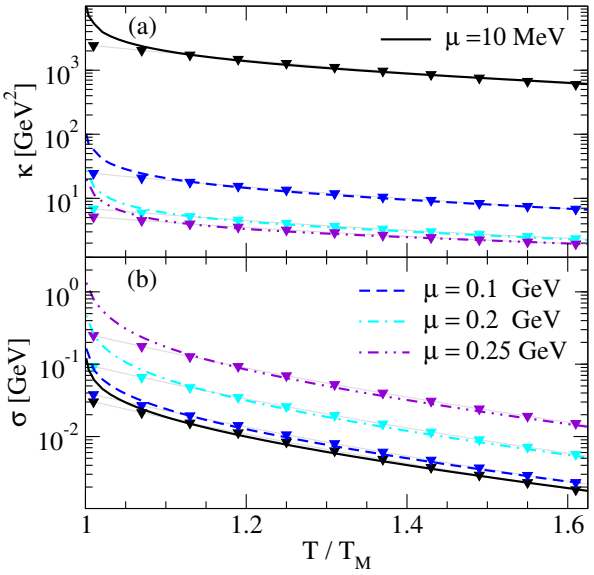


Figure 3.17: The thermal conductivity $\kappa$ (a) and the electrical conductivity $\sigma$ (b) as functions of the scaled temperature $T/T_{\rm M}$ at several values of the chemical potential.

(ii) for small chemical potentials the thermal conductivity diverges, whereas the electrical conductivity remains almost independent of the chemical potential. The difference arises from those terms in Eq. (3.52) for $\kappa$ which contain the enthalpy $h'$. In the relevant temperature-density range, the minimal value of the enthalpy per particle is $h'_{\rm min} \simeq 0.8$ GeV, see Fig. 3.10 in Sec. 3.5. This value already exceeds the cutoff parameter $\Lambda \simeq 0.65$ GeV, which is the characteristic energy scale of the model, therefore one may conclude that the dominant terms in $\kappa$ are the terms containing $h'$, *i.e.*, the terms arising from the second and third correlators on the right-hand side of Eq. (3.11). The enthalpy per particle rapidly increases with the decrease of the chemical potential, therefore at small chemical potentials the main contribution comes from the third term. Numerically we find that the first two terms are negligible compared to the third one for $\mu \leq 0.1$ GeV. The second correlator becomes important once $\mu \geq 0.1$ GeV, whereas the first one is always suppressed for $\mu \leq 0.25$ GeV. Thus, using Eqs. (3.5), (3.6), (3.11) and (3.42), we obtain for small chemical potentials $\mu \leq 0.1$ GeV a simple relation between the thermal and electrical conductivities

$$\frac{\kappa}{\sigma} = \frac{N_f}{{\rm Tr}\hat{Q}^2}\frac{h'^2}{T} = \frac{9h'^2}{10\pi\alpha T}. \tag{3.179}$$

Note that the first equality holds for any number of flavors, whereas in the second step we substituted $N_f = 2$. For $\mu \ll T$ we have the asymptotic behavior $h' \simeq 7\pi^2T^2/15\mu$, therefore the thermal conductivity diverges at vanishing baryon density as $\kappa \propto \mu^{-2}$, which is consistent with the result of Ref. [80]. Substituting the expression for $h'$ in Eq. (3.179) we find in the nondegenerate regime

$$\frac{\kappa\mu^2}{\sigma T^3} = \frac{N_f}{{\rm Tr}\hat{Q}^2}\left(\frac{7\pi^2}{15}\right)^2 = \frac{49\pi^3}{250\alpha} \simeq 830. \tag{3.180}$$

It is seen that the Wiedemann-Franz law $\sigma T/\kappa \sim const$ does not hold in this case. Finally, we note that away from the Mott line we have the scalings $\sigma \propto T^{-6}$ and $\kappa \propto T^{-\gamma}$ with $\gamma = 3$ for $\mu \leq 0.1$ GeV and $\gamma = 2$ for $\mu \geq 0.2$ GeV.

The dependence of the conductivities on the chemical potential is shown in Fig. 3.15. The electrical conductivity is seen to be nearly independent of the chemical potential away from the Mott transition

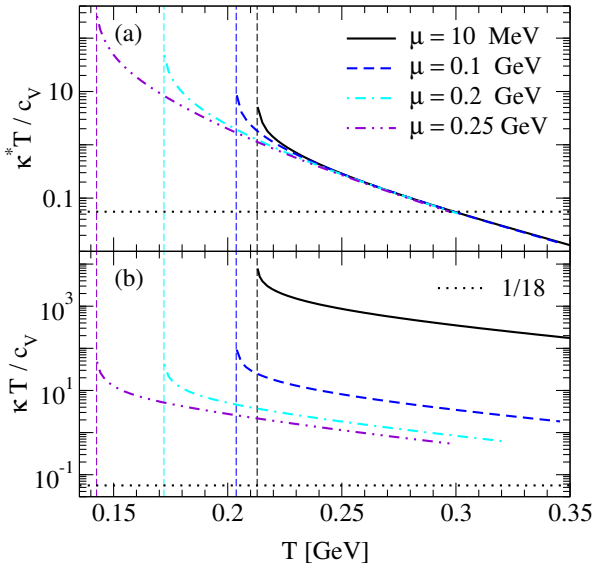


Figure 3.18: The ratios $\kappa^* T/c_V$ (a) and $\kappa T/c_V$ (b) as functions of the temperature at several values of the chemical potential.

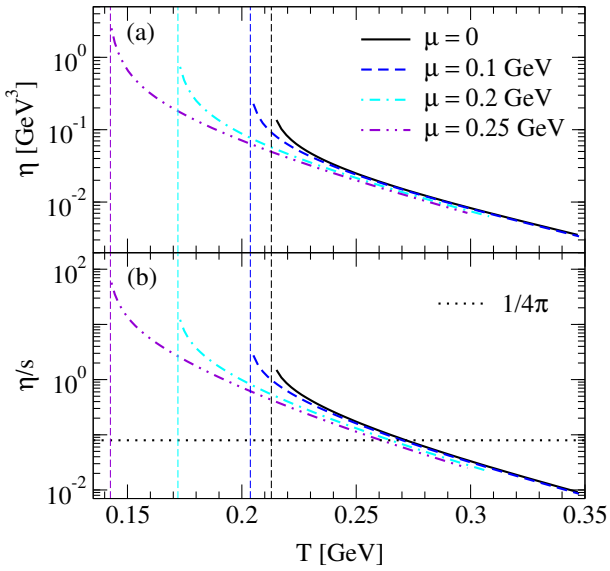


Figure 3.19: The temperature dependence of the shear viscosity $\eta$ (a) and its ratio to the entropy density (b) at various chemical potentials.

line. Only close to this transition $\sigma$ increases because of the vanishing of the spectral width at $T_{\rm M}$. Note that for temperatures $T \geq 0.25$ GeV the electrical conductivity remains almost constant because of the absence of the Mott line at these temperatures. However, the thermal conductivity is always a rapidly decreasing function of the chemical potential because of the reasons discussed above, and becomes infinitely large in the limit $\mu \to 0$.

At nonzero $\mu$ the symmetry between quarks and antiquarks is broken; its consequences discussed above are illustrated in Fig. 3.16, where the quark and antiquark contributions to $\sigma$ are shown separately. At temperatures close to $T_{\rm M}$ both contributions decrease with quarks contributing dominantly. For temperatures away from the Mott transition line, the moderate increase in the conductivity of quarks up to $\mu \simeq 0.2$ GeV is accompanied by a rapid decrease in the contribution of antiquarks, which becomes negligible at $\mu > 0.2$ GeV. The sum of these two contributions turns out to be a slowly decreasing function of $\mu$ in the entire range of $\mu$ and $T$, see also Fig. 3.15.

In order to remove the effect of the variations of the position of the Mott line with the chemical potential, we show in Fig. 3.17 again the conductivities as in Fig. 3.14, but with the temperature axis scaled by the corresponding $T_{\rm M}(\mu)$. In this case the conductivities display a universal dependence on this scaled temperature, their values being only shifted by a $\mu$-dependent constant.

Apart from the Wiedemann-Franz relation, the ratios the $\kappa T/c_V$ and $\kappa^* T/c_V$ are of interest. Here $\kappa^*$ is defined by Eq. (3.52) with $h' = 0$ and $c_V$ is the specific heat capacity as defined in Sec. 3.5. These ratios are shown in Fig. 3.18.

We conjecture that the ratio $\kappa^* T/c_V$, which is associated with the energy transfer only, is bounded from below due to the quantum mechanical uncertainty principle. To motivate this conjecture we refer to the kinetic theory of non-interacting gases. Because for temperatures $T > T_{\rm M}$ the quark masses are negligible compared to other scales, we can set their average velocity $\bar{v} \simeq 1$. Furthermore, in this regime the characteristic energy $\varepsilon \simeq 3T$. Now, according to the kinetic theory of dilute gases the thermal conductivity is estimated as

$$\kappa^{\rm kin} \simeq \frac{1}{3} c_V \bar{v} l \simeq \frac{1}{3} c_V \tau, \tag{3.181}$$

where $l$ is the mean free path and $\tau = l/\bar{v}$ is the mean collision time. Therefore, we find that at high temperatures $\kappa T/c_V \simeq T\tau/3 \simeq \varepsilon\tau/9$. Because of the uncertainty principle $\varepsilon\tau \geq 1/2$, we find

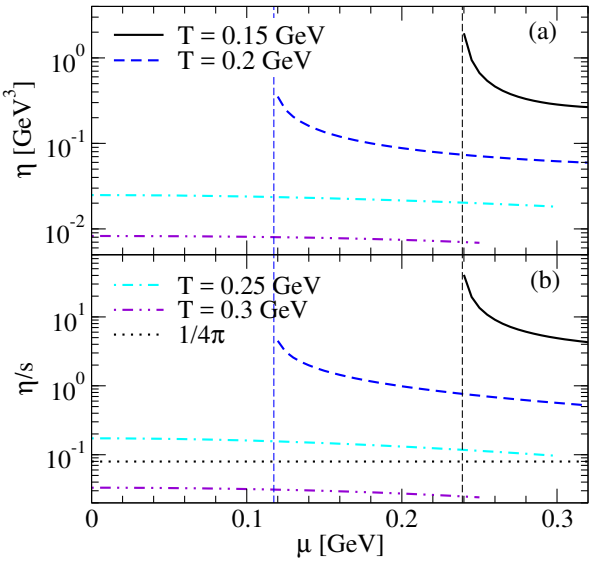


Figure 3.20: The dependence of the shear viscosity (a) and the ratio $\eta/s$ (b) on the chemical potential at various temperatures. The vertical lines show the value of the chemical potential where $T = T_{\rm M}(\mu)$.

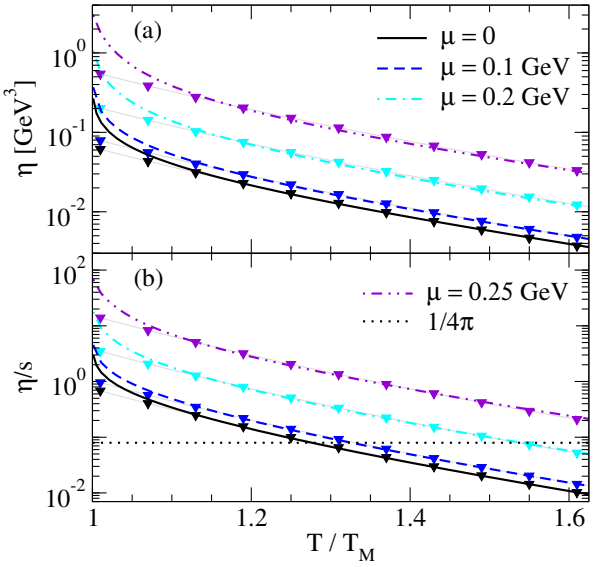


Figure 3.21: The shear viscosity (a) and the ratio $\eta/s$ (b) as functions of the scaled temperature $T/T_{\rm M}$ at several values of chemical potential. The horizontal line shows the KSS bound $1/4\pi$ [81].

(recovering the natural constants) the following bound

$$\frac{\kappa^{\rm kin} T}{c_V} \geq \frac{\hbar c^2}{18 k_B}. \tag{3.182}$$

In the present context $\kappa^{\rm kin}$ in Eq. (3.182) should be associated with $\kappa^*$ because this quantity serves as the analogue of the thermal conductivity defined in the kinetic theory of gases. Indeed, both quantities involve the total energy transport and do not separate the convective particle current which is excluded from $\kappa$ by definition.

Note that in the case of the shear viscosity the discussion of an analogous bound was given by Ref. [80] and a more stringent limit (the so-called KSS bound) was suggested later on from gauge-gravity duality considerations [81].

According to the panel (a) of Fig. 3.18, the bound (3.182) is violated for the ratio involving $\kappa^*$ at high temperatures $T \gtrsim 0.3$ GeV. It is remarkable that this occurs in the same range where the shear-viscosity bound is violated (see below, Sec. 3.6.2). The inclusion of gluonic degrees of freedom will mitigate this violation. The quark-meson exchange processes will not be the most dominant processes away from the Mott temperature and the gluonic degrees of freedom are expected to play a significant role in thermal transport.

### 3.6.2 Shear viscosity

The shear viscosity of quark matter has been studied extensively because of the experimental evidence for its very low value in heavy-ion collisions where the quark matter formation is expected and because of the conjectured universal lower bound of the ratio $\eta/s$ derived from the gauge-gravity duality [81]. We now evaluate the expression for $\eta$ given by Eq. (3.63) and compare it to earlier studies, in particular those based on the two-flavor NJL model.

Figure 3.19 shows the temperature dependence of the shear viscosity and the ratio $\eta/s$. As in the case of the conductivities, the shear viscosity is a decreasing function of the temperature, for the reasons already explained in detail above: the dispersive effects increase with the temperature and

| $\chi_{\rm fit}$ | $C$ | $\alpha$ | $a_1$ | $a_2$ | $a_3$ |
|---|---|---|---|---|---|
| $\sigma$ | 0.032 | 6 | 2.64 | 1.23 | 2.67 |
| $\kappa$ | 2.10 | 3 | −0.95 | 1.27 | 0.0 |
| $\kappa^*$ | 1.55 | 7 | 3.47 | 1.08 | 3.34 |
| $\eta$ | 0.065 | 6 | 2.92 | 0.95 | 2.7 |
| $\eta/s$ | 0.75 | 9 | 3.89 | 1.72 | 3.47 |

Table 3.1: The values of the fit parameters in Eq. (3.184).

the viscosity of matter is reduced. The entropy density of quark matter is an increasing function of temperature (linear in the degenerate regime $T \ll \mu$ and cubic in the nondegenerate regime $T \gg \mu$), therefore the ratio $\eta/s$ decreases faster than $\eta$ with increasing temperature. In the high-temperature regime $\eta$ and $\eta/s$ have the scaling $T^{-6}$ and $T^{-9}$, respectively. The enhancement of both quantities in the limit $T \to T_{\rm M}$ is understood as due to vanishing of the relevant on-shell self-energies at the Mott temperature. At high temperatures $T \gtrsim 0.27$ GeV the ratio $\eta/s$ undershoots the KSS bound $1/4\pi$ [81]. This is an indication of the change in the processes that dominate the viscosity, namely from quark-meson fluctuations to those including gluonic degrees of freedom, which are integrated out from the NJL model. Their contribution becomes increasingly important at high temperatures and leads to an increase of the viscosity with temperature, see Refs. [92–95].

The dependence of $\eta$ and $\eta/s$ on the chemical potential is shown in Fig. 3.20. As in the case of the electrical conductivity, these are slowly decreasing functions of $\mu$ at fixed temperature except at the corresponding Mott line where $\eta$ formally diverges. Finally, in Fig. 3.21 we show these quantities as functions of the ratio $T/T_{\rm M}$. As in the case of the conductivities, we observe a universal behavior of $\eta$ and $\eta/s$ on $T/T_{\rm M}$ for fixed $\mu$ values, *i.e.*, the curves belonging to different values of $\mu$ are only shifted vertically by a $\mu$-dependent constant.

### 3.6.3 Fitting conductivities and shear viscosity

The observed nearly universal behavior of the transport coefficients with the scaled temperature $T/T_{\rm M}$ for fixed values of the chemical potential suggests fitting transport coefficients as functions of $T/T_{\rm M}$ and the chemical potential, as displayed in Figs. 3.17 and 3.21 with triangles.

For this purpose we first fit the Mott temperature, displayed in Fig. 3.6, with the formula

$$T_{\rm M}^{\rm fit}(\mu) = T_0 \begin{cases} 1 - \sqrt{\gamma y} e^{-\pi/(\gamma y)} & 0 \le y \le 0.5, \\ \sqrt{1.55(1-y) + 0.04(1-y)^2} & 0.5 < y \le 1, \end{cases} \tag{3.183}$$

with $T_0 = T_{\rm M}(\mu = 0) = 0.213$ GeV, $y = \mu/\mu_0$, where $\mu_0 = 0.345$ GeV corresponds to the point where $T_{\rm M} = 0$ and the chemical potential attains its maximum on the Mott line, and $\gamma = 2.7$. The formula (3.183) has relative accuracy $\le 3\%$ for chemical potentials $\mu \le 0.32$ GeV.

Next, all transport coefficients discussed in this section can be fitted with a generic formula

$$\chi_{\rm fit} = C \left(\frac{T}{T_{\rm M}}\right)^{-\alpha} \exp[a_1 y^2 + a_2 y^4 + a_3 y^6] \times \chi_{\rm div}, \tag{3.184}$$

where $\chi_{\rm fit} \in \{\sigma, \kappa, \kappa^*, \eta, \eta/s\}$. The term $\chi_{\rm div}$ is diverging in the limit $\mu \to 0$ in the case of $\kappa$ and is given by the formula

$$\chi_{\rm div} = \left(\frac{T}{T_{\rm M}}\right)^2 + y^{-2}. \tag{3.185}$$

For all other coefficients $\chi_{\rm div} = 1$. The values of the constants in formula (3.184) are given in Table 3.1

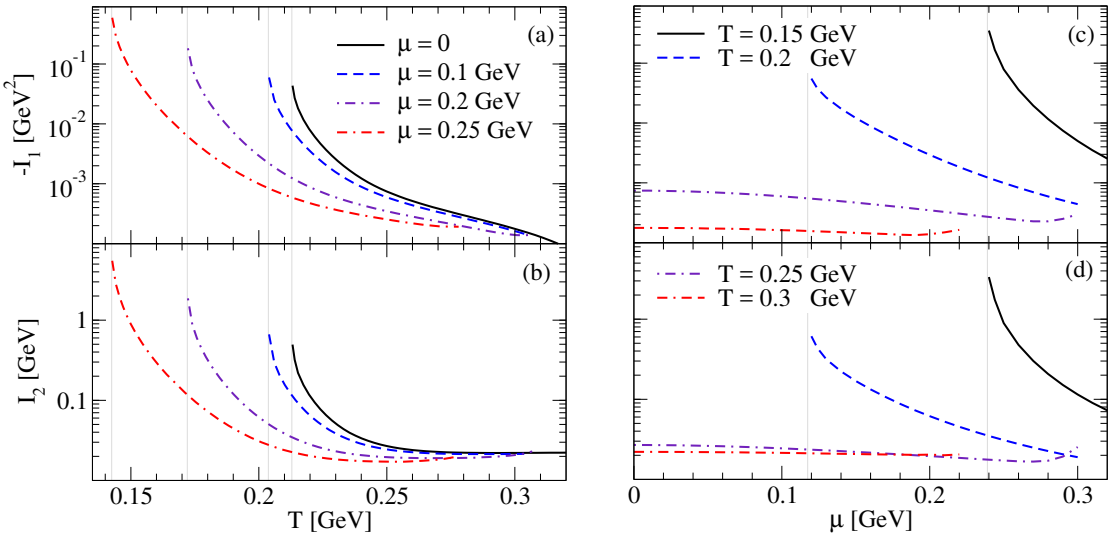


Figure 3.22: Dependence of the integrals $I_1$ (a), (c) and $I_2$ (b), (d) on the temperature for several values of the chemical potential (left panels) and on the chemical potential for several values of the temperature (right panels). The corresponding Mott lines are shown by vertical lines.

(for each transport coefficient $C$ is given in relevant units).

A comparison between the exact results and the fits is shown in Figs. 3.17 and 3.21, where an excellent agreement is observed for temperatures above $T/T_{\rm M} \geq 1.1$. In this domain all fit formulas have relative accuracy $\leq 10\%$.

## 3.7 Numerical results for bulk viscosity

We start our analysis with an examination of the influence of various factors entering the expressions for bulk viscosities $\zeta_0$, $\zeta_1$ and $\zeta_2$ (see Sec. 3.2.4). Readers interested only in the results on the bulk viscosity can skip to the following subsection.

### 3.7.1 Preliminaries

The behavior of the two-dimensional integrals determining $\zeta_0$, $I_1$ and $I_2$ through Eqs. (3.73), (3.79) and (3.80) is as follows. For a given value of $\varepsilon$ the inner integrands are peaked at $p \simeq |\varepsilon|$, as it was the case for the other transport coefficients. The heights of the peaks rapidly increase with the value of $|\varepsilon|$. As a consequence, the inner (momentum) integrals are increasing functions of $|\varepsilon|$ for $|\varepsilon| \leq \Lambda$. For energies larger than $\Lambda$ the peaks are outside of the momentum-integration range (because of the momentum cutoff $p \leq \Lambda$), and the momentum integral rapidly decreases with $|\varepsilon|$. It vanishes asymptotically in the limit $\varepsilon \to \pm\infty$ for $I_1$ and $I_2$, but tends to a constant value for $\zeta_0$. This asymptotic behavior is easily seen from Eq. (3.73). Its inner integrand can be roughly estimated as $\propto p^2\Big[2(\varepsilon^2 A_0 - p^2 A_v)^2 - (\varepsilon^2 - p^2)(\varepsilon^2 A_0^2 - p^2 A_v^2)\Big] = p^2\Big[(\varepsilon^2 A_0 - p^2 A_v)^2 + \varepsilon^2 p^2 (A_0 - A_v)^2\Big]$, where we approximated $\gamma \simeq 1/3$ and $\delta \simeq 0$ (see Sec. 3.5) and neglected the scalar component of the spectral function, which is small compared to the vector and temporal components. If $|\varepsilon| \gg p$, we can approximate Eqs. (3.121) and (3.122) as $n_1 = \varepsilon^2(1 - \varrho_0^2)$, $n_2 = \varepsilon^2 \varrho_0$. The dominant term in the integrand in this case is $\propto p^2\varepsilon^4 A_0^2 = p^2\varepsilon^4(\varrho_0 n_1 - 2n_2)^2/(n_1^2 + 4n_2^2)^2 = p^2\varrho_0^2/(1 + \varrho_0^2)^2$, which does not depend on $\varepsilon$ in the on-shell approximation to the self-energy. As a result, the momentum integral tends to a constant value for $|\varepsilon| \geq \Lambda$. The Fermi-factor $\partial n(\varepsilon)/\partial\varepsilon$ in the outer integrals of Eqs. (3.73), (3.79) and (3.80) has a maximum at the energy $\varepsilon = \mu$ and suppresses the contribution from energies, that are far from this value. We have verified numerically that it is sufficient to integrate up to the

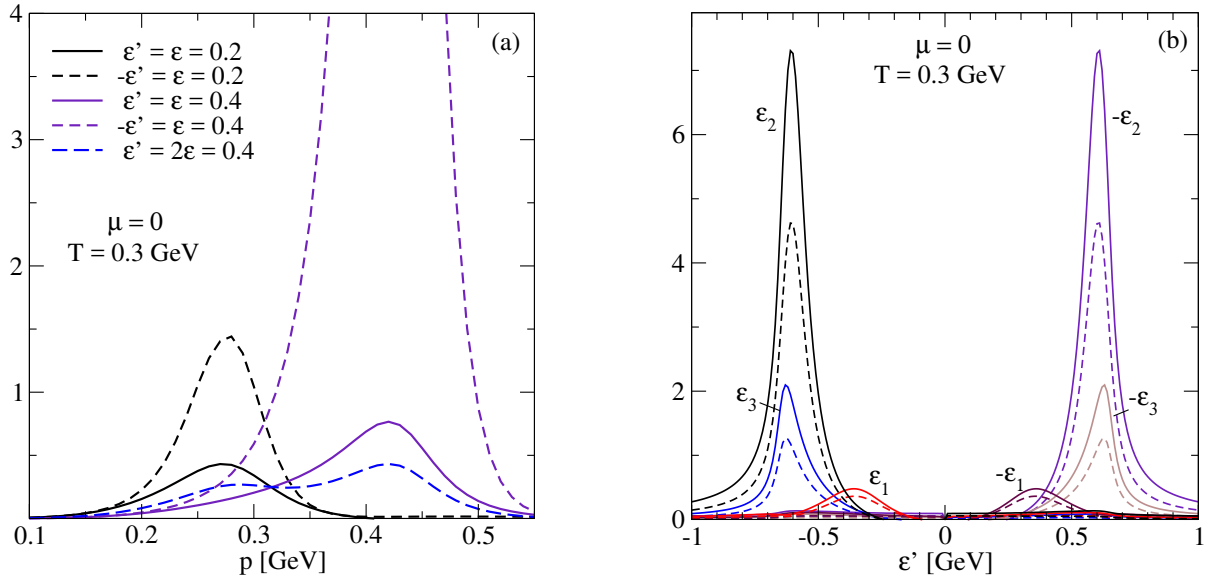


Figure 3.23: The integrands of the integral $R_0$: (a) the inner integrand as a function of quark momentum at various values of $\varepsilon$ and $\varepsilon'$ (shown in GeV units); (b) the $p$-integral of $R_0$ (solid lines, in GeV units) and its product with the factor $[n(\varepsilon) - n(\varepsilon')]/(\varepsilon - \varepsilon')$ (dashed lines) as functions of $\varepsilon'$ for various values of $\varepsilon$: $\varepsilon_1 = 0.3$, $\varepsilon_2 = 0.6$ and $\varepsilon_3 = 0.7$ GeV.

energy $|\varepsilon| \leq 2$ GeV. Next we note that the outer integral samples the contribution of antiquarks from the range $(-\infty, 0)$ and that of quarks from the range $(0, +\infty)$, and we are in a position to examine the contributions from quarks and antiquarks separately. We find that when $\mu = 0$, the integrands of Eqs. (3.73), (3.79), and (3.80) are even functions of $\varepsilon$, *i.e.*, the quark and antiquark contributions are the same. At nonzero chemical potentials the quark–antiquark symmetry is broken and the contributions from quarks and antiquarks differ. While the contributions of quarks and antiquarks to the (inner) momentum integrands are comparable at nonzero $\mu$, the factor $\partial n/\partial\varepsilon$ in the energy integration makes the quark contribution dominant.

The dependence of the integrals $I_1$ and $I_2$ on temperature and chemical potential is shown in Fig. 3.22. Both are rapidly decreasing functions of temperature (at fixed chemical potential) or chemical potential (at fixed temperature) in the regime close to the Mott line, as expected. In the whole temperature-density range considered $I_1$ is always negative, while $I_2$ is always positive. $-I_1$ is always a decreasing function of the temperature, whereas $I_2$ tends to a constant value at high temperatures for small chemical potentials, but shows a slight minimum at higher chemical potentials.

Next we turn to the discussion of three-dimensional integrals $R_0$ and $\bar{R}$, given by Eqs. (3.78) and (3.81). A new feature that appears in these expressions is the convolution of two spectral functions. As a result, the integrands of $R_0$ and $X$ have sharp peaks at $p \simeq |\varepsilon|$ if $|\varepsilon| \simeq |\varepsilon'|$, and they transform into broad structures with two smaller maxima located at $p \simeq |\varepsilon|$ and $p \simeq |\varepsilon'|$ when $|\varepsilon| \neq |\varepsilon|$, see Fig. 3.23, (a). Therefore, the main contribution to the integrals arises from the domain where $p \simeq |\varepsilon| \simeq |\varepsilon'|$. Because the integration range covers both positive and negative values of $\varepsilon$ there are two possibilities $\varepsilon' = \pm\varepsilon$ for the maximum to arise. In the case of $R_0$ integral only the minus sign is realized. Indeed, because the temporal and vector components of the spectral function have the same order of magnitude, the inner integrand of $R_0$ can be roughly estimated as $aa' + bb' - cc' \simeq \varepsilon\varepsilon' A_0 A_0' - p^2 A_v A_v' \simeq (\varepsilon\varepsilon' - p^2) A_0 A_0'$, see Eqs. (3.78). Therefore, the peaks around $p \simeq \varepsilon \simeq \varepsilon'$ originating from the temporal and vector components almost cancel each other, and the momentum integral is mainly concentrated around $\varepsilon' \simeq -\varepsilon$, see Fig. 3.23, (b). The integral $\bar{R}$ contains additional terms which support also a peak at $\varepsilon' \simeq \varepsilon$ and, consequently, the momentum integrand obtains contributions at two locations. In both cases of $R_0$ and $\bar{R}$ the height of the peaks rapidly increases with the increase of

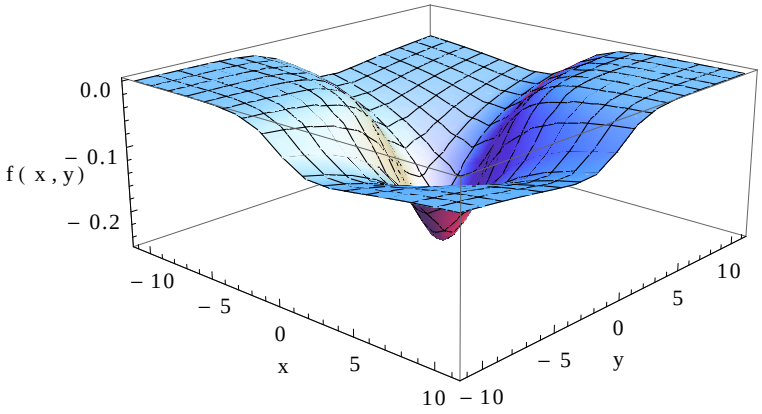


Figure 3.24: The factor $f(x,y) \equiv [n(x) - n(y)]/(x-y)$ in the integrand of $R_0$ with $x = (\varepsilon - \mu)/T$, $y = (\varepsilon' - \mu)/T$ and $n(x) = 1/(e^x + 1)$.

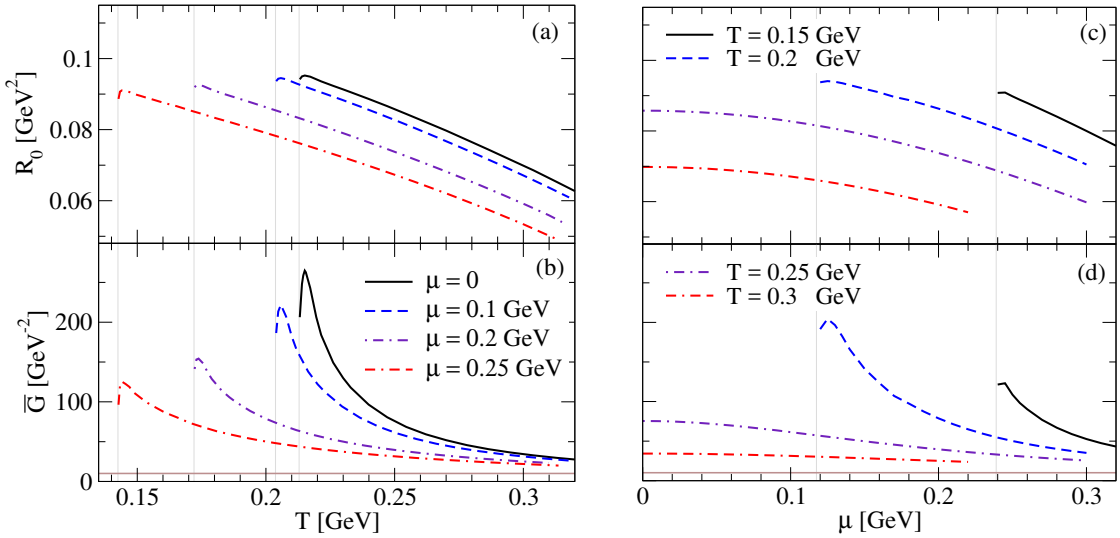


Figure 3.25: The integral $R_0$ (a), (c) and the renormalized coupling $\bar{G}$ (b), (d) as functions of the temperature for several values of the chemical potential (left panels) and as functions of the chemical potential for several values of the temperature (right panels). The value of the bare coupling constant $G$ is shown by the solid horizontal line. The corresponding Mott transition lines are shown by vertical lines.

$|\varepsilon|$ as long as $|\varepsilon| \leq \Lambda$ and becomes negligible for higher values of $|\varepsilon|$. The integration over $\varepsilon'$ contains also the factor $[n(\varepsilon) - n(\varepsilon')]/(\varepsilon - \varepsilon')$, which at low temperatures is strongly peaked at the energies $\varepsilon = \varepsilon' = \mu$, as seen from Fig. 3.24. At high temperatures it transforms into a bell-shaped broad structure (without change of the location of the maximum) and samples energies far away from $\mu$. It decreases faster at high energies in the case where $\varepsilon - \mu$ and $\varepsilon' - \mu$ have the same sign. The integrand of $\bar{R}$ contains an additional combination of Fermi functions $[\varepsilon n(\varepsilon) - \varepsilon' n(\varepsilon')]/(\varepsilon - \varepsilon') - 1/2$, which tends to the finite limits $-1/2$ and $1/2$, when $\varepsilon, \varepsilon' \to +\infty$ and $\varepsilon, \varepsilon' \to -\infty$, respectively.

The outer integrands of $R_0$ and $\bar{R}$ are rapidly increasing functions of $|\varepsilon|$ for $|\varepsilon| \leq \Lambda$ and they sharply drop at higher values of $|\varepsilon|$, as it was the case for the two-dimensional integrals $I_1$ and $I_2$. Our analysis shows that the momentum integrals in Eqs. (3.78) and (3.81) are invariant under the simultaneous transformations $\varepsilon \to -\varepsilon$, $\varepsilon' \to -\varepsilon'$ and $\mu \to -\mu$, as expected. Due to this property all integrals are even functions of the chemical potential.

Figure 3.25 illustrates the temperature and chemical potential dependence of the integral $R_0$

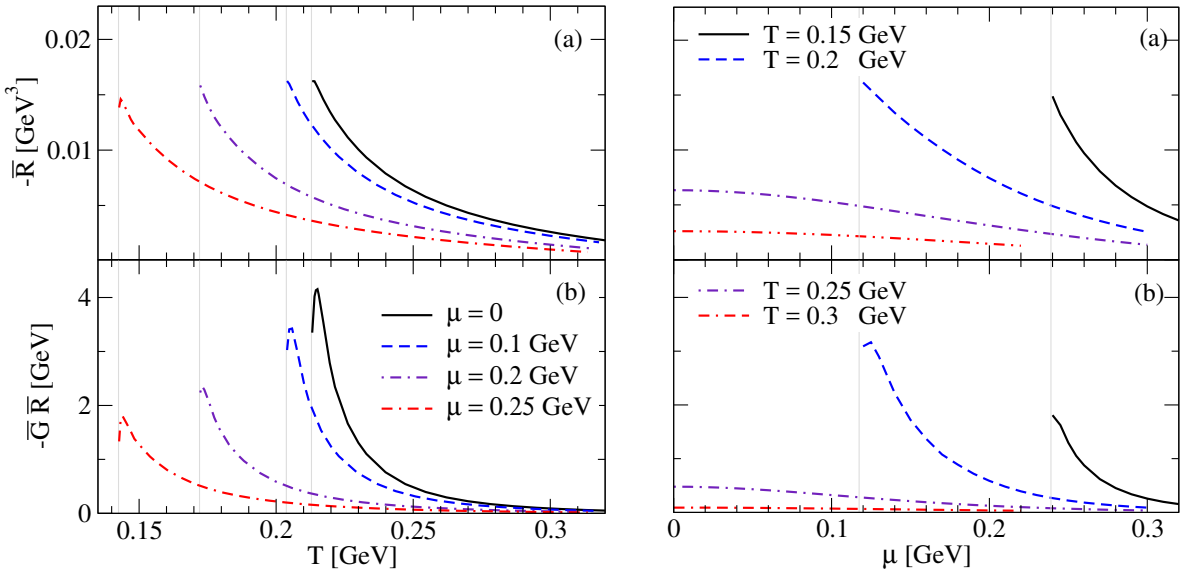


Figure 3.26: Integral $\bar{R}$ (a), (c) and the product $\bar{G}\bar{R}$ (b), (d) as functions of the temperature for various values of the chemical potential (left panels) and as functions of the chemical potential for various values of the temperature (right panels). The vertical lines show the corresponding Mott lines.

and the renormalized coupling $\bar{G} = G/(1 - GR_0)$ [see Eq. (B.23)]. The same dependence for the integral $\bar{R}$ and the product $\bar{G}\bar{R}$ is shown in Fig. 3.26. The latter combination enters the formulas of $\zeta_{1,2}$ components of the bulk viscosity, see Eq. (3.76). It is remarkable that $R_0$ and $\bar{R}$ remain finite at the Mott temperature in contrast to the integrals $I_1$ and $I_2$. The reason for this behavior can be understood if we recall that at the Mott temperature the imaginary parts of the self-energies essentially vanish, therefore the spectral functions transform into $\delta$-functions: $A_j(p, \varepsilon) \propto \delta(p^2 + m^2 - \varepsilon^2)$, where $j$ index labels the Lorentz component. Therefore, the integrands of the expressions (3.78) and (3.81) will contain a product of two $\delta$-functions at different arguments. When integrated over the variables $\varepsilon$ and $\varepsilon'$, the integral will consequently have a finite value. (This was not the case for two-dimensional intergals, where a single energy-integration led to two $\delta$-functions at the same argument and, therefore, to a divergent integral.) Apart from the different asymptotics for $T \to T_{\mathrm{M}}$, the generic quantitative temperature-density dependence of the three-dimensional intergrals $R_0$ and $\bar{R}$ does not differ significantly from that of two-dimensional integrals discussed above. Close to the Mott line we find $R_0 \simeq 0.1$ GeV$^2$ and therefore $\bar{G} \gg G \simeq 10$ GeV$^{-2}$. At high temperatures and chemical potentials $R_0$ decreases and $\bar{G}$ tends to its "bare" value. Thus, we anticipate that the renormalization of the coupling constant by multi-loop contributions and its impact on the bulk viscosity should be important in the low-temperature regime close to the Mott transition line. We also note that $\bar{R}$ is alway negative, which in combination with $I_1 < 0$ and $I_2 > 0$ guarantees the positivity of both $\zeta_1$ and $\zeta_2$ components in the entire temperature-density range.

### 3.7.2 Bulk viscosities

With the analysis above we are in a position to study the behavior of the components of the bulk viscosity $\zeta_0$, $\zeta_1$, $\zeta_2$ and their sum $\zeta$. Figures 3.27 and 3.28 show these quantities as functions of temperature and chemical potential, respectively. Because, as we have seen, the functions $|I_1|$, $I_2$, as well as $R_0$, $\bar{G}$ and $|\bar{R}|$ display a maximum at (or close to) the Mott line and decay with increasing temperature or chemical potential, the multi-loop contributions to the bulk viscosity $\zeta_1$ and $\zeta_2$ are expected to show analogous behavior. The one-loop result $\zeta_0$ is maximal at the Mott line as well, decreases with increasing $T$ or $\mu$, passes a minimum and increases according to a power law. At high temperatures the temperature scaling is $\zeta_0 \propto T^3$. This functional behavior arises from the fact that $\zeta_0$

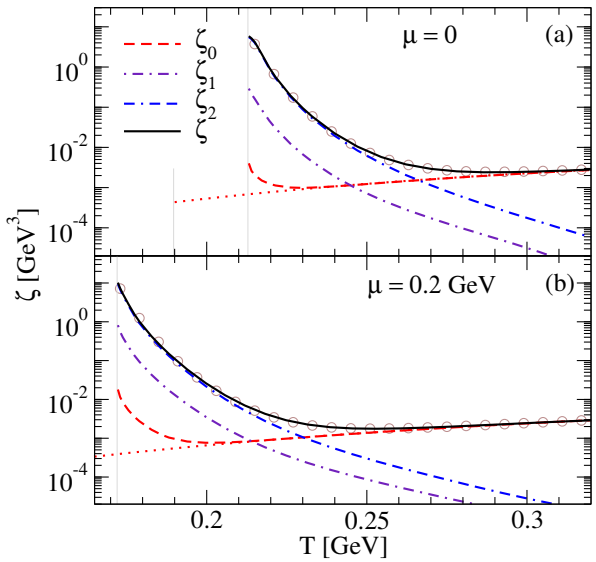


Figure 3.27: The three components of the bulk viscosity and their sum as functions of the temperature. The dotted lines correspond to the chiral limit $m_0 = 0$. The results of the fit formula (3.187) are shown by circles.

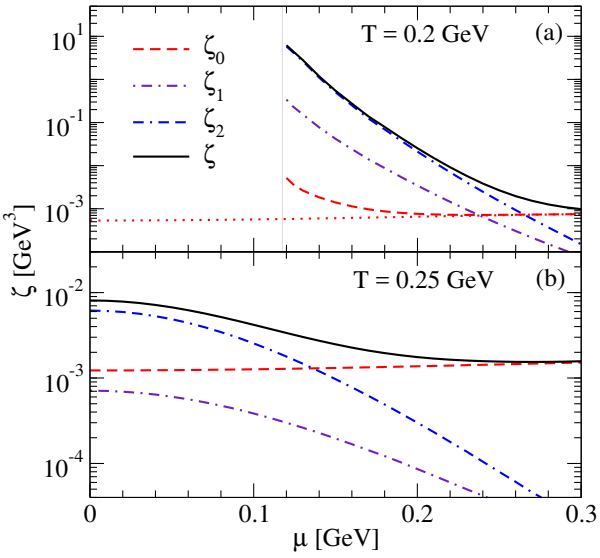


Figure 3.28: The three components of the bulk viscosity and their sum as functions of the chemical potential for two values of the temperature. The dotted lines correspond to the chiral limit $m_0 = 0$.

depends essentially on the difference of the temporal and vector components of the spectral function, see Eqs. (3.73)–(3.75), and its asymptotic increase for large $\mu$ or $T$ has been verified to be the result of the increase of the difference between those components with increasing $T$ or $\mu$, see Fig. 3.9. This is also the reason why the bulk viscosity evaluated in the one-loop approximation is negligible compared to the shear viscosity, which, as we have seen in the previous section, depends on the average amplitude of the components of the spectral function [91].

The contribution from the multi-loop processes dominates the one-loop result close to the corresponding Mott line, *i.e.*, at sufficiently low temperatures or chemical potentials, see Figs. 3.27 and 3.28. In this regime all three components $\zeta_0$, $\zeta_1$, $\zeta_2$ and, therefore, also the net bulk viscosity $\zeta$ drop rapidly with increasing temperature or chemical potential. The functional behavior of three components of the bulk viscosity around the Mott line is described by the universal formula

$$\zeta_i \propto \exp\left(\frac{a_i}{T/T_{\rm M} - b_i}\right), \quad i = 0, 1, 2, \tag{3.186}$$

where $a_i$ and $b_i \lesssim 1$ depend only on the chemical potential. In this regime the following inequalities hold $\zeta \simeq \zeta_2 \gg \zeta_1 \gg \zeta_0$, and we see from Figs. 3.27 and 3.28 that the one-loop result $\zeta_0$ underestimates the net bulk viscosity by three orders of magnitude.

The situation reverses for high $T$ and $\mu$, where the multi-loop contributions $\zeta_1$ and $\zeta_2$ decrease rapidly and one finds $\zeta \simeq \zeta_0 \gg \zeta_2 \gg \zeta_1$. As a consequence, the net bulk viscosity has a mild minimum as a function of temperature. In the high-temperature regime it increases as $\zeta \propto T^3$, but is almost independent on the chemical potential.

Thus, we conclude that in the high-$T$ or high-$\mu$ limits the single-loop approximation correctly represents the bulk viscosity, *i.e.*, the single loop provides indeed the leading-order contribution. This is clearly not the case in the low-$T$ or low-$\mu$ limits, close to the Mott line, where $\zeta_0$ fails to describe correctly the bulk viscosity, which is dominated by the multi-loop contributions from $\zeta_2$.

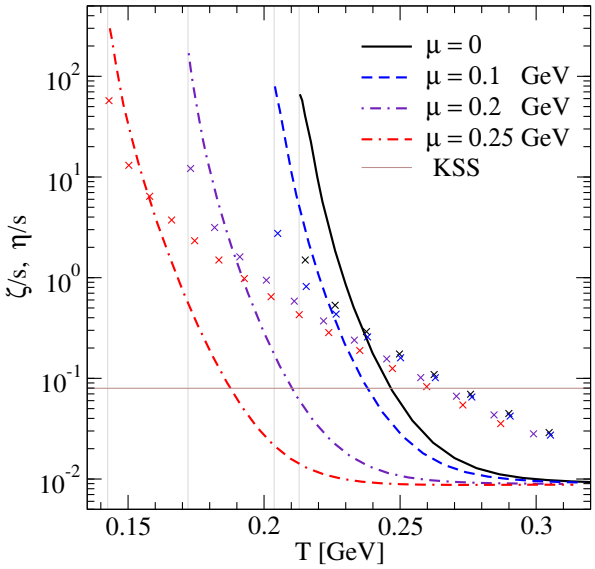


Figure 3.29: The ratio $\zeta/s$ as a function of the temperature for several values of the chemical potential. The corresponding $\eta/s$ ratios are shown for comparison by crosses. The solid horizontal line shows the KSS bound [81].

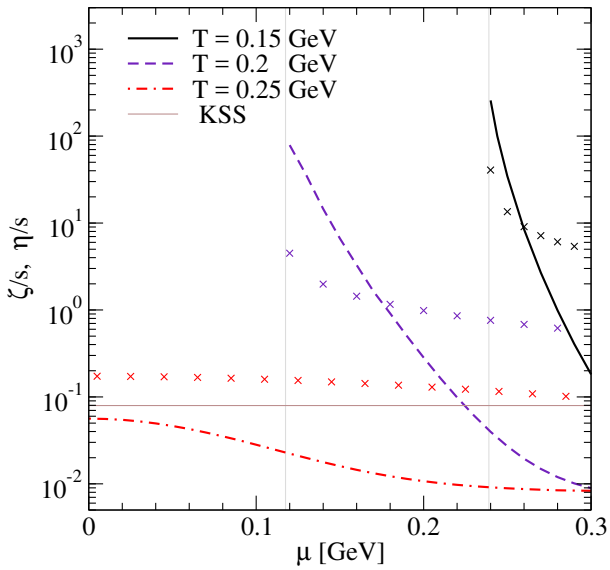


Figure 3.30: The ratio $\zeta/s$ as a function of the chemical potential for several values of the temperature. The corresponding ratios $\eta/s$ are shown by crosses. The solid horizontal line shows the KSS bound [81].

### 3.7.3 Chiral limit

It is interesting to explore also the case when the chiral symmetry is intact ($m_0 = 0$). In this case quarks become massless above the critical (Mott) temperature $T_c$, which implies vanishing multi-loop contributions, as already mentioned in Sec. 3.2.4. Consequently, the bulk viscosity is determined by the single-loop result (3.73) with $m = m_0 = 0$. As seen from Figs. 3.27 and 3.28, $\zeta_0$ in the chiral limit behaves quite differently from the case of $m_0 \neq 0$ close to the Mott temperature. It is smooth at the critical temperature and increases with the temperature as a power law in the entire parameter range. This behavior can be understood as follows. At $T \to T_c$ we have $m = 0$, $m_M \to 0$, therefore from Eqs. (3.132)–(3.138) we find $\varrho_0 \simeq \varrho_v \to 0$ for high momenta which contribute mostly to $\zeta_0$. Therefore, from Eqs. (3.121), (3.122) and (3.124) we estimate $n_1 \simeq p_0^2 - p^2$, $n_2 \simeq (p_0^2 - p^2)\varrho_0 \to 0$ and $A_{0,v}(p_0, p) \simeq -n_2/(n_1^2 + 4n_2^2) \sim \delta(p_0^2 - p^2)$. Now, substituting $\gamma = 1/3$, $\delta = 0$ in Eqs. (3.73)–(3.75) (see Section 3.5) we find that the integrand of $\zeta_0$ is proportional to $2(\varepsilon^2 A_0 - p^2 A_v)^2 - (\varepsilon^2 - p^2)(\varepsilon^2 A_0^2 - p^2 A_v^2) \sim (\varepsilon^2 - p^2)^2 \delta(\varepsilon^2 - p^2)^2 \to 0$, which implies that the integral remains regular in the limit $T \to T_c$. In the high-$T$ regime the results for $\zeta_0$ coincide with those of the case of explicit chiral symmetry breaking.

We note that according to the discussion above $\zeta_0$ component will vanish in any theory with weakly-interacting massless particles. The weakness of the interaction implies small spectral widths and, therefore, nearly on-mass-shell particles with $p \simeq \varepsilon$. As a consequence, the integrand in Eq. (3.73) vanishes, as expected.

### 3.7.4 Comparison to the shear viscosity

In Figs. 3.29 and 3.30 we show the dependence of the ratio $\zeta/s$ on temperature and chemical potential. For comparison we show also the ratio $\eta/s$ as computed in Ref. [91] and revised in Sec. 3.6.2, as well as the AdS/CFT lower bound $1/4\pi$ on that ratio [81]. As a general trend, the ratio $\zeta/s$ increases rapidly close to the Mott transition line with decreasing temperature or chemical potential and attains its maximum on this line. It becomes weakly dependent on these quantities as one moves away from this regime to high-$\mu$ and high-$T$ limit. The $\eta/s$ displays similar behavior, but the increase in the vicinity of the Mott line is not as steep as for $\zeta/s$. Numerically we find in this regime $\zeta \geq \eta$ with

| $T^*$ | $\alpha$ | $\Delta$ [MeV] |
|---|---|---|
| $T^0_{\rm min}$ | 0.65 | 90 |
| $T_{\rm min}$ | 0.86 | 106 |
| $T_{02}$ | 0.84 | 87 |
| $T_{\eta=\zeta}$ | 1.13 | $-6$ |

Table 3.2: The values of the fit parameters in Eq. (3.193).

$\zeta/\eta \simeq 5 \div 20$ on the Mott line. Thus, we conclude that close to the Mott transition line *the bulk viscosity dominates the shear viscosity by large factors and this dominance arises from the multi-loop processes.* We stress that had we kept only the one-loop contribution to the bulk viscosity, it would have been negligible compared to the shear viscosity. As the temperature or the chemical potential increases away from the Mott line, $\zeta$ decreases faster than $\eta$ and eventually one reaches the point where $\zeta = \eta$, beyond which shear viscosity dominates. This crossover point appears earlier than the point where $\zeta_0 \simeq \zeta_2$, beyond which $\zeta_0$ dominates the bulk viscosity, see the next subsection. Consequently, we conclude that if only $\zeta_0$ contribution is kept, then shear viscosity is the dominant source of dissipation in the entire temperature-density regime.

### 3.7.5 Fits to the bulk viscosity

The observed nearly universal low-$T$ behavior (3.186) of $\zeta_2$ component with the scaled temperature $T/T_{\rm M}$ for fixed values of the chemical potential and the high-$T$ asymptotics of $\zeta_0$ suggest fitting the net bulk viscosity in the whole temperature range by the formula

$$\zeta_{\rm fit}(T,\mu) = a(y)\exp\left[\frac{c(y)}{T/T_{\rm M}(y) - b(y)}\right] + d(y)T^3. \tag{3.187}$$

The coefficients $a, b, c, d$ depend on the chemical potential via the formulas [$y = \mu/(0.345\ \text{GeV})$]

$$a(y) = (2.57 - 5.65y^2) \times 10^{-6}\ [\text{GeV}^3], \tag{3.188}$$
$$b(y) = 0.806 - 0.055y^2 - 0.617y^4, \tag{3.189}$$
$$c(y) = 2.89 + 0.96y^2 + 12.73y^4, \tag{3.190}$$
$$d(y) = 0.082 + 0.02y^2. \tag{3.191}$$

The fit formula (3.187) is valid for chemical potentials $\mu \leq 0.2$ GeV, where its relative error is $\leq 10\%$. A comparison of the fit with the numerical result is shown in Fig. 3.27.

In the chiral limit the first term in Eq. (3.187) vanishes, and we are left with a pure power-law increase in the whole temperature-density range

$$\zeta_{\rm ch}(T,\mu) = T^3(0.082 + 0.168\mu^2), \tag{3.192}$$

where $T$ and $\mu$ are in GeV units.

Now we define several characteristic temperatures: $T^0_{\rm min}$ and $T_{\rm min}$, corresponding to the minimums of $\zeta_0$ and $\zeta$, respectively; $T_{02}$ - the temperature of the intersection of $\zeta_0$ and $\zeta_2$ components; and $T_{\zeta=\eta}$ - the temperature of the intersection of $\zeta$ and $\eta$. These temperatures vary with the chemical potential, or, equivalently, with the corresponding value of the Mott temperature. Interestingly, all these characteristic temperatures turn out to be linear functions of the Mott temperature with 1% accuracy and can be fitted as

$$T^*(\mu) = \alpha T_{\rm M}(\mu) + \Delta, \tag{3.193}$$

with $T^* = \{T^0_{\rm min}, T_{\rm min}, T_{02}, T_{\zeta=\eta}\}$, and the coefficients $\alpha$ and $\Delta$ do not depend on the chemical potential. Their numerical values are listed in Table 3.2.

## 3.8 Conclusions

In this chapter we have studied the electrical and thermal conductivities and the bulk viscosity as well as provided an update on the shear viscosity of quark matter within the two-flavor NJL model using the Kubo formalism [58, 59]. We have derived formulas for these transport coefficients of a relativistic quark plasma taking into account the full Lorentz structure of the self-energies (spectral functions) of the quarks. The two-point correlation functions are evaluated with the full propagator and within the $1/N_c$ approximation to the multi-loop contributions; these then imply that vertex corrections are suppressed and the leading-order contributions to the correlation functions arise from diagrams containing only loops. These diagrams reduce to a single-loop diagram for the conductivities and the shear viscosity, whereas an infinite series of loop diagrams should be summed up to find the leading-order contribution to the bulk viscosity. It is worthwhile to note that our Kubo formulas have generic validity and can be applied in the broader context of field theories of relativistic plasmas in a straightforward manner when the vertex corrections are suppressed by some mechanism.

We have applied this general formalism to compute the transport coefficients of the NJL model for quark matter in the regime where the dispersive effects arise from quark-meson scattering above the Mott temperature for dissolution of mesons into quarks. We find that the thermal and electrical conductivities are decreasing functions of temperature at fixed chemical potential; they show nearly universal behavior when the temperature is scaled by the Mott temperature, *i.e.*, as functions of $T/T_{\rm M}$. We also find that the ratio $\kappa/\sigma$ does not follow the Wiedemann-Franz law. Furthermore, we recomputed the shear viscosity of the model; we find a qualitative agreement with previous results of Refs. [91, 224, 225, 227]. In particular, the ratio of $\eta/s$ tends to the KSS bound $1/4\pi$ [81], but undershoots this bound at some intermediate temperature and fails to describe the high-temperature limit where gluonic degrees become important. We have also conjectured a lower bound on the ratio $\kappa^* T/c_V \geq 1/18$ on the basis of the uncertainty principle. This conjecture needs further studies from different standpoints, including methods well suited for non-perturbative calculations. Within the NJL model we find that this ratio undershoots the lower bound $1/18$ at high temperatures.

One of our key results is the observation that the single-loop contributions, which are dominant for the shear viscosity and the conductivities, are insufficient for the evaluation of the bulk viscosity. We demonstrated that close to the Mott temperature the multi-loop contributions, which require resummations of infinite geometrical series of loops, dominate the one-loop contribution. In the regime of interest the bulk viscosity is a decreasing function of temperature at fixed chemical potential, but after passing a minimum it increases again. The decreasing behavior is dominated by multi-loop contribution, whereas the high-$T$ increasing segment is dominated by the one-loop contribution.

Another key result of this study is the observation that the bulk viscosity dominates the shear viscosity of quark matter in the vicinity of the Mott temperature by factors of $5 \div 20$ depending on the chemical potential. With increasing temperature the bulk viscosity decreases faster than the shear viscosity and above a certain temperature we find $\eta \geq \zeta$. The range of validity of our comparison is limited by the temperature at which the ratio $\eta/s$ undershoots the KSS bound $1/4\pi$ and obviously the dispersive effects due to mesonic decays into quarks become insufficient to account for the shear viscosity of quark matter. Nevertheless, the observation of large bulk viscosity in the parameter domain of this study may have interesting and important implications for the hydrodynamical description of heavy-ion collisions at RHIC and LHC.

For practical implementations we have provided also simple fit formulas for the electrical and thermal conductivities as well as the shear and the bulk viscosities with a good relative accuracy, which can be utilized in numerical simulations of hydrodynamics of the quark plasma.

Looking ahead, we anticipate that the formalism described here can be straightforwardly extended

to include heavier flavor quarks, the most important being the strange quark. The NJL-model Lagrangian (3.1) employed in this work can be extended to include vector interactions and/or Polyakov loop contributions. The role of the confinement can be assessed by extending the NJL model to include the Polyakov loop at finite temperatures. The mesons, which appear in the present model as scatterers, can carry momentum and charge in heavy-ion experiments and can contribute to transport, as established in numerical simulations of such experiments (see Refs. [94, 230–232] and references therein). As the gluonic degrees of freedom are integrated out in the NJL-type models from the outset, the pure gauge contributions can be accounted only if one starts with an effective model that captures the gauge sector of QCD. In addition, having an access to the spectral functions of quarks, will allow us to compute the rates of the photon and dilepton emission from quark matter in the present model, which is again of interest for the tomography of heavy-ion collisions.

# Chapter 4

# Electrical conductivity of a warm neutron star crust in magnetic fields

## 4.1 Introduction

Electrical conductivity of crustal matter in neutron stars and interiors of white dwarfs plays a central role in the astrophysical description of these compact stars. The spectrum of problems where the conductivity of material is important includes magnetic field evolution [96–101], dissipation of MHD waves [102–105], etc. Transport in highly compressed matter has been studied extensively in the cold regime, *i.e.*, for temperatures $T \leq 1$ MeV ($1.16 \times 10^{10}$ K), which is relevant for neutron stars several minutes to hours past their formation in a supernova event, as well as for the interiors of white dwarfs. Initial studies of transport in dense matter appropriate for white dwarf stars go back to the work by Mestel and Hoyle [106] and Lee [107] in the 1950s, who computed the thermal conductivity of the electron-ion plasma in nonrelativistic electron regime, relevant for the radiative and thermal transport in white dwarfs. The electrical conductivity of ultracompressed matter, where electrons become relativistic (at zero temperature this corresponds to density $10^6$ g cm$^{-3}$) was computed by Abrikosov in 1963 [108] including the regime where matter is solid. These initial estimates were followed by a series of works in the 1960s and 1970s [109–117], among which the variational study of Flowers and Itoh [118] provides the most comprehensive account of transport in the solid and liquid regimes of crustal matter, as well as of the neutron drip regime, where free neutrons contribute to the thermal conductivity and the shear viscosity of matter. An alternative formulation in terms of Coulomb logarithm and a detailed comparison of results of various authors was given in Ref. [119]. The regime where ions form a liquid was studied in Ref. [121], where it was shown that the screening of electron-ion interactions can lead to substantial corrections in this case. These studies were further improved and extended in Refs. [102,103,120,122–127,129], which cover a broad range of densities and compositions appropriate for matter in white dwarfs and crusts of neutron stars in the case of strongly degenerate electrons and spherical nuclei. The special case of non-spherical nuclei (pasta phase) at the base of a neutron star crust, which may have very low electrical resistivity, is discussed in Ref. [130]. The implementation of the transport coefficients of dense matter in the dissipative MHD equations was discussed and the associated transport coefficients in strong magnetic fields were computed for the crust of a cold neutron star in the presence of magnetic fields by a number of authors [102, 103]. We confine our attention to non-quantizing fields in this work, *i.e.*, fields below the critical field $B \simeq 10^{14}$ G above which the Landau quantization of electron trajectories becomes important [128].

The early computations of conductivity of cold neutron star matter described above were motivated by the studies of magnetic field decay in neutron star interiors. Recent resistive MHD simulations of magnetized neutron stars in general relativity [73–75], including binary magnetized neutron star mergers and hypermassive neutron stars formed in the post-merger phase [76] require as an input the conductivity of warm (heated) crustal matter. In this regime the plasma forms a liquid state of

correlated ions and ionized electrons at nonzero temperature and in nonzero magnetic field. Such matter is also expected in proto-neutron stars newly formed in the aftermath of a supernova explosion as well as in the crusts of neutron stars accreting material from a companion.

In this chapter we start addressing the necessary input for resistive MHD simulations of such matter, specifically its electrical conductivity. In this regime electrons are the most mobile charge carriers and the key mechanism of the electrical conduction is the electron scattering off the ions. There are important statistical corrections to the free-space scattering rate: following earlier calculations we incorporate structure factors of one-component plasma (OCP) (we do not consider here the possibility of matter featuring a mixture of nuclei with different mass numbers and/or charges); in addition we include dynamical screening of exchanged photons which accounts for a frequency-dependent scattering rate. The photon self-energy is computed within the HTL effective field theory approach to the polarization tensor.

This chapter is organized as follows. Section 4.2 discusses the phase diagram of electron-ion plasma in the regimes of interest for neutron stars and white dwarfs. In Sec. 4.3 we derive the electrical conductivity tensor in magnetic field starting from the linearized Boltzmann equation for electrons. Section 4.4 computes the matrix element for electron-ion scattering including the screening of the interaction in the HTL approximation. We also discuss the input structure factor of ions (OCP). In Sec. 4.5 we present the numerical results for the electrical conductivity in the density, temperature and $B$-field regimes of interest. Our results are summarized in Sec. 4.6. Appendix C.1 gives the details of the derivation of the relaxation time used in the main text. We describe the computations of polarization tensor in Appendix C.2.

We use the natural units with $e = \sqrt{\alpha}$, $\alpha = 1/137$. This chapter is based on the papers [131, 132].

## 4.2 Physical conditions

Matter in the interiors of white dwarfs and in the neutron star crusts is in a plasma state - the ions are fully ionized while free electrons are the most mobile carriers of charge. Electron density is related to the ion charge $Z$ by the charge neutrality condition $n_e = Zn_i$, where $n_i$ is the number density of nuclei. Electrons to a good accuracy form non-interacting gas which becomes degenerate below the Fermi temperature $T_F = \varepsilon_F - m$, where the Fermi energy is defined as $\varepsilon_F = (p_F^2 + m^2)^{1/2}$, the electron Fermi momentum is given by $p_F = (3\pi^2 n_e)^{1/3}$ and $m$ is the electron mass. The state of ions with mass number $A$ and charge $Z$ is controlled by the value of the Coulomb plasma parameter

$$\Gamma = \frac{e^2 Z^2}{T a_i} \simeq 22.73 \frac{Z^2}{T_6} \left( \frac{\rho_6}{A} \right)^{1/3}, \tag{4.1}$$

where $e$ is the elementary charge, $T$ is the temperature, $a_i = (4\pi n_i/3)^{-1/3}$ is the radius of the spherical volume per ion, $T_6$ is the temperature in units $10^6$ K, and $\rho_6$ is the density in units of $10^6$ g cm$^{-3}$. If $\Gamma \ll 1$ or, equivalently $T \gg T_C \equiv Z^2 e^2/a_i$, ions form a weakly coupled Boltzmann gas. In the regime $\Gamma \geq 1$ ions are strongly coupled and form a liquid for values of $\Gamma \leq \Gamma_m \simeq 160$ and a lattice for $\Gamma > \Gamma_m$. The melting temperature of the lattice associated with $\Gamma_m$ is defined as $T_m = (Ze)^2/\Gamma_m a_i$. For temperatures below the ion plasma temperature

$$T_p = \left( \frac{4\pi Z^2 e^2 n_i}{M} \right)^{1/2}, \tag{4.2}$$

where $M$ is the ion mass, the quantization of oscillations of the lattice becomes important. Figure 4.1 shows the temperature-density phase diagram of the crustal material in the cases where it is composed of iron $^{56}$Fe, carbon $^{12}$C, helium $^4$He, and hydrogen $^1$H.

The general structure of the phase diagram for $^{56}$Fe shares many common features with the phase diagram of $^{12}$C. However, there is one important difference: as the temperature is lowered the quan-

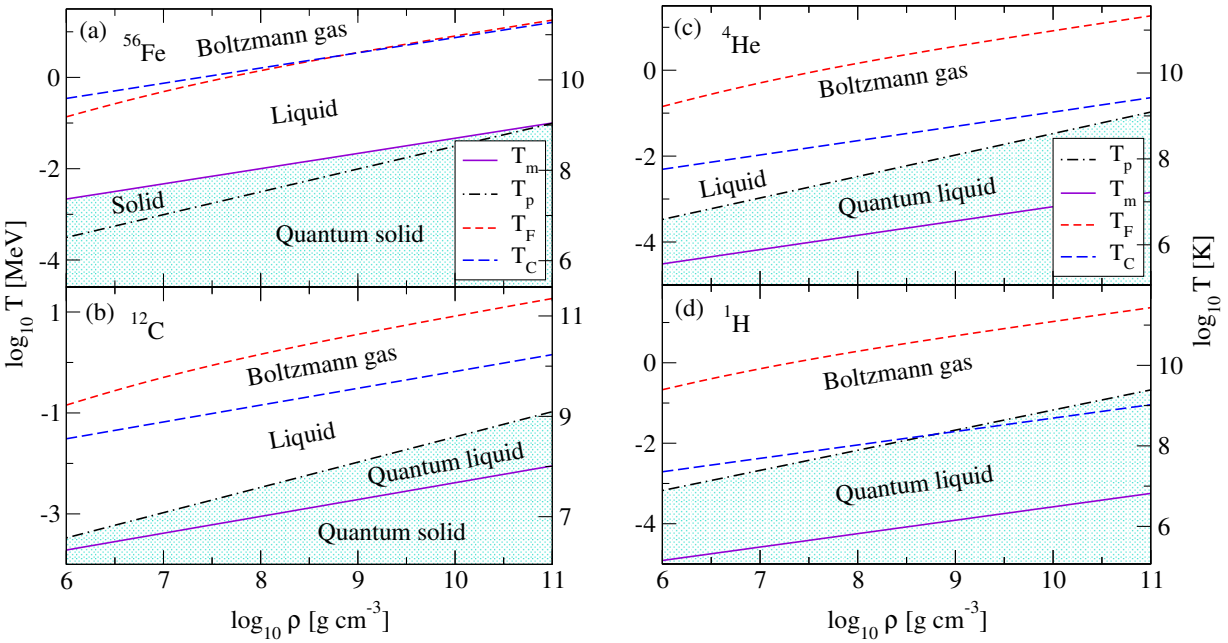


Figure 4.1: The temperature-density phase diagram of dense plasma composed of iron $^{56}$Fe (a), carbon $^{12}$C (b), helium $^{4}$He (c) and hydrogen $^{1}$H (d). The electron gas degeneracy sets in below the Fermi temperature $T_F$ (short dashed lines). The ionic component solidifies below the melting temperature $T_m$ (solid lines), while quantum effects become important below the plasma temperature (dash-dotted lines). For temperatures above $T_C$ (long dashed lines) the ionic component forms a Boltzmann gas. Note that for light elements $^{12}$C, $^{4}$He and $^{1}$H quantum effects become important in the portion of the phase diagram lying between the lines $T_p(\rho)$ and $T_m(\rho)$. The present study does not cover the shaded portion of the phase diagram.

tum effects become important for carbon prior to solidification, whereas iron solidifies close to the temperature where ionic quantum effects become important. The same feature is also seen in the phase diagrams of helium and hydrogen, where the quantum effects become important already in the liquid phase. Except for hydrogen and perhaps helium both of which may not solidify because of quantum zero point motions all heavier elements $Z > 2$ solidify at low enough temperature. Figure 4.2 shows the same phase diagram in the case of density-dependent crust composition adopted from Ref. [274], where nuclei are in weak equilibrium with electrons at zero temperature. As seen from the figure, in this case the general structure of the phase diagram is similar to that of matter composed of iron. Our studies do not cover the shaded portions of phase diagrams, where either lattice structure or quantum effects of crustal matter are important.

## 4.3 Electrical conductivity tensor

The kinetics of electrons is described by the Boltzmann equation for electron distribution function [71]

$$\frac{\partial f}{\partial t} + \boldsymbol{v}\frac{\partial f}{\partial \boldsymbol{r}} - e(\boldsymbol{E} + [\boldsymbol{v} \times \boldsymbol{B}])\frac{\partial f}{\partial \boldsymbol{p}} = I[f], \tag{4.3}$$

where $\boldsymbol{E}$ and $\boldsymbol{B}$ are the electric and magnetic fields, $\boldsymbol{v}$ is the electron velocity, $e$ is the unit charge, and $I[f]$ is the collision integral. In the relevant density and temperature regime electron-ion collisions are

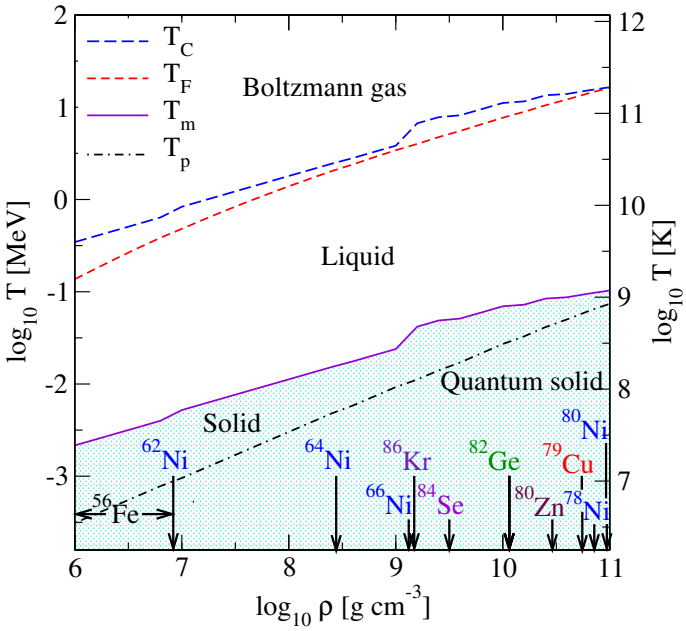


Figure 4.2: The temperature-density phase diagram of dense stellar matter in the crust of a neutron star. Various phases are labeled in the figure. The vertical arrows show the density at which the indicated element first appears. The crust composition is taken from Ref. [274]. The shaded portion of the phase diagram indicates the regime which is not covered by our study.

responsible for the conductivity of matter. [1] The collision integral has the form

$$I = -(2\pi)^4 \sum_{234} |\mathcal{M}_{12\to 34}|^2 \delta^{(4)}(p + p_2 - p_3 - p_4)[f(1-f_3)g_2 - f_3(1-f)g_4], \tag{4.4}$$

where $f = f(p)$ and $f_3 = f(p_3)$ are the distribution functions of the incoming and outgoing electrons, respectively; $g_{2,4} = g(p_{2,4})$ are the distribution functions of the ion before and after the collision; here and below we use the shorthand notation: $\sum_i = \int d\boldsymbol{p}_i/(2\pi)^3$. We will assume that ions form a classical ensemble in equilibrium, *i.e.*, their distribution function $g(p)$ is given by the Maxwell-Boltzmann distribution

$$g(p) = n_i \left(\frac{2\pi}{MT}\right)^{3/2} e^{-\beta\varepsilon}, \tag{4.5}$$

where $\varepsilon = p^2/2M$ and $\beta = T^{-1}$ is the inverse temperature. We are interested in perturbations that introduce small deviations from equilibrium, in which case the Boltzmann equation can be linearized. We thus consider small perturbation around the equilibrium Fermi-Dirac distribution function of electrons given by

$$f^0(\varepsilon) = \frac{1}{e^{\beta(\varepsilon-\mu)}+1}, \tag{4.6}$$

where $\varepsilon = \sqrt{p^2+m^2}$ and $\mu$ is the chemical potential and write

$$f = f^0 + \delta f, \qquad \delta f = -\phi \frac{\partial f^0}{\partial \varepsilon}, \tag{4.7}$$

[1] Here we neglect the possible contribution from positrons, which can be sizable only in the very low density and high temperature matter.

where $\delta f \ll f_0$ is a small perturbation. In the case of electrical conduction we can keep only the last term on the left-hand side of Eq. (4.3). We substitute the electron distribution function (4.7) in Eq. (4.3) and take into account the identities

$$\frac{\partial f^0}{\partial \boldsymbol{p}} = \boldsymbol{v}\frac{\partial f^0}{\partial \varepsilon}, \quad \frac{\partial f^0}{\partial \varepsilon} = -\beta f^0(1-f^0), \tag{4.8}$$

which follow directly from Eq. (4.6). To linear order in perturbation $\phi$ the Boltzmann equation reads

$$e\boldsymbol{v}\cdot\boldsymbol{E}\frac{\partial f^0}{\partial \varepsilon} - e[\boldsymbol{v}\times\boldsymbol{B}]\frac{\partial f^0}{\partial \varepsilon}\frac{\partial \phi}{\partial \boldsymbol{p}} = -I[f], \tag{4.9}$$

where the collision integral in the same approximation is given by

$$I[f] = -(2\pi)^4\beta\sum_{234}|\mathcal{M}_{12\to 34}|^2\delta^{(4)}(p+p_2-p_3-p_4)f^0(1-f_3^0)g_2(\phi-\phi_3). \tag{4.10}$$

The electric field appears in the drift term of linearized Boltzmann equation (4.9) at the order $O(1)$ (with respect to $\phi$), whereas the term involving magnetic field at order $O(\phi)$, because $[\boldsymbol{v}\times\boldsymbol{B}](\partial f^0/\partial\boldsymbol{p}) \propto [\boldsymbol{v}\times\boldsymbol{B}]\boldsymbol{v} = 0$. We next specify the form of the function $\phi$ in the case of conduction as

$$\phi = \boldsymbol{p}\cdot\boldsymbol{\Xi}(\varepsilon), \tag{4.11}$$

which after substitution into Eqs. (4.9) and (4.10) gives

$$e\boldsymbol{v}\frac{\partial f^0}{\partial \varepsilon}\left[\boldsymbol{E}+(\boldsymbol{\Xi}\times\boldsymbol{B})\right] = -I[f], \tag{4.12}$$

with

$$\begin{aligned} I[f] &= -(2\pi)^4\beta\sum_{234}|\mathcal{M}_{12\to 34}|^2\delta^{(4)}(p+p_2-p_3-p_4)f^0(1-f_3^0)g_2(\boldsymbol{p}\cdot\boldsymbol{\Xi}-\boldsymbol{p}\cdot\boldsymbol{\Xi}_3) \\ &= -(2\pi)^4\beta\boldsymbol{\Xi}\int d^4q\sum_{234}|\mathcal{M}_{12\to 34}|^2\delta^{(4)}(p-p_3-q)\delta^{(4)}(p_2-p_4+q) \\ &\quad\times f^0(1-f_3^0)g_2(\boldsymbol{p}-\boldsymbol{p}_3) = \frac{\partial f^0}{\partial\varepsilon}(2\pi)^{-5}\boldsymbol{\Xi}\int d\omega d\boldsymbol{q}\int d\boldsymbol{p}_2|\mathcal{M}_{12\to 34}|^2 \\ &\quad\times\delta(\varepsilon-\varepsilon_3-\omega)\delta(\varepsilon_2-\varepsilon_4+\omega)\frac{1-f_3^0}{1-f^0}g_2\boldsymbol{q} = \frac{\partial f^0}{\partial\varepsilon}(\boldsymbol{p}\cdot\boldsymbol{\Xi})\tau^{-1}(\varepsilon), \end{aligned} \tag{4.13}$$

where the relaxation time is defined by

$$\tau^{-1}(\varepsilon) = (2\pi)^{-5}\int d\omega d\boldsymbol{q}\int d\boldsymbol{p}_2|\mathcal{M}_{12\to 34}|^2\frac{\boldsymbol{q}\cdot\boldsymbol{p}}{p^2}\delta(\varepsilon-\varepsilon_3-\omega)\delta(\varepsilon_2-\varepsilon_4+\omega)g_2\frac{1-f_3^0}{1-f^0}. \tag{4.14}$$

In transforming the linearized collision integral (4.13) we approximated $\boldsymbol{\Xi}\approx\boldsymbol{\Xi}_3$ and introduced a dummy integration over energy and momentum transfers, *i.e.*, $\omega = \varepsilon-\varepsilon_3$ and $\boldsymbol{q} = \boldsymbol{p}-\boldsymbol{p}_3$. Equations (4.12) and (4.13) lead to

$$e\boldsymbol{v}\cdot\left[\boldsymbol{E}+(\boldsymbol{\Xi}\times\boldsymbol{B})\right] = -\boldsymbol{\Xi}\cdot\boldsymbol{p}\;\tau^{-1}(\varepsilon), \tag{4.15}$$

or, equivalently

$$eE\tau\varepsilon^{-1}\boldsymbol{e}+\omega_c\tau(\boldsymbol{\Xi}\times\boldsymbol{b})+\boldsymbol{\Xi} = 0, \tag{4.16}$$

where $\boldsymbol{b}\equiv\boldsymbol{B}/B$, $\boldsymbol{e}\equiv\boldsymbol{E}/E$, and $\omega_c = eB\varepsilon^{-1}$ is the cyclotron frequency of electrons.

It remains to express the vector $\boldsymbol{\Xi}$ describing the perturbation in terms of physical fields. Its most general decomposition is given by

$$\boldsymbol{\Xi} = \alpha \boldsymbol{e} + \beta \boldsymbol{b} + \gamma [\boldsymbol{e} \times \boldsymbol{b}], \tag{4.17}$$

where the coefficients $\alpha$, $\beta$ and $\gamma$ are functions of the electron energy. Substituting Eq. (4.17) in Eq. (4.16) one finds that $\alpha = -eE\tau/\varepsilon(1+\omega_c^2\tau^2)$, $\beta/\alpha = (\omega_c\tau)^2(\boldsymbol{e}\cdot\boldsymbol{b})$ and $\gamma/\alpha = -\omega_c\tau$. As a result, the most general form of the perturbation (4.11) is given by

$$\phi = -\frac{e\tau}{1+(\omega_c\tau)^2} v_i \left[\delta_{ij} - \omega_c\tau\varepsilon_{ijk}b_k + (\omega_c\tau)^2 b_i b_j\right] E_j, \tag{4.18}$$

where the Latin indices label the components of Cartesian coordinates. The electrical current is defined in terms of perturbation $\phi$ as

$$j_i = 2\int \frac{d\boldsymbol{p}}{(2\pi)^3} e v_i \phi \frac{\partial f^0}{\partial \varepsilon} \tag{4.19}$$

and, at the same time, it is related to the conductivity tensor $\sigma_{ij}$ by

$$j_i = \sigma_{ij} E_j. \tag{4.20}$$

Substituting Eq. (4.18) in Eq. (4.19) and combining it with Eq. (4.20) we find for the conductivity tensor

$$\sigma_{ij} = \delta_{ij}\sigma_0 - \varepsilon_{ijm}b_m\sigma_1 + b_i b_j \sigma_2, \tag{4.21}$$

where

$$\sigma_n = \frac{e^2\beta}{3\pi^2}\int_m^\infty d\varepsilon \frac{p^3}{\varepsilon}\frac{\tau(\omega_c\tau)^n}{1+(\omega_c\tau)^2} f^0(1-f^0), \quad n = 0,1,2. \tag{4.22}$$

The conductivity tensor has a simple form when the magnetic field is along the $z$-direction

$$\hat{\sigma} = \begin{pmatrix} \sigma_0 & -\sigma_1 & 0 \\ \sigma_1 & \sigma_0 & 0 \\ 0 & 0 & \sigma \end{pmatrix}, \tag{4.23}$$

where the longitudinal component $\sigma$ is the conductivity in the absence of magnetic field and is given by

$$\sigma = \frac{e^2\beta}{3\pi^2}\int_m^\infty d\varepsilon \frac{p^3}{\varepsilon}\tau f^0(1-f^0) = \sigma_0 + \sigma_2. \tag{4.24}$$

In this case the conduction becomes isotropic with $\boldsymbol{j} = \sigma\boldsymbol{E}$. The other two components of the matrix (4.23) are called transverse ($\sigma_0$) and Hall conductivities ($\sigma_1$), respectively.

## 4.4 Collision integral and relaxation time

We now turn to the evaluation of the collision integral, or, equivalently, the relaxation time, assuming that for temperatures and densities of interest relativistic electrons are scattered by correlated nuclei. In free space this process is described by the well-known Mott scattering by a Coulomb center. We use the standard QED methods to compute the transition probability, but include in addition the screening of the interaction by the medium in terms of polarization tensor.

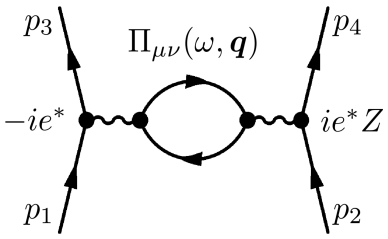


Figure 4.3: Feynman diagram describing the scattering of electron of charge $e^* = \sqrt{4\pi}e$ off a nucleus of charge $e^*Z$ (left and right straight arrows, respectively) via exchange of photon (wavy line). The photon self-energy is given by the polarization tensor $\Pi_{\mu\nu}(\omega, \boldsymbol{q})$ shown by the closed loop. Dots stand for QED vertices.

### 4.4.1 Scattering matrix element

The scattering amplitude for electron scattering off a nucleus characterized by its charge $Z$ is given by (see Fig. 4.3 and Appendix C.2 for details)

$$\mathcal{M}_{12\to34} = -\frac{J_0 J_0'}{q^2 + \Pi_L'} + \frac{\boldsymbol{J}_\perp \boldsymbol{J}_\perp'}{q^2 - \omega^2 + \Pi_T} = -\mathcal{M}_L + \mathcal{M}_T, \tag{4.25}$$

where

$$J^\mu = -e^* \bar{u}^{s_3}(p_3)\gamma^\mu u^{s_1}(p_1), \tag{4.26}$$
$$J'^\mu = Ze^* v'^\mu = Ze^*(1, \boldsymbol{p}'/M), \tag{4.27}$$

$e^* = \sqrt{4\pi}e$, and $\boldsymbol{J}_\perp, \boldsymbol{J}_\perp'$ are the components of the currents transverse to $\boldsymbol{q}$ ($\boldsymbol{p}_1 \equiv \boldsymbol{p}$, $\boldsymbol{p}_2 \equiv \boldsymbol{p}'$). The screening of the interaction is taken into account in terms of the longitudinal $\Pi_L(\omega, \boldsymbol{q})$ and transverse $\Pi_T(\omega, \boldsymbol{q})$ components of the polarization tensor, with $\Pi_L'(\omega, \boldsymbol{q}) \equiv \Pi_L(\omega, \boldsymbol{q})/(1 - \omega^2/q^2)$.

The form of the matrix element (4.25) includes thus the dynamical screening of the electron-ion interaction due to the exchange of transverse photons. Such separation has been employed previously in the treatment of transport of unpaired [275] and superconducting ultrarelativistic quark matter [215].

Standard QED diagrammatic rules can be applied to compute the transition probability from the diagram shown in Fig. 4.3. The square of the scattering matrix element can be written as

$$|\mathcal{M}_{12\to34}|^2 = |\mathcal{M}_L|^2 + |\mathcal{M}_T|^2 - 2\mathrm{Re}(\mathcal{M}_L \mathcal{M}_T^*), \tag{4.28}$$

where

$$|\mathcal{M}_L|^2 = \frac{J_0 J_0^* J_0' J_0'^*}{|q^2 + \Pi_L'|^2}, \tag{4.29}$$
$$|\mathcal{M}_T|^2 = \frac{J_i J_k^* J_{\perp i}' J_{\perp k}'^*}{|q^2 - \omega^2 + \Pi_T|^2}, \tag{4.30}$$
$$\mathcal{M}_L \mathcal{M}_T^* = \frac{J_0 J_i^* J_0' J_{\perp i}'^*}{(q^2 + \Pi_L')(q^2 - \omega^2 + \Pi_T^*)}, \tag{4.31}$$

*i.e.*, the scattering probability splits into longitudinal, transverse, and interference contributions. The scattering probability per unit volume should be obtained after averaging the scattering amplitude (4.28) over initial spins of electrons, summing over final spins, and multiplying with the structure factor of ions $S(q)$ and the square of nuclear formfactor $F^2(q)$.

In order to average over the spin variables we recall the sum rule

$$\sum_s u^s(p)\bar{u}^s(p) = \frac{\not{p}+m}{2\varepsilon}, \tag{4.32}$$

to obtain

$$\sum_{s_1 s_3}[\bar{u}^{s_3}(p_3)\gamma_\mu u^{s_1}(p_1)][\bar{u}^{s_3}(p_3)\gamma_\nu u^{s_1}(p_1)]^* = \frac{1}{4\varepsilon_1\varepsilon_3}\mathrm{Tr}\left[\gamma_\mu(\not{p}_1+m)\gamma_\nu(\not{p}_3+m)\right]. \tag{4.33}$$

The trace computation gives

$$\mathrm{Tr}\left[\gamma^\mu(\not{p}_1+m)\gamma^\nu(\not{p}_3+m)\right] = 4\left[p_1^\mu p_3^\nu + p_1^\nu p_3^\mu - g^{\mu\nu}((p_1p_3)-m^2)\right]. \tag{4.34}$$

Combining Eqs. (4.26), (4.33) and (4.34) we obtain for the current-current couplings

$$\frac{1}{2}\sum_{s_1 s_3} J_\mu J_\nu^* = \frac{e^{*2}}{2\varepsilon_1\varepsilon_3}\left[p_{1\mu}p_{3\nu} + p_{1\nu}p_{3\mu} - g_{\mu\nu}(\varepsilon_1\varepsilon_3 - \boldsymbol{p}_1\cdot\boldsymbol{p}_3 - m^2)\right]. \tag{4.35}$$

For various components we have

$$\frac{1}{2}\sum_{s_1 s_3} J_0 J_0^* = \frac{e^{*2}}{2\varepsilon_1\varepsilon_3}(\varepsilon_1\varepsilon_3 + \boldsymbol{p}_1\cdot\boldsymbol{p}_3 + m^2), \tag{4.36}$$

$$\frac{1}{2}\sum_{s_1 s_3} J_i J_k^* = \frac{e^{*2}}{2\varepsilon_1\varepsilon_3}\left[p_{1i}p_{3k} + p_{1k}p_{3i} + \delta_{ik}(\varepsilon_1\varepsilon_3 - \boldsymbol{p}_1\cdot\boldsymbol{p}_3 - m^2)\right], \tag{4.37}$$

$$\frac{1}{2}\sum_{s_1 s_3} J_0 J_i^* = \frac{e^{*2}}{2\varepsilon_1\varepsilon_3}(\varepsilon_1 p_{3i} + \varepsilon_3 p_{1i}). \tag{4.38}$$

Substituting these expressions into Eqs. (4.29)–(4.31) we obtain

$$\frac{1}{2}\sum_{s_1 s_3}|\mathcal{M}_L|^2 = \frac{1}{2}\sum_{s_1 s_3}\frac{J_0 J_0^* J_0' J_0'^*}{|q^2+\Pi_L'|^2} = \frac{Z^2e^{*4}}{2\varepsilon_1\varepsilon_3}\frac{\varepsilon_1\varepsilon_3 + \boldsymbol{p}_1\cdot\boldsymbol{p}_3 + m^2}{|q^2+\Pi_L'|^2}, \tag{4.39}$$

$$\begin{aligned}\frac{1}{2}\sum_{s_1 s_3}|\mathcal{M}_T|^2 &= \frac{1}{2}\sum_{s_1 s_3}\frac{J_i J_k^* J_{\perp i}' J_{\perp k}'^*}{|q^2-\omega^2+\Pi_T|^2} = \frac{Z^2e^{*4}}{2\varepsilon_1\varepsilon_3}\frac{1}{M^2|q^2-\omega^2+\Pi_T|^2}\\ &\times\left[2(\boldsymbol{p}_1\cdot\boldsymbol{p}_\perp')(\boldsymbol{p}_3\cdot\boldsymbol{p}_\perp') + (\boldsymbol{p}_\perp')^2\left(\varepsilon_1\varepsilon_3 - \boldsymbol{p}_1\cdot\boldsymbol{p}_3 - m^2\right)\right],\end{aligned} \tag{4.40}$$

$$\frac{1}{2}\sum_{s_1 s_3}\mathcal{M}_L\mathcal{M}_T^* = \frac{1}{2}\sum_{s_1 s_3}\frac{J_0 J_{\perp i}^* J_0' J_{\perp i}'^*}{(q^2+\Pi_L')(q^2-\omega^2+\Pi_T^*)} = \frac{Z^2e^{*4}}{2\varepsilon_1\varepsilon_3 M}\frac{[\varepsilon_1(\boldsymbol{p}_3\cdot\boldsymbol{p}_\perp') + \varepsilon_3(\boldsymbol{p}_1\cdot\boldsymbol{p}_\perp')]}{(q^2+\Pi_L')(q^2-\omega^2+\Pi_T^*)}. \tag{4.41}$$

From Eqs. (4.28), (4.39)–(4.41) we obtain for the entire matrix element

$$\begin{aligned}\frac{1}{2}\sum_{s_1 s_3}|\mathcal{M}_{12\to34}|^2 = \frac{Z^2e^{*4}}{2\varepsilon_1\varepsilon_3}\Bigg\{&\frac{\varepsilon_1\varepsilon_3 + \boldsymbol{p}_1\cdot\boldsymbol{p}_3 + m^2}{|q^2+\Pi_L'|^2} - \frac{2}{M}\frac{\varepsilon_1(\boldsymbol{p}_3\cdot\boldsymbol{p}_\perp') + \varepsilon_3(\boldsymbol{p}_1\cdot\boldsymbol{p}_\perp')}{\mathrm{Re}[(q^2+\Pi_L')(q^2-\omega^2+\Pi_T^*)]}\\ &+\frac{2(\boldsymbol{p}_1\cdot\boldsymbol{p}_\perp')(\boldsymbol{p}_3\cdot\boldsymbol{p}_\perp') + (\boldsymbol{p}_\perp')^2\left(\varepsilon_1\varepsilon_3 - \boldsymbol{p}_1\cdot\boldsymbol{p}_3 - m^2\right)}{M^2|q^2-\omega^2+\Pi_T|^2}\Bigg\}.\end{aligned} \tag{4.42}$$

The nominators can be further simplified by using the relations $\boldsymbol{p}_3 = \boldsymbol{p}-\boldsymbol{q}$ and $\varepsilon_3 = \varepsilon-\omega$. Taking

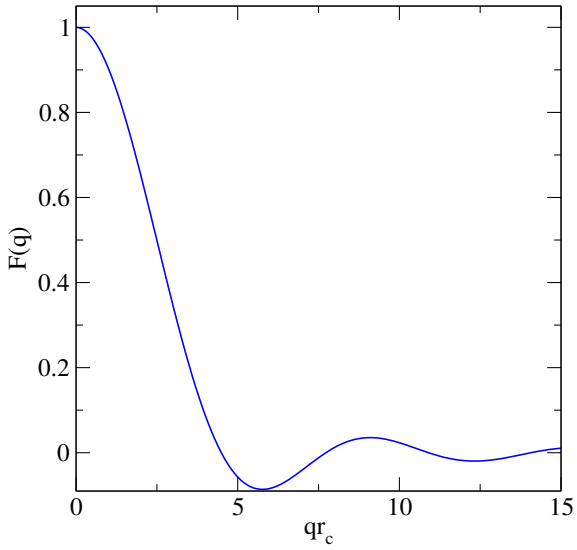


Figure 4.4: Dependence of the nuclear formfactor on the magnitude of momentum transfer $q$ in units of inverse nuclear radius $r_c$.

into account that $\boldsymbol{q}\cdot\boldsymbol{p}'_\perp = 0$ and dropping the index 1 we obtain

$$\frac{1}{2}\sum_{s_1 s_3}|\mathcal{M}_{12\to 34}|^2 = \frac{Z^2 e^{*4}}{2\varepsilon(\varepsilon-\omega)}\left\{\frac{\varepsilon(2\varepsilon-\omega)-\boldsymbol{p}\cdot\boldsymbol{q}}{|q^2+\Pi'_L|^2}+\frac{2(\boldsymbol{p}_\perp\cdot\boldsymbol{p}'_\perp)^2+(p'_\perp)^2(\boldsymbol{p}\cdot\boldsymbol{q}-\varepsilon\omega)}{M^2|q^2-\omega^2+\Pi_T|^2}\right.$$
$$\left.-\frac{2(2\varepsilon-\omega)(\boldsymbol{p}_\perp\cdot\boldsymbol{p}'_\perp)}{M\mathrm{Re}[(q^2+\Pi'_L)(q^2-\omega^2+\Pi^*_T)]}\right\}S(q)F^2(q). \tag{4.43}$$

In the last step we added also the ion structure factor $S(q)$ and the nuclear formfactor $F(q)$, which account for the ion-ion correlation and the finite size of the nuclei, respectively. We use the simple expression for the nuclear formfactor [122]

$$F(q) = -3\frac{qr_c\cos(qr_c)-\sin(qr_c)}{(qr_c)^3}, \tag{4.44}$$

where $r_c$ is the charge radius of the nucleus given by $r_c = 1.15\,A^{1/3}$ fm. The function $F(q)$ is shown in Fig. 4.4.

### 4.4.2 Relaxation time

Substituting the transition probability (4.43) into the expression for the relaxation time (4.14) and carrying our the integrations (see Appendix C.1 for details) we finally obtain

$$\tau^{-1}(\varepsilon) = \frac{\pi Z^2 e^4 n_i}{\varepsilon p^3}\int_{-\infty}^{\varepsilon-m} d\omega e^{-\omega/2T}\frac{f^0(\varepsilon-\omega)}{f^0(\varepsilon)}\int_{q_-}^{q_+} dq(q^2-\omega^2+2\varepsilon\omega)S(q)F^2(q)\frac{1}{\sqrt{2\pi}\theta}$$
$$\times\; e^{-\omega^2/2q^2\theta^2}e^{-q^2/8MT}\left\{\frac{(2\varepsilon-\omega)^2-q^2}{|q^2+\Pi'_L|^2}+\theta^2\frac{(q^2-\omega^2)[(2\varepsilon-\omega)^2+q^2]-4m^2q^2}{q^2|q^2-\omega^2+\Pi_T|^2}\right\}, \tag{4.45}$$

where $\theta=\sqrt{T/M}$, $q_\pm = |\pm p+\sqrt{p^2-(2\omega\varepsilon-\omega^2)}|$ and $\varepsilon=\sqrt{p^2+m^2}$ for non-interacting electrons. The contributions of longitudinal and transverse photons in Eq. (4.45) separate (first and second terms in the braces). The dynamical screening effects contained in the transverse contribution are parametrically suppressed by the factor $T/M$ at low temperatures and for heavy nuclei. This contribution is clearly important in the cases where electron-electron ($e$-$e$) scattering contributes to the collision

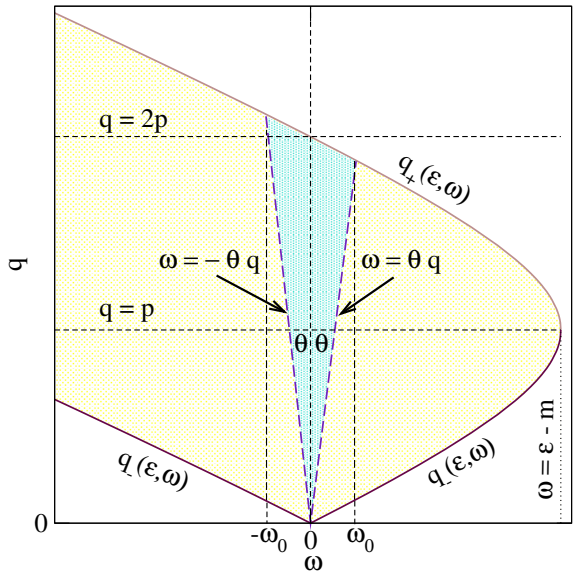


Figure 4.5: The integration region in Eq. (4.45) in the plane $(\omega, q)$ (light shaded area) bounded by the functions $q_\pm(\varepsilon,\omega)$. The major contribution to the integral comes from the triangle bound by the lines $\omega = \pm\theta q$ with the narrow opening angle $2\theta$ (dark shaded area).

integral. This is the case, for example, when ions form a solid lattice and, therefore, Umklapp $e$-$e$ processes are allowed, or in the case of thermal conduction and shear stresses when the $e$-$e$ collisions contribute to the dissipation.

In our numerical calculations the temperature varies mostly in the range $0.1 \leq T \leq 10$ MeV and the masses of the nuclei lie in the range $10^3 \leq M \leq 10^5$ MeV. Therefore, the parameter $\theta$ changes in the range $10^{-3} \leq \theta \leq 10^{-1} \ll 1$. As a result, one can expect that the dynamical part of the scattering amplitude should be suppressed compared with the static part by several orders of magnitude. Numerical calculations show that the contribution of the dynamical part is smaller than 1.5% for $^1$H and 0.4% for $^4$He, and has the order of $\theta^2$, as expected. For heavy nuclei these corrections are negligible, *e.g.*, 0.15% for $^{12}$C and 0.04% for $^{56}$Fe. Due to the exponential factor $e^{-\omega^2/2q^2\theta^2}$ in the integrand of Eq. (4.45) only small values of $\omega$ ($|\omega| \lesssim q\theta$) contribute significantly to the integral (4.45). Therefore, the effective phase volume of the double integration in Eq. (4.45) reduces to the triangle limited by the lines

$$\omega = \pm\theta q, \quad q_+(\varepsilon,\omega) = 2p - \omega v^{-1} \approx 2p. \tag{4.46}$$

as illustrated in Fig. 4.5. It is seen from this figure that the effective width of $\omega$ variable is given by $\omega_0 = 2p\theta$.

### 4.4.3 Recovering limiting cases

In Eq. (4.45) we can take the limit where the ionic component of the plasma is at zero temperature (the temperature of the electronic component is arbitrary so far). Then, because

$$\lim_{\theta\to 0} \frac{1}{\theta\sqrt{2\pi}} \mathrm{e}^{-x^2/2\theta^2} = \delta(x), \tag{4.47}$$

we obtain

$$\tau^{-1}(\varepsilon) = \frac{\pi Z^2 e^4 n_i}{\varepsilon p^3} \int_0^{2p} dq q^3 S(q) F^2(q) e^{-q^2/8MT} \frac{4\varepsilon^2 - q^2}{|q^2 + \Pi'_L|^2}, \tag{4.48}$$

where we took into account the fact that for $\omega = 0$ the limits on momentum transfer reduce to $q_- = 0$ and $q_+ = 2p$. Neglecting also the nuclear recoil (which amounts to replacing the exponential factor $e^{-q^2/8MT}$ by unity) we obtain the well-known expression of the relaxation time

$$\tau^{-1}(\varepsilon) = \frac{\pi Z^2 e^4 n_i}{\varepsilon\, p^3} \int_0^{2p} dq q^3 S(q) F^2(q) \frac{4\varepsilon^2 - q^2}{|q^2 + \Pi'_L|^2}. \tag{4.49}$$

Note that the nuclear recoil factor $e^{-q^2/8MT}$ can be important at very low temperatures and high densities for light nuclei, where it can reduce the scattering amplitude significantly. For example, in the extreme cases $T = 0.01$ MeV, $\log_{10}\rho = 11$ for $^{12}$C or $T = 0.1$ MeV, $\log_{10}\rho = 11$ for $^{1}$H we find that the relative error could be larger than a factor of 2. Therefore, Eq. (4.48) is a better approximation than Eq. (4.49) in the static limit $\omega \to 0$. However, in the main density-temperature range we consider the nuclear recoil and the dynamical screening introduce only small corrections and do not change the general behavior of the conductivity. The maximum deviations between Eqs. (4.49) and (4.45) (mostly at high densities $\log_{10}\rho \simeq 11$ and low temperatures $T \lesssim 0.1$ MeV) are 30% for $^{1}$H and $^{4}$He, 12% for $^{12}$C and 5% for $^{56}$Fe. The only exception where the dynamical effects change the behaviour of the relaxation time is hydrogen at high densities and low temperatures, see Sec. 4.5.1 for details.

It can be shown that at densities $\rho \leq 10^{11}$ g cm$^{-3}$ the effect of nuclear form factor is small as well. Indeed, for the heaviest nucleus that we consider ($^{86}$Kr, see Fig. 4.2) $r_c \simeq 0.025$ MeV$^{-1}$ and the maximal value of the parameter is $qr_c \simeq 0.5$. For small $qr_c$ we can use the approximate formula obtained from Eq. (4.44)

$$F^2(q) \approx 1 - 0.2(qr_c)^2, \tag{4.50}$$

therefore the maximal correction for $^{86}$Kr is 5%, which is consistent with numerical results. The corrections are smaller than 4% for $^{56}$Fe, 2% for $^{12}$C and 1% for $^{2}$He and $^{1}$H.

Consider now two limiting cases with respect to the temperature of the electronic component of the plasma: (i) the degenerate limit, *i.e.*, $T \ll T_F$; and (ii) the nondegenerate limit, *i.e.*, $T \gg T_F$. In the zero-temperature limit Eqs. (4.22) and (4.24) simplify via the substitution $\partial f^0/\partial\varepsilon = -\beta f^0(1 - f^0) \to -\delta(\varepsilon - \varepsilon_F)$, *i.e.*,

$$\sigma_n = \frac{e^2}{3\pi^2} \frac{p_F^3}{\varepsilon_F} \tau_F \frac{(\omega_{cF}\tau_F)^n}{1 + (\omega_{cF}\tau_F)^2} \tag{4.51}$$

and

$$\sigma = \frac{n_e e^2 \tau_F}{\varepsilon_F}, \qquad \sigma_0 = \frac{\sigma}{1 + (\omega_{cF}\tau_F)^2}, \qquad \sigma_1 = (\omega_{cF}\tau_F)\sigma_0, \tag{4.52}$$

where we used the expression for the electron Fermi momentum $p_F = (3\pi^2 n_e)^{1/3}$ and defined $\tau_F \equiv \tau(\varepsilon_F)$ and $\omega_{cF} \equiv eB/\varepsilon_F$. The first relation in Eq. (4.52) is the well-known Drude formula. From Eq. (4.49) we find in the low-temperature limit

$$\tau_F^{-1} = \frac{4Ze^4\varepsilon_F}{3\pi} \int_0^{2p_F} dq\, q^3 \frac{S(q)F^2(q)}{|q^2 + \Pi'_L|^2} \left(1 - \frac{q^2}{4\varepsilon_F^2}\right), \tag{4.53}$$

where we used the charge neutrality condition $n_e = Zn_i$. Neglecting the screening ($\Pi'_L \to 0$) and the nuclear formfactor [$F(q) \to 1$] we obtain from Eq. (4.53)

$$\tau_F^{-1} = \frac{4Ze^4\varepsilon_F}{3\pi} \int_0^{2p_F} \frac{dq}{q} \left(1 - \frac{q^2}{4\varepsilon_F^2}\right) S(q), \tag{4.54}$$

which coincides with Eqs. (9) and (11) of Ref. [121].

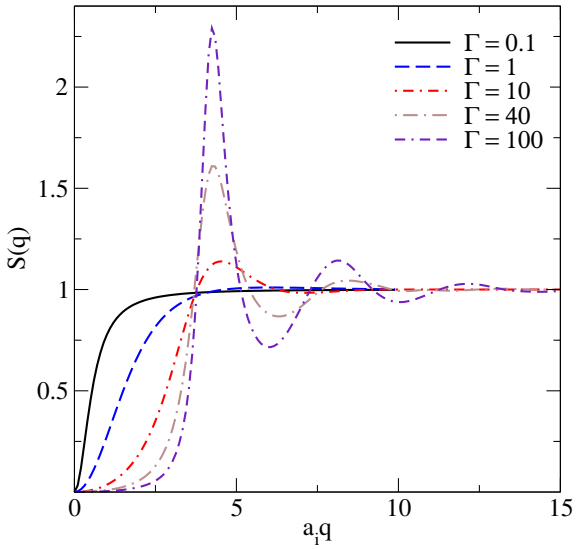


Figure 4.6: Dependence of the structure factor of one-component plasma (OCP) on the magnitude of momentum transfer $q$ in units of inverse $a_i$. For $\Gamma \geq 2$ the structure factor is taken from Monte-Carlo calculations of Galam and Hansen [133]. For $\Gamma < 2$ we obtain the structure factor from the analytical expressions provided by Tamashiro *et al.* [276].

In the limit of nondegenerate electrons $f^0 \ll 1$ and, therefore,

$$\sigma_n \simeq \frac{e^2}{3\pi^2 T}\int_m^\infty p^2 dp \frac{p^2}{\varepsilon^2}\frac{\tau(\omega_c\tau)^n}{1+(\omega_c\tau)^2} f^0 = \frac{n_e e^2}{3T}\langle v^2 \frac{\tau(\omega_c\tau)^n}{1+(\omega_c\tau)^2}\rangle, \tag{4.55}$$

where the quantities in the brackets are taken at some average energy $\bar{\varepsilon} \sim T$, which can be identified with the average thermal energy of a particle (electron) in the Boltzmann limit. We recall that the statistical average of an energy-dependent quantity $F(\varepsilon)$ is defined as

$$\langle F(\varepsilon)\rangle = \frac{2}{n_e}\int \frac{d\boldsymbol{p}}{(2\pi)^3} F(\varepsilon) f^0(\varepsilon), \tag{4.56}$$

where the factor 2 arises from the spin of electrons. In Eq. (4.55) we can further replace $v^2/3T \to 1/\bar{\varepsilon}$, consequently

$$\sigma \simeq \frac{n_e e^2 \bar{\tau}}{\bar{\varepsilon}}, \qquad \sigma_0 \simeq \frac{\sigma}{1+(\bar{\omega}_c\bar{\tau})^2}, \qquad \sigma_1 \simeq \frac{\bar{\omega}_c\bar{\tau}\sigma}{1+(\bar{\omega}_c\bar{\tau})^2}, \tag{4.57}$$

where $\bar{\omega}_c = eB/\bar{\varepsilon}$, $\bar{\tau} = \tau(\bar{\varepsilon})$. Thus, the formulas in both strongly degenerate and nondegenerate regimes have the same form, but different characteristic energy scale, which is $\varepsilon_F$ in the degenerate regime and $\bar{\varepsilon} \simeq 3T$ in the nondegenerate, ultrarelativistic regime. In the case where $T \sim m$ we use $\bar{\varepsilon} = 3T/2 + \sqrt{(3T/2)^2 + m^2}$, which arises from the condition $\bar{v}^2\bar{\varepsilon} = 3T$, where $\bar{v}$ is the mean velocity.

### 4.4.4 Ion structure factor

For the numerical computations we need to specify the ion structure factor $S(q)$. We assume that only one sort of ions exists at a given density, so that the structure factor of OCP can be used. This has been extensively computed using various numerical methods. We adopt the Monte Carlo results of Galam and Hansen [133] for Coulomb OCP provided in tabular form for $\Gamma \geq 2$ and set a two-dimension spline function in the space spanned by the magnitude of the momentum transfer $q$ and the plasma parameter $\Gamma$. For small momentum transfers $qa_i < 1$ we use the formulas (A1) and

(A2) of Ref. [120].

In the low-Γ regime ($\Gamma \leq 2$), not covered by the Monte Carlo results, we use the analytical (leading order) expressions for Coulomb OCP by Tamashiro *et al.* [276], derived using density functional methods. The dependence of the resulting structure factors on the dimensionless parameter $a_i q$, where $a_i$ is the ion-sphere radius as defined after Eq. (4.1), is shown in Fig. 4.6 for various values of the plasma parameter Γ. Note that these correlation functions were derived for classical plasma, therefore the quantum aspects of motion of light elements with $Z \leq 6$ in the temperature regime $T_p \geq T \geq T_m$ are not accounted for. It is seen that the structure factor universally suppresses the contribution from small-$q$ scattering. The suppression sets in for larger $q$ at larger values of Γ. The large-$q$ asymptotics is independent of Γ as $S(q) \to 1$. The major difference arises for intermediate values of $q$ where the structure factor oscillates and the amplitude of oscillations increases with the value of Γ parameter.

### 4.4.5 Polarization tensor

The screening of longitudinal and transverse interactions is determined by the corresponding components of the photon polarization tensor. The expression (4.45) is exact with respect to the form of the polarization tensor. We will use an approximation to Eq. (4.45) derived within the HTL effective field theory of QED [277,278] in Appendix C.2; see also the related work on astrophysical relativistic, dense gases of Refs. [279–281]. Our computations, outlined in detail in Appendix C.2, are carried out at nonzero temperature and density and include the mass of electrons; formally, we require the four-momentum of the photon to be small compared with the four-momentum of the fermions in the loop. For the longitudinal and transverse components of the polarization tensor we find

$$\Pi_L(q,\omega) = \left(1-x^2\right)\int_0^\infty dp\mathcal{F}(\varepsilon)\left[1-\frac{x}{2v}\log\frac{x+v}{x-v}\right], \tag{4.58}$$

$$\Pi_T(q,\omega) = \frac{1}{2}\int_0^\infty dp\mathcal{F}(\varepsilon)\left[x^2+\left(v^2-x^2\right)\frac{x}{2v}\log\frac{x+v}{x-v}\right], \tag{4.59}$$

where $x=\omega/q$ and $v=\partial\varepsilon/\partial p = p/\varepsilon$ is the particle velocity and

$$\mathcal{F}(\varepsilon) = -\frac{4e^2}{\pi}p^2\left[\frac{\partial f^+(\varepsilon)}{\partial\varepsilon}+\frac{\partial f^-(\varepsilon)}{\partial\varepsilon}\right]. \tag{4.60}$$

In the degenerate or ultrarelativistic limits the velocity has a constant value $\bar{v}$ and Eqs. (4.58) and (4.59) can be written as

$$\Pi_L = q_D^2\left(1-x^2\right)\left[1-\frac{x}{2\bar{v}}\log\frac{x+\bar{v}}{x-\bar{v}}\right], \tag{4.61}$$

$$\Pi_T = \frac{1}{2}q_D^2\left[x^2+\left(\bar{v}^2-x^2\right)\frac{x}{2\bar{v}}\log\frac{x+\bar{v}}{x-\bar{v}}\right], \tag{4.62}$$

where $\bar{v}=v_F$ in the degenerate and $\bar{v}=1$ in the ultrarelativistic limits, respectively, and the Debye wave number $q_D$ is given by the radial part of the phase-space integral

$$q_D^2 = \int_0^\infty dp\ \mathcal{F}(\varepsilon). \tag{4.63}$$

Dropping the contribution of antiparticles we find in the limiting cases of highly degenerate and nondegenerate matter

$$q_D^2 \simeq 4e^2\begin{cases} p_F\,\varepsilon_F/\pi, & T\ll T_F,\\ \pi\,n_e\,/T, & T\gg T_F,\end{cases} \tag{4.64}$$

where in the last line we introduced the electron number density ($f^0 \equiv f^+$)

$$n_e = 2\int \frac{d\boldsymbol{p}}{(2\pi)^3} f^0(\varepsilon). \tag{4.65}$$

Equations (4.61) and (4.62) coincide with Eqs. (8) and (9) of Ref. [280], if we take into account the first line of Eq. (4.64) and substitute $e^2 \to e^2/4\pi$ in our equations. Note that Eqs. (4.61) and (4.62) can be also applied in the general case, if $\bar{v}$ is defined as the characteristic velocity of electrons.

At temperatures of interest it is more economical to use low $x \ll 1$ expansions for the polarization tensor (see Sec. 4.4.2); we keep the next-to-leading in $x$ terms and find

$$\Pi'_L(q,\omega) = q_D^2 \chi_l, \qquad \Pi_T(q,\omega) = q_D^2 \chi_t, \tag{4.66}$$

where the susceptibilities to order $O(x^2)$ are given by

$$\mathrm{Re}\chi_l(q,\omega) = 1 - \frac{x^2}{\bar{v}^2}, \quad \mathrm{Im}\chi_l(q,\omega) = -\frac{\pi x}{2\bar{v}}, \tag{4.67}$$

$$\mathrm{Re}\chi_t(q,\omega) = x^2, \qquad \mathrm{Im}\chi_t(q,\omega) = \frac{\pi}{4} x\bar{v}. \tag{4.68}$$

Because the terms containing $\bar{v}$ are small as well as electrons are ultrarelativistic in the entire regime of interest with exception of very low densities we approximate $\bar{v} = 1$ in our numerical calculations.

## 4.5 Numerical results

Numerically the electrical conductivity is evaluated using the relaxation time given by Eq. (4.45) in the most general case with the ion structure factor given in Fig. 4.6 and polarization tensor given by Eqs. (4.66)–(4.68). With this relaxation time we evaluate the components of the conductivity tensor using Eq. (4.22). We recall that for large magnetic fields the tensor structure of the conductivity is important, while in the limit of negligible fields only the single quantity (scalar or longitudinal conductivity) $\sigma = \sigma_0 + \sigma_2$ is relevant, see Eq. (4.24).

### 4.5.1 Results for relaxation times

We provide in Figs. 4.7–4.9 numerical values of the relaxation time for a number of cases of interest. We stress that $\tau$ is energy-dependent and is evaluated in the degenerate case at the Fermi energy and in the nondegenerate case at $\bar{\varepsilon} \simeq 3T$, which is the thermal energy of ultrarelativistic electrons, see Sec. 4.4.3. In Fig. 4.7 we show the dependence of the relaxation time and the factor $\omega_c\tau$ on density for two values of temperature, which correspond either to the degenerate [panels (a) and (b)] or to the nondegenerate regime [panels (c) and (d)]. It is seen that in the degenerate regime ($T = 0.1$ MeV) the slope of decrease in the relaxation time is smaller than in the case of the nondegenerate regime. We see that only in the case of hydrogen the relaxation time changes its behaviour from a decreasing to an increasing function at sufficiently high densities and low temperatures. This effect is found to be a consequence of the nuclear recoil effect. (However, this result for hydrogen might not be very trustworthy as the quantum effects which are not accounted for in our approach are already important at the relevant temperature-density range, see Fig. 4.1.)

We see also from Fig. 4.7 (b) and (d) that the factor $\omega_c\tau$ makes a crossover from being much larger than unity at small densities to being much smaller at high densities. This indicates that in low-density matter the effects of anisotropy are much more important than in the high-density matter. In fact, in the nondegenerate case the low-density matter has highly anisotropic conductivity with, for example, $\omega_c\tau \sim 10^3$ for $B_{12} = 1$. We see also, that anisotropy in the conduction becomes more pronounced for lighter elements. For example, for $^4$He and $^1$H the crust is practically anisotropic in the entire density-temperature range considered here.

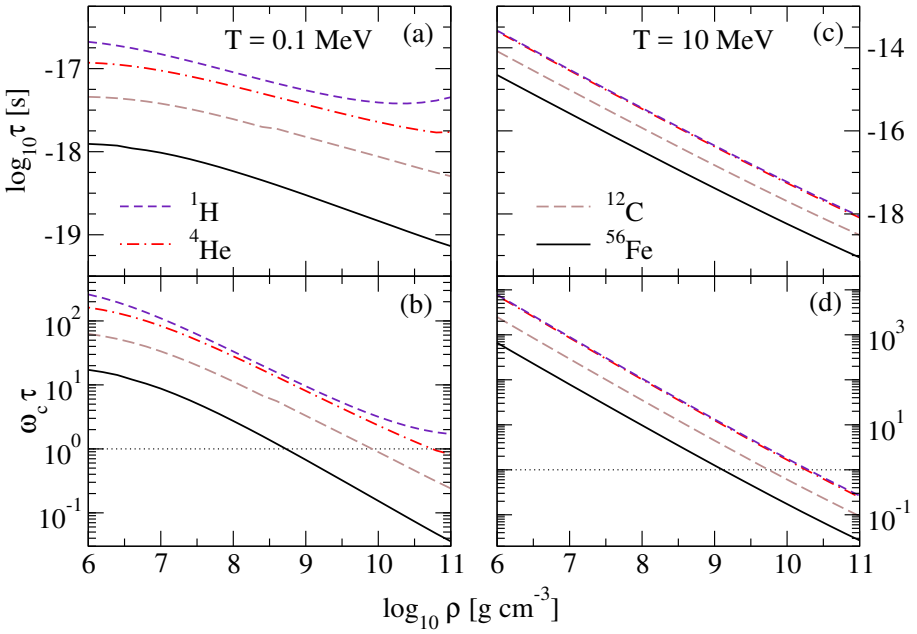


Figure 4.7: The relaxation time [(a) and (c)] and dimensionless product $\omega_c\tau$ [(b) and (d)] as functions of density. The temperature is fixed at $T = 0.1$ MeV in (a) and (b) (degenerate regime) and at $T = 10$ MeV in (c) and (d) (nondegenerate regime). The magnetic field is fixed at $B_{12} = 1$.

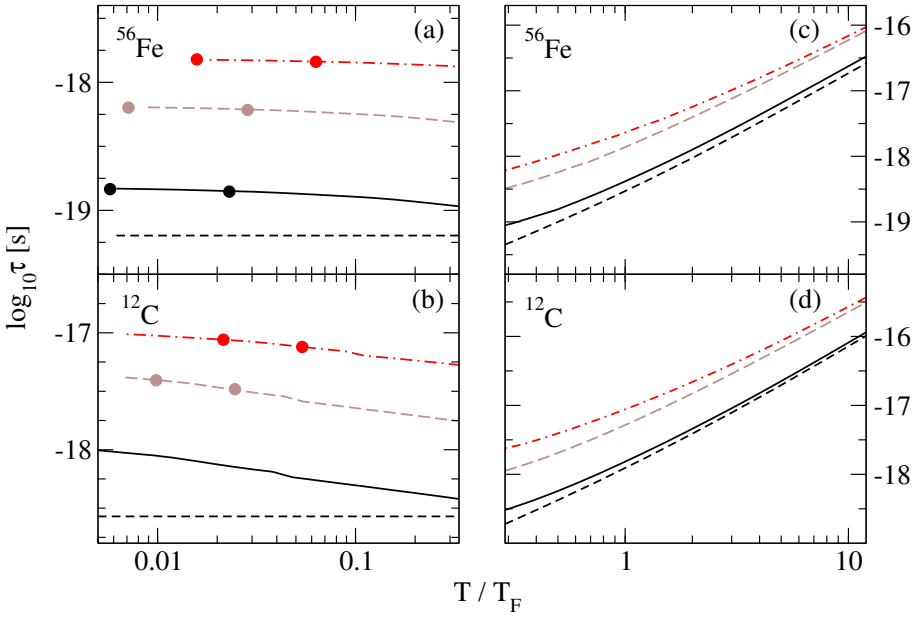


Figure 4.8: The relaxation time as a function of dimensionless ratio $T/T_F$ for three values of density: $\log_{10}\rho = 10$ (solid lines), $\log_{10}\rho = 8$ (dashed lines), $\log_{10}\rho = 6$ (dash-dotted lines) for $^{56}$Fe [(a) and (c)] and $^{12}$C [(b) and (d)]. Panels (a) and (b) correspond to the degenerate and (c) and (d) - to the nondegenerate regime. To demonstrate the effect of ion-ion correlations, we show the results for $\log_{10}\rho = 10$ in the case where $S(q) = 1$ by short-dashed lines. The open circles reproduce the results of Ref. [121].

Figures 4.8 and 4.9 show the temperature dependence of the relaxation time in the degenerate [panels (a) and (b)] and the nondegenerate [panels (c) and (d)] regimes. Our results agree well with those of Nandkumar and Pethick [121] in the degenerate regime. It is seen that $\tau$ decreases as a

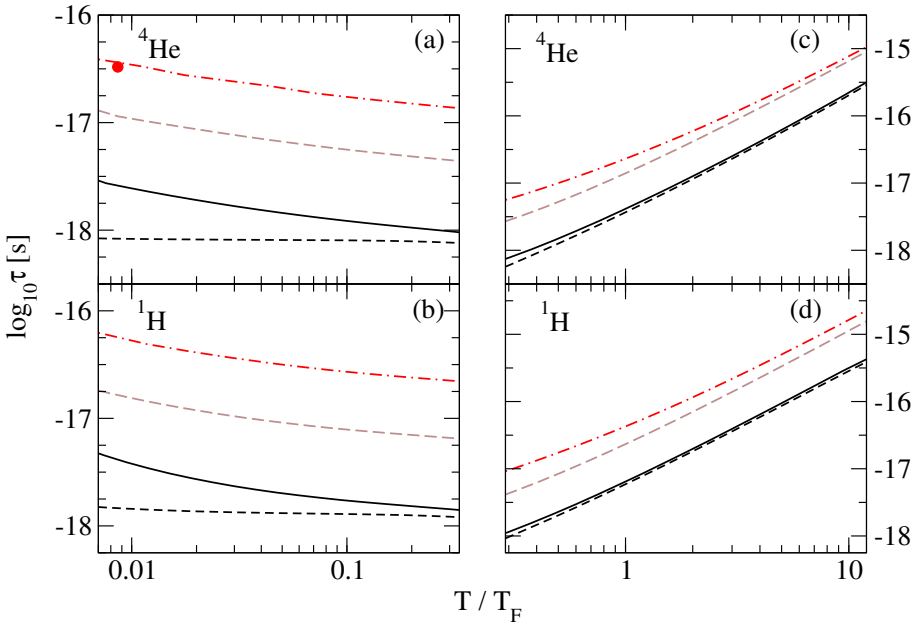


Figure 4.9: Same as in Fig. 4.8, but for $^4$He [(a) and (c)], and $^1$H [(b) and (d)].

function of temperature in the degenerate regime and increases in the nondegenerate regime. The temperature decrease in the degenerate regime is caused almost entirely by the structure factor $S(q)$. For comparison we evaluated also the relaxation time without taking into account the structure factor in Figs. 4.8 and 4.9. In the nondegenerate regime the temperature dependence of $\tau$ is dominated by the energy increase of electrons with temperature and the role of $S(q)$ is less important, especially for light nuclei. This is due to the fact that when $T \geq T_F$, *i.e.*, electrons are nondegenerate, the ionic component forms a weakly coupled Boltzmann gas for composition consisting of $^{56}$Fe nuclei with $\Gamma \lesssim 1$ and for compositions consisting of $^{12}$C, $^4$He and $^1$H nuclei with $\Gamma \ll 1$ (see Fig. 4.1).

### 4.5.2 Results for longitudinal conductivity

We start our analysis of the numerical results for the conductivity tensor with the density, temperature and composition dependence of the scalar (longitudinal) conductivity $\sigma$ given by Eq. (4.24). We relegate to the next subsection the discussion of the $\sigma_0$ and $\sigma_1$ components, which is straightforward after we have clarified the basic features of $\sigma$. We will also first study the cases of crustal matter consisting of one element ($^{56}$Fe, $^{12}$C, $^4$He and $^1$H) and later on consider density-dependent composition in Sec. 4.5.4.

The upper panels of Figs. 4.10 and 4.11 show $\sigma$ as a function of density for various temperatures. The value of the magnetic field is fixed at $B_{12} = 1$; here and below we use the units $B_{12} = B/(10^{12}$ G) to characterize the magnetic field. The temperature values range from the nondegenerate regime ($T = 10$ MeV) to the degenerate regime ($T = 0.1$ MeV) where the case $T = 1$ MeV is a representative for transition from the nondegenerate to the degenerate regime, which occurs around $\rho \simeq 10^8$ g cm$^{-3}$ for all nuclei (see Fig. 4.1). In each case $\sigma$ shows a power-law dependence on density $\sigma \propto \rho^{\alpha}$; in the degenerate regime $\alpha \simeq 0.4$ for $^{56}$Fe, $\alpha \simeq 0.45$ for $^{12}$C, and $\alpha \simeq 0.5$ for both $^4$He and $^1$H. Note that at high-dentity regime $^1$H shows a sharper increase because of the reversed behaviour of the relaxation time in this domain. As was mentioned above, this is a consequence of the nuclear recoil effect. In the nondegenerate regime the increase in the conductivity is less steep with $\alpha \simeq 0.1$ for all nuclei.

The behavior of the conductivity in the degenerate and nondegenerate regimes can be traced back to the different density and temperature dependence of the relaxation time in these regimes. The conductivity depends in both regimes on the ratio $\tau(\varepsilon)/\varepsilon$ and is proportional to $n_e$, see Eqs. (4.52)

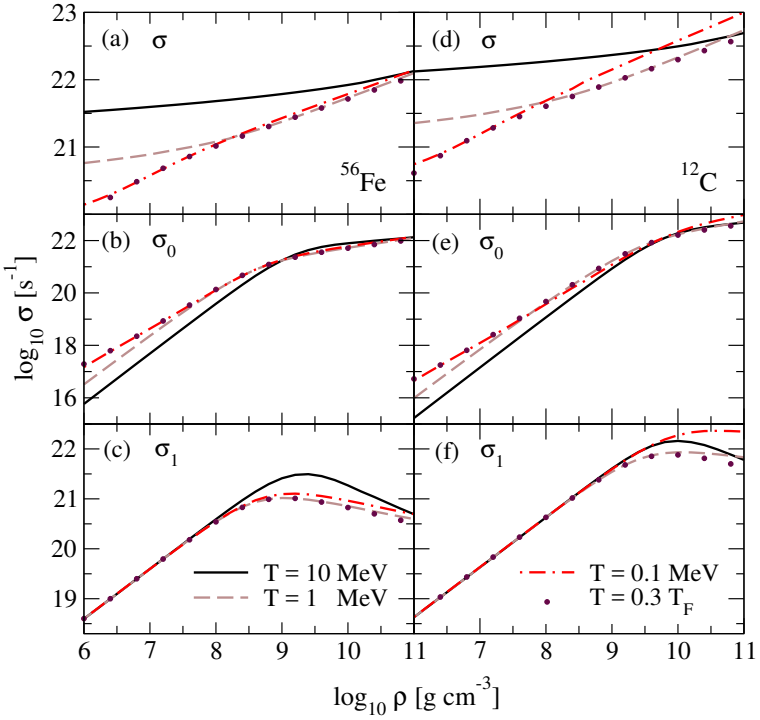


Figure 4.10: Dependence of three components of the electrical conductivity tensor on density for various values of temperature indicated in the plot and $B_{12} = 1$ [$B_{12} \equiv B/(10^{12}$ G)]. Panels (a)–(c) show the conductivities for $^{56}$Fe, panels (d)–(f) - the same for $^{12}$C. The circles show the minimum/maximum of the components of the conductivity tensor at the given density.

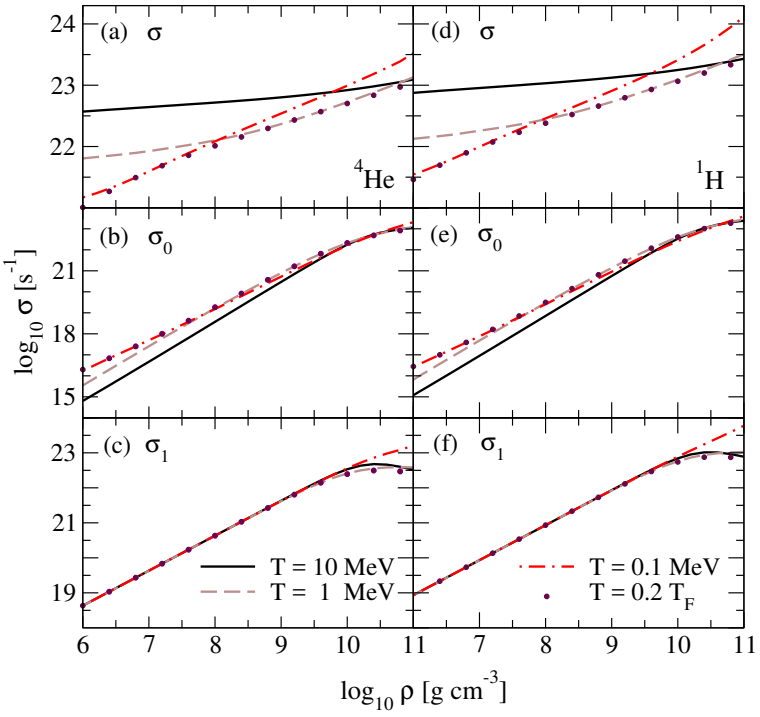


Figure 4.11: Same as in Fig. 4.10, but for $^{4}$He [(a)–(c)], and $^{1}$H [(d)–(f)].

and (4.57). For any fixed temperature and density, the ratio $\tau(\varepsilon)/\varepsilon$ scales approximately as $\varepsilon$. In the degenerate regime $\varepsilon$ is the Fermi energy, therefore $\varepsilon \propto \rho^{1/3}$, while in the nondegenerate regime $\bar{\varepsilon} \propto T$ independent of density. Apart from these differences, $\tau^{-1} \propto n_i$, which guarantees that the

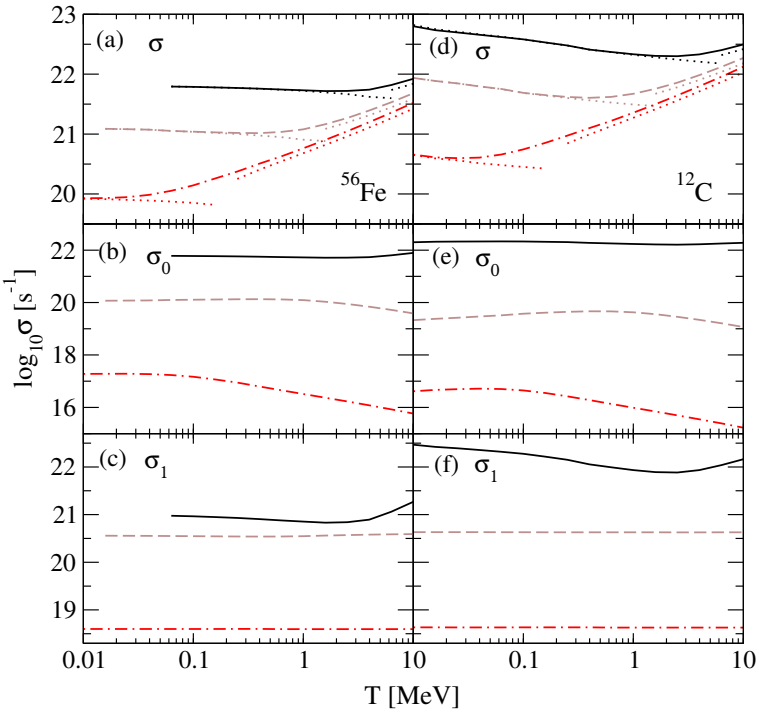


Figure 4.12: The temperature dependence of three components of the electrical conductivity tensor for $B_{12} = 1$ and three values of density - $\log_{10}\rho = 10$ (solid lines), $\log_{10}\rho = 8$ (dashed lines) and $\log_{10}\rho = 6$ (dash-dotted lines) in units g cm$^{-3}$. Panels (a)–(c) show the conductivities for $^{56}$Fe, panels (d)–(f) - the same for $^{12}$C. The dots represent the results obtained with Eqs. (4.52) and (4.57).

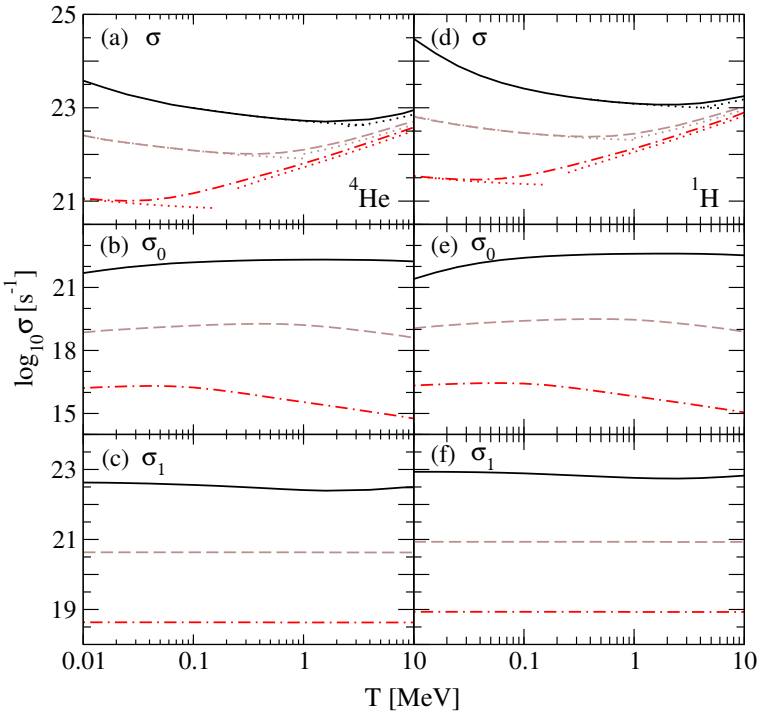


Figure 4.13: Same as in Fig. 4.12, but for $^4$He [(a)–(c)], and $^1$H [(d)–(f)].

relaxation time decreases with density in both cases. These factors combined lead to slower increase of the conductivity in the nondegenerate regime as compared to the degenerate one. Note that $\omega_c\tau$ scales as $\tau/\varepsilon$ in both cases.

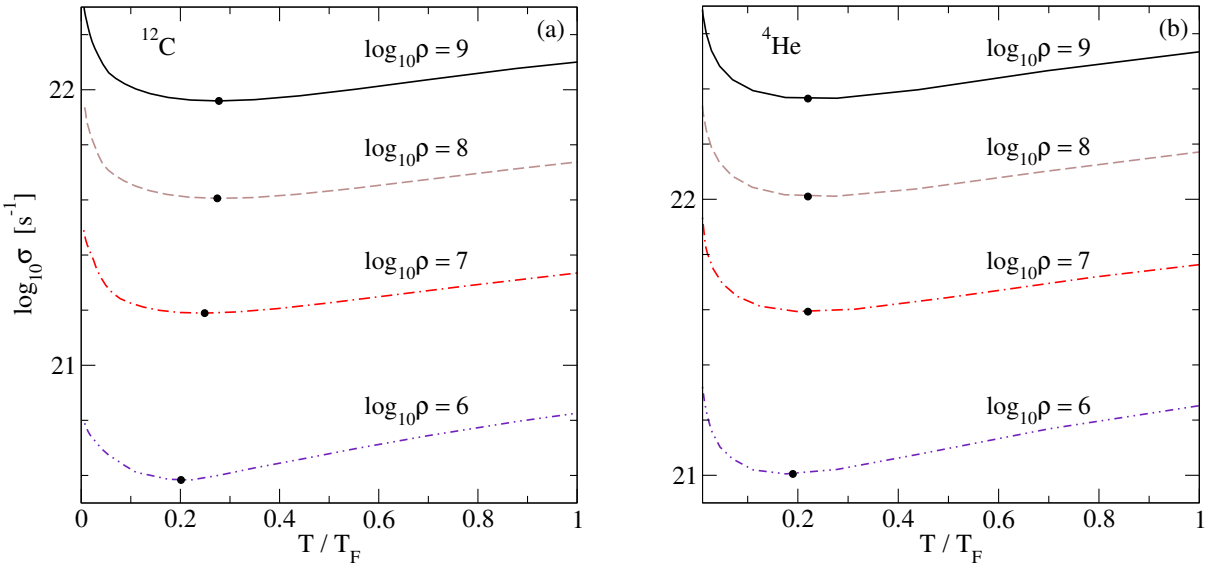


Figure 4.14: Dependence of the conductivity on the scaled temperature for various densities for (a) $^{12}$C, and (b) $^{4}$He. The minimum of the conductivity arises at $T \simeq (0.2 \div 0.3)T_F$.

The main difference between the values of $\sigma$ for different nuclei characterized by their mass number $A$ and charge $Z$ is due to the scaling $\sigma \sim n_e\tau \sim Zn_i(Z^2n_i)^{-1} \sim Z^{-1}$, see Eqs. (4.45), (4.52) and (4.57). Therefore, we find for the ratio of conductivities: $\sigma_C/\sigma_{Fe} \simeq 4.3$, $\sigma_{He}/\sigma_C \simeq 3$ and (in the nondegenerate limit) $\sigma_H/\sigma_{He} \simeq 2$, which is consistent with the results shown in Figs. 4.10 and 4.11.

Let us turn to the temperature dependence of the conductivity. The most prominent effect seen in the temperature dependence of $\sigma$, shown in panels (a) and (d) of Figs. 4.12 and 4.13, is the existence of a minimum as a function of temperature. The dotted lines in the low-temperature regime correspond to the formula (4.52) and extend to the point where $T \simeq T_F$. We see that the Drude formula works very well for $T \leq 0.1T_F$ and we find a good agreement between our conductivities and those in Refs. [121, 127] in this regime. The dotted lines in the high-temperature regime correspond to the formula (4.57). As we see from the plots, Eq. (4.57) gives the correct qualitative behavior of the electrical conductivity at high temperatures, but quantitatively underestimates it by about 20%. The minimum in $\sigma$ arises at about the transition from the degenerate to the nondegenerate regime and is identified empirically with $T \simeq 0.3T_F$ for $^{56}$Fe and $^{12}$C and with $T \simeq 0.2T_F$ for $^{4}$He and $^{1}$H. This approximately corresponds to the requirement that the Fermi energy becomes equal to the thermal energy of a nondegenerate relativistic gas. We show in Fig. 4.14 the dependence of $\sigma$ on appropriately scaled temperature for a number of densities for $^{12}$C and $^{4}$He (the results are similar also for $^{56}$Fe and $^{1}$H). As seen from these figures, the minimum in the conductivity shifts slightly to lower values of the scaled temperature $T/T_F$ with decreasing density and nucleus charge number. We also show the density dependence of the conductivity at this minimum in Figs. 4.10 and 4.11 by small circles.

The conductivity decreases with temperature at low temperatures, where the electrons are degenerate. This decrease arises (almost) solely from the temperature dependence of the correlation function $S(q)$. In the case where $S(q) = 1$ the electrical conductivity is nearly temperature-independent, whereas in full calculation it decreases with temperature, as expected. Indeed, as seen from Fig. 4.6, with increasing temperature and, consequently, decreasing $\Gamma$ small momentum transfer scattering becomes more important, which increases the effective scattering cross-section.

In the degenerate regime the temperature dependence of $\sigma$ (or $\tau$) is stronger for lighter elements, because for the given density and temperature the parameter $\Gamma$ is smaller for lighter elements ($\Gamma \sim Z^2/A^{1/3}$, *e.g.*, $\Gamma_{Fe}/\Gamma_C \simeq 11$, $\Gamma_C/\Gamma_{He} \simeq 6$), and the factor $S(q;\Gamma)$ varies faster for small values of $\Gamma$ (at small $a_iq$), see Fig. 4.6.

In the nondegenerate regime the temperature dependence of $\tau$ changes because of the scaling $\bar{\tau} \propto \bar{\varepsilon}^2$. Therefore, the conductivity scales as $\sigma \propto \bar{\tau}/\bar{\varepsilon} \propto T$, as suggested in Ref. [118] (the exact calculations give $\sigma \propto T^\beta$ with $\beta \simeq 0.7 \div 0.8$).

### 4.5.3 Results for transverse and Hall conductivities

For strong magnetic fields the tensor structure of the conductivity becomes important and we need to discuss the remaining components of this tensor given by Eqs. (4.52) and (4.57). These components depend strongly on the value of "anisotropy parameter" $\omega_c\tau$. Assuming density-independent values of the magnetic fields, we find that the parameter $\omega_c\tau$ decreases as a function of density because of the decrease of the relaxation time in any regime, see Fig. 4.7. Note that in the degenerate case $\omega_c$ decreases as well because of its inverse dependence on the energy of electrons. It is seen that at high densities for $^{56}$Fe and $^{12}$C nuclei $\omega_c\tau \ll 1$ (isotropic region) and $\sigma_0 \simeq \sigma$. At low densities, where $\omega_c\tau \gg 1$, we have strong anisotropy with

$$\sigma_0 \simeq \frac{\sigma}{(\omega_c\tau)^2} \simeq \left(\frac{n_e e}{B}\right)^2 \sigma^{-1} \ll \sigma. \tag{4.69}$$

Because $\omega_c\tau$ decreases with density, $\sigma_0$ increases with density much faster than $\sigma$: $\sigma_0 \propto \rho^\beta$, $\beta \simeq 1.4$ in the degenerate and $\beta \simeq 1.7$ in the nondegenerate regime, see Figs. 4.10 and 4.11. At low densities $\sigma_0$ is smaller than $\sigma$ by several orders of magnitude, the exact value being dependent on magnetic field.

We see from Eq. (4.69) that for a given density $\sigma_0 \sim \sigma^{-1}$, therefore $\sigma_0$ shows a reversed temperature dependence in the anisotropic regime, as seen from Figs. 4.10–4.13, panels (b) and (e). It increases in the degenerate regime, decreases in the nondegenerate regime, and has a maximum around the temperature $T \simeq (0.2 \div 0.3)T_F$, which is shown with dots in Figs. 4.10 and 4.11. The reversed behavior applies also to the $Z$-dependence, *i.e.*, $\sigma_0 \sim \tau^{-1} \sim Z$, therefore in this regime $\sigma_0$ is smaller for lighter elements as long as $Z/A \simeq 0.5$. The only exception is $^1$H, for which the factor $n_e \propto Z/A$ is twice larger than for the other elements. As a result, $\sigma_0$ for hydrogen is always twice larger than that for helium. The curves corresponding to different temperatures in Figs. 4.10 and 4.11 (b) and (e) intersect when $\omega_c\tau \simeq 1$ at high densities ($\rho \simeq 10^9$ g cm$^{-3}$ for $^{56}$Fe and $\rho \simeq 10^{10}$ g cm$^{-3}$ for the other cases) as a consequence of the transition from anisotropic to isotropic conduction (see also Fig. 4.7). In addition, there are also intersections related to the transition from the degenerate (high-density) to the nondegenerate (low-density) regime, as already discussed in the case of $\sigma$.

For $\sigma_1$ component we have

$$\sigma_1 \simeq \sigma\omega_c\tau \simeq \frac{B}{n_e e}\sigma^2, \quad \omega_c\tau \ll 1, \tag{4.70}$$

$$\sigma_1 \simeq \frac{\sigma}{\omega_c\tau} \simeq \frac{n_e e}{B}, \quad \omega_c\tau \gg 1. \tag{4.71}$$

At low densities ($\omega_c\tau \gg 1$) $\sigma_1$ is proportional to the electron number density but is independent of the temperature, see Eq. (4.71). It is almost the same for nuclei with $A/Z \simeq 2$ and is twice larger for hydrogen, see Figs. 4.10–4.13, panels (c) and (f). At high densities where the isotropy is restored $\sigma_1$ becomes a decreasing function of density because of the additional factor $\omega_c\tau$ in Eq. (4.70), the decrease being faster at higher temperatures, see Figs. 4.10 and 4.11. We find the scaling $\sigma_1 \propto \rho^{-\gamma}$, $\gamma \simeq 0.2$ in the degenerate and $\gamma \simeq 0.7$ in the nondegenerate regime for $^{56}$Fe and $^{12}$C (for $^4$He and $^1$H the isotropic region is negligible).

As a function of density $\sigma_1$ has a maximum at $\omega_c\tau \simeq 1$, where $\sigma_0 \simeq \sigma_1 \simeq \sigma/2$. In isotropic region $\sigma_1$ depends on the temperature through the scaling $\sigma_1 \sim \sigma^2$ and has a minimum as the scalar conductivity. For $Z > 1$ we have the scaling $\sigma_1 \sim Z^{-2}$, therefore $\sigma_1$ is larger for $^4$He as compared to $^{12}$C by an order of magnitude and more than two orders of magnitude as compared to $^{56}$Fe. As

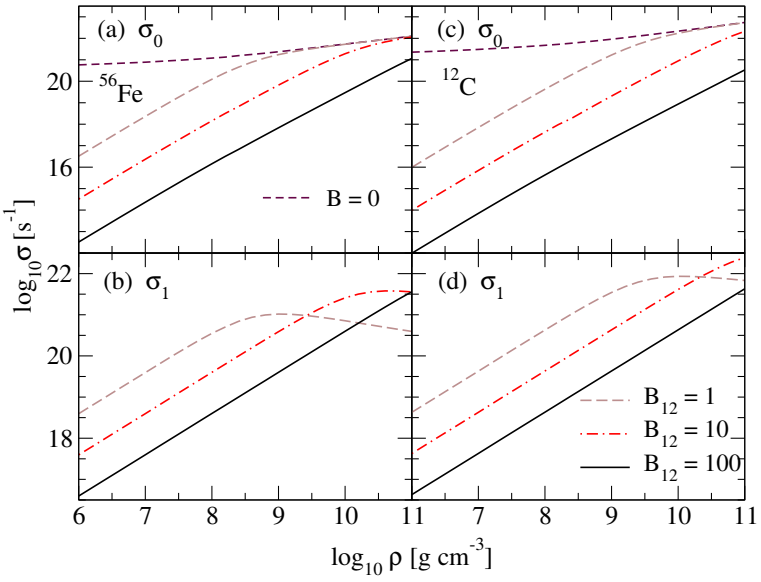


Figure 4.15: Dependence of $\sigma_0$ [(a) and (c)] and $\sigma_1$ [(b) and (d)] components of the conductivity tensor on density for various values of the $B$-field. Panels (a) and (b) show these components for $^{56}$Fe, panels (c) and (d) - the same for $^{12}$C. The temperature is fixed at $T = 1$ MeV.

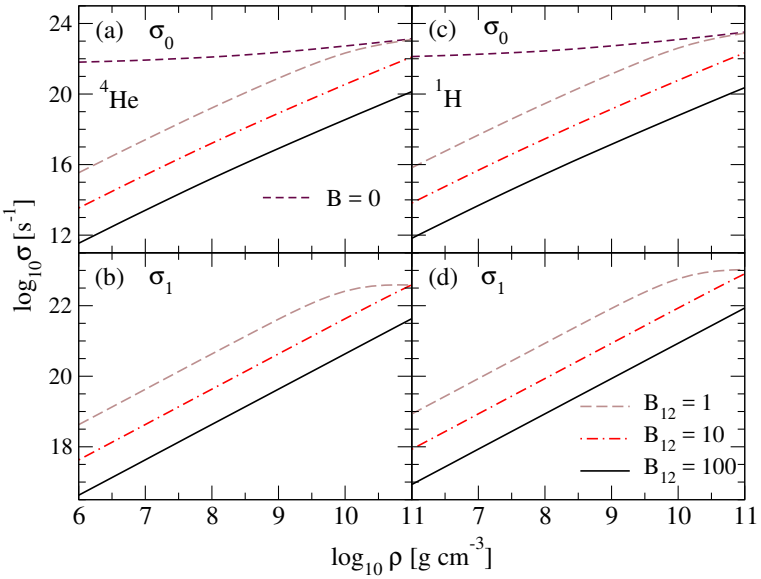


Figure 4.16: Same as in Fig. 4.15, but for $^4$He [(a) and (b)], and $^1$H [(c) and (d)].

$\omega_c\tau$ is larger for light elements [see Fig. 4.7], the anisotropic region for these elements is larger, and the maximum of $\sigma_1$ versus density is shifted to higher densities and its value increases, as can be seen from Figs. 4.10 and 4.11. Note that in both isotropic and strongly anisotropic cases $\sigma_1 \ll \sigma$.

Figures 4.15 and 4.16 show the density dependence of $\sigma_0$ and $\sigma_1$ for different values of the magnetic field. As $\omega_c \propto B$, the density region where the conductivity is anisotropic becomes larger with the increase of magnetic field, and the maximum of $\sigma_1$ as a function of density is shifted to higher densities.

Figures 4.17 and 4.18 show the dependence of $\sigma_0$ and $\sigma_1$ on magnetic field. As we see, for low magnetic fields $\sigma_0 \simeq \sigma$. With increasing magnetic field $\sigma_0$ decreases and for $\omega_c\tau \gg 1$ we find that $\sigma_0 \propto B^{-2}$, see Eq. (4.69). For $\omega_c\tau \ll 1$ and $\omega_c\tau \gg 1$ cases we have $\sigma_1 \propto B$ and $\sigma_1 \sim B^{-1}$, respectively, see Eqs. (4.70) and (4.71), therefore $\sigma_1$ should have a maximum as a function of magnetic field. As seen from Figs. 4.17 and 4.18, the maximum of $\sigma_1$ occurs where $\sigma_0$ begins to drop ($\omega_c\tau \simeq 1$). This

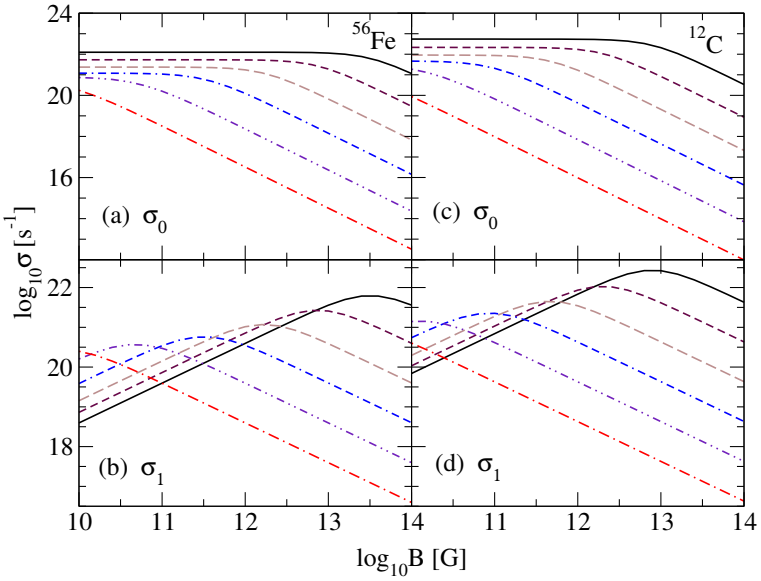


Figure 4.17: Dependence of $\sigma_0$ [(a) and (c)] and $\sigma_1$ [(b) and (d)] components of the conductivity tensor on the magnetic field for $^{56}$Fe [(a) and (b)] and $^{12}$C [(c) and (d)] at six values of density - $\log_{10}\rho = 11$, $\log_{10}\rho = 10$, $\log_{10}\rho = 9$, $\log_{10}\rho = 8$, $\log_{10}\rho = 7$ and $\log_{10}\rho = 6$ (from top to bottom). The temperature is fixed at $T = 1$ MeV.

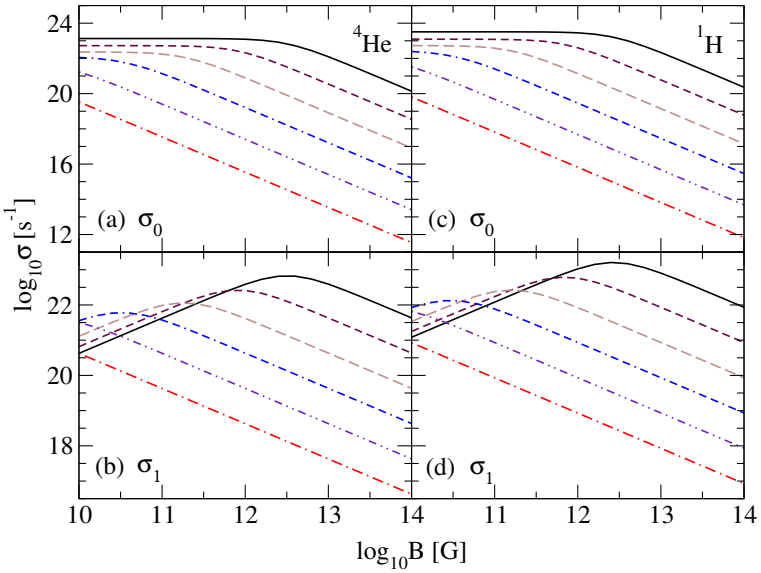


Figure 4.18: Same as in Fig. 4.17, but for $^{4}$He [(a) and (b)], and $^{1}$H [(c) and (d)].

maximum shifts to lower magnetic fields with the decrease of density and nucleus charge number $Z$. For $B = 10^{12}$ G the crust is anisotropic at densities $\rho < 10^{9}$ g cm$^{-3}$ for $^{56}$Fe and $\rho < 10^{10}$ g cm$^{-3}$ for $^{12}$C. For magnetic fields $B \geq 10^{13}$ G the outer crust is almost completely anisotropic for all nuclei.

We now turn to the study of combined effects of temperature and magnetic field, *i.e.*, how the anisotropy induced by the magnetic field is affected by the temperature. To characterize the anisotropy we consider the ratio $\sigma_0/\sigma$, which is shown in Figs. 4.19 and 4.20 as a function of dimensionless ratios $3T/T_F$ (for $^{56}$Fe and $^{12}$C nuclei) and $5T/T_F$ (for $^{4}$He and $^{1}$H nuclei) for various densities and magnetic fields. We see that the position of the maximum is almost independent of density and magnetic field. At this maximum the anisotropy of the crust is the smallest. Because in the anisotropic regime $\sigma_0/\sigma \propto \sigma^{-2}$, see Eq. (4.69), this ratio increases with the temperature in the degenerate regime. In

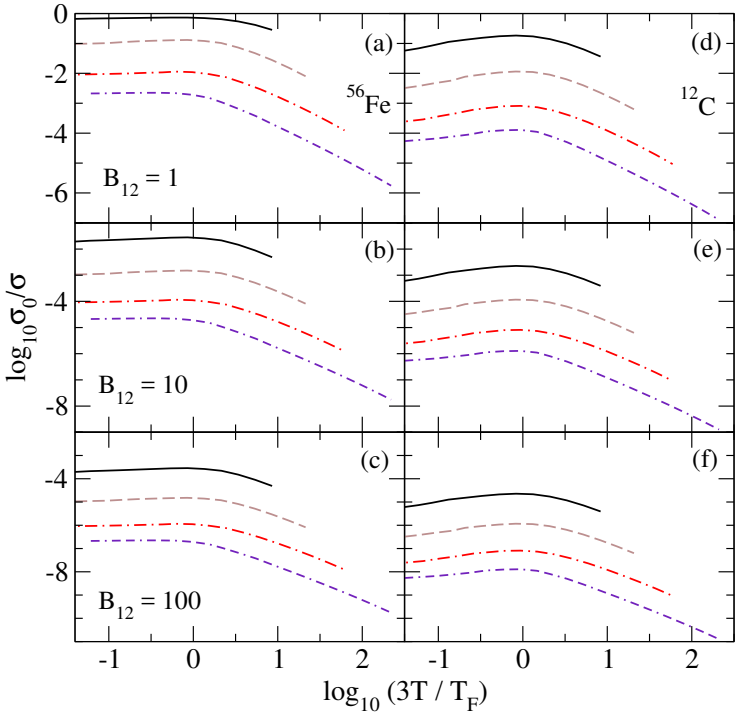


Figure 4.19: The ratio $\sigma_0/\sigma$ as a function of scaled temperature $3T/T_F$ at various densities $\log_{10}\rho = 9$ (solid lines), $\log_{10}\rho = 8$ (dashed lines), $\log_{10}\rho = 7$ (dash-dotted lines) and $\log_{10}\rho = 6$ (double-dash-dotted lines) and for three values of the magnetic field $B_{12} = 1$ [(a) and (d)], $B_{12} = 10$ [(b) and (e)], and $B_{12} = 100$ [(c) and (f)]. Panels (a)–(c) show the ratio for $^{56}$Fe, panels (d)–(f) - the same for $^{12}$C.

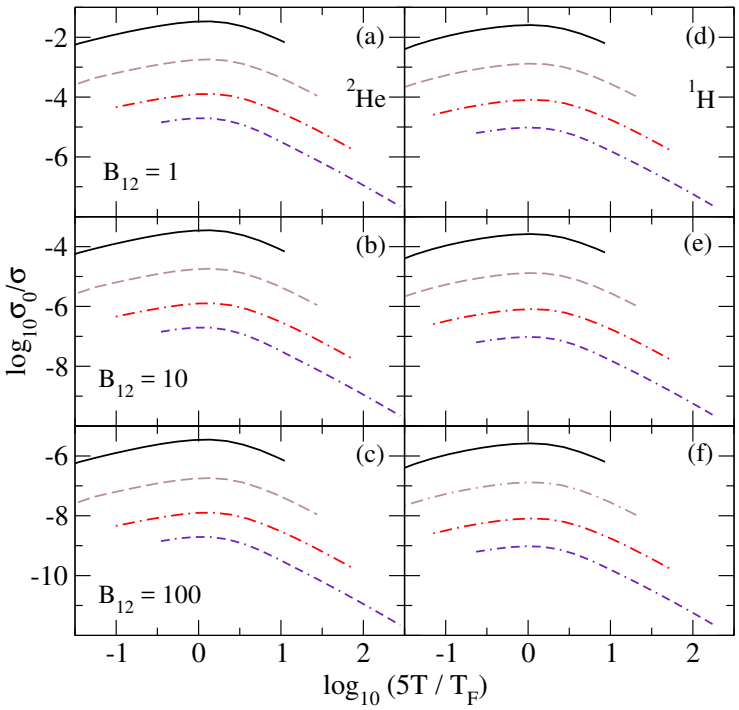


Figure 4.20: Same ratio as in Fig. 4.19 as a function of the scaled temperature defined as $5T/T_F$ for $^4$He [(a)–(c)] and $^1$H [(d)–(f)].

the nondegenerate regime $\sigma$ increases with temperature, therefore $\sigma_0/\sigma$ decreases approximately as $T^{-3/2}$. At very high temperatures the crust becomes strongly anisotropic.

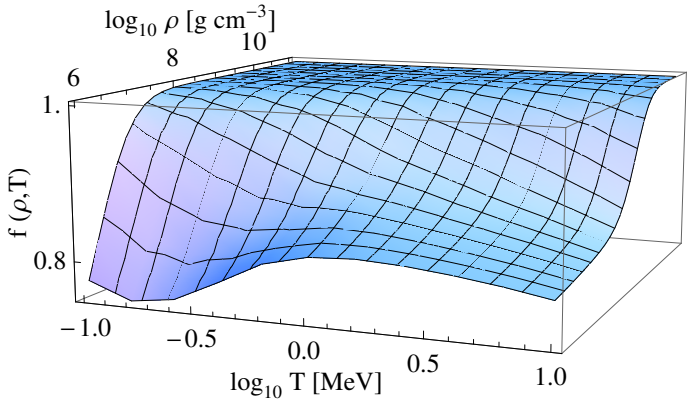


Figure 4.21: The function $f(\rho, T)$ defined in Eq. (4.72) for $^{56}$Fe at magnetic field $B_{12} = 1$.

From Eqs. (4.52) and (4.57) we can obtain a simple relation between the three components of the conductivity tensor

$$f(\rho, T) \equiv \frac{\sigma_0}{\sigma}\left[1 + \left(\frac{\sigma_1}{\sigma_0}\right)^2\right] = 1. \tag{4.72}$$

At temperatures close to the Fermi temperature Eqs. (4.52) and (4.57) break down, however, according to Fig. 4.21, the relation (4.72) is satisfied quite well in the whole crust. While Fig. 4.21 shows the case for $^{56}$Fe, we have verified that similar results hold also for the other nuclei and composition dependent crust and are weakly dependent on the magnitude of the magnetic field in the range $10^{-2} \leq B_{12} \leq 10^2$.

### 4.5.4 Density-dependent composition

We now turn to the case where the composition of matter depends on the density. We will assume that the composition does not depend strongly on the temperature in the range of temperatures studied here ($T \leq 10$ MeV) and will proceed with composition derived for $T = 0$. The conservation of baryon number, electric charge and the condition of $\beta$-equilibrium uniquely determines the energetically most preferable state of matter for any given model of nuclear forces in the density range of interest $10^6 \leq \rho \leq \rho_{\rm drip}$, where $\rho_{\rm drip} \simeq 4 \times 10^{11}$ g cm$^{-3}$ is the neutron drip density.

The laboratory information on nuclear masses can be used as an input to eliminate the uncertainties related to the nuclear Hamiltonian [282], therefore various studies of the composition of the crust predict nearly identical sequences of nuclei as a function of density.

In our calculations we adopted the nuclear sequence taken from Ref. [274] and shown in Fig. 4.2. The matter composed of iron below the density $\log_{10}\rho \leq 7$ is followed by a sequence of nuclei with charges in the range $28 \leq Z \leq 36$. This composition can be compared to the initial studies of nuclear sequences below neutron drip density [283,284] (displayed in Table 2.1 of Ref. [284]) and a more recent study based on improved data and theory [285]. These deviate from the composition adopted here only marginally.

To assess the differences that arise from the replacement of, for example, iron nuclei studied above by density-dependent composition recall that for nuclei with mass number $A$ and charge $Z$ the relaxation time scales as $\tau^{-1} \propto Z^2 n_i \propto Z^2/A$. Because $\tau \propto \varepsilon^2$, in the degenerate regime there will be additional density dependence in the conductivity arising from the factor $\tau/\varepsilon \propto n_e^{1/3}$. For the conductivity in the degenerate regime we find the scaling

$$\sigma \propto \frac{n_e \tau_F}{\varepsilon_F} \propto \left(\frac{Z}{A}\right)^{1/3} Z^{-1}. \tag{4.73}$$

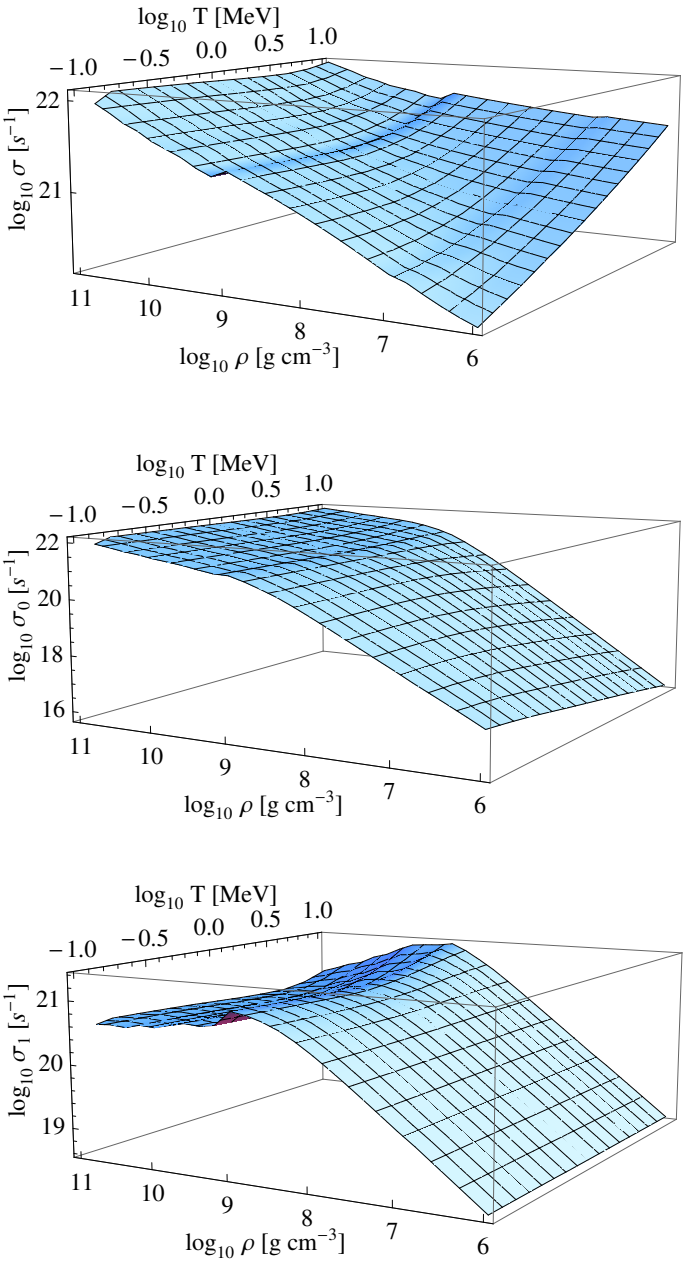


Figure 4.22: Dependence of three components of the electrical conductivity tensor on density and temperature for $B_{12} = 1$ and composition taken from Ref. [274].

In the nondegenerate regime

$$\sigma \propto \frac{n_e \bar{\tau}}{\bar{\varepsilon}} \propto Z^{-1}. \tag{4.74}$$

To give a few numerical examples, we quote the ratio $\mathcal{R}$ of conductivities of elements present in density-dependent matter composition to that of iron: $\mathcal{R}[^{62}\mathrm{Ni}] = 0.92$, $\mathcal{R}[^{64}\mathrm{Ni}] = 0.91$, $\mathcal{R}[^{86}\mathrm{Kr}] = 0.70$, $\mathcal{R}[^{84}\mathrm{Se}] = 0.73$, $\mathcal{R}[^{82}\mathrm{Ge}] = 0.77$, $\mathcal{R}[^{80}\mathrm{Zn}] = 0.81$, $\mathcal{R}[^{80}\mathrm{Ni}] = 0.85$ in the degenerate regime and $\mathcal{R}[^{62}\mathrm{Ni}] = \mathcal{R}[^{64}\mathrm{Ni}] = 0.93$, $\mathcal{R}[^{86}\mathrm{Kr}] = 0.72$, $\mathcal{R}[^{84}\mathrm{Se}] = 0.76$, $\mathcal{R}[^{82}\mathrm{Ge}] = 0.81$, $\mathcal{R}[^{80}\mathrm{Zn}] = 0.87$, $\mathcal{R}[^{80}\mathrm{Ni}] = 0.93$ in the nondegenerate regime. The differences between these estimates based on the scalings (4.73), (4.74) and our numerical results are smaller than 5% and arise from the additional dependence of the relaxation time on $Z$ and $A$ via the structure factor and the Debye momentum. We conclude, that the results of density-dependent composition differ from those found for iron by a factor $\leq 1.4$.

The three components of the conductivity tensor in the case of density-dependent composition are shown in Fig. 4.22 and, according to the arguments above, show all the basic features already discussed in the case of $^{56}$Fe.

### 4.5.5 Fit formulas for the electrical conductivity tensor

We have performed fits to the longitudinal component of the conductivity tensor using the formula

$$\sigma_{\rm fit} = \frac{1.5\times10^{22}}{Z}\left(\frac{T_F}{1\ {\rm MeV}}\right)^a\left(\frac{T}{T_F}\right)^{-b}\left(\frac{T}{T_F}+d\right)^{b+c}\ {\rm s}^{-1}. \tag{4.75}$$

The density dependence of $\sigma_{\rm fit}$ arises from its dependence on the Fermi temperature, which in general has the form $T_F = 0.511\left[\sqrt{1+(Z\rho_6/A)^{2/3}}-1\right]$ MeV. For ultrarelativistic electrons this simplifies to $T_F = 0.511(Z\rho_6/A)^{1/3} \simeq 0.4\rho_6^{1/3}$ MeV, where the second relation is valid for $Z/A \simeq 0.5$. Substituting this into Eq. (4.75) we obtain a fit formula with explicit dependence on density

$$\sigma_{\rm fit} = \frac{C}{Z}\rho_6^{(a+b)/3}T_1^{-b}\left(T_1\rho_6^{-1/3}+d'\right)^{b+c}\ {\rm s}^{-1}, \tag{4.76}$$

where $T_1 \equiv T/(1\ {\rm MeV})$; $C = 1.5\times10^{22}\times0.4^{a-c}$ and $d' = 0.4d$ for $Z \geq 2$, and $C = 1.5\times10^{22}\times0.5^{a-c}$ and $d' = 0.5d$ for $Z = 1$. The fit parameters $a, b, c, d$ depend on the nucleus charge number via the following formulas:

$$a(Z) = 0.924 - 0.009\log Z + 0.003\log^2 Z, \tag{4.77}$$
$$b(Z) = 0.507 - 0.028\log Z - 0.025\log^2 Z, \tag{4.78}$$
$$c(Z) = 0.788 + 0.010\log Z + 0.003\log^2 Z, \tag{4.79}$$
$$d(Z) = 0.279 + 0.056\log Z + 0.035\log^2 Z. \tag{4.80}$$

The relative error of the fit formula (4.75) defined as $\gamma = 100|\sigma^{\rm fit}-\sigma|/\sigma$ is 10% for $^{56}$Fe and $\beta$-equilibrium composition in the temperature range 0.1 MeV $\leq T \leq$ 10 MeV, and 5% for $^{12}$C, $^4$He and $^1$H in the temperature range 0.4 MeV $\leq T \leq$ 10 MeV.

The form of Eq. (4.75) provides the correct temperature and density dependence of the conductivity in the limiting cases of strongly degenerate and nondegenerate electrons. For the first case $T \ll T_F$ and $\sigma \propto T_F^{a+b}T^{-b}$. In the nondegenerate limit $T \gg T_F$ and $\sigma \propto T_F^{a-c}T^c$. As to the explicit density dependence in these limits, one finds that $\sigma \propto \rho^{(a+b)/3}T^{-b}$ when $T \ll T_F$ and $\sigma \propto \rho^{(a-c)/3}T^c$ when $T \gg T_F$, assuming the ultrarelativistic limit. Averaging over the fit parameters we finally quote the rough scaling of the conductivity in the two limiting cases: $\sigma \propto \rho^{4.7}T^{-0.5}$ for $^1$H and $^4$He; $\sigma \propto \rho^{4.3}T^{-0.4}$ for $^{12}$C and $\sigma \propto \rho^{3.5}T^{-0.15}$ for $^{56}$Fe in the degenerate regime and $\sigma \propto \rho^{1/30}T^{4/5}$ in the nondegenerate regime, which agree quite well with exact result discussed in Sec. 4.5.2. The conductivity given by the fit formula (4.75) attains its minimum at the temperature $T/T_F = bd/c \simeq 0.2$.

For the other two components of the conductivity tensor the following formulas can be used

$$\sigma_0^{\rm fit} = \frac{\nu\sigma_{\rm fit}}{1+\delta^2\nu^2\sigma_{\rm fit}^2}, \qquad \sigma_1^{\rm fit} = \frac{\delta\sigma_{\rm fit}^2}{1+\delta^2\sigma_{\rm fit}^2}, \tag{4.81}$$

where $\nu = (T_F/\varepsilon_F)^{0.16}$ and $\delta = B(n_e ec)^{-1}$ in cgs units with $c$ being the speed of light. The relative error of formulas (4.81) is $\gamma \simeq 10\%$ for $Z \leq 6$ and $\gamma \simeq 15\%$ for the other cases in the entire range of density and magnetic field considered above.

## 4.6 Conclusions

Motivated by recent advances in numerical simulations of astrophysical phenomena, such as mergers of neutron star binaries within the resistive MHD framework, we have computed here the conductivity of warm matter ($10^9 \leq T \leq 10^{11}$ K) at densities corresponding to the outer crusts of neutron stars and the interiors of white dwarfs. Our results apply to arbitrary temperatures above the solidification temperature of matter and cover the transition from the degenerate to the nondegenerate regime. In this liquid plasma regime the conductivity is dominated by the electrons which scatter off the correlated nuclei via screened electromagnetic force. The correlations in the plasma in the liquid state are included in terms of ion structure factor extracted from the data on Monte Carlo simulations of OCP. A key feature of our computation is the inclusion of the dynamical screening of photon exchange and inelastic processes, which we show to be small in the temperature-density regime considered. The use of OCP structure factor implies that our results should be applied with caution in the case where matter is composed of mixture of nuclei, in which case the interspecies correlations are not accounted for. We have implemented the HTL QED polarization susceptibilities in the low-frequency limit combined with nonzero-temperature screening Debye length, which should be a good approximation where the inelastic processes are suppressed by the large mass of nuclei. A further simplifying approximation that went into our formalism, which is well justified by the MHD regime of astrophysical studies, is the assumption of weakly non-equilibrium state of the plasma. This allowed us to express the solution of the Boltzmann kinetic equation in relaxation time approximation.

We find that the conductivity as a function of the temperature shows a minimum around $T \simeq (0.2 \div 0.3) T_F$ almost independent of the density. The position of the minimum weakly depends on the composition of matter. This minimum arises as a result of the transition from the degenerate regime ($T \ll T_F$) to the nondegenerate regime ($T \gg T_F$). Thus, the conductivity decreases with increasing temperature in the degenerate regime up to the point of minimum; further increase in the temperature leads to a power-law increase in the conductivity as the system enters the nondegenerate regime. We further find that at fixed temperature the conductivity always increases with density, but the slope of this increase is much weaker in the nondegenerate regime.

We have further extracted the components of the conductivity tensor in the entire density and temperature range for non-quantizing magnetic fields $10^{10} \leq B \leq 10^{14}$ G. Because the product of the relaxation time and the electron cyclotron frequency is a decreasing function of density in the complete temperature range, low-density matter features anisotropic conductivity at lower magnetic fields. For example, the component of the conductivity transverse to the field ($\sigma_0$) tends to the longitudinal conductivity ($\sigma$) in the high density limit, but it is substantially suppressed at low densities. This underlines the importance of proper inclusion of anisotropy of conductivity in astrophysical studies of dilute magnetized matter even at relatively low magnetic fields.

Our results can be implemented in numerical studies via fit formulas (4.75)–(4.81). An alternative is to use plain text tables of conductivities, provided as a supplemental material in Ref. [131].

Finally, our results show that the conductivity depends weakly on the composition of matter. For example, the conductivity of matter composed of heavy elements with $26 \leq Z \leq 36$ in $\beta$-equilibrium with electrons differs from the conductivity of matter composed of $^{56}$Fe at the same density and temperature by a factor $\leq 1.4$. It would be interesting, however, to study the conductivity of warm multicomponent matter which is composed of nuclei in statistical equilibrium, in which case the composition may become an important factor.

# Chapter 5

# Summary and perspectives

The aim of this thesis is the investigation of relativistic dissipative hydrodynamics and transport coefficients of strongly correlated systems. Our studies are relevant for the description of heavy-ion collisions, as well as compact stellar objects at finite temperatures and in strong magnetic fileds.

In Chapter 2 we provide a novel derivation of the second-order relativistic hydrodynamics using Zubarev's non-equilibrium statistical operator approach [79]. We consider a generic quantum system, the dynamics of which is described by means of the operators of the energy-momentum tensor and the currents of multiple conserved charges. Following the method proposed in Refs. [66, 67], we first construct a non-equilibrium statistical operator for the given values of the energy-momentum tensor and the conserved currents. The statistical operator which is the retarded solution of the quantum Liouville equation differs form the local grand canonical distribution by a non-equilibrium term. The latter involves the gradients of temperature, chemical potentials and fluid velocity (thermodynamic forces) and can be treated as a perturbation for small deviations from equilibrium.

In the next step the statistical operator is expanded into Taylor series with respect to the thermodynamic forces up to the second order. Averaging the operators of the shear viscous tensor, the bulk viscous pressure and the charge diffusion currents over the non-equilibrium part of the statistical operator we obtain transport (evolution) equations for these dissipative quantities. We observe that the second-order corrections to the dissipative quantities arise from (i) the quadratic terms of the Taylor expansion of the statistical operator and (ii) the linear terms of this expansion, where non-local effects are properly taken into account. In particular, we find that the relaxation terms, which are necessary for the causal description of relativistic fluids, arise from these non-local corrections. Apart from that, the terms of the type (ii) generate additional second-order terms which represent the coupling of the transport equations with the conservation laws.

The first- and the second-order transport coefficients appearing in the transport equations are expressed via certain two- and three-point equilibrium correlation functions, computation of which can be performed by applying standard thermal field theory methods. The characteristic relaxation times, which are necessary for the maintenance of the causality, are expressed via the frequency-derivatives of the relevant first-order transport coefficients taken in the zero-frequency limit.

The research accomplished in this chapter can be extended to include strong gravitational fields, which are of great interest in relativistic astrophysics and cosmology. Another extension of this study could be the inclusion of electromagnetic fields, which play a central role in the MHD description of various phenomena in compact stars, and might be an important issue for heavy-ion phenomenology as well. One can further extend these studies to include also quantum anomalies (*e.g.*, vorticity terms), which have been intensively studied in recent years.

In Chapter 3 we compute the four transport coefficients (electrical and thermal conductivities, shear and bulk viscosities) of strongly coupled relativistic quark plasma within the two-flavor NJL model in the isospin-symmetric limit [82, 83]. Our starting point are the Kubo formulas, which express these transport coefficients via two-point correlation functions between the operators of corresponding dis-

sipative fluxes. In general, these correlation functions contain an infinite series of Feynman diagrams, resummation of which requires non-perturbative methods. We apply here the effective $1/N_c$ power counting scheme to choose the leading-order diagrams which contribute to the required correlators. This approximation implies that the ladder diagrams, *i.e.*, the diagrams with vertex corrections are suppressed, and the leading contribution to the transport coefficients consists of a geometrical series of multi-loop diagrams with full (dressed) quark propagators.

Further analysis of the Dirac structure of these correlation functions shows that the infinite series of loop-diagrams reduces to a single-loop correlator in the cases of the conductivities and the shear viscosity. We compute the corresponding two-point correlation functions in the imaginary-time (Matsubara) formalism to obtain compact expressions for them in terms of the quark spectral function. We show that the proper inclusion of the full Dirac structure of the quark self-energy and the spectral function is crucial to obtain correct results for the transport coefficients. The relevant scattering processes which lead to dispersive effects and thereby finite values of transport coefficients are the quark-meson fluctuations above the Mott transition temperature $T_{\rm M}$, where meson decay into two on-mass-shell quarks is kinematically allowed.

The numerical results for the transport coefficients are obtained for the temperature-density range relevant mainly to heavy-ion collisions. The conductivities and the shear viscosity are found to be decreasing functions of temperature and baryonic chemical potential, the main source of the decrease being the increasing difference between the quark and meson masses. Interestingly, these coefficients show a nearly universal behavior when temperature is scaled by the corresponding Mott temperature. We find that the Wiedemann-Franz law for the ratio of the thermal and the electrical conductivities does not hold in the regime of interest. The thermal conductivity diverges quadratically at vanishing chemical potential, which is consistent with the results of Ref. [80]. The ratio of the shear viscosity to the entropy density is of the order of 10 close to the Mott temperature, but undershoots the AdS/CFT bound $1/4\pi$ [81] at high temperatures. This violation is a consequence of the absence of gluonic degrees of freedom in the NJL model. We also conjecture a lower bound on the ratio $\kappa^* T/c_V \geq 1/18$, where $\kappa^*$ is the relativistic analogue of the thermal conductivity of nonrelativistic gases, and $c_V$ is the heat capacity per unit volume. This lower bound, predicted by the uncertainty principle, is found to be violated within the NJL model roughly at temperatures where the AdS/CFT bound for the ratio $\eta/s$ is violated.

In contrast to the cases of these transport coefficients, the computation of the bulk viscosity in the relevant temperature-density range requires resummation of an infinite series of multi-loop diagrams which form a geometrical progression. One of our key results is that the multi-loop contributions to the bulk viscosity dominate the single-loop contribution close to the Mott line, whereas at high temperatures the one-loop contribution becomes dominant. The exponential decrease of the multi-loop-dominated bulk viscosity close to the Mott temperature is followed by the cubic (in temperature) increase of the one-loop contribution in the high-temperature regime. The combination of these two contributions leads to a mild minimum in the temperature dependence of the bulk viscosity. Another key result of our studies is that the bulk viscosity exceeds the shear viscosity close to the Mott temperature by factors $5 \div 20$ (depending on the chemical potential). In the high-temperature regime the bulk viscosity becomes negligible compared to the shear viscosity. We comment also on the chiral symmetric case, where the multi-loop contributions to the bulk viscosity automatically vanish. In this case the bulk viscosity is negligible compared to the shear viscosity in the entire regime of interest.

The studies of the transport coefficients of quark matter close to the chiral phase transition line can be further improved by including vector interactions and/or Polyakov loop contributions in the NJL-model Lagrangian. Another possibility is to extend the current studies to the multi-flavor, in particular, the three-flavor case. These studies can be extended also to the low-temperature and high-density domain and to isospin-asymmetric quark matter in the presence of leptons. This set-up is relevant for the quark cores of compact stars. Another challenging task would be the computation of second-order transport coefficients of quark matter, which are necessary for causal hydrodynamical

description of heavy-ion collisions.

In Chapter 4 we compute the electrical conductivity tensor of warm magnetized QED plasma relevant to the outer crusts of neutron stars as well as interiors of white dwarfs [131, 132]. We apply the Boltzmann kinetic theory within the relaxation time approximation, which provides an accurate estimate for the transport coefficients with the assumption that the deviations from thermodynamic equilibrium are sufficiently small. Our calculations are applicable in a broad range of temperatures, densities and magnetic fields, where the plasma is in the liquid state. In this liquid regime the electrical conductivity is dominated by relativistic electrons, the main dissipation mechanism of which is the scattering off the correlated nuclei via screened electromagnetic force. The ion-ion correlations in the plasma are included via two-point structure factor extracted from the Monte Carlo simulations of classical one-component plasma. One of the key features of our computation is the inclusion of inelastic scattering processes, which are incorporated in terms of the dynamical screening of photon exchange, as well as the thermal distribution of nuclei.

In the presence of strong magnetic fields the conduction phenomena are described in terms of three different components of the conductivity tensor. Focusing on non-quantizing magnetic fields $B \leq 10^{14}$ G, we study numerically the three components of the conductivity tensor as functions of temperature, density, magnetic field and the nuclear charge number. Varying the temperature and the density we study how the transition from the degenerate ($T \ll T_F$) to the nondegenerate regime ($T \gg T_F$) of electrons changes the behavior of the conductivity ($T_F$ is the Fermi temperature of electrons). We find that the longitudinal conductivity increases with density, but the slope of this increase is much weaker in the nondegenerate regime as compared to the degenerate regime. The transition in the behavior of the conductivity occurs at the characteristic temparature $T \simeq (0.2 \div 0.3)T_F$, where the scalar conductivity crosses a minimum as a function of temperature. In the case of the transverse conductivities this transition point appears in the form of either a minimum, or a maximum, depending on the value of the magnetic field.

The next topic of our studies is the investigation of the magnetic field dependence of the transverse components of the conductivity tensor. Because the electron mean free path is larger at lower densities, the bending of the electron trajectories by the magnetic field between two subsequent collisions is more sizable in this case. As a result, the effect of anisotropy on the conduction is more significant at lower densities. Further analysis of combined effects of temperature and magnetic field shows that the anisotropy decreases with the increase of temperature as long as electrons are degenerate, but becomes increasingly important in the nondegenerate regime. Thus, the crust is in the "most isotropic" state at the transition point $T \simeq (0.2 \div 0.3)T_F$. At temperatures $T \simeq 10$ MeV and typical magnetic fields $B \simeq 10^{12} \div 10^{14}$ G the transverse conductivity in the outer crust of a neutron star can be reduced by $8 \div 12$ orders of magnitude, as compared to the longitudinal conductivity.

As a final step we analyze the composition-dependence of the conductivity. We first consider crustal matter consisting of a single type of atomic nucleus ($^{56}$Fe, $^{12}$C, $^{4}$He and $^{1}$H), and then extend our studies for density-dependent composition. The scalar conductivity shows a universal scaling with the nuclear charge number $\sigma \propto Z^{-1}$. The results derived for the density-dependent composition with elements with $26 \leq Z \leq 36$ in $\beta$-equilibrium with electrons are found to be close (both qualitatively and quantitatively) to those obtained for the iron nuclei, with the maximum deviation being by a factor of 1.4.

The studies of this chapter can be extended in several ways, including computation of the conductivity of hot multicomponent plasma with temperature-dependent composition. A number of interesting astrophysical problems motivate also the studies of other transport coefficients (*e.g.*, thermal conductivity, thermopower, viscosities) in the regime of high temperatures and strong magnetic fields. It would be interesting also to consider the case of extremely large magnetic fields, which are relevant for magnetars.

# Appendix A

# Correlation functions and the Kubo formulas

## A.1 Derivation of the Kubo formulas

In this Appendix we derive the relations between the first-order transport coefficients defined in Sec. 2.4.3 and retarded Green's functions, closely following similar derivations in Refs. [68, 70]. We recall that in the evaluation of the transport coefficients any non-uniformities in the thermodynamic parameters can be neglected, *i.e.*, the *local equilibrium* distribution can be replaced by a *global equilibrium* distribution with some average temperature $T = \beta^{-1}$ and chemical potentials $\mu_a$.

Consider a generic two-point correlator given by Eq. (2.166). In equilibrium and in the fluid rest frame we have $\hat{A} = \beta\hat{K}$, $\hat{K} = \hat{H} - \sum_a \mu_a \hat{\mathcal{N}}_a$ [see Eq. (2.99)], therefore from Eqs. (2.155) and (2.166) we obtain

$$\Big(\hat{X}(\boldsymbol{x},t),\hat{Y}(\boldsymbol{x}_1,t_1)\Big) = \int_0^1 d\tau \langle \hat{X}(\boldsymbol{x},t)\left[e^{-\beta\tau\hat{K}}\hat{Y}(\boldsymbol{x}_1,t_1)e^{\beta\tau\hat{K}} - \langle\hat{Y}(\boldsymbol{x}_1,t_1)\rangle_l\right]\rangle_l. \tag{A.1}$$

The time evolution of any operator in Heisenberg picture is governed by the equation

$$\hat{Y}(\boldsymbol{x},t) = e^{i\hat{K}t}\hat{Y}(\boldsymbol{x},0)e^{-i\hat{K}t}, \tag{A.2}$$

therefore we have $\hat{Y}(\boldsymbol{x},t+\delta t) = e^{i\hat{K}(t+\delta t)}\hat{Y}(\boldsymbol{x},0)e^{-i\hat{K}(t+\delta t)} = e^{i\hat{K}\delta t}\hat{Y}(\boldsymbol{x},t)e^{-i\hat{K}\delta t}$. Performing an analytic continuation $\delta t \to i\tau'$ we obtain

$$\hat{Y}(\boldsymbol{x},t+i\tau') = e^{-\hat{K}\tau'}\hat{Y}(\boldsymbol{x},t)e^{\hat{K}\tau'}, \tag{A.3}$$

from where we obtain also the relations

$$\langle\hat{Y}(\boldsymbol{x},t+i\tau')\rangle_l = \langle\hat{Y}(\boldsymbol{x},t)\rangle_l, \tag{A.4}$$

$$\langle\hat{X}(\boldsymbol{x},t)\hat{Y}(\boldsymbol{x}_1,t'+i\beta)\rangle_l = \langle\hat{Y}(\boldsymbol{x}_1,t')\hat{X}(\boldsymbol{x},t)\rangle_l. \tag{A.5}$$

The relation (A.5) is known as Kubo-Martin-Schwinger relation.

Performing a variable change $\beta\tau = \tau'$ in Eq. (A.1) and employing Eqs. (A.3) and (A.4) we obtain

$$\Big(\hat{X}(\boldsymbol{x},t),\hat{Y}(\boldsymbol{x}_1,t_1)\Big) = \frac{1}{\beta}\int_0^\beta d\tau' \langle \hat{X}(\boldsymbol{x},t)\left[\hat{Y}(\boldsymbol{x}_1,t_1+i\tau') - \langle\hat{Y}(\boldsymbol{x}_1,t_1+i\tau')\rangle_l\right]\rangle_l. \tag{A.6}$$

Assuming that the correlations vanish in the limit $t_1 \to -\infty$ [68, 70], *i.e.*,

$$\lim_{t_1\to-\infty}\Big(\langle\hat{X}(\boldsymbol{x},t)\hat{Y}(\boldsymbol{x}_1,t_1+i\tau')\rangle_l - \langle\hat{X}(\boldsymbol{x},t)\rangle_l\langle\hat{Y}(\boldsymbol{x}_1,t_1+i\tau')\rangle_l\Big) = 0, \tag{A.7}$$

we can modify the integrand in Eq. (A.6) as follows

$$\begin{aligned}
&\langle\hat{X}(\boldsymbol{x},t)\hat{Y}(\boldsymbol{x}_1,t_1+i\tau')\rangle_l - \langle\hat{X}(\boldsymbol{x},t)\rangle_l\langle\hat{Y}(\boldsymbol{x}_1,t_1+i\tau')\rangle_l \\
&= \langle\hat{X}(\boldsymbol{x},t)\int_{-\infty}^{t_1}dt'\frac{d}{dt'}\hat{Y}(\boldsymbol{x}_1,t'+i\tau')\rangle_l - \langle\hat{X}(\boldsymbol{x},t)\rangle_l\int_{-\infty}^{t_1}dt'\frac{d}{dt'}\langle\hat{Y}(\boldsymbol{x}_1,t'+i\tau')\rangle_l \\
&= -i\int_{-\infty}^{t_1}dt'\langle\hat{X}(\boldsymbol{x},t)\frac{d}{d\tau'}\hat{Y}(\boldsymbol{x}_1,t'+i\tau')\rangle_l + i\int_{-\infty}^{t_1}dt'\langle\hat{X}(\boldsymbol{x},t)\rangle_l\frac{d}{d\tau'}\langle\hat{Y}(\boldsymbol{x}_1,t'+i\tau')\rangle_l.
\end{aligned}$$

Substituting this back into Eq. (A.6) and using the relations (A.4) and (A.5) we obtain

$$\Big(\hat{X}(\boldsymbol{x},t),\hat{Y}(\boldsymbol{x}_1,t_1)\Big) = \frac{i}{\beta}\int_{-\infty}^{t_1}dt'\langle\big[\hat{X}(\boldsymbol{x},t),\hat{Y}(\boldsymbol{x}_1,t')\big]\rangle_l, \tag{A.8}$$

where the square brackets denote the commutator. Taking into account that $t' \le t_1 \le t$, we can write for Eq. (A.8)

$$\Big(\hat{X}(\boldsymbol{x},t),\hat{Y}(\boldsymbol{x}_1,t_1)\Big) = -\frac{1}{\beta}\int_{-\infty}^{t_1}dt' G^R_{\hat{X}\hat{Y}}(\boldsymbol{x}-\boldsymbol{x}_1,t-t'), \tag{A.9}$$

where

$$G^R_{\hat{X}\hat{Y}}(\boldsymbol{x}-\boldsymbol{x}',t-t') = -i\theta(t-t')\langle\big[\hat{X}(\boldsymbol{x},t),\hat{Y}(\boldsymbol{x}',t')\big]\rangle_l \tag{A.10}$$

is the two-point retarded Green's function for a uniform medium.

Now consider a generic transport coefficient given by the integral

$$I[\hat{X},\hat{Y}](\omega) = \beta\int d^3x_1\int_{-\infty}^{t}dt_1 e^{i\omega(t-t_1)}e^{\varepsilon(t_1-t)}\Big(\hat{X}(\boldsymbol{x},t),\hat{Y}(\boldsymbol{x}_1,t_1)\Big), \qquad \omega>0, \tag{A.11}$$

where we introduced also a non-zero frequency $\omega$ for the convenience of calculations: we will go to the limit $\omega\to 0$ at the end. According to Eq. (A.9) we can write Eq. (A.11) as

$$I[\hat{X},\hat{Y}](\omega') = -\int_{-\infty}^{0}dt' e^{(\varepsilon-i\omega')t'}\int_{-\infty}^{t'}dt\int d^3x G^R_{\hat{X}\hat{Y}}(-\boldsymbol{x},-t). \tag{A.12}$$

Performing a Fourier-transformation

$$G^R_{\hat{X}\hat{Y}}(\boldsymbol{x},t) = \int\frac{d^3k}{(2\pi)^3}\int_{-\infty}^{\infty}\frac{d\omega}{2\pi}e^{-i(\omega t-\boldsymbol{k}\boldsymbol{x})}G^R_{\hat{X}\hat{Y}}(\boldsymbol{k},\omega), \tag{A.13}$$

we obtain

$$\int d^3x G^R_{\hat{X}\hat{Y}}(-\boldsymbol{x},-t) = \int_{-\infty}^{\infty}\frac{d\omega}{2\pi}e^{i\omega t}G^R_{\hat{X}\hat{Y}}(\omega), \tag{A.14}$$

where $G^R_{\hat{X}\hat{Y}}(\omega)\equiv\lim_{\boldsymbol{k}\to 0}G^R_{\hat{X}\hat{Y}}(\boldsymbol{k},\omega)$. Then we have from Eq. (A.12)

$$\begin{aligned}
I[\hat{X},\hat{Y}](\omega') &= -\int_{-\infty}^{\infty}\frac{d\omega}{2\pi}G^R_{\hat{X}\hat{Y}}(\omega)\int_{-\infty}^{0}dt' e^{(\varepsilon-i\omega')t'}\frac{e^{i\omega t'}}{i\omega} \\
&= \frac{i}{\omega'+i\varepsilon}\oint\frac{d\omega}{2\pi i}\left[\frac{1}{\omega-\omega'-i\varepsilon}-\frac{1}{\omega}\right]G^R_{\hat{X}\hat{Y}}(\omega),
\end{aligned} \tag{A.15}$$

where the integral is closed in the upper-half plane where the retarded Green's function is analytic.

Applying Cauchy's integral formula and performing the limit $\varepsilon \to +0$ we obtain

$$I[\hat{X},\hat{Y}](\omega') = \frac{i}{\omega'}\left[G^R_{\hat{X}\hat{Y}}(\omega') - G^R_{\hat{X}\hat{Y}}(0)\right]. \tag{A.16}$$

Going to the zero-frequency limit $\omega \to 0$ we obtain the final formula

$$I[\hat{X},\hat{Y}](0) = i\frac{d}{d\omega}G^R_{\hat{X}\hat{Y}}(\omega)\Big|_{\omega=0}, \tag{A.17}$$

with

$$G^R_{\hat{X}\hat{Y}}(\omega) = -i\int_0^\infty dt e^{i\omega t}\int d^3x \langle\left[\hat{X}(\boldsymbol{x},t),\hat{Y}(\boldsymbol{0},0)\right]\rangle_l. \tag{A.18}$$

Form Eqs. (A.18) and (A.16) we find that

$$\left\{G^R_{\hat{X}\hat{Y}}(\omega)\right\}^* = G^R_{\hat{X}\hat{Y}}(-\omega), \qquad \left\{I[\hat{X},\hat{Y}](\omega)\right\}^* = I[\hat{X},\hat{Y}](-\omega). \tag{A.19}$$

Indeed, since $\hat{X}(\boldsymbol{x},t)$ and $\hat{Y}(\boldsymbol{x},t)$ are hermitian operators, we have the property

$$\langle\left[\hat{X}(\boldsymbol{x},t)\hat{Y}(\boldsymbol{x}',t')\right]\rangle^*_l = -\langle\left[\hat{X}(\boldsymbol{x},t)\hat{Y}(\boldsymbol{x}',t')\right]\rangle_l, \tag{A.20}$$

therefore the retarded Greens' function given by Eq. (A.10) is real, which is used to obtain the first relation in Eq. (A.19). From Eq. (A.19) we have also

$$\mathrm{Re}G^R_{\hat{X}\hat{Y}}(-\omega) = \mathrm{Re}G^R_{\hat{X}\hat{Y}}(\omega), \qquad \mathrm{Im}G^R_{\hat{X}\hat{Y}}(-\omega) = -\mathrm{Im}G^R_{\hat{X}\hat{Y}}(\omega), \tag{A.21}$$

therefore from Eqs. (A.11) and (A.17) we obtain in the zero-frequency limit

$$\beta\int d^4x_1\Big(\hat{X}(x),\hat{Y}(x_1)\Big) = -\frac{d}{d\omega}\mathrm{Im}G^R_{\hat{X}\hat{Y}}(\omega)\Big|_{\omega=0}, \tag{A.22}$$

where we used the shorthand notation defined in Eq. (2.163).

Now let as show that the Green's function (A.18) is symmetric in its arguments if the operators $\hat{X}$ and $\hat{Y}$ have the same parity under the time reversal. We have

$$\begin{aligned} G^R_{\hat{Y}\hat{X}}(\omega) &= i\int_0^\infty dt e^{i\omega t}\int d^3x\langle\left[\hat{X}(\boldsymbol{0},0),\hat{Y}(\boldsymbol{x},t)\right]\rangle_l \\ &= i\int_0^\infty dt e^{i\omega t}\int d^3x\langle\left[\hat{X}(-\boldsymbol{x},-t),\hat{Y}(\boldsymbol{0},0)\right]\rangle_l \\ &= i\int_0^\infty dt e^{i\omega t}\int d^3x\langle\left[\hat{X}(\boldsymbol{x},-t),\hat{Y}(\boldsymbol{0},0)\right]\rangle_l, \end{aligned} \tag{A.23}$$

where we used the uniformity of the medium. For hermitian operators we have the following transformation rule under the rime-reversal

$$\hat{X}_T(\boldsymbol{x},t) = \eta_X\hat{X}(\boldsymbol{x},-t), \qquad \hat{Y}_T(\boldsymbol{x},t) = \eta_Y\hat{Y}(\boldsymbol{x},-t), \tag{A.24}$$

with $\eta_{X,Y} = \pm 1$. For Eq. (A.23) we then have

$$\begin{aligned} G^R_{\hat{Y}\hat{X}}(\omega) &= i\eta_X\eta_Y\int_0^\infty dt e^{i\omega t}\int d^3x\langle\left[\hat{X}_T(\boldsymbol{x},t),\hat{Y}_T(\boldsymbol{0},0)\right]\rangle_l \\ &= i\eta_X\eta_Y\int_0^\infty dt e^{i\omega t}\int d^3x\langle\left[\hat{X}(\boldsymbol{x},t),\hat{Y}(\boldsymbol{0},0)\right]\rangle_{l,T}. \end{aligned} \tag{A.25}$$

Finally, taking into account that the statistical average of a commutator of hermitian operators is pure imaginary, and the operator of time-reversion is antiunitary (*i.e.*, transforms a number to its complex conjugate), we obtain

$$G^R_{\hat{Y}\hat{X}}(\omega) = -i\eta_X\eta_Y \int_0^\infty dt e^{i\omega t} \int d^3x \langle \big[\hat{X}(\boldsymbol{x},t), \hat{Y}(\boldsymbol{0},0)\big]\rangle_l = \eta_X\eta_Y G^R_{\hat{X}\hat{Y}}(\omega). \tag{A.26}$$

Thus, if $\eta_X = \eta_Y$, we obtain $G^R_{\hat{Y}\hat{X}}(\omega) = G^R_{\hat{X}\hat{Y}}(\omega)$, and, therefore, $I[\hat{Y},\hat{X}](\omega) = I[\hat{X},\hat{Y}](\omega)$, which is Onsager's symmetry principle for transport coefficients. Using now Eq. (A.22) and the definitions of the transport coefficients given by Eqs. (2.201), (2.202), (2.205) and (2.208), we obtain the formulas (2.209) and (2.210) of the main text.

In the derivation of the second-order transport equations we deal with vectors of the type $[x \equiv (\boldsymbol{x},t)]$

$$I^\tau[\hat{X},\hat{Y}](\omega) = \beta \int d^4x_1 e^{i\omega(t-t_1)} \Big(\hat{X}(x), \hat{Y}(x_1)\Big)(x_1 - x)^\tau, \tag{A.27}$$

where we used again the shorthand notation (2.163). The correlator $\big(\hat{X}(x), \hat{Y}(x_1)\big)$ evaluated in the local rest frame depends on the spatial coordinates only via the difference $|\boldsymbol{x} - \boldsymbol{x}_1|$, *i.e.*, it is an even function of $\boldsymbol{x} - \boldsymbol{x}_1$. Then Eq. (A.27) implies that the spatial components of the vector $I^\tau$ vanish in that frame, and for the temporal component we have

$$\begin{aligned} I^0[\hat{X},\hat{Y}](\omega) &= \beta \int d^4x_1 e^{i\omega(t-t_1)} \Big(\hat{X}(x), \hat{Y}(x_1)\Big)(t_1 - t) \\ &= i\beta \frac{d}{d\omega} \int d^4x_1 e^{i\omega(t-t_1)} \Big(\hat{X}(x), \hat{Y}(x_1)\Big) = i\frac{d}{d\omega} I[\hat{X},\hat{Y}](\omega), \end{aligned} \tag{A.28}$$

where we used Eq. (A.11). From Eqs. (A.17) and (A.28) we obtain in the limit $\omega \to 0$

$$I^0[\hat{X},\hat{Y}](0) = K[\hat{X},\hat{Y}], \tag{A.29}$$

where we defined

$$K[\hat{X},\hat{Y}] = -\frac{d^2}{d\omega^2} G^R_{\hat{X}\hat{Y}}(\omega)\Big|_{\omega=0} = -\frac{d^2}{d\omega^2} \mathrm{Re} G^R_{\hat{X}\hat{Y}}(\omega)\Big|_{\omega=0}. \tag{A.30}$$

Note that in Eqs. (A.17) and (A.30) the Green's function should be evaluated in the fluid rest frame. The relation (A.29) can be cast now into a covariant form

$$\beta \int d^4x_1 \Big(\hat{X}(x), \hat{Y}(x_1)\Big)(x_1 - x)^\tau = K[\hat{X},\hat{Y}]u^\tau. \tag{A.31}$$

## A.2 Properties of the non-local projectors $\Delta_{\mu\nu}(x,x_1)$ and $\Delta_{\mu\nu\rho\sigma}(x,x_1)$

Using Eqs. (2.7) and (2.237) we find the following properties for the second-rank projector $\Delta_{\mu\nu}(x,x_1)$

$$\begin{aligned} \Delta_{\mu\nu}(x,x_1) = \Delta_{\nu\mu}(x_1,x), \qquad & u^\mu(x)\Delta_{\mu\nu}(x,x_1) = \Delta_{\mu\nu}(x,x_1)u^\nu(x_1) = 0, \\ \Delta_{\mu\nu}(x,x) = \Delta_{\mu\nu}(x), \qquad & \Delta^\mu_\alpha(x)\Delta_{\mu\nu}(x,x_1) = \Delta_{\alpha\nu}(x,x_1). \end{aligned} \tag{A.32}$$

Form Eqs. (2.27) and (2.238) we find for the forth-rank projector $\Delta_{\mu\nu\rho\sigma}(x,x_1)$

$$\begin{gathered} \Delta_{\mu\nu\rho\sigma}(x,x_1) = \Delta_{\nu\mu\rho\sigma}(x,x_1) = \Delta_{\nu\mu\sigma\rho}(x,x_1) = \Delta_{\rho\sigma\mu\nu}(x_1,x), \\ u^\mu(x)\Delta_{\mu\nu\rho\sigma}(x,x_1) = 0, \quad \Delta_{\mu\nu\rho\sigma}(x,x_1)u^\rho(x_1) = 0, \\ \Delta_{\mu\nu\rho\sigma}(x,x) = \Delta_{\mu\nu\rho\sigma}(x), \quad \Delta^\mu{}_{\mu\rho\sigma}(x,x_1) = 0, \quad \Delta_{\mu\nu\rho\sigma}(x,x_1)\Delta^{\rho\sigma}_{\alpha\beta}(x_1) = \Delta_{\mu\nu\alpha\beta}(x,x_1). \end{gathered} \tag{A.33}$$

For our further calculations it is enough to expand the non-local projectors around the point $x_1 = x$ keeping only the linear terms in the difference $x_1 - x$. We thus approximate

$$u_\mu(x_1) \simeq u_\mu(x) + (x_1 - x)^\alpha \partial_\alpha u_\mu(x), \tag{A.34}$$

which due to the identity $u^\mu \partial_\alpha u_\mu = 0$ gives $u^\mu(x) u_\mu(x_1) \simeq 1$. In this approximation we find for the projector (2.237)

$$\Delta_{\mu\nu}(x,x_1) = g_{\mu\nu} - u_\mu(x_1)u_\nu(x) = \Delta_{\mu\nu}(x) - u_\nu(x)(x_1 - x)^\alpha \partial_\alpha u_\mu(x), \tag{A.35}$$

and from Eqs. (A.32) and (A.35) we obtain

$$\begin{gathered}
\Delta^\mu_\mu(x,x_1) = 3, \qquad \Delta^\alpha_\nu(x)\Delta_{\mu\alpha}(x,x_1) = \Delta_{\mu\nu}(x), \\
\Delta_{\mu\nu}(x,x_1)\Delta^{\mu\nu}(x,x_1) = \Delta_{\mu\lambda}(x)\Delta^{\mu\nu}(x,x_1)\Delta^\lambda_\nu(x_1) = \Delta_{\mu\lambda}(x)\Delta^{\mu\lambda}(x,x_1) = 3, \\
\Delta_{\mu\nu}(x,x_1)\Delta^{\nu\mu}(x,x_1) = \Delta_{\mu\lambda}(x)\Delta^{\nu\mu}(x,x_1)\Delta^\lambda_\nu(x_1) = \Delta^\nu_\lambda(x)\Delta^\lambda_\nu(x_1) = 3.
\end{gathered} \tag{A.36}$$

The forth-rank projector $\Delta_{\mu\nu\rho\sigma}(x,x_1)$ in the same approximation can be written as

$$\Delta_{\mu\nu\rho\sigma}(x,x_1) = \frac{1}{2}\big[\Delta_{\mu\rho}(x,x_1)\Delta_{\nu\sigma}(x,x_1) + \Delta_{\mu\sigma}(x,x_1)\Delta_{\nu\rho}(x,x_1)\big] - \frac{1}{3}\Delta_{\mu\nu}(x)\Delta_{\rho\sigma}(x_1), \tag{A.37}$$

which together with the properties (A.36) gives

$$\Delta_{\mu\nu}{}^{\mu\nu}(x,x_1) = 5. \tag{A.38}$$

Equation (A.38) together with the first relation in Eq. (A.36) was used in Eqs. (2.235) and (2.236) for the right normalization of the corresponding correlation functions.

Using the relation $\partial_\alpha \Delta_{\gamma\delta} = -u_\gamma \partial_\alpha u_\delta - u_\delta \partial_\alpha u_\gamma$, from Eq. (2.26) we obtain

$$\begin{aligned}
\partial_\alpha \Delta_{\gamma\delta\rho\sigma} \;=\; & -\frac{1}{2}\Big[\Delta_{\gamma\rho}(u_\sigma \partial_\alpha u_\delta + u_\delta \partial_\alpha u_\sigma) + \Delta_{\delta\sigma}(u_\gamma \partial_\alpha u_\rho + u_\rho \partial_\alpha u_\gamma) + \rho \leftrightarrow \sigma\Big] \\
& + \frac{1}{3}\Big[\Delta_{\gamma\delta}(u_\rho \partial_\alpha u_\sigma + u_\sigma \partial_\alpha u_\rho) + \Delta_{\rho\sigma}(u_\gamma \partial_\alpha u_\delta + u_\delta \partial_\alpha u_\gamma)\Big].
\end{aligned} \tag{A.39}$$

Multiplying Eq. (A.39) by $\Delta^{\gamma\delta}_{\mu\nu}(x)$ and using the properties (2.27) we obtain

$$\frac{\partial}{\partial x_1^\alpha}\Delta_{\mu\nu\rho\sigma}(x,x_1)\Big|_{x_1=x} = \Delta^{\gamma\delta}_{\mu\nu}\partial_\alpha \Delta_{\gamma\delta\rho\sigma} = -(\Delta_{\mu\nu\rho\beta}u_\sigma + \Delta_{\mu\nu\sigma\beta}u_\rho)\partial_\alpha u^\beta, \tag{A.40}$$

where we recalled Eq. (2.238).

# Appendix B

# Details of the NJL model calculations

## B.1 Calculation of the bulk viscosity

Substituting Eq. (3.68) into Eq. (3.67) and taking into account the isotropy of the medium ($[T_{11}, T_{33}] = [T_{11}, T_{22}]$, etc.) and the symmetry property of correlation function with respect to its arguments we obtain

$$\Pi^R_\zeta(\omega) = -i\int_0^\infty dt e^{i\omega t}\int d\boldsymbol{r}\langle\frac{1}{3}[T_{11},T_{11}]+\frac{2}{3}[T_{11},T_{22}]-2\gamma[T_{11},T_{00}] \\ -2\delta[T_{11},N_0]+2\gamma\delta[T_{00},N_0]+\gamma^2[T_{00},T_{00}]+\delta^2[N_0,N_0]\rangle_0. \tag{B.1}$$

Further progress requires substituting the explicit expressions for the components of the energy-momentum tensor (3.2) and the particle current (3.3) in this expression. We first switch to the imaginary time formalism via the replacement $t \to -i\tau$ and introduce the notation

$$\Pi^{(kl)}[\hat{a},\hat{b}](\omega_n) = \left(\frac{G}{2}\right)^{k+l-2}\int_0^\beta d\tau\, e^{i\omega_n\tau}\int d\boldsymbol{r}\langle T_\tau\big((\bar\psi\hat{a}\psi)^k\Big|_{(\boldsymbol{r},\tau)},(\bar\psi\hat{b}\psi)^l\Big|_0\big)\rangle_0, \tag{B.2}$$

where $\hat{a}$ and $\hat{b}$ are either differential operators contracted with Dirac $\gamma$-matrices (or simply $\gamma$-matrices), or interaction vertices $\Gamma^0_{s/ps}$ coming from Eqs. (3.1)–(3.3). Then the result of the substitution can be written as a sum of three terms

$$\Pi^M_\zeta(\omega_n) = \Pi^{M,11}_\zeta(\omega_n)+\Pi^{M,12}_\zeta(\omega_n)+\Pi^{M,22}_\zeta(\omega_n), \tag{B.3}$$

where

$$\begin{aligned}
-\Pi^{M,11}_\zeta(\omega_n) &= \frac{1}{3}\Pi^{(11)}[i\gamma_1\partial_1,i\gamma_1\partial_1]+\frac{2}{3}\Pi^{(11)}[i\gamma_1\partial_1,i\gamma_2\partial_2]-2\gamma\Pi^{(11)}[i\gamma_1\partial_1,-\gamma_0\partial_\tau] \\
&- 2\delta\Pi^{(11)}[i\gamma_1\partial_1,\gamma_0]+2\gamma\delta\Pi^{(11)}[-\gamma_0\partial_\tau,\gamma_0]+\gamma^2\Pi^{(11)}[-\gamma_0\partial_\tau,-\gamma_0\partial_\tau] \\
&+ \delta^2\Pi^{(11)}[\gamma_0,\gamma_0]+2(1+\gamma)\Big\{\Pi^{(11)}[i\gamma_1\partial_1,i\not\partial_\tau-m_0]-\delta\Pi^{(11)}[\gamma_0,i\not\partial_\tau-m_0] \\
&- \gamma\Pi^{(11)}[-\gamma_0\partial_\tau,i\not\partial_\tau-m_0]+\frac{1+\gamma}{2}\Pi^{(11)}[i\not\partial_\tau-m_0,i\not\partial_\tau-m_0]\Big\},
\end{aligned} \tag{B.4}$$

$$\begin{aligned}
-\Pi^{M,12}_\zeta(\omega_n) &= \sum_{\Gamma=\{1,i\boldsymbol{\tau}\gamma_5\}}\Big\{2(1+\gamma)\Pi^{(12)}[i\gamma_1\partial_1,\Gamma]-2\gamma(1+\gamma)\Pi^{(12)}[-\gamma_0\partial_\tau,\Gamma] \\
&\quad -2\delta(1+\gamma)\Pi^{(12)}[\gamma_0,\Gamma]+2(1+\gamma)^2\Pi^{(12)}[i\not\partial_\tau-m_0,\Gamma]\Big\},
\end{aligned} \tag{B.5}$$

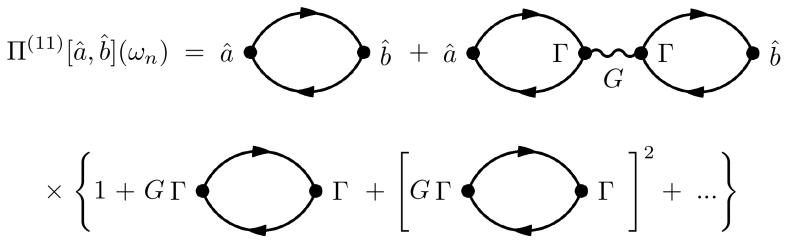


Figure B.1: Loop resummation for the correlation function $\Pi^{(11)}[\hat{a},\hat{b}]$ defined in Eq. (B.2) at the leading order in $1/N_c$ expansion.

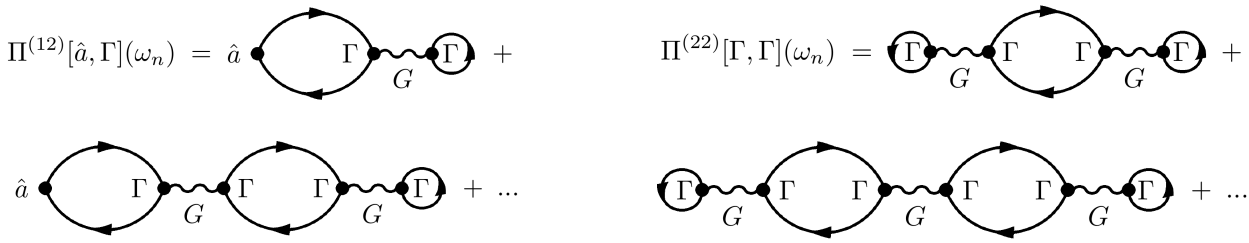


Figure B.2: Same as Fig. B.1, but for the functions $\Pi^{(12)}[\hat{a},\Gamma]$ (left figure) and $\Pi^{(22)}[\Gamma,\Gamma]$ (right figure).

and

$$-\Pi_\zeta^{M,22}(\omega_n) = (1+\gamma)^2 \sum_{\Gamma,\Gamma'=\{1,i\boldsymbol{\tau}\gamma_5\}} \Pi^{(22)}[\Gamma,\Gamma']. \tag{B.6}$$

The three types of correlation functions entering Eqs. (B.3)–(B.6) are shown diagrammatically at the leading order in Figs. B.1 and B.2. Next we note that $\Pi^{(12)}[\hat{a},\Gamma](\omega_n) = \Pi^{(22)}[\Gamma,\Gamma'](\omega_n) = 0$, because both contain bubble diagrams with one vertex $\Gamma$, which permits only $\omega_n = 0$. Thus, the second and the third terms in Eq. (B.3) vanish. We also note that the pseudoscalar vertex with $\gamma_5$ does not appear in this expression, therefore we are left in all diagrams with the vertex $\Gamma = 1$.

The remaining terms in the two-point correlation function can be expressed through the single-loop diagrams given by Eq. (3.71) of the main text. With this definition and from Fig. B.1 we find that

$$\Pi^{(11)}[\hat{a},\hat{b}](\omega_n) = \Pi_0[\hat{a},\hat{b}](\omega_n) + \tilde{G}(\omega_n)\Pi_0[\hat{a},1](\omega_n)\Pi_0[1,\hat{b}](\omega_n), \tag{B.7}$$

where we introduced a frequency-dependent coupling constant

$$\tilde{G}(\omega_n) = \frac{G}{1 - G\Pi_0[1,1](\omega_n)}. \tag{B.8}$$

To perform the Matsubara summations we need to take into account that the operators $\hat{a}$ and $\hat{b}$ may depend on $i\omega_l$. (For example, if $\hat{a} = -\gamma_0\partial_\tau$, in the momentum space we have $\hat{a} = i\gamma_0\bar{\omega}_l$, $\bar{\omega}_l = \omega_l + \omega_n/2$.) We separate the $i\bar{\omega}_l$-dependent parts of these operators by formally factorizing $\hat{a}...\hat{b}... = f(i\bar{\omega}_l)\hat{a}_0...\hat{b}_0...$, where $\hat{a}_0$ and $\hat{b}_0$ are $i\bar{\omega}_l$-independent parts of operators $\hat{a}$ and $\hat{b}$. Now we define

$$\begin{aligned} S[\hat{a},\hat{b}](\boldsymbol{p},i\omega_n) &= T\sum_l \mathrm{Tr}\big[\hat{a}G(\boldsymbol{p},i\omega_l+i\omega_n)\hat{b}G(\boldsymbol{p},i\omega_l)\big] \\ &= T\sum_l f(i\bar{\omega}_l)\mathrm{Tr}\big[\hat{a}_0G(\boldsymbol{p},i\omega_l+i\omega_n)\hat{b}_0G(\boldsymbol{p},i\omega_l)\big]. \end{aligned} \tag{B.9}$$

The calculation is completely analogous to that of $S_{\mu\nu}[f]$ functions defined in Eq. (3.28) and gives

$$S[\hat{a},\hat{b}](\boldsymbol{p},\omega)=\int_{-\infty}^{\infty}d\varepsilon\int_{-\infty}^{\infty}d\varepsilon'\mathrm{Tr}[\hat{a}_0A(\boldsymbol{p},\varepsilon')\hat{b}_0A(\boldsymbol{p},\varepsilon)]\frac{\tilde{n}(\varepsilon)f(\varepsilon+\omega/2)-\tilde{n}(\varepsilon')f(\varepsilon'-\omega/2)}{\varepsilon-\varepsilon'+\omega+i\delta}. \tag{B.10}$$

This implies that the single-loop polarization tensor is given by

$$\begin{aligned}\Pi_0[\hat{a},\hat{b}](\omega)=\int\frac{d\boldsymbol{p}}{(2\pi)^3}\int_{-\infty}^{\infty}d\varepsilon\int_{-\infty}^{\infty}d\varepsilon'\mathrm{Tr}[\hat{a}_0A(\boldsymbol{p},\varepsilon')\hat{b}_0A(\boldsymbol{p},\varepsilon)]\\ \times\frac{\tilde{n}(\varepsilon')f(\varepsilon'-\omega/2)-\tilde{n}(\varepsilon)f(\varepsilon+\omega/2)}{\varepsilon-\varepsilon'+\omega+i\delta}.\end{aligned} \tag{B.11}$$

The real and imaginary parts of the polarization tensor can now be computed by applying the Dirac identity. In particular, we find

$$\mathrm{Im}\Pi_0[\hat{a},\hat{b}](\omega)\Big|_{\omega=0}=\frac{d}{d\omega}\mathrm{Re}\Pi_0[\hat{a},\hat{b}](\omega)\Big|_{\omega=0}=0. \tag{B.12}$$

Next we compute the relevant structure of the polarization tensor needed for the bulk viscosity. From Eq. (B.7) we find

$$\mathrm{Im}\Pi^{(11)}[\hat{a},\hat{b}]=\mathrm{Im}\Pi_0[\hat{a},\hat{b}]+\mathrm{Re}\tilde{G}\mathrm{Im}\big\{\Pi_0[\hat{a},1]\Pi_0[1,\hat{b}]\big\}+\mathrm{Im}\tilde{G}\mathrm{Re}\big\{\Pi_0[\hat{a},1]\Pi_0[1,\hat{b}]\big\}. \tag{B.13}$$

For the real and imaginary parts of $\tilde{G}$ we find from Eq. (B.8)

$$\mathrm{Re}\tilde{G}(\omega) = G\frac{1-G\mathrm{Re}\Pi_0[1,1](\omega)}{\{1-G\mathrm{Re}\Pi_0[1,1](\omega)\}^2+\{G\mathrm{Im}\Pi_0[1,1](\omega)\}^2}, \tag{B.14}$$

$$\mathrm{Im}\tilde{G}(\omega) = G\frac{G\mathrm{Im}\Pi_0[1,1](\omega)}{\{1-G\mathrm{Re}\Pi_0[1,1](\omega)\}^2+\{G\mathrm{Im}\Pi_0[1,1](\omega)\}^2}, \tag{B.15}$$

which, upon using Eq. (B.12), gives

$$\mathrm{Re}\tilde{G}(0)\equiv\bar{G},\qquad \frac{d}{d\omega}\mathrm{Re}\tilde{G}(\omega)\Big|_{\omega=0}=-\bar{G}^2\frac{d}{d\omega}\mathrm{Re}\Pi_0[1,1](\omega)\Big|_{\omega=0}=0, \tag{B.16}$$

$$\mathrm{Im}\tilde{G}(0)=0,\qquad \frac{d}{d\omega}\mathrm{Im}\tilde{G}(\omega)\Big|_{\omega=0}=\bar{G}^2\frac{d}{d\omega}\mathrm{Im}\Pi_0[1,1](\omega)\Big|_{\omega=0}. \tag{B.17}$$

From Eqs. (B.13), (B.16) and (B.17) we obtain

$$\frac{d}{d\omega}\mathrm{Im}\Pi^{(11)}[\hat{a},\hat{b}](\omega)\Big|_{\omega=0}=L_0[\hat{a},\hat{b}]+\bar{G}L_1[\hat{a},\hat{b}]+\bar{G}^2L_2[\hat{a},\hat{b}], \tag{B.18}$$

where

$$L_0[\hat{a},\hat{b}] = \frac{d}{d\omega}\mathrm{Im}\Pi_0[\hat{a},\hat{b}](\omega)\Big|_{\omega=0}, \tag{B.19}$$

$$L_1[\hat{a},\hat{b}] = R_0[\hat{a},1]L_0[1,\hat{b}]+R_0[1,\hat{b}]L_0[\hat{a},1], \tag{B.20}$$

$$L_2[\hat{a},\hat{b}] = L_0[1,1]R_0[\hat{a},1]R_0[1,\hat{b}], \tag{B.21}$$

$$R_0[\hat{a},\hat{b}] = \mathrm{Re}\Pi_0[\hat{a},\hat{b}](\omega)\Big|_{\omega=0}, \tag{B.22}$$

and the effective zero-frequency coupling is given by

$$\bar{G}=\frac{G}{1-GR_0[1,1]}. \tag{B.23}$$

Now we calculate the relevant pieces of the polarization tensor for specific $\hat{a}$ and $\hat{b}$ operator combinations. Using Eqs. (3.46) and (3.47) we can write the relevant real parts in the generic form

$$R_0[\hat{a},\hat{b}] = -\frac{2N_cN_f}{\pi^4}\int_0^\Lambda p^2dp\int_{-\infty}^{\infty}d\varepsilon\int_{-\infty}^{\infty}d\varepsilon'\frac{\varepsilon^k\tilde{n}(\varepsilon)-\varepsilon'^k\tilde{n}(\varepsilon')}{\varepsilon-\varepsilon'}\mathcal{O}_R(p,\varepsilon,\varepsilon'), \tag{B.24}$$

where the factors $N_c = 3$ and $N_f = 2$ arise from the trace in the color and flavor spaces, respectively; $\Lambda$ is the 3-momentum cutoff parameter. For each specific value of $\hat{a}$ and $\hat{b}$ operators we have the following functions $\mathcal{O}_R$

$$R_0\,[1,1] \qquad \mathcal{O}_R = (m^2A_sA_s' + \varepsilon\varepsilon' A_0A_0' - p^2A_vA_v'), \tag{B.25a}$$
$$R_0\,[1,i\gamma_1\partial_1] \qquad \mathcal{O}_R = \frac{1}{3}mp^2(A_s'A_v + A_sA_v'), \tag{B.25b}$$
$$R_0\,[1,\gamma_0] \qquad \mathcal{O}_R = m(\varepsilon A_s'A_0 + \varepsilon' A_sA_0'), \tag{B.25c}$$
$$R_0\,[1,-\gamma_0\partial_\tau] \qquad \mathcal{O}_R = m(\varepsilon A_s'A_0 + \varepsilon' A_sA_0'), \tag{B.25d}$$

and $k = 0$ for the first three cases and $k = 1$ for the last case.

The generic form of the imaginary parts is given by

$$L_0[\hat{a},\hat{b}] = -\frac{2N_cN_f}{\pi^3}\int_0^\Lambda p^2dp\int_{-\infty}^{\infty}d\varepsilon\frac{\partial n(\varepsilon)}{\partial\varepsilon}\mathcal{O}_I(p,\varepsilon), \tag{B.26}$$

where for each specific value of $\hat{a}$ and $\hat{b}$ operators the following $\mathcal{O}_I$ functions should be substituted

$$L_0[1,1] \qquad \mathcal{O}_I = m^2A_s^2 + \varepsilon^2A_0^2 - p^2A_v^2, \tag{B.27a}$$
$$L_0[1,\gamma_0] \qquad \mathcal{O}_I = 2m\varepsilon A_sA_0, \tag{B.27b}$$
$$L_0[1,-\gamma_0\partial_\tau] \qquad \mathcal{O}_I = 2m\varepsilon^2A_sA_0, \tag{B.27c}$$
$$L_0[1,i\gamma_1\partial_1] \qquad \mathcal{O}_I = \frac{2}{3}mp^2A_sA_v, \tag{B.27d}$$
$$L_0[\gamma_0,\gamma_0] \qquad \mathcal{O}_I = m^2A_s^2 + \varepsilon^2A_0^2 + p^2A_v^2, \tag{B.27e}$$
$$L_0[-\gamma_0\partial_\tau,-\gamma_0\partial_\tau] \qquad \mathcal{O}_I = \varepsilon^2(m^2A_s^2 + \varepsilon^2A_0^2 + p^2A_v^2), \tag{B.27f}$$
$$L_0[\gamma_0,-\gamma_0\partial_\tau] \qquad \mathcal{O}_I = \varepsilon(m^2A_s^2 + \varepsilon^2A_0^2 + p^2A_v^2), \tag{B.27g}$$
$$L_0[i\gamma_1\partial_1,\gamma_0] \qquad \mathcal{O}_I = \frac{2}{3}p^2\varepsilon A_0A_v, \tag{B.27h}$$
$$L_0[i\gamma_1\partial_1,-\gamma_0\partial_\tau] \qquad \mathcal{O}_I = \frac{2}{3}p^2\varepsilon^2A_0A_v, \tag{B.27i}$$
$$L_0[i\gamma_1\partial_1,i\gamma_1\partial_1] \qquad \mathcal{O}_I = \frac{p^2}{15}(-5m^2A_s^2 + 5\varepsilon^2A_0^2 + p^2A_v^2), \tag{B.27j}$$
$$L_0[i\gamma_1\partial_1,i\gamma_2\partial_2] \qquad \mathcal{O}_I = \frac{2}{15}p^4A_v^2. \tag{B.27k}$$

With these ingredients the bulk viscosity can be computed by writing $\zeta = \zeta_0 + \zeta_1 + \zeta_2$, where the indices on these quantities match those of the $L$-functions in Eq. (B.18). From Eq. (B.4) we find

$$\begin{aligned}\zeta_0 &= \frac{1}{3}(2+3\gamma)^2L_0[i\gamma_1\partial_1,i\gamma_i\partial_i] - 2(2+3\gamma)L_0[i\gamma_1\partial_1,-\gamma_0\partial_\tau]\\ &+ 2\delta(2+3\gamma)L_0[i\gamma_1\partial_1,\gamma_0] - 2\delta L_0[-\gamma_0\partial_\tau,\gamma_0] + L_0[-\gamma_0\partial_\tau,-\gamma_0\partial_\tau]\\ &+ 2m_0(1+\gamma)(2+3\gamma)L_0[1,i\gamma_1\partial_1] - 2m_0(1+\gamma)L_0[1,-\gamma_0\partial_\tau]\\ &+ \delta^2L_0[\gamma_0,\gamma_0] + 2m_0\delta(1+\gamma)L_0[1,\gamma_0] + m_0^2(1+\gamma)^2L_0[1,1].\end{aligned} \tag{B.28}$$

The components $\zeta_{1,2}$ can be written as $\zeta_1 = 2(\bar{G}\bar{R})I_1$, $\zeta_2 = (\bar{G}\bar{R})^2 L_0[1,1]$ with

$$\begin{aligned} \bar{R} &= (2+3\gamma)R_0[1, i\gamma_1\partial_1] + m_0(1+\gamma)R_0[1,1] + \delta R_0[1,\gamma_0] - R_0[1,-\gamma_0\partial_\tau], && \text{(B.29)} \\ I_1 &= (2+3\gamma)L_0[1, i\gamma_1\partial_1] + m_0(1+\gamma)L_0[1,1] + \delta L_0[1,\gamma_0] - L_0[1,-\gamma_0\partial_\tau]. && \text{(B.30)} \end{aligned}$$

The final expressions for three contributions to $\zeta$ are given by Eqs. (3.73)–(3.81) of the main text.

## B.2 Meson-exchange quark self-energy

Here we provide some details of the computation of the self-energy (3.125) and its imaginary part. Analogous calculations for relativistic nucleonic matter were carried out in Ref. [273] and for two-flavor quark matter in Ref. [91]. Substituting the quark and meson propagators into Eq. (3.125) [see Eqs. (3.84), (3.85) and (3.113)], we find

$$\Sigma^M(\boldsymbol{p},\omega_n) = g_M^2 \int \frac{d\boldsymbol{q}}{(2\pi)^3 2} \sum_{\pm} \frac{1}{2E_q^{\pm}} T \sum_m \frac{\Gamma_M(E_q^{\pm}\gamma_0 - \boldsymbol{\gamma}\cdot\boldsymbol{q} + m)\Gamma_M}{(i\omega_m - E_q^{\pm})[(\omega_n-\omega_m)^2 + E_M^2]}, \tag{B.31}$$

where $E_M^2 = (\boldsymbol{p}-\boldsymbol{q})^2 + m_M^2$. For $\Gamma_\sigma = 1$ and $\Gamma_\pi = i\gamma_5\tau_j$ we can write $\Gamma_M(E_q^{\pm}\gamma_0 - \boldsymbol{\gamma}\cdot\boldsymbol{q} + m)\Gamma_M = E_q^{\pm}\gamma_0 - \boldsymbol{\gamma}\cdot\boldsymbol{q} + P_M m$, with $P_\sigma = 1$, $P_\pi = -1$, therefore

$$\Sigma^M(\boldsymbol{p},\omega_n) = P_M m \Sigma_s^M + i\omega_n\gamma_0\Sigma_0^M - \boldsymbol{p}\cdot\boldsymbol{\gamma}\Sigma_v^M, \tag{B.32}$$

where we defined

$$\begin{aligned} \Sigma_s^M &= g_M^2 \int \frac{d\boldsymbol{q}}{(2\pi)^3} \sum_{\pm} \frac{\mathscr{S}^{\pm}}{2E_q^{\pm}}, && \text{(B.33)} \\ \Sigma_0^M &= g_M^2 \int \frac{d\boldsymbol{q}}{(2\pi)^3} \frac{1}{2i\omega_n} \sum_{\pm} \mathscr{S}^{\pm}, && \text{(B.34)} \\ \Sigma_v^M &= g_M^2 \int \frac{d\boldsymbol{q}}{(2\pi)^3} \frac{\boldsymbol{q}\cdot\boldsymbol{p}}{p^2} \sum_{\pm} \frac{\mathscr{S}^{\pm}}{2E_q^{\pm}}, && \text{(B.35)} \end{aligned}$$

and

$$\begin{aligned} \mathscr{S}^{\pm} &= T\sum_m \frac{1}{(i\omega_m - E_q^{\pm})[(\omega_n-\omega_m)^2 + E_M^2]} = \frac{1}{2E_M} T\sum_m \\ &\times \left[\frac{1}{(i\omega_m - E_q^{\pm})(i\omega_m - i\omega_n + E_M)} - \frac{1}{(i\omega_m - E_q^{\pm})(i\omega_m - i\omega_n - E_M)}\right]. \end{aligned} \tag{B.36}$$

Using Cauchy's integral formula we find

$$\begin{aligned} \int_C \frac{dz}{2\pi i} \frac{n^+(z)}{(z - E_q^{\pm})(z - i\omega_n - E_M)} &= T\sum_m \frac{1}{(i\omega_m - E_q^{\pm})(i\omega_m - i\omega_n - E_M)} \\ &= \frac{n^+(E_q^{\pm}) - n^+(E_M + i\omega_n)}{E_q^{\pm} - E_M - i\omega_n} = \frac{n^+(E_q^{\pm}) + n_B(E_M)}{E_q^{\pm} - E_M - i\omega_n}, \end{aligned} \tag{B.37}$$

where $n_B(z) = (e^{\beta z} - 1)^{-1}$ is the Bose distribution function, therefore

$$\mathscr{S}^{\pm} = \frac{1}{2E_M}\left[\frac{n^+(E_q^{\pm}) + n_B(-E_M)}{E_q^{\pm} + E_M - i\omega_n} - \frac{n^+(E_q^{\pm}) + n_B(E_M)}{E_q^{\pm} - E_M - i\omega_n}\right]. \tag{B.38}$$

Defining $E_\pm = E_q \pm E_M$ and using the properties $n_B(-E) = -1 - n_B(E)$, $n^+(-E) = 1 - n^-(E)$

we obtain

$$\sum_{\pm} \mathscr{S}^{\pm} = \frac{1}{2E_M}\left[\frac{E_+\mathscr{C}_3 - 2i\omega_n\mathscr{C}_1}{E_+^2+\omega_n^2} - \frac{E_-\mathscr{C}_3 + 2i\omega_n\mathscr{C}_2}{E_-^2+\omega_n^2}\right], \tag{B.39}$$

where $\mathscr{C}_1$, $\mathscr{C}_2$, and $\mathscr{C}_3$ are defined in Eqs. (3.129). In the same manner we obtain

$$\sum_{\pm} \frac{\mathscr{S}^{\pm}}{2E_q^{\pm}} = \frac{1}{4E_qE_M}\left[\frac{i\omega_n\mathscr{C}_3 - 2E_+\mathscr{C}_1}{E_+^2+\omega_n^2} - \frac{i\omega_n\mathscr{C}_3 + 2E_-\mathscr{C}_2}{E_-^2+\omega_n^2}\right]. \tag{B.40}$$

Now using Eqs. (B.39) and (B.40) in Eqs. (B.33)–(B.35) we obtain Eqs. (3.127) and (3.128) of the main text.

We now turn to the computation of the imaginary parts of Eqs. (3.127) and (3.128), which are extracted using the Dirac identity by writing

$$\mathrm{Im}\frac{1}{E^2+\omega_n^2}\bigg|_{i\omega_n\to p_0+i\varepsilon} = \pi\mathrm{sgn}(p_0)\delta(E^2-p_0^2) = \frac{\pi}{2p_0}[\delta(E+p_0)+\delta(E-p_0)]. \tag{B.41}$$

For on-shell quarks with $p_0 = \sqrt{\boldsymbol{p}^2+m^2}$ Eqs. (3.127) and (3.128) generate four contributions after analytical continuation and application of the Dirac identity, each of which is proportional to a $\delta$-function

$$\delta(E_M+E_q+p_0) \equiv \delta_1, \qquad \delta(E_M+E_q-p_0) \equiv \delta_2, \tag{B.42}$$

$$\delta(E_M-E_q+p_0) \equiv \delta_3, \qquad \delta(E_M-E_q-p_0) \equiv \delta_4. \tag{B.43}$$

For $p_0 \geq 0$, the term $\delta_1$ vanishes trivially. As we will show later, the terms $\delta_2$ and $\delta_3$ do not give any contribution as well. Using the relation $E_M^2-(E_q+p_0)^2 = m_M^2-2m^2-2pqx-2E_qp_0$, where $x=\cos(\widehat{\boldsymbol{p}\boldsymbol{q}})$, for $\delta_4$ we can write

$$\begin{aligned}\delta_4 = \delta(E_M-E_q-p_0)+\delta(E_M+E_q+p_0) &= 2E_M\delta[E_M^2-(E_q+p_0)^2] \\ &= \frac{E_M}{pq}\delta(x-x_-), \quad x_- = \frac{m_M^2-2m^2-2E_qp_0}{2pq},\end{aligned} \tag{B.44}$$

and for an arbitrary function $f(\boldsymbol{q}) = f(q,x)$ we then have

$$\begin{aligned}&\int \frac{d\boldsymbol{q}}{(2\pi)^3}f(\boldsymbol{q})\delta_4 = \int_0^{\Lambda}\frac{q^2dq}{(2\pi)^2}\int_{-1}^{1}dx f(q,x)\frac{E_M}{pq}\delta(x-x_-) \\ &= \int_m^{E_\Lambda}\frac{dE_q}{(2\pi)^2}\frac{E_qE_M}{p}f(q,x_-)\theta(1-x_-^2) = \int_{E_{\min}}^{E_{\max}}\frac{dE_q}{(2\pi)^2}\frac{E_qE_M}{p}f(q,x_-),\end{aligned} \tag{B.45}$$

where the limits of integration are found from the condition $x_-^2 \leq 1$ or

$$\left(\frac{m_M^2-2m^2-2E_qp_0}{2pq}\right)^2 \leq 1, \tag{B.46}$$

which leads us to Eqs. (3.135) and (3.138) of the main text in the cases $m \neq 0$ and $m=0$, respectively.

By analogy with Eqs. (B.44) and (B.45) we have

$$\begin{aligned}\delta_2+\delta_3 = \delta(E_M+E_q-p_0)+\delta(E_M-E_q+p_0) &= 2E_M\delta[E_M^2-(E_q-p_0)^2] \\ &= \frac{E_M}{pq}\delta(x-x_+), \quad x_+ = \frac{m_M^2-2m^2+2E_qp_0}{2pq},\end{aligned} \tag{B.47}$$

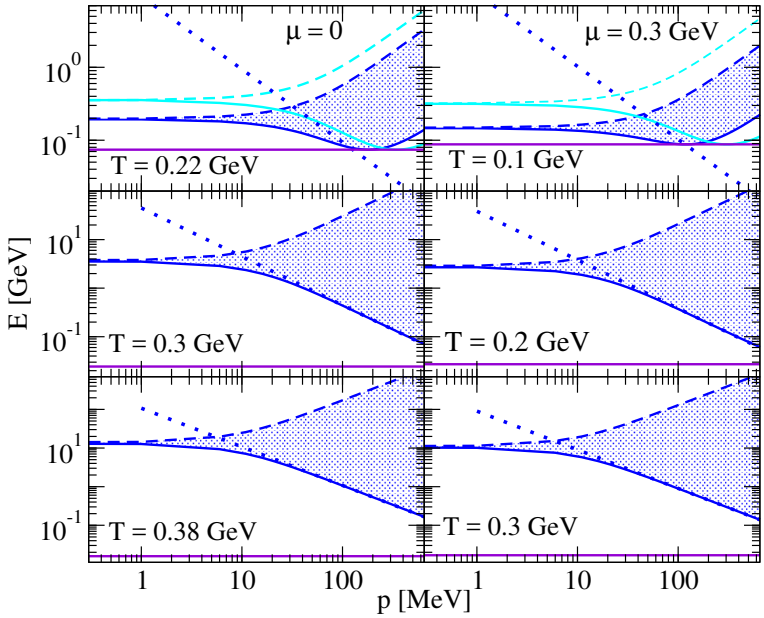


Figure B.3: Dependence of the ranges of integration (3.135) (the shaded area) in the self-energies (3.132) and (3.134) on momentum at various values of temperature and chemical potential. The ranges are limited by $E_{\min,\pi}$ (heavy solid line) and $E_{\max,\pi}$ (heavy dashed line) for $\pi$-mesons and by $E_{\min,\sigma}$ (light solid line) and $E_{\max,\sigma}$ (light dashed line) for $\sigma$-mesons. The chiral limit given by (3.138) is shown by the dotted lines. The value of the quark mass is shown by the heavy horizontal line.

therefore

$$\int \frac{d\boldsymbol{q}}{(2\pi)^3} f(\boldsymbol{q})(\delta_2+\delta_3) = \int_m^\infty \frac{dE_q}{(2\pi)^2}\frac{E_q E_M}{p} f(q,x_+)\theta(1-x_+^2). \tag{B.48}$$

The condition $x_+^2 \le 1$ is satisfied for $E_q \in (E'_{\min}, E'_{\max})$ with $E'_{\min} = -E_{\max}$, $E'_{\max} = -E_{\min}$, as can be seen from Eq. (3.135) (note that $x_+$ is obtained from $x_-$ by the inversion $p_0 \to -p_0$). In this case the integration range is empty, and the integral vanishes.

We are now in a position to take the imaginary parts of the self-energies; keeping the only non-vanishing part $\propto \mathrm{Im}[E_-^2+\omega_n^2]^{-1} = \pi(2p_0)^{-1}\delta_4$, we find form Eqs. (3.127)–(3.130) and (B.45)

$$\begin{aligned}\mathrm{Im}\Sigma^M_{s,v} &= -g_M^2 \int \frac{d\boldsymbol{q}}{(2\pi)^3}\mathscr{Q}_{s,v}(\boldsymbol{q})\frac{p_0\mathscr{C}_3 + 2E_-\mathscr{C}_2}{4E_qE_M}\frac{1}{E_-^2+\omega_n^2}\\ &= \frac{g_M^2}{16\pi p}\int_{E_{\min}}^{E_{\max}} dE_q \mathscr{T}_{s,v}(q,x_-)[n_B(E_M)+n^-(E_q)],\end{aligned} \tag{B.49}$$

and

$$\begin{aligned}\mathrm{Im}\Sigma^M_{0} &= g_M^2 \int \frac{d\boldsymbol{q}}{(2\pi)^3}\mathscr{Q}_{0}(q)\frac{2p_0\mathscr{C}_2 + E_-\mathscr{C}_3}{4E_qE_M}\frac{1}{E_-^2+\omega_n^2}\\ &= \frac{g_M^2}{16\pi p}\int_{E_{\min}}^{E_{\max}} dE_q \mathscr{T}_{0}(q)[n_B(E_M)+n^-(E_q)],\end{aligned} \tag{B.50}$$

where the functions $\mathscr{T}_i, i = s, 0, v$ are defined in Eq. (3.133). Combining Eqs. (B.49) and (B.50) we finally obtain Eq. (3.132) of the main text. The imaginary part of the on-shell self-energy of antiquarks ($p_0 = -E_p$), given by Eq. (3.134), is obtained through a similar calculation. To support the discussion of the various contributions to the self-energies (3.132) and (3.134) in the main text we show in Fig. B.3 the ranges of integration in these equations.

# Appendix C

# Collision integral of QED plasma: details of computations

## C.1 Evaluating the relaxation time

The purpose of this appendix is to give the details of the transition from Eq. (4.14) to Eq. (4.45) for the relaxation time. We start by defining several angles by the relations $\boldsymbol{p}\cdot\boldsymbol{q} = pq\cos\alpha$, $\boldsymbol{p}_\perp\cdot\boldsymbol{p}'_\perp = p_\perp p'_\perp\cos\phi$ and $\boldsymbol{q}\cdot\boldsymbol{p}' = qp'\cos\vartheta$, where $\boldsymbol{p}_\perp$ and $\boldsymbol{p}'_\perp$ are the components of the vectors $\boldsymbol{p}$ and $\boldsymbol{p}'$ transverse to $\boldsymbol{q}$. Writing the second $\delta$-function in Eq. (4.14) as $\delta(\varepsilon_2-\varepsilon_4+\omega) = (M/p'q)\delta(\cos\vartheta - x_0)$, where $x_0 = (2\omega M - q^2)/2p'q$, we find

$$\tau^{-1}(\varepsilon) = \frac{(2\pi)^{-5}M}{p}\int d\omega d\boldsymbol{q}\cos\alpha\,\delta(\varepsilon-\varepsilon_3-\omega)S(q)F^2(q)\frac{1-f_3^0}{1-f^0}\int_0^\infty dp'p'g(p')I_\Omega, \tag{C.1}$$

where

$$\begin{aligned} I_\Omega &= \int d(\cos\vartheta)d\phi\frac{Z^2e^{*4}}{2\varepsilon\varepsilon_3}\left[\frac{2\varepsilon^2-\varepsilon\omega-pq\cos\alpha}{|q^2+\Pi'_L|^2}\right. \\ &+ \frac{p'^2\sin^2\vartheta[2(p\cos\phi)^2\sin^2\alpha+qp\cos\alpha-\varepsilon\omega]}{M^2|q^2-\omega^2+\Pi_T|^2} \\ &- \left.\frac{2}{M}\frac{(2\varepsilon-\omega)(pp'\sin\alpha\sin\vartheta\cos\phi)}{\mathrm{Re}[(q^2+\Pi'_L)(q^2-\omega^2+\Pi^*_T)]}\right]\delta(\cos\vartheta-x_0), \end{aligned} \tag{C.2}$$

and we substituted the expression for the matrix element (4.43). After integration over the angle $\phi$ we obtain

$$I_\Omega = \pi\frac{Z^2e^{*4}}{\varepsilon(\varepsilon-\omega)}\left[\frac{2\varepsilon^2-\varepsilon\omega-pq\cos\alpha}{|q^2+\Pi'_L|^2}+p'^2(1-x_0^2)\frac{p^2\sin^2\alpha+qp\cos\alpha-\varepsilon\omega}{M^2|q^2-\omega^2+\Pi_T|^2}\right]\theta(1-|x_0|). \tag{C.3}$$

The step-function $\theta$ defines the minimum value $p'_{\min} = |2\omega M - q^2|/2q$ for the integration over this variable. We substitute Eq. (C.3) in Eq. (C.1), implement the integration bound on $p'$ and find

$$\begin{aligned} \tau^{-1}(\varepsilon) &= \frac{(2\pi)^{-5}\pi M}{p}\frac{Z^2e^{*4}}{\varepsilon}\int d\omega d\boldsymbol{q}\frac{S(q)F^2(q)\cos\alpha}{\varepsilon-\omega}\delta(\varepsilon-\varepsilon_3-\omega)\frac{1-f_3^0}{1-f^0}\int_{p'_{\min}}^\infty dp'p'g(p') \\ &\times \left[\frac{2\varepsilon^2-\varepsilon\omega-pq\cos\alpha}{|q^2+\Pi'_L|^2}+p'^2(1-x_0^2)\frac{p^2\sin^2\alpha+qp\cos\alpha-\varepsilon\omega}{M^2|q^2-\omega^2+\Pi_T|^2}\right]. \end{aligned} \tag{C.4}$$

The remaining $\delta$ function is written as $\delta(\varepsilon - \varepsilon_3 - \omega) = [(\varepsilon - \omega)/pq]\delta(\cos\alpha - y_0)\vartheta(\varepsilon - \omega)$, where $y_0 = (q^2 - \omega^2 + 2\varepsilon\omega)/2pq$. In the next step we integrate over $p'$ using Eq. (4.5)

$$\int_{p'_{\rm min}}^{\infty} dp'p'g(p') = MTg(p'_{\rm min}), \tag{C.5}$$

$$\int_{p'_{\rm min}}^{\infty} dp'p'g(p')p'^2 = 2(MT)^2 g(p'_{\rm min})(1 + \beta\varepsilon_{\rm min}), \tag{C.6}$$

$$\int_{p'_{\rm min}}^{\infty} dp'p'^3 g(p')(1 - x_0^2) = \int_{p_{\rm min}}^{\infty} dp'p'g(p')\ (p'^2 - p'^2_{\rm min}) = 2(MT)^2 g(p'_{\rm min}), \tag{C.7}$$

where $\varepsilon_{\rm min} = p'^2_{\rm min}/2M$. Then for Eq. (C.4) we obtain

$$\begin{aligned}\tau^{-1}(\varepsilon) &= \frac{M^2T}{8(2\pi)^3}\frac{Z^2e^{*4}}{\varepsilon p^3}\int_{-\infty}^{\varepsilon} d\omega \frac{1 - f(\varepsilon - \omega)}{1 - f^0(\varepsilon)}\int_0^{\infty} dqS(q)F^2(q)g(p'_{\rm min})(q^2 - \omega^2 + 2\varepsilon\omega)\\ &\times\ \theta(1 - |y_0|)\left[\frac{(2\varepsilon - \omega)^2 - q^2}{|q^2 + \Pi'_L|^2} + \frac{T}{Mq^2}\frac{(q^2 - \omega^2)[(2\varepsilon - \omega)^2 + q^2] - 4q^2m^2}{|q^2 - \omega^2 + \Pi_T|^2}\right],\end{aligned} \tag{C.8}$$

where we integrated over the angles and substituted the expression for $y_0$. Finally, the $\theta$-function puts some limitations on the integration region over $q$, specifically $q_- \le q \le q_+$, where $q_\pm = |\pm\sqrt{\varepsilon^2 - m^2} + \sqrt{(\varepsilon - \omega)^2 - m^2}|$. Note also that to have a real $q$ we need $\omega \le \varepsilon - m$. Implementing these limits we obtain

$$\begin{aligned}\tau^{-1}(\varepsilon) &= \frac{M^2T}{8(2\pi)^3}\frac{Z^2e^{*4}}{\varepsilon p^3}\int_{-\infty}^{\varepsilon-m} d\omega \frac{1 - f^0(\varepsilon - \omega)}{1 - f^0(\varepsilon)}\int_{q_-}^{q_+} dqS(q)F^2(q)g(p'_{\rm min})(q^2 - \omega^2 + 2\varepsilon\omega)\\ &\times\ \left[\frac{(2\varepsilon - \omega)^2 - q^2}{|q^2 + \Pi'_L|^2} + \frac{T}{Mq^2}\frac{(q^2 - \omega^2)[(2\varepsilon - \omega)^2 + q^2] - 4q^2m^2}{|q^2 - \omega^2 + \Pi_T|^2}\right].\end{aligned} \tag{C.9}$$

Finally, we write Eq. (4.5) as

$$g(p'_{\rm min}) = n_i\left(\frac{2\pi}{MT}\right)^{3/2} e^{-x^2/2\theta^2}e^{\omega/2T}e^{-q^2/8MT}, \tag{C.10}$$

where $x = \omega/q$ and $\theta = \sqrt{T/M}$, and substitute in Eq. (C.9) to obtain Eq. (4.45) of the main text.

## C.2 Polarization tensor

In this appendix we outline the derivation of the polarization tensor in the HTL effective field theory. Most of the HTL computation are carried out in the ultrarelativistic (massless) limit; here we keep the particle mass nonzero and implement HTL approximation by requiring that the external photon four-momenta are small compared to the fermionic four-momenta within the fermionic loop.

The full photon propagator $D_{\mu\nu}$ can be found from the Dyson equation

$$[D^{-1}]_{\mu\nu} = [D_0^{-1}]_{\mu\nu} - \Pi_{\mu\nu}, \tag{C.11}$$

where $D_0^{\mu\nu} = g^{\mu\nu}/Q^2$ is the free photon propagator with $Q^2 = \omega^2 - q^2$; $\Pi_{\mu\nu}$ is the photon polarization tensor and can be decomposed into transverse and longitudinal modes

$$\Pi_{\mu\nu} = \Pi_T P^T_{\mu\nu} + \Pi_L P^L_{\mu\nu}. \tag{C.12}$$

We work in the plasma rest frame where the projectors $P^T_{\mu\nu}$ and $P^L_{\mu\nu}$ have the following components

$$P^T_{00}=0,\quad P^T_{0i}=0,\quad P^T_{ij}=-\delta_{ij}+q_iq_j/q^2, \tag{C.13}$$

$$P^L_{00}=-q^2/Q^2,\quad P^L_{0i}=-\omega q_i/Q^2,\quad P^L_{ij}=-\frac{\omega^2}{Q^2}\frac{q_iq_j}{q^2}. \tag{C.14}$$

They satisfy the relations

$$P^T_{\mu\alpha}P^{T\alpha\nu}=P^{T\nu}_{\mu},\quad P^L_{\mu\alpha}P^{L\alpha\nu}=P^{L\nu}_{\mu},\quad P^T_{\mu\alpha}P^{L\alpha\nu}=0. \tag{C.15}$$

From Eqs. (C.11)–(C.15) it is easy to find the full photon propagator

$$D^{\mu\nu}=\frac{1}{Q^2}\left[g^{\mu\nu}+\frac{\Pi_T}{Q^2-\Pi_T}P^{T\mu\nu}+\frac{\Pi_L}{Q^2-\Pi_L}P^{L\mu\nu}\right]. \tag{C.16}$$

Using Eq. (C.16) and the current conservation law $q^\mu J_\mu=\omega J_0+q^iJ_i=0$, we can express the scattering amplitude via two scalar functions $\Pi_L$ and $\Pi_T$

$$\mathcal{M}=J_\mu D^{\mu\nu}J'_\nu=-\frac{J_0J'_0}{q^2+\Pi'_L}+\frac{\boldsymbol{J}_\perp\boldsymbol{J}'_\perp}{q^2-\omega^2+\Pi_T}, \tag{C.17}$$

where we introduced transverse currents $J_{\perp i}=J_j(\delta_{ij}-q_iq_j/q^2)$ and $\Pi'_L=-\Pi_Lq^2/Q^2=\Pi_L/(1-x^2)$ and $x=\omega/q$. The one-loop diagram in the imaginary-time formalism is given by [see Fig. 4.3]

$$\Pi_{\mu\nu}(\boldsymbol{q},\omega_n)=e^{*2}\int\frac{d\boldsymbol{p}}{(2\pi)^3}T\sum_m\mathrm{Tr}[\gamma_\mu S(\boldsymbol{p},\omega_m)\gamma_\nu S(\boldsymbol{p}-\boldsymbol{q},\omega_m-\omega_n)], \tag{C.18}$$

where $S(\boldsymbol{p},\omega_n)$ is the free electron-positron propagator and the sum is over fermionic (odd) Matsubara frequencies $\omega_m=(2m+1)\pi T-i\mu$ (note that $\omega_n=2n\pi T$ is a bosonic, *i.e.*, an even Matsubara frequency). The propagator $S(\boldsymbol{p},\omega_n)$ is given by

$$S(\boldsymbol{p},\omega_m)=i\sum_\pm\frac{\Lambda^\pm_p\gamma_0}{i\omega_n-E^\pm_p}, \tag{C.19}$$

where $\Lambda^\pm_p$ are the projection operators onto positive and negative energy states

$$\Lambda^\pm_p=\frac{\not{p}^\pm+m}{2E^\pm_p}\gamma_0,\qquad p^\pm=(E^\pm_p,\boldsymbol{p})=(\pm E_p,\boldsymbol{p}). \tag{C.20}$$

Substitution of Eq. (C.19) into Eq. (C.18) gives

$$\Pi_{\mu\nu}(\boldsymbol{q},\omega_n)=-e^{*2}\int\frac{d\boldsymbol{p}}{(2\pi)^3}\sum_{\pm\pm}T\sum_m\frac{\mathrm{Tr}[\gamma_\mu\Lambda^\pm_p\gamma_0\gamma_\nu\Lambda^\pm_{p-q}\gamma_0]}{(i\omega_m-E^\pm_p)(i\omega_m-i\omega_n-E^\pm_{p-q})}. \tag{C.21}$$

The trace is evaluated using standard field theory methods after substituting therein the projectors (C.20):

$$\mathrm{Tr}[\gamma_\mu\Lambda^\pm_p\gamma_0\gamma_\nu\Lambda^\pm_{p-q}\gamma_0]=\frac{p^\pm_\mu p'^\pm_\nu+p^\pm_\nu p'^\pm_\mu-g_{\mu\nu}[(p^\pm p'^\pm)-m^2]}{E^\pm_pE^\pm_{p'}},\qquad \boldsymbol{p}'=\boldsymbol{p}-\boldsymbol{q}. \tag{C.22}$$

The summation over the Matsubara frequencies gives

$$T\sum_m\frac{1}{(i\omega_m-E^\pm_p)(i\omega_m-i\omega_n-E^\pm_{p-q})}=\frac{f^+(E^\pm_p)-f^+(E^\pm_{p-q})}{E^\pm_p-E^\pm_{p-q}-i\omega_n}, \tag{C.23}$$

where $f^{\pm}(E) = [e^{\beta(E\mp\mu)}+1]^{-1}$ (note that in the main text we use $f^0$ instead of $f^+$). Substituting Eqs. (C.22) and (C.23) into Eq. (C.21) we obtain

$$\Pi_{\mu\nu}(\boldsymbol{q},\omega_n) = -e^{*2}\int\frac{d\boldsymbol{p}}{(2\pi)^3}\sum_{\pm\pm}\frac{p^{\pm}_{\mu}p'^{\pm}_{\nu}+p^{\pm}_{\nu}p'^{\pm}_{\mu}-g_{\mu\nu}[(p^{\pm}p'^{\pm})-m^2]}{E^{\pm}_{p}E^{\pm}_{p'}}\frac{f^+(E^{\pm}_{p})-f^+(E^{\pm}_{p-q})}{E^{\pm}_{p}-E^{\pm}_{p-q}-i\omega_n}. \quad \text{(C.24)}$$

Consider the spatial components of Eq. (C.24)

$$\begin{aligned}\Pi_{ij}(\boldsymbol{q},\omega_n) &= -e^{*2}\int\frac{d\boldsymbol{p}}{(2\pi)^3}\Bigg\{\frac{p_ip'_j+p_jp'_i-\delta_{ij}(m^2-E_pE_{p-q}+\boldsymbol{p}\cdot\boldsymbol{p}')}{E_pE_{p-q}}\\ &\times\left[\frac{f^+(E_p)-f^+(E_{p-q})}{E_p-E_{p-q}-i\omega_n}+\frac{f^+(-E_p)-f^+(-E_{p-q})}{-E_p+E_{p-q}-i\omega_n}\right]\\ &-\frac{p_ip'_j+p_jp'_i-\delta_{ij}(m^2+E_pE_{p-q}+\boldsymbol{p}\cdot\boldsymbol{p}')}{E_pE_{p-q}}\\ &\times\left[\frac{f^+(E_p)-f^+(-E_{p-q})}{E_p+E_{p-q}-i\omega_n}+\frac{f^+(-E_p)-f^+(E_{p-q})}{-E_p-E_{p-q}-i\omega_n}\right]\Bigg\}. \quad \text{(C.25)}\end{aligned}$$

The part of the polarization tensor $\propto\delta_{ij}$ gives

$$\begin{aligned}\Pi^{(1)}_{ij}(\boldsymbol{q},\omega_n) &= -e^{*2}\delta_{ij}\int\frac{d\boldsymbol{p}}{(2\pi)^3}\Bigg\{-\frac{m^2-E_pE_{p-q}+\boldsymbol{p}\cdot\boldsymbol{p}'}{E_pE_{p-q}}\left[\frac{f^+(E_p)-f^+(E_{p-q})}{E_p-E_{p-q}-i\omega_n}\right.\\ &+\left.\frac{f^+(-E_p)-f^+(-E_{p-q})}{-E_p+E_{p-q}-i\omega_n}\right]+\frac{m^2+E_pE_{p-q}+\boldsymbol{p}\cdot\boldsymbol{p}'}{E_pE_{p-q}}\\ &\times\left[\frac{f^+(E_p)-f^+(-E_{p-q})}{E_p+E_{p-q}-i\omega_n}+\frac{f^+(-E_p)-f^+(E_{p-q})}{-E_p-E_{p-q}-i\omega_n}\right]\Bigg\}. \quad \text{(C.26)}\end{aligned}$$

In the spirit of the HTL approximation we next put $\boldsymbol{q}=0$ in the pre-factors multiplying the occupation numbers, use the relation $f^+(-E)=1-f^-(E)$ and drop the vacuum contributions $\propto 1$ to obtain

$$\Pi^{(1)}_{ij}(\boldsymbol{q},\omega_n) = -2e^{*2}\delta_{ij}\int\frac{d\boldsymbol{p}}{(2\pi)^3}\left[\frac{f^+(E_p)+f^-(E_p)}{E_p}\right]. \quad \text{(C.27)}$$

In the remaining part of the polarization tensor we set $(p_ip'_j+p_jp'_i)/(E_pE_{p-q})\simeq 2p_ip_j/E_p^2$ to find

$$\begin{aligned}\Pi^{(2)}_{ij}(\boldsymbol{q},\omega_n) &= -2e^{*2}\int\frac{d\boldsymbol{p}}{(2\pi)^3}\frac{p_ip_j}{E_p^2}\Bigg\{\left[\frac{f^+(E_p)-f^+(E_{p-q})}{E_p-E_{p-q}-i\omega_n}+\frac{f^+(-E_p)-f^+(-E_{p-q})}{-E_p+E_{p-q}-i\omega_n}\right]\\ &-\left[\frac{f^+(E_p)-f^+(-E_{p-q})}{E_p+E_{p-q}-i\omega_n}+\frac{f^+(-E_p)-f^+(E_{p-q})}{-E_p-E_{p-q}-i\omega_n}\right]\Bigg\}. \quad \text{(C.28)}\end{aligned}$$

We further approximate

$$E_{p-q} = E_p-\frac{(\boldsymbol{p}\cdot\boldsymbol{q})}{E_p}, \quad \text{(C.29)}$$

$$f^+(E_p)-f^+(E_{p-q}) = \frac{(\boldsymbol{p}\cdot\boldsymbol{q})}{E_p}\frac{\partial f^+(E_p)}{\partial E_p}, \quad \text{(C.30)}$$

$$f^+(-E_p)-f^+(-E_{p-q}) = -\frac{(\boldsymbol{p}\cdot\boldsymbol{q})}{E_p}\frac{\partial f^-(E_p)}{\partial E_p}, \quad \text{(C.31)}$$

and drop the vacuum terms to obtain

$$\Pi^{(2)}_{ij}(\boldsymbol{q},\omega_n) = -2e^{*2}\int\frac{d\boldsymbol{p}}{(2\pi)^3}\frac{p_ip_j}{E_p^2}\Bigg\{\left[\frac{\partial f^+(E_p)}{\partial E_p}+\frac{\partial f^-(E_p)}{\partial E_p}\right]+ + \frac{i\omega_nE_p}{(\boldsymbol{p}\cdot\boldsymbol{q})-i\omega_nE_p}\left[\frac{\partial f^+(E_p)}{\partial E_p}+\frac{\partial f^-(E_p)}{\partial E_p}\right]-\frac{f^+(E_p)+f^-(E_p)}{E_p}\Bigg\}. \tag{C.32}$$

Now we add Eq. (C.27) to this to obtain

$$\Pi_{ij}(\boldsymbol{q},\omega_n) = -2e^{*2}\int\frac{p^2dp}{2\pi^2}\int\frac{d\Omega}{4\pi}\Bigg\{\delta_{ij}\left[\frac{f^+(E_p)+f^-(E_p)}{E_p}\right]-\frac{p_ip_j}{E_p^2}\left[\frac{f^+(E_p)+f^-(E_p)}{E_p}\right] + \frac{p_ip_j}{E_p^2}\left[\frac{\partial f^+(E_p)}{\partial E_p}+\frac{\partial f^-(E_p)}{\partial E_p}\right]-\frac{p_ip_j}{E_p^2}\frac{i\omega_nE_p}{i\omega_nE_p-(\boldsymbol{p}\cdot\boldsymbol{q})}\left[\frac{\partial f^+(E_p)}{\partial E_p}+\frac{\partial f^-(E_p)}{\partial E_p}\right]\Bigg\}. \tag{C.33}$$

In the first three terms in Eq. (C.33) the angular and radial integrals separate. For the angular part we have

$$\int\frac{d\Omega}{4\pi}\frac{p_ip_j}{p^2}=\frac{\delta_{ij}}{3}. \tag{C.34}$$

By partial integration we find ($\epsilon\equiv E_p$)

$$\int d\epsilon\frac{p^3}{\epsilon}\frac{d}{d\epsilon}[f^+(\epsilon)+f^-(\epsilon)]=-3\int[f^+(\epsilon)+f^-(\epsilon)]\left(1-\frac{p^2}{3\epsilon^2}\right)pd\epsilon, \tag{C.35}$$

which implies that the sum of these terms vanishes. For the remainder we find

$$\Pi_{ij}(\boldsymbol{q},\omega)=\frac{4e^2}{\pi}\int p^2dp\left[\frac{\partial f^+(E_p)}{\partial E_p}+\frac{\partial f^-(E_p)}{\partial E_p}\right]v^2\int\frac{d\Omega}{4\pi}n_in_j\frac{\omega}{\omega+i\delta-v(\boldsymbol{n}\cdot\boldsymbol{q})}, \tag{C.36}$$

where $v=(\partial E_p/\partial p)=p/E_p$, $\boldsymbol{n}=\boldsymbol{p}/p$, and in the last term we have performed the analytical continuation $i\omega_n\to\omega+i\delta$. The spatial part of the polarization tensor can be decomposed as

$$\Pi_{ij}(\boldsymbol{q},\omega)=P^T_{ij}\Pi_T(\boldsymbol{q},\omega)+P^L_{ij}\Pi_L(\boldsymbol{q},\omega). \tag{C.37}$$

Contracting Eq. (C.37) with $\delta_{ij}$ and using Eqs. (C.13) and (C.14) we find

$$2\Pi_T(\boldsymbol{q},\omega)+\frac{\omega^2}{\omega^2-q^2}\Pi_L(\boldsymbol{q},\omega)=\left(-\frac{4e^2}{\pi}\right)\int p^2dp\left[\frac{\partial f^+(E_p)}{\partial E_p}+\frac{\partial f^-(E_p)}{\partial E_p}\right]v^2L_v(\boldsymbol{q},\omega), \tag{C.38}$$

where

$$L_v(\boldsymbol{q},\omega)\equiv\int\frac{d\Omega}{4\pi}\frac{\omega}{\omega+i\delta-v(\boldsymbol{n}\cdot\boldsymbol{q})}=\frac{x}{2v}\log\frac{x+v}{x-v},\qquad x\equiv\omega/q. \tag{C.39}$$

Next contract Eq. (C.37) with $q_iq_j$ to find (note that $q_iq_jP^T_{ij}=0$)

$$\frac{q^2}{\omega^2-q^2}\Pi^L(\boldsymbol{q},\omega)=\left(-\frac{4e^2}{\pi}\right)\int p^2dp\left[\frac{\partial f^+(E_p)}{\partial E_p}+\frac{\partial f^-(E_p)}{\partial E_p}\right][L_v(\boldsymbol{q},\omega)-1]. \tag{C.40}$$

Using Eqs. (C.38)–(C.40) we obtain Eqs. (4.58) and (4.59) of the main text.

# Bibliography


[1] M. Gyulassy and L. McLerran, *New forms of QCD matter discovered at RHIC*, *Nuclear Physics A* **750** (2005) 30–63, [nucl-th/0405013].

[2] R. Baier, P. Romatschke and U. A. Wiedemann, *Dissipative hydrodynamics and heavy-ion collisions*, *Phys. Rev. C* **73** (2006) 064903, [hep-ph/0602249].

[3] L. P. Csernai, J. I. Kapusta and L. D. McLerran, *Strongly Interacting Low-Viscosity Matter Created in Relativistic Nuclear Collisions*, *Phys. Rev. Lett.* **97** (2006) 152303, [nucl-th/0604032].

[4] P. Romatschke and U. Romatschke, *Viscosity Information from Relativistic Nuclear Collisions: How Perfect is the Fluid Observed at RHIC?*, *Physical Review Letters* **99** (2007) 172301, [0706.1522].

[5] H. Song and U. Heinz, *Causal viscous hydrodynamics in 2 + 1 dimensions for relativistic heavy-ion collisions*, *Phys. Rev. C* **77** (2008) 064901, [0712.3715].

[6] M. Luzum and P. Romatschke, *Conformal relativistic viscous hydrodynamics: Applications to RHIC results at $\sqrt{s_{NN}}$=200 GeV*, *Phys. Rev. C* **78** (2008) 034915, [0804.4015].

[7] M. Luzum and P. Romatschke, *Viscous Hydrodynamic Predictions for Nuclear Collisions at the LHC*, *Physical Review Letters* **103** (2009) 262302, [0901.4588].

[8] M. Luzum, *Elliptic flow at energies available at the CERN Large Hadron Collider: Comparing heavy-ion data to viscous hydrodynamic predictions*, *Phys. Rev. C* **83** (2011) 044911, [1011.5173].

[9] H. Song, S. A. Bass, U. Heinz, T. Hirano and C. Shen, *200 A GeV Au+Au Collisions Serve a Nearly Perfect Quark-Gluon Liquid*, *Physical Review Letters* **106** (2011) 192301, [1011.2783].

[10] H. Niemi, G. S. Denicol, P. Huovinen, E. Molnár and D. H. Rischke, *Influence of Shear Viscosity of Quark-Gluon Plasma on Elliptic Flow in Ultrarelativistic Heavy-Ion Collisions*, *Phys. Rev. Lett.* **106** (2011) 212302, [1101.2442].

[11] Z. Qiu, C. Shen and U. Heinz, *Hydrodynamic elliptic and triangular flow in Pb-Pb collisions at $\sqrt{s_{NN}}$ = 2.76 A TeV*, *Physics Letters B* **707** (2012) 151–155, [1110.3033].

[12] U. Heinz, *Towards the Little Bang Standard Model*, *Journal of Physics Conference Series* **455** (2013) 012044, [1304.3634].

[13] D. H. Rischke, S. Bernard and J. A. Maruhn, *Relativistic hydrodynamics for heavy-ion collisions. I. General aspects and expansion into vacuum*, *Nuclear Physics A* **595** (1995) 346–382, [nucl-th/9504018].

[14] D. H. Rischke, *Fluid Dynamics for Relativistic Nuclear Collisions*, in *Hadrons in Dense Matter and Hadrosynthesis*, vol. 516 of *Lecture Notes in Physics, Berlin Springer Verlag*, p. 21, 1999. nucl-th/9809044. DOI.

[15] P. F. Kolb and U. Heinz, *Hydrodynamic Description of Ultrarelativistic Heavy Ion Collisions*, in *Quark-Gluon Plasma*, p. 634, 2004. nucl-th/0305084.

[16] P. Houvinen and P. V. Ruuskanen, *Hydrodynamic Models for Heavy Ion Collisions*, *Annual Review of Nuclear and Particle Science* **56** (2006) 163–206, [nucl-th/0605008].

[17] J. Y. Ollitrault, *Relativistic hydrodynamics for heavy-ion collisions*, *European Journal of Physics* **29** (2008) 275–302, [0708.2433].

[18] T. Hirano, N. van der Kolk and A. Bilandzic, *Hydrodynamics and Flow*, in *Lecture Notes in Physics, Berlin Springer Verlag*, vol. 785 of *Lecture Notes in Physics, Berlin Springer Verlag*, p. 139, 2010. 0808.2684. DOI.

[19] U. Heinz, *Early Collective Expansion: Relativistic Hydrodynamics and the Transport Properties of QCD Matter*, *Landolt Börnstein* **23** (2010) 240, [0901.4355].

[20] D. A. Teaney, *Viscous Hydrodynamics and the Quark Gluon Plasma*, pp. 207–266. World Scientific Publishing Co, 2010. 0905.2433.

[21] P. Romatschke, *New Developments in Relativistic Viscous Hydrodynamics*, *International Journal of Modern Physics E* **19** (2010) 1–53, [0902.3663].

[22] A. K. Chaudhuri, *Viscous Hydrodynamic Model for Relativistic Heavy Ion Collisions*, *Advances in High Energy Physics* **58** (2013) 693180.

[23] U. Heinz and R. Snellings, *Collective Flow and Viscosity in Relativistic Heavy-Ion Collisions*, *Annual Review of Nuclear and Particle Science* **63** (2013) 123–151, [1301.2826].

[24] A. Jaiswal and V. Roy, *Relativistic hydrodynamics in heavy-ion collisions: general aspects and recent developments*, *ArXiv e-prints* (2016) , [1605.08694].

[25] W. Florkowski, M. P. Heller and M. Spaliński, *New theories of relativistic hydrodynamics in the LHC era*, *Reports on Progress in Physics* **81** (2018) 046001, [1707.02282].

[26] H. Song, Y. Zhou and K. Gajdosova, *Collective flow and hydrodynamics in large and small systems at the LHC*, *ArXiv e-prints* (2017) , [1703.00670].

[27] C. Eckart, *The Thermodynamics of Irreversible Processes. III. Relativistic theory of the simple fluid*, *Physical Review* **58** (1940) 919–924.

[28] L. Landau and E. Lifshitz, *Fluid Mechanics*. Butterworth-Heinemann, Oxford, 1987.

[29] W. A. Hiscock and L. Lindblom, *Stability and causality in dissipative relativistic fluids*, *Annals of Physics* **151** (1983) 466–496.

[30] W. A. Hiscock and L. Lindblom, *Generic instabilities in first-order dissipative relativistic fluid theories*, *Phys. Rev. D* **31** (1985) 725–733.

[31] W. A. Hiscock and L. Lindblom, *Linear plane waves in dissipative relativistic fluids*, *Phys. Rev. D* **35** (1987) 3723–3732.

[32] G. S. Denicol, T. Kodama, T. Koide and P. Mota, *Stability and causality in relativistic dissipative hydrodynamics*, *Journal of Physics G Nuclear Physics* **35** (2008) 115102, [0807.3120].

[33] S. Pu, T. Koide and D. H. Rischke, *Does stability of relativistic dissipative fluid dynamics imply causality?*, *Phys. Rev. D* **81** (2010) 114039, [0907.3906].

[34] I. Müller, *Zum Paradoxon der Wärmeleitungstheorie*, *Zeitschrift fur Physik* **198** (1967) 329–344.

[35] W. Israel, *Nonstationary irreversible thermodynamics: A causal relativistic theory*, *Annals of Physics* **100** (1976) 310–331.

[36] W. Israel and J. M. Stewart, *Transient relativistic thermodynamics and kinetic theory*, *Annals of Physics* **118** (1979) 341–372.

[37] A. Muronga, *Relativistic dynamics of non-ideal fluids: Viscous and heat-conducting fluids. II. Transport properties and microscopic description of relativistic nuclear matter*, *Phys. Rev. C* **76** (2007) 014910, [nucl-th/0611091].

[38] T. Tsumura, T. Kunihiro and K. Ohnishi, *Derivation of covariant dissipative fluid dynamics in the renormalization-group method*, *Physics Letters B* **646** (2007) 134–140, [hep-ph/0609056].

[39] R. Baier, P. Romatschke, D. Thanh Son, A. O. Starinets and M. A. Stephanov, *Relativistic viscous hydrodynamics, conformal invariance, and holography*, *Journal of High Energy Physics* **4** (2008) 100, [0712.2451].

[40] M. A. York and G. D. Moore, *Second order hydrodynamic coefficients from kinetic theory*, *Phys. Rev. D* **79** (2009) 054011, [0811.0729].

[41] B. Betz, D. Henkel and D. H. Rischke, *From kinetic theory to dissipative fluid dynamics*, *Progress in Particle and Nuclear Physics* **62** (2009) 556–561, [0812.1440].

[42] G. S. Denicol, T. Koide and D. H. Rischke, *Dissipative Relativistic Fluid Dynamics: A New Way to Derive the Equations of Motion from Kinetic Theory*, *Physical Review Letters* **105** (2010) 162501, [1004.5013].

[43] A. Monnai and T. Hirano, *Relativistic dissipative hydrodynamic equations at the second order for multi-component systems with multiple conserved currents*, *Nuclear Physics A* **847** (2010) 283–314, [1003.3087].

[44] B. Betz, G. S. Denicol, T. Koide, E. Molnár, H. Niemi and D. H. Rischke, *Second order dissipative fluid dynamics from kinetic theory*, in *European Physical Journal Web of Conferences*, vol. 13 of *European Physical Journal Web of Conferences*, p. 07005, 2011. 1012.5772. DOI.

[45] G. S. Denicol, E. Molnár, H. Niemi and D. H. Rischke, *Derivation of fluid dynamics from kinetic theory with the 14-moment approximation*, *European Physical Journal A* **48** (2012) 170, [1206.1554].

[46] G. S. Denicol, H. Niemi, E. Molnár and D. H. Rischke, *Derivation of transient relativistic fluid dynamics from the Boltzmann equation*, *Phys. Rev. D* **85** (2012) 114047, [1202.4551].

[47] A. Jaiswal, R. S. Bhalerao and S. Pal, *New relativistic dissipative fluid dynamics from kinetic theory*, *Physics Letters B* **720** (2013) 347–351, [1204.3779].

[48] A. Jaiswal, R. S. Bhalerao and S. Pal, *Complete relativistic second-order dissipative hydrodynamics from the entropy principle*, *Phys. Rev. C* **87** (2013) 021901, [1302.0666].

[49] A. Jaiswal, *Relativistic dissipative hydrodynamics from kinetic theory with relaxation-time approximation*, *Phys. Rev. C* **87** (2013) 051901, [1302.6311].

[50] A. Jaiswal, R. Ryblewski and M. Strickland, *Transport coefficients for bulk viscous evolution in the relaxation-time approximation*, *Phys. Rev. C* **90** (2014) 044908, [1407.7231].

[51] G. S. Denicol, *Kinetic foundations of relativistic dissipative fluid dynamics*, *Journal of Physics G Nuclear Physics* **41** (2014) 124004.

[52] R. S. Bhalerao, A. Jaiswal, S. Pal and V. Sreekanth, *Relativistic viscous hydrodynamics for heavy-ion collisions: A comparison between the Chapman-Enskog and Grad methods*, *Phys. Rev. C* **89** (2014) 054903, [1312.1864].

[53] A. Jaiswal, B. Friman and K. Redlich, *Relativistic second-order dissipative hydrodynamics at finite chemical potential*, *Physics Letters B* **751** (2015) 548–552, [1507.02849].

[54] W. Florkowski, A. Jaiswal, E. Maksymiuk, R. Ryblewski and M. Strickland, *Relativistic quantum transport coefficients for second-order viscous hydrodynamics*, *Phys. Rev. C* **91** (2015) 054907, [1503.03226].

[55] K. Tsumura, Y. Kikuchi and T. Kunihiro, *Relativistic causal hydrodynamics derived from Boltzmann equation: A novel reduction theoretical approach*, *Phys. Rev. D* **92** (2015) 085048, [1506.00846].

[56] L. Tinti, A. Jaiswal and R. Ryblewski, *Quasiparticle second-order viscous hydrodynamics from kinetic theory*, *Phys. Rev. D* **95** (2017) 054007, [1612.07329].

[57] H. Mori, *A Quantum-statistical Theory of Transport Processes*, *Journal of the Physical Society of Japan* **11** (1956) 1029–1044.

[58] R. Kubo, *Statistical-Mechanical Theory of Irreversible Processes. I*, *Journal of the Physical Society of Japan* **12** (1957) 570–586.

[59] R. Kubo, M. Yokota and S. Nakajima, *Statistical-Mechanical Theory of Irreversible Processes. II. Response to Thermal Disturbance*, *Journal of the Physical Society of Japan* **12** (1957) 1203–1211.

[60] H. Mori, *Statistical-Mechanical Theory of Transport in Fluids*, *Physical Review* **112** (1958) 1829–1842.

[61] H. Mori, *Correlation Function Method for Transport Phenomena*, *Physical Review* **115** (1959) 298–300.

[62] B. Robertson, *Equations of Motion in Nonequilibrium Statistical Mechanics*, *Physical Review* **144** (1966) 151–161.

[63] B. Robertson, *Equations of Motion in Nonequilibrium Statistical Mechanics. II. Energy Transport*, *Physical Review* **160** (1967) 175–183.

[64] D. N. Zubarev and S. V. Tishchenko, *Nonlocal hydrodynamics with memory*, *Physica* **59** (1972) 285–304.

[65] D. Zubarev, *Nonequilibrium Statistical Thermodynamics*. Studies in Soviet science. Consultants Bureau, 1974.

[66] D. Zubarev, V. Morozov and G. Röpke, *Statistical Mechanics of Nonequilibrium Processes*. John Wiley & Sons, 1997.

[67] D. N. Zubarev, A. V. Prozorkevich and S. A. Smolyanskii, *Derivation of nonlinear generalized equations of quantum relativistic hydrodynamics*, *Theoretical and Mathematical Physics* **40** (1979) 821–831.

[68] A. Hosoya, M.-a. Sakagami and M. Takao, *Nonequilibrium thermodynamics in field theory: Transport coefficients*, *Annals of Physics* **154** (1984) 229–252.

[69] R. Horsley and W. Schoenmaker, *Quantum field theories out of thermal equilibrium. (I). General considerations*, *Nuclear Physics B* **280** (1987) 716–734.

[70] X.-G. Huang, A. Sedrakian and D. H. Rischke, *Kubo formulas for relativistic fluids in strong magnetic fields*, *Annals of Physics* **326** (2011) 3075–3094, [1108.0602].

[71] E. Lifshitz and L. Pitaevski, *Physical Kinetics*. Butterworth-Heinemann, Oxford, 1981.

[72] L. P. Kadanoff and P. C. Martin, *Hydrodynamic Equations and Correlation Functions*, *Annals of Physics* **281** (2000) 800–852.

[73] C. Palenzuela, L. Lehner, O. Reula and L. Rezzolla, *Beyond ideal MHD: towards a more realistic modelling of relativistic astrophysical plasmas*, *MNRAS* **394** (2009) 1727–1740, [0810.1838].

[74] K. Dionysopoulou, D. Alic, C. Palenzuela, L. Rezzolla and B. Giacomazzo, *General-relativistic resistive magnetohydrodynamics in three dimensions: Formulation and tests*, *Phys. Rev. D* **88** (2013) 044020, [1208.3487].

[75] C. Palenzuela, L. Lehner, S. L. Liebling, M. Ponce, M. Anderson, D. Neilsen et al., *Linking electromagnetic and gravitational radiation in coalescing binary neutron stars*, *Phys. Rev. D* **88** (2013) 043011, [1307.7372].

[76] K. Dionysopoulou, D. Alic and L. Rezzolla, *General-relativistic resistive-magnetohydrodynamic simulations of binary neutron stars*, *Phys. Rev. D* **92** (2015) 084064, [1502.02021].

[77] L. Rezzolla and O. Zanotti, *Relativistic Hydrodynamics*. Oxford University Press, 2013.

[78] S. Weinberg, *Gravitation and Cosmology: Principles and Applications of the General Theory of Relativity*. 1972.

[79] A. Harutyunyan, A. Sedrakian and et al., *Second-order relativistic hydrodynamics from a non-equilibrium statistical operator*, in preparation.

[80] P. Danielewicz and M. Gyulassy, *Dissipative phenomena in quark-gluon plasmas*, *Phys. Rev. D* **31** (1985) 53–62.

[81] P. K. Kovtun, D. T. Son and A. O. Starinets, *Viscosity in Strongly Interacting Quantum Field Theories from Black Hole Physics*, *Physical Review Letters* **94** (2005) 111601, [hep-th/0405231].

[82] A. Harutyunyan, D. H. Rischke and A. Sedrakian, *Transport coefficients of two-flavor quark matter from the Kubo formalism*, *Phys. Rev. D* **95** (2017) 114021, [1702.04291].

[83] A. Harutyunyan and A. Sedrakian, *Bulk viscosity of two-flavor quark matter from the Kubo formalism*, *Phys. Rev. D* **96** (2017) 034006, [1705.09825].

[84] Y. Nambu and G. Jona-Lasinio, *Dynamical Model of Elementary Particles Based on an Analogy with Superconductivity. I*, *Phys. Rev.* **122** (1961) 345–358.

[85] Y. Nambu and G. Jona-Lasinio, *Dynamical Model of Elementary Particles Based on an Analogy with Superconductivity. II*, *Phys. Rev.* **124** (1961) 246–254.

[86] U. Vogl and W. Weise, *The Nambu and Jona-Lasinio model: Its implications for Hadrons and Nuclei*, *Progress in Particle and Nuclear Physics* **27** (1991) 195–272.

[87] S. P. Klevansky, *The Nambu–Jona-Lasinio model of quantum chromodynamics*, *Reviews of Modern Physics* **64** (1992) 649–708.

[88] T. Hatsuda and T. Kunihiro, *QCD phenomenology based on a chiral effective Lagrangian*, *Phys. Rep.* **247** (1994) 221–367, [hep-ph/9401310].

[89] M. Buballa, *NJL-model analysis of dense quark matter*, *Phys. Rep.* **407** (2005) 205–376, [hep-ph/0402234].

[90] E. Quack and S. P. Klevansky, *Effective $1/N_c$ expansion in the Nambu–Jona-Lasinio model*, *Phys. Rev. C* **49** (1994) 3283–3288.

[91] R. Lang, N. Kaiser and W. Weise, *Shear viscosities from Kubo formalism in a large-$N_c$ Nambu–Jona-Lasinio model*, *European Physical Journal A* **51** (2015) 127, [1506.02459].

[92] P. Arnold, G. D. Moore and L. G. Yaffe, *Transport coefficients in high temperature gauge theories (I): leading-log results*, *Journal of High Energy Physics* **11** (2000) 001, [hep-ph/0010177].

[93] P. Arnold, G. D. Moore and L. G. Yaffe, *Transport coefficients in high temperature gauge theories, 2. Beyond leading log*, *Journal of High Energy Physics* **5** (2003) 051, [hep-ph/0302165].

[94] Z. Xu and C. Greiner, *Shear Viscosity in a Gluon Gas*, *Phys. Rev. Lett.* **100** (2008) 172301, [0710.5719].

[95] N. Christiansen, M. Haas, J. M. Pawlowski and N. Strodthoff, *Transport Coefficients in Yang-Mills Theory and QCD*, *Phys. Rev. Lett.* **115** (2015) 112002, [1411.7986].

[96] P. Goldreich and A. Reisenegger, *Magnetic field decay in isolated neutron stars*, *ApJ* **395** (1992) 250–258.

[97] D. Bhattacharya, *The Evolution of the Magnetic Fields of Neutron Stars*, *Journal of Astrophysics and Astronomy* **16** (1995) 217.

[98] A. Muslimov and D. Page, *Magnetic and Spin History of Very Young Pulsars*, *ApJ* **458** (1996) 347, [astro-ph/9505116].

[99] V. Urpin, D. Konenkov and V. Urpin, *Magnetic and spin evolution of isolated neutron stars with the crustal magnetic field*, *MNRAS* **292** (1997) 167, [astro-ph/9801077].

[100] S. Konar and D. Bhattacharya, *Magnetic field evolution of accreting neutron stars*, *MNRAS* **284** (1997) 311–317.

[101] M. E. Gusakov, E. M. Kantor and D. D. Ofengeim, *Evolution of the magnetic field in neutron stars*, *Phys. Rev. D* **96** (2017) 103012, [1705.00508].

[102] I. Easson and C. J. Pethick, *Magnetohydrodynamics of neutron star interiors*, *ApJ* **227** (1979) 995–1012.

[103] D. M. Sedrakyan and A. K. Avetisyan, *Magnetohydrodynamics of Plasma in the Crust of a Neutron Star*, *Astrophysics* **26** (1987) 295–302.

[104] D. M. Sedrakian, A. S. Harutyunyan and M. V. Hayrapetyan, *Magnetosonic waves in the crust of a neutron star*, *Astrophysics* **56** (2013) 229–245.

[105] D. M. Sedrakian, A. S. Harutunyan and M. V. Hayrapetyan, *Absorption of Magnetosonic Waves in the Crust of Neutron Stars. Radio Emission from Pulsars*, *Astrophysics* **57** (2014) 530–549.

[106] L. Mestel and F. Hoyle, *On the thermal conductivity in dense stars*, *Proceedings of the Cambridge Philosophical Society* **46** (1950) 331.

[107] T. D. Lee, *Hydrogen Content and Energy-Productive Mechanism of White Dwarfs*, *ApJ* **111** (1950) 625.

[108] A. Abrikosov, *The conductivity of strongly compressed matter*, *Soviet Physics JETP* **18** (1964) 1399.

[109] W. B. Hubbard, *Studies in Stellar Evolution. V. Transport Coefficients of Degenerate Stellar Matter*, *ApJ* **146** (1966) 858.

[110] L. Mestel and M. A. Ruderman, *The energy content of a white dwarf and its rate of cooling*, *MNRAS* **136** (1967) 27.

[111] M. Lampe, *Transport Coefficients of Degenerate Plasma*, *Physical Review* **170** (1968) 306–319.

[112] I. Iben, Jr., *Electron Conduction in Red Giants*, *ApJ* **154** (1968) 557.

[113] M. Lampe, *Transport Theory of a Partially Degenerate Plasma*, *Physical Review* **174** (1968) 276–280.

[114] W. B. Hubbard and M. Lampe, *Thermal Conduction by Electrons in Stellar Matter*, *ApJS* **18** (1969) 297.

[115] A. B. Solinger, *Electrical and Thermal Conductivity in a Superdense Lattice. I. High-Temperature Conductivity*, *ApJ* **161** (1970) 553.

[116] V. Canuto, *Electrical Conductivity and Conductive Opacity of a Relativistic Electron Gas*, *ApJ* **159** (1970) 641.

[117] A. Kovetz and G. Shaviv, *The Electrical and Thermal Conductivities of Stellar Degenerate Matter*, *A&A* **28** (1973) 315.

[118] E. Flowers and N. Itoh, *Transport properties of dense matter*, *ApJ* **206** (1976) 218–242.

[119] D. G. Yakovlev and V. A. Urpin, *Thermal and Electrical Conductivity in White Dwarfs and Neutron Stars*, *Soviet Ast.* **24** (1980) 303.

[120] N. Itoh, S. Mitake, H. Iyetomi and S. Ichimaru, *Electrical and thermal conductivities of dense matter in the liquid metal phase. I - High-temperature results*, *ApJ* **273** (1983) 774–782.

[121] R. Nandkumar and C. J. Pethick, *Transport coefficients of dense matter in the liquid metal regime*, *MNRAS* **209** (1984) 511–524.

[122] N. Itoh, Y. Kohyama, N. Matsumoto and M. Seki, *Electrical and thermal conductivities of dense matter in the crystalline lattice phase*, *ApJ* **285** (1984) 758–765.

[123] S. Mitake, S. Ichimaru and N. Itoh, *Electrical and thermal conductivities of dense matter in the liquid metal phase. II - Low-temperature quantum corrections*, *ApJ* **277** (1984) 375–378.

[124] N. Itoh and Y. Kohyama, *Electrical and thermal conductivities of dense matter in the crystalline lattice phase. II - Impurity scattering*, *ApJ* **404** (1993) 268–270.

[125] N. Itoh, H. Hayashi and Y. Kohyama, *Electrical and Thermal Conductivities of Dense Matter in the Crystalline Lattice Phase. III. Inclusion of Lower Densities*, *ApJ* **418** (1993) 405.

[126] D. A. Baiko, A. D. Kaminker, A. Y. Potekhin and D. G. Yakovlev, *Ion Structure Factors and Electron Transport in Dense Coulomb Plasmas*, *Physical Review Letters* **81** (1998) 5556–5559, [physics/9811052].

[127] A. Y. Potekhin, D. A. Baiko, P. Haensel and D. G. Yakovlev, *Transport properties of degenerate electrons in neutron star envelopes and white dwarf cores*, *A&A* **346** (1999) 345–353, [astro-ph/9903127].

[128] A. Y. Potekhin, *Electron conduction in magnetized neutron star envelopes*, *A&A* **351** (1999) 787–797, [astro-ph/9909100].

[129] N. Itoh, S. Uchida, Y. Sakamoto, Y. Kohyama and S. Nozawa, *The Second Born Corrections to the Electrical and Thermal Conductivities of Dense Matter in the Liquid Metal Phase*, *ApJ* **677** (2008) 495–502, [0708.2967].

[130] C. J. Horowitz, D. K. Berry, C. M. Briggs, M. E. Caplan, A. Cumming and A. S. Schneider, *Disordered Nuclear Pasta, Magnetic Field Decay, and Crust Cooling in Neutron Stars*, *Physical Review Letters* **114** (2015) 031102, [1410.2197].

[131] A. Harutyunyan and A. Sedrakian, *Electrical conductivity of a warm neutron star crust in magnetic fields*, *Phys. Rev. C* **94** (2016) 025805, [1605.07612].

[132] A. Harutyunyan and A. Sedrakian, *Electrical conductivity tensor of dense plasma in magnetic fields*, *Proceedings of Science* (2016) (MPCS2015)011, [1607.04541].

[133] S. Galam and J.-P. Hansen, *Statistical mechanics of dense ionized matter. VI. Electron screening corrections to the thermodynamic properties of the one-component plasma*, *Phys. Rev. A* **14** (1976) 816–832.

[134] D. H. Rischke, *The quark-gluon plasma in equilibrium*, *Progress in Particle and Nuclear Physics* **52** (2004) 197–296, [nucl-th/0305030].

[135] A. Sedrakian, *The physics of dense hadronic matter and compact stars*, *Progress in Particle and Nuclear Physics* **58** (2007) 168–246, [nucl-th/0601086].

[136] M. G. Alford, A. Schmitt, K. Rajagopal and T. Schäfer, *Color superconductivity in dense quark matter*, *Reviews of Modern Physics* **80** (2008) 1455–1515, [0709.4635].

[137] T. Muta, *Foundations Of Quantum Chromodynamics: An Introduction to Perturbative Methods in Gauge Theories*. World Scientific Books, 2009.

[138] M. Gell-Mann, *A schematic model of baryons and mesons*, *Physics Letters* **8** (1964) 214–215.

[139] D. J. Gross and F. Wilczek, *Ultraviolet Behavior of Non-Abelian Gauge Theories*, *Physical Review Letters* **30** (1973) 1343–1346.

[140] H. D. Politzer, *Reliable Perturbative Results for Strong Interactions?*, *Physical Review Letters* **30** (1973) 1346–1349.

[141] https://www.liverpool.ac.uk/physics/research/nuclear-physics/research/thermodynamics/.

[142] J. B. Natowitz, K. Hagel, Y. Ma, M. Murray, L. Qin, R. Wada et al., *Limiting Temperatures and the Equation of State of Nuclear Matter*, *Physical Review Letters* **89** (2002) 212701, [nucl-ex/0204015].

[143] J. C. Collins and M. J. Perry, *Superdense matter: Neutrons or asymptotically free quarks?*, *Physical Review Letters* **34** (1975) 1353–1356.

[144] N. Cabibbo and G. Parisi, *Exponential hadronic spectrum and quark liberation*, *Physics Letters B* **59** (1975) 67–69.

[145] M. Alford, *Color-Superconducting Quark Matter*, *Annual Review of Nuclear and Particle Science* **51** (2001) 131–160, [hep-ph/0102047].

[146] K. Rajagopal and F. Wilczek, *The Condensed Matter Physics of QCD*, pp. 2061–2151. World Scientific Publishing Co, 2001. hep-ph/0011333.

[147] O. Scavenius, Á. Mócsy, I. N. Mishustin and D. H. Rischke, *Chiral phase transition within effective models with constituent quarks*, *Phys. Rev. C* **64** (2001) 045202, [nucl-th/0007030].

[148] Z. Fodor and S. D. Katz, *A new method to study lattice QCD at finite temperature and chemical potential*, *Physics Letters B* **534** (2002) 87–92, [hep-lat/0104001].

[149] Y. Aoki, G. Endrődi, Z. Fodor, S. D. Katz and K. K. Szabó, *The order of the quantum chromodynamics transition predicted by the standard model of particle physics*, *Nature* **443** (2006) 675–678, [hep-lat/0611014].

[150] Y. Aoki, S. Borsányi, S. Dürr, Z. Fodor, S. D. Katz, S. Krieg et al., *The QCD transition temperature: results with physical masses in the continuum limit II*, *Journal of High Energy Physics* **6** (2009) 088, [0903.4155].

[151] Y. Aoki, S. Borsanyi, S. Durr, Z. Fodor, S. D. Katz, S. Krieg et al., *QCD transition temperature: approaching the continuum on the lattice*, *Nuclear Physics A* **830** (2009) 805–808.

[152] Z. Fodor, *QCD thermodynamics on the lattice: Approaching the continuum limit with physical quark masses*, in *Journal of Physics Conference Series*, vol. 230 of *Journal of Physics Conference Series*, 2010. DOI.

[153] S. Borsányi, G. Endrődi, Z. Fodor, A. Jakovác, S. D. Katz, S. Krieg et al., *The QCD equation of state with dynamical quarks*, *Journal of High Energy Physics* **11** (2010) 77, [1007.2580].

[154] M. Stephanov, K. Rajagopal and E. Shuryak, *Event-by-event fluctuations in heavy ion collisions and the QCD critical point*, *Phys. Rev. D* **60** (1999) 114028, [hep-ph/9903292].

[155] Z. Fodor and S. D. Katz, *Critical point of QCD at finite $T$ and $\mu$, lattice results for physical quark masses*, *Journal of High Energy Physics* **4** (2004) 050, [hep-lat/0402006].

[156] J. Gasser and H. Leutwyler, *Quark masses*, *Phys. Rep.* **87** (1982) 77–169.

[157] S. Weinberg, *Nuclear forces from chiral lagrangians*, *Physics Letters B* **251** (1990) 288–292.

[158] S. Weinberg, *Effective chiral lagrangians for nucleon-pion interactions and nuclear forces*, *Nuclear Physics B* **363** (1991) 3–18.

[159] G. Ecker, *Chiral perturbation theory*, *Progress in Particle and Nuclear Physics* **35** (1995) 1–80, [hep-ph/9501357].

[160] V. Bernard, N. Kaiser and U.-G. Meißner, *Chiral Dynamics in Nucleons and Nuclei*, *International Journal of Modern Physics E* **4** (1995) 193–344, [hep-ph/9501384].

[161] F. Karsch, *Lattice QCD at Finite Temperature*, in *New States of Matter in Hadronic Interactions*, vol. 631 of *American Institute of Physics Conference Series*, pp. 112–141, 2002. DOI.

[162] E. Laermann and O. Philipsen, *Lattice QCD at Finite Temperature*, *Annual Review of Nuclear and Particle Science* **53** (2003) 163–198, [hep-ph/0303042].

[163] O. Philipsen, *Status of the QCD phase diagram from the Lattice*, in *APS Division of Nuclear Physics Meeting Abstracts*, 2012. 1111.5370.

[164] O. Philipsen, *Towards a theoretical description of dense QCD*, in *European Physical Journal Web of Conferences*, vol. 137 of *European Physical Journal Web of Conferences*, p. 03016, 2017. 1612.03400. DOI.

[165] A. Chodos, R. L. Jaffe, K. Johnson, C. B. Thorn and V. F. Weisskopf, *New extended model of hadrons*, *Phys. Rev. D* **9** (1974) 3471–3495.

[166] A. Chodos, R. L. Jaffe, K. Johnson and C. B. Thorn, *Baryon structure in the bag theory*, *Phys. Rev. D* **10** (1974) 2599–2604.

[167] T. Degrand, R. L. Jaffe, K. Johnson and J. Kiskis, *Masses and other parameters of the light hadrons*, *Phys. Rev. D* **12** (1975) 2060–2076.

[168] J. Maldacena, *The Large-N Limit of Superconformal Field Theories and Supergravity*, *International Journal of Theoretical Physics* **38** (1999) 1113–1133, [hep-th/9711200].

[169] O. Aharony, S. S. Gubser, J. Maldacena, H. Ooguri and Y. Oz, *Large N field theories, string theory and gravity*, *Phys. Rep.* **323** (2000) 183–386, [hep-th/9905111].

[170] J. Casalderrey-Solana, H. Liu, D. Mateos, K. Rajagopal and U. A. Wiedemann, *Gauge/String Duality, Hot QCD and Heavy Ion Collisions*, *ArXiv e-prints* (2011) , [1101.0618].

[171] O. DeWolfe, S. S. Gubser, C. Rosen and D. Teaney, *Heavy ions and string theory*, *Progress in Particle and Nuclear Physics* **75** (2014) 86–132, [1304.7794].

[172] B. Friman, C. Höhne, J. Knoll, S. Leupold, J. Randrup, R. Rapp et al., *The CBM Physics Book: Compressed Baryonic Matter in Laboratory Experiments*. Lecture Notes in Physics. Springer Berlin Heidelberg, 2011.

[173] D. Blaschke, J. Aichelin, E. Bratkovskaya, V. Friese, M. Gazdzicki, J. Randrup et al., *Topical issue on exploring strongly interacting matter at high densities - nica white paper*, *Eur. Phys. J. A* **52** (2016) 267.

[174] G. Policastro, D. T. Son and A. O. Starinets, *Shear Viscosity of Strongly Coupled $N = 4$ Supersymmetric Yang-Mills Plasma*, *Physical Review Letters* **87** (2001) 081601, [hep-th/0104066].

[175] M. Gyulassy, *The QGP Discovered at RHIC*, *ArXiv Nuclear Theory e-prints* (2004) , [nucl-th/0403032].

[176] T. K. Nayak, *Heavy ions: Results from the Large Hadron Collider*, *Pramana* **79** (2012) 719–735, [1201.4264].

[177] N. N. Bogolyubov, *Problems of dynamic theory in statistical physics*. 1960.

[178] V. G. Morozov and G. Röpke, *Zubarev's method of a nonequilibrium statistical operator and some challenges in the theory of irreversible processes*, *Condensed Matter Physics* **1** (1998) 673–686.

[179] C. Cattaneo, *Sulla conduzione del calore*, *Atti. Semin. Mat. Fis. Univ. Modena* **3** (1948) 83.

[180] A. A. Abrikosov, L. P. Gorkov, I. E. Dzyaloshinski, R. A. Silverman and G. H. Weiss, *Methods of Quantum Field Theory in Statistical Physics*, *Physics Today* **17** (1964) 78.

[181] A. L. Fetter and J. D. Walecka, *Quantum theory of many-particle systems*. 1971.

[182] G. Mahan, *Many-particle physics*. Plenum Press, New York, 1990.

[183] J. I. Kapusta and C. Gale, *Finite-Temperature Field Theory: Principles and Applications*. Cambridge University Press, 2006.

[184] https://commons.wikimedia.org/wiki/File:Neutron_star_structure.JPG.

[185] N. Chamel and P. Haensel, *Physics of Neutron Star Crusts*, *Living Reviews in Relativity* **11** (2008) 10, [0812.3955].

[186] A. Y. Potekhin, G. Chabrier and D. G. Yakovlev, *Internal temperatures and cooling of neutron stars with accreted envelopes.*, *A&A* **323** (1997) 415–428, [astro-ph/9706148].

[187] D. Page, *Fast Cooling of Neutron Stars: Superfluidity versus Heating and Accreted Envelope*, *ApJ* **479** (1997) L43–L46, [astro-ph/9610191].

[188] D. Page, *Thermal Evolution of Isolated Neutron Stars*, in *NATO Advanced Science Institutes (ASI) Series C*, vol. 515 of *NATO Advanced Science Institutes (ASI) Series C*, p. 539, 1998. astro-ph/9706259.

[189] C. Cutler and L. Lindblom, *The effect of viscosity on neutron star oscillations*, *ApJ* **314** (1987) 234–241.

[190] N. Andersson, D. I. Jones, K. D. Kokkotas and N. Stergioulas, *R-Mode Runaway and Rapidly Rotating Neutron Stars*, *ApJ* **534** (2000) L75–L78, [astro-ph/0002114].

[191] H. Grad, *On the kinetic theory of rarefied gases*, *Comm. Pure Appl. Math.* **2** (1949) 331.

[192] S. Chapman, T. G. Cowling and D. Park, *The Mathematical Theory of Non-Uniform Gases*, *American Journal of Physics* **30** (1962) 389–389.

[193] S. Chapman and T. G. Cowling, *The Mathematical Theory of Non-uniform Gases*. 1991.

[194] S. Bhattacharyya, S. Minwalla, V. E. Hubeny and M. Rangamani, *Nonlinear fluid dynamics from gravity*, *Journal of High Energy Physics* **2** (2008) 045, [0712.2456].

[195] M. Rangamani, *Gravity and hydrodynamics: lectures on the fluid-gravity correspondence*, *Classical and Quantum Gravity* **26** (2009) 224003, [0905.4352].

[196] S. I. Finazzo, R. Rougemont, H. Marrochio and J. Noronha, *Hydrodynamic transport coefficients for the non-conformal quark-gluon plasma from holography*, *Journal of High Energy Physics* **2** (2015) 51, [1412.2968].

[197] P. Romatschke, *Relativistic viscous fluid dynamics and non-equilibrium entropy*, *Classical and Quantum Gravity* **27** (2010) 025006, [0906.4787].

[198] G. D. Moore and K. A. Sohrabi, *Thermodynamical second-order hydrodynamic coefficients*, *Journal of High Energy Physics* **11** (2012) 148, [1210.3340].

[199] A. Czajka and S. Jeon, *Kubo formulas for the shear and bulk viscosity relaxation times and the scalar field theory shear $\tau_\pi$ calculation*, *Phys. Rev. C* **95** (2017) 064906, [1701.07580].

[200] T. Koide, G. S. Denicol, P. Mota and T. Kodama, *Relativistic dissipative hydrodynamics: A minimal causal theory*, *Phys. Rev. C* **75** (2007) 034909, [hep-ph/0609117].

[201] T. Koide and T. Kodama, *Transport coefficients of non-Newtonian fluid and causal dissipative hydrodynamics*, *Phys. Rev. E* **78** (2008) 051107, [0806.3725].

[202] T. Hayata, Y. Hidaka, T. Noumi and M. Hongo, *Relativistic hydrodynamics from quantum field theory on the basis of the generalized Gibbs ensemble method*, *Phys. Rev. D* **92** (2015) 065008, [1503.04535].

[203] S. Weinberg, *Entropy Generation and the Survival of Protogalaxies in an Expanding Universe*, *ApJ* **168** (1971) 175.

[204] W. Israel and J. M. Stewart, *Thermodynamics of nonstationary and transient effects in a relativistic gas*, *Physics Letters A* **58** (1976) 213–215.

[205] L. Landau and E. Lifshitz, *Statistical Physics*. Pergamon Press, Oxford, 1980.

[206] D. N. Zubarev and V. P. Kalashnikov, *Derivation of the nonequilibrium statistical operator from the extremum of the information entropy*, *Physica* **46** (1970) 550–554.

[207] Z. Onyszkiewicz, *Derivation of the generalized nonequilibrium statistical operator from the extremum of the Von Neumann Entropy*, *Physica A Statistical Mechanics and its Applications* **143** (1987) 287–295.

[208] S. R. de Groot, P. Mazur and S. Choi, *Non-Equilibrium Thermodynamics*, *Physics Today* **16** (1963) 70.

[209] S. R. de Groot, P. Mazur and A. L. King, *Non-equilibrium Thermodynamics*, *American Journal of Physics* **31** (1963) 558–559.

[210] P. Arnold, Ç. Doğan and G. D. Moore, *Bulk viscosity of high-temperature QCD*, *Phys. Rev. D* **74** (2006) 085021, [hep-ph/0608012].

[211] K. Dusling and T. Schäfer, *Bulk viscosity, particle spectra, and flow in heavy-ion collisions*, *Phys. Rev. C* **85** (2012) 044909, [1109.5181].

[212] M. Buzzegoli, E. Grossi and F. Becattini, *General equilibrium second-order hydrodynamic coefficients for free quantum fields*, *Journal of High Energy Physics* **10** (2017) 91, [1704.02808].

[213] I. A. Shovkovy and P. J. Ellis, *Thermal conductivity of dense quark matter and cooling of stars*, *Phys. Rev. C* **66** (2002) 015802, [hep-ph/0204132].

[214] C. Manuel, A. Dobado and F. J. Llanes-Estrada, *Shear viscosity in a CFL quark star*, *Journal of High Energy Physics* **9** (2005) 076, [hep-ph/0406058].

[215] M. G. Alford, H. Nishimura and A. Sedrakian, *Transport coefficients of two-flavor superconducting quark matter*, *Phys. Rev. C* **90** (2014) 055205, [1408.4999].

[216] S. Sarkar and R. Sharma, *Shear viscosity of two-flavor inhomogenous color superconducting quark matter*, *Phys. Rev. D* **96** (2017) 094025, [1701.00010].

[217] H. Heiselberg, *Viscosities of quark-gluon plasmas*, *Phys. Rev. D* **49** (1994) 4739–4750, [hep-ph/9401309].

[218] Y. Hidaka and R. D. Pisarski, *Suppression of the shear viscosity in a "semi"-quark-gluon plasma*, *Phys. Rev. D* **78** (2008) 071501, [0803.0453].

[219] J.-W. Chen, Y.-F. Liu, S. Pu, Y.-K. Song and Q. Wang, *Negative off-diagonal conductivities in a weakly coupled quark-gluon plasma at the leading-log order*, *Phys. Rev. D* **88** (2013) 085039, [1308.2945].

[220] M. Greif, I. Bouras, C. Greiner and Z. Xu, *Electric conductivity of the quark-gluon plasma investigated using a perturbative QCD based parton cascade*, *Phys. Rev. D* **90** (2014) 094014, [1408.7049].

[221] K. Hattori, S. Li, D. Satow and H.-U. Yee, *Longitudinal conductivity in strong magnetic field in perturbative QCD: Complete leading order*, *Phys. Rev. D* **95** (2017) 076008, [1610.06839].

[222] K. Hattori and D. Satow, *Electrical conductivity of quark-gluon plasma in strong magnetic fields*, *Phys. Rev. D* **94** (2016) 114032, [1610.06818].

[223] H. Defu, *Shear viscosity of hot QCD from transport theory and thermal field theory in real time formalism*, *ArXiv High Energy Physics - Phenomenology e-prints* (2005) , [hep-ph/0501284].

[224] M. Iwasaki, H. Ohnishi and T. Fukutome, *Shear viscosity of the quark matter*, *Journal of Physics G Nuclear Physics* **35** (2008) 035003, [hep-ph/0703271].

[225] W. M. Alberico, S. Chiacchiera, H. Hansen, A. Molinari and M. Nardi, *Shear viscosity and entropy of quark matter*, *European Physical Journal A* **38** (2008) 97–103, [0707.4442].

[226] S.-x. Qin and D. H. Rischke, *Charmonium spectral functions and transport properties of quark-gluon plasma*, *Physics Letters B* **734** (2014) 157–161, [1403.3025].

[227] R. Lang and W. Weise, *Shear viscosity from Kubo formalism: NJL model study*, *European Physical Journal A* **50** (2014) 63, [1311.4628].

[228] R. Lang, *Shear Viscosities from Kubo Formalism in Large-$N_c$ Nambu–Jona-Lasinio Model*. Doctoral Dissertation. Technische Universität München, 2015.

[229] S. Ghosh, T. C. Peixoto, V. Roy, F. E. Serna and G. Krein, *Shear and bulk viscosities of quark matter from quark-meson fluctuations in the Nambu–Jona-Lasinio model*, *Phys. Rev. C* **93** (2016) 045205, [1507.08798].

[230] S. Plumari, A. Puglisi, F. Scardina and V. Greco, *Shear viscosity of a strongly interacting system: Green-Kubo correlator versus Chapman-Enskog and relaxation-time approximations*, *Phys. Rev. C* **86** (2012) 054902, [1208.0481].

[231] R. Marty, E. Bratkovskaya, W. Cassing, J. Aichelin and H. Berrehrah, *Transport coefficients from the Nambu–Jona-Lasinio model for $SU(3)_f$*, *Phys. Rev. C* **88** (2013) 045204, [1311.3159].

[232] A. Puglisi, S. Plumari and V. Greco, *Electric conductivity from the solution of the relativistic Boltzmann equation*, *Phys. Rev. D* **90** (2014) 114009, [1408.7043].

[233] A. S. Khvorostukhin, V. D. Toneev and D. N. Voskresensky, *Viscosity coefficients for hadron and quark-gluon phases*, *Nuclear Physics A* **845** (2010) 106–146, [1003.3531].

[234] K. Heckmann, M. Buballa and J. Wambach, *Chiral restoration effects on the shear viscosity of a pion gas*, *European Physical Journal A* **48** (2012) 142, [1202.0724].

[235] S. Ghosh, A. Lahiri, S. Majumder, R. Ray and S. K. Ghosh, *Shear viscosity due to Landau damping from the quark-pion interaction*, *Phys. Rev. C* **88** (2013) 068201, [1311.4070].

[236] H. B. Meyer, *Calculation of the shear viscosity in SU(3) gluodynamics*, *Phys. Rev. D* **76** (2007) 101701, [0704.1801].

[237] G. Aarts, C. Allton, J. Foley, S. Hands and S. Kim, *Spectral Functions at Small Energies and the Electrical Conductivity in Hot Quenched Lattice QCD*, *Physical Review Letters* **99** (2007) 022002, [hep-lat/0703008].

[238] H. B. Meyer, *Transport properties of the quark-gluon plasma from lattice QCD*, *Nuclear Physics A* **830** (2009) 641–648, [0907.4095].

[239] A. Amato, G. Aarts, C. Allton, P. Giudice, S. Hands and J.-I. Skullerud, *Electrical Conductivity of the Quark-Gluon Plasma Across the Deconfinement Transition*, *Physical Review Letters* **111** (2013) 172001, [1307.6763].

[240] G. Aarts, C. Allton, A. Amato, P. Giudice, S. Hands and J.-I. Skullerud, *Electrical conductivity and charge diffusion in thermal QCD from the lattice*, *Journal of High Energy Physics* **2** (2015) 186, [1412.6411].

[241] S. S. Gubser, A. Nellore, S. S. Pufu and F. D. Rocha, *Thermodynamics and Bulk Viscosity of Approximate Black Hole Duals to Finite Temperature Quantum Chromodynamics*, *Physical Review Letters* **101** (2008) 131601, [0804.1950].

[242] S. I. Finazzo and J. Noronha, *Holographic calculation of the electric conductivity of the strongly coupled quark-gluon plasma near the deconfinement transition*, *Phys. Rev. D* **89** (2014) 106008, [1311.6675].

[243] R. Rougemont, J. Noronha and J. Noronha-Hostler, *Suppression of Baryon Diffusion and Transport in a Baryon Rich Strongly Coupled Quark-Gluon Plasma*, *Physical Review Letters* **115** (2015) 202301, [1507.06972].

[244] D. Li, S. He and M. Huang, *Temperature dependent transport coefficients in a dynamical holographic QCD model*, *Journal of High Energy Physics* **6** (2015) 46, [1411.5332].

[245] S. I. Finazzo and R. Rougemont, *Thermal photon, dilepton production, and electric charge transport in a baryon rich strongly coupled QGP from holography*, *Phys. Rev. D* **93** (2016) 034017, [1510.03321].

[246] A. Hosoya and K. Kajantie, *Transport coefficients of QCD matter*, *Nuclear Physics B* **250** (1985) 666–688.

[247] G. D. Moore and O. Saremi, *Bulk viscosity and spectral functions in QCD*, *Journal of High Energy Physics* **9** (2008) 015, [0805.4201].

[248] J.-W. Chen, Y.-F. Liu, Y.-K. Song and Q. Wang, *Shear and bulk viscosities of a weakly coupled quark gluon plasma with finite chemical potential and temperature: Leading-log results*, *Phys. Rev. D* **87** (2013) 036002, [1212.5308].

[249] H. B. Meyer, *Calculation of the Bulk Viscosity in SU(3) Gluodynamics*, *Physical Review Letters* **100** (2008) 162001, [0710.3717].

[250] K. Paech and S. Pratt, *Origins of bulk viscosity in relativistic heavy ion collisions*, *Phys. Rev. C* **74** (2006) 014901, [nucl-th/0604008].

[251] K. Rajagopal and N. Tripuraneni, *Bulk viscosity and cavitation in boost-invariant hydrodynamic expansion*, *Journal of High Energy Physics* **3** (2010) 18, [0908.1785].

[252] F. Karsch, D. Kharzeev and K. Tuchin, *Universal properties of bulk viscosity near the QCD phase transition*, *Physics Letters B* **663** (2008) 217–221, [0711.0914].

[253] D. Kharzeev and K. Tuchin, *Bulk viscosity of QCD matter near the critical temperature*, *Journal of High Energy Physics* **9** (2008) 093, [0705.4280].

[254] C. Sasaki and K. Redlich, *Transport coefficients near chiral phase transition*, *Nuclear Physics A* **832** (2010) 62–75, [0811.4708].

[255] P. Chakraborty and J. I. Kapusta, *Quasiparticle theory of shear and bulk viscosities of hadronic matter*, *Phys. Rev. C* **83** (2011) 014906, [1006.0257].

[256] V. Chandra, *Bulk viscosity of anisotropically expanding hot QCD plasma*, *Phys. Rev. D* **84** (2011) 094025, [1107.1195].

[257] A. Dobado, F. J. Llanes-Estrada and J. M. Torres-Rincon, *Bulk viscosity and energy-momentum correlations in high energy hadron collisions*, *European Physical Journal C* **72** (2012) 1873, [1101.1801].

[258] S.-S. Xiao, P.-P. Guo, L. Zhang and D.-F. Hou, *Bulk viscosity of hot dense Quark matter in the PNJL model*, *Chinese Physics C* **38** (2014) 054101, [1306.3842].

[259] F. Werner and Y. Castin, *Unitary gas in an isotropic harmonic trap: Symmetry properties and applications*, *Phys. Rev. A* **74** (2006) 053604, [cond-mat/0607821].

[260] D. T. Son, *Vanishing Bulk Viscosities and Conformal Invariance of the Unitary Fermi Gas*, *Physical Review Letters* **98** (2007) 020604, [cond-mat/0511721].

[261] T. Enss, R. Haussmann and W. Zwerger, *Viscosity and scale invariance in the unitary Fermi gas*, *Annals of Physics* **326** (2011) 770–796, [1008.0007].

[262] K. Dusling and T. Schäfer, *Bulk Viscosity and Conformal Symmetry Breaking in the Dilute Fermi Gas near Unitarity*, *Physical Review Letters* **111** (2013) 120603, [1305.4688].

[263] M. G. Alford, M. Braby, S. Reddy and T. Schäfer, *Bulk viscosity due to kaons in color-flavor-locked quark matter*, *Phys. Rev. C* **75** (2007) 055209, [nucl-th/0701067].

[264] B. A. Sa'd, I. A. Shovkovy and D. H. Rischke, *Bulk viscosity of spin-one color superconductors with two quark flavors*, *Phys. Rev. D* **75** (2007) 065016, [astro-ph/0607643].

[265] B. A. Sa'd, I. A. Shovkovy and D. H. Rischke, *Bulk viscosity of strange quark matter: Urca versus nonleptonic processes*, *Phys. Rev. D* **75** (2007) 125004, [astro-ph/0703016].

[266] H. Dong, N. Su and Q. Wang, *Baryon number conservation and enforced electric charge neutrality for bulk viscosity in quark matter*, *Phys. Rev. D* **75** (2007) 074016, [astro-ph/0702104].

[267] M. G. Alford, M. Braby and A. Schmitt, *Bulk viscosity in kaon-condensed color flavor-locked quark matter*, *Journal of Physics G Nuclear Physics* **35** (2008) 115007, [0806.0285].

[268] X.-G. Huang, M. Huang, D. H. Rischke and A. Sedrakian, *Anisotropic hydrodynamics, bulk viscosities, and r-modes of strange quark stars with strong magnetic fields*, *Phys. Rev. D* **81** (2010) 045015, [0910.3633].

[269] I. A. Shovkovy and X. Wang, *Bulk viscosity in the nonlinear and anharmonic regimes of strange quark matter*, *New Journal of Physics* **13** (2011) 045018, [1012.0354].

[270] J. Berdermann, D. Blaschke, T. Fischer and A. Kachanovich, *Neutrino emissivities and bulk viscosity in neutral two-flavor quark matter*, *Phys. Rev. D* **94** (2016) 123010, [1609.05201].

[271] L. I. Mandelstam and M. A. Leontovich, *On the theory of sound absorption in fluids*, *Zh. Exp. Theor. Fiz.* **7** (1937) 438.

[272] E. E. Kolomeitsev and D. N. Voskresensky, *Viscosity of neutron star matter and r-modes in rotating pulsars*, *Phys. Rev. C* **91** (2015) 025805, [1412.0314].

[273] G. Colucci, A. Sedrakian and D. H. Rischke, *Leading-order nucleon self-energy in relativistic chiral effective field theory*, *Phys. Rev. C* **88** (2013) 015209, [1303.1270].

[274] J. M. Pearson, S. Goriely and N. Chamel, *Properties of the outer crust of neutron stars from Hartree-Fock-Bogoliubov mass models*, *Phys. Rev. C* **83** (2011) 065810.

[275] H. Heiselberg and C. J. Pethick, *Transport and relaxation in degenerate quark plasmas*, *Phys. Rev. D* **48** (1993) 2916–2928.

[276] M. N. Tamashiro, Y. Levin and M. C. Barbosa, *The one-component plasma: a conceptual approach*, *Physica A Statistical Mechanics and its Applications* **268** (1999) 24–49, [cond-mat/9810213].

[277] E. Braaten and R. D. Pisarski, *Soft amplitudes in hot gauge theories: A general analysis*, *Nuclear Physics B* **337** (1990) 569–634.

[278] E. Braaten and R. D. Pisarski, *Deducing hard thermal loops from Ward identities*, *Nuclear Physics B* **339** (1990) 310–324.

[279] T. Altherr and U. Kraemmer, *Gauge field theory methods for ultra-degenerate and ultra-relativistic plasmas*, *Astroparticle Physics* **1** (1992) 133–158.

[280] T. Altherr, E. Petitgirard and T. del Río Gaztelurrutia, *Photon propagation in dense media*, *Astroparticle Physics* **1** (1993) 289–295, [hep-ph/9212264].

[281] T. Altherr, E. Petitgirard and T. del Río Gaztelurrutia, *Axion emission from red giants and white dwarfs*, *Astroparticle Physics* **2** (1994) 175–186, [hep-ph/9310304].

[282] R. N. Wolf, D. Beck, K. Blaum, C. Böhm, C. Borgmann, M. Breitenfeldt et al., *Plumbing Neutron Stars to New Depths with the Binding Energy of the Exotic Nuclide Zn82*, *Physical Review Letters* **110** (2013) 041101.

[283] G. Baym, C. Pethick and P. Sutherland, *The Ground State of Matter at High Densities: Equation of State and Stellar Models*, *ApJ* **170** (1971) 299.

[284] S. L. Shapiro and S. A. Teukolsky, *Black Holes, White Dwarfs and Neutron Stars: The Physics of Compact Objects*. Wiley, 1986.

[285] S. B. Rüster, M. Hempel and J. Schaffner-Bielich, *Outer crust of nonaccreting cold neutron stars*, *Phys. Rev. C* **73** (2006) 035804, [astro-ph/0509325].

# Arus Harutyunyan

*Curriculum Vitae*

## Personal data

| | |
|---|---|
| Date of birth | 10$^{th}$ January, 1992 |
| Nationality | Armenian |
| Gender | Female |
| Family status | Single |
| Address | Max-von-Laue str. 1, 60438 Frankfurt am Main, Germany |
| Phone | +49 (0) 151 468 462 26, +374 76 50 16 |
| Email | arus@th.physik.uni-frankfurt.de, arusharutyunyan5@gmail.com |

## Education

2012–2014 **Master student**, Department of Theoretical Physics, Yerevan State University, Armenia; Diploma with Honors.

2008–2012 **Bachelor student**, Department of Theoretical Physics, Yerevan State University, Armenia; Diploma with Honors.

2005–2008 **High School Student**, Yerevan Physical-Mathematical School, Armenia; Diploma with Gold Medal.

## Current position

Since 01.12.2014 **Graduate student**, Institute for Theoretical Physics,
Title of the thesis: *"Relativistic hydrodynamics and transport in strongly correlated systems".*
Scientific supervisor: Prof. Dr. Armen Sedrakian.
Date of defense: 9 April, 2018.

## Publications

### Refereed journal articles

6. A. Harutyunyan, A. Sedrakian,
*Bulk viscosity of two-flavor quark matter from the Kubo formalism.*
Phys. Rev. D **96**, 034006, (2017) [18 pages]; arXiv:1705.09825 [hep-ph].

5. A. Harutyunyan, D. H. Rischke and A. Sedrakian,
*Transport coefficients of two-flavor quark matter from the Kubo formalism.*
Phys. Rev. D **95**, 114021, (2017) [24 pages]; arXiv:1702.04291 [nucl-th].

4. A. Harutyunyan, A. Sedrakian,
*Electrical conductivity of a warm neutron star crust in magnetic fields.*
Phys. Rev. C **94**, 025805, (2016) [18 pages + 11 pages of supplemental tables]; arXiv:1605.07612 [astro-ph.HE].
3. D. M. Sedrakian, A. S. Harutyunyan, M. V. Hayrapetyan,
*Absorption of magnetosonic waves in the crust of neutron stars. Radio emission from pulsars.*
Astrophysics **56**, 530-549, (2014) [20 pages].
2. D. M. Sedrakian, A. S. Harutyunyan, M. V. Hayrapetyan,
*Magnetosonic waves in the crust of a neutron star.*
Astrophysics **56**, 229-245, (2013) [17 pages].
1. D. M. Sedrakian, A. S. Harutyunyan, M. V. Hayrapetyan,
*Magnetohydrodynamic equations for the crust of neutron stars.*
Astrophysics **56**, 76-87, (2013) [12 pages].

### Conference proceedings

2. A. Harutyunyan, A. Sedrakian,
*Electrical conductivity tensor of dense plasma in magnetic fields*,
PoS(MPCS2015)011, [12 pages + 7 pages of supplemental tables]; arXiv:1607.04541 [astro-ph.HE].
1. D. M. Sedrakian, A. S. Harutyunyan, M. V. Hayrapetyan,
*Magnetosonic waves in the crust of a neutron star*,
Journal of Physics: Conference Series **496**, 012017, (2014) [6 pages].

### Preprints

4. A. Harutyunyan, A. Sedrakian, *et al.*,
*Second-order relativistic hydrodynamics from a non-equilibrium statistical operator.*
In preparation.
3. A. Harutyunyan, A. Sedrakian, *et al.*,
*Bulk viscosity of hot quark plasma from the Kubo-Zubarev formalism.*
In preparation.
2. A. Harutyunyan, A. Sedrakian, D. Rischke,
*Relativistic Dissipative Fluid Dynamics from Non-Equilibrium Statistical Operator.*
In preparation.
1. A. Harutyunyan, A. Nathanail, L. Rezzolla, A. Sedrakian,
*Electrical Resistivity and Hall effect in Binary Neutron-Star Mergers.*
In preparation.

## Participation in Conferences and Schools

**2017**

6. *"The Modern Physics of Compact Stars and Relativistic Gravity"*,
   September 18-22, 2017, Yerevan, Armenia.

5. *NewCompStar School 2017 - "Neutron stars: theory, observations and gravitational waves emission"*,
   September 11-15, 2017, University of Sofia, Bulgaria.

4. *"Neutron stars and their environments"*,
   July 3-7, 2017, Institute of Space Sciences, Bellaterra (Barcelona), Spain.

3. *"Hot and dense matter"*,
   May 8-12, 2017, Kloster Schöntal, Germany.

2. *"Annual NewCompStar Conference 2017"*,
   March 27-31, 2017, Warsaw, Poland.

1. *"Neutron star mergers: From gravitational waves to nucleosynthesis"*,
   January 15-21, 2017, Hirschegg, Kleinwalsertal, Austria.

**2016**

4. *"Giersch International Symposion",*
   September 26-30, 2016, FIAS, Frankfurt am Main, Germany.

3. *NewCompStar School 2016 - "Neutron stars: gravitational physics theory and observations"*,
   September 5-9, 2016, Department of Physics, University of Coimbra, Portugal.

2. *"Pulsars and their environments"*,
   May 18-20, 2016, Meudon Campus of Paris Observatory, France.

1. *"Frontiers in Nuclear and Hadronic Physics"*,
   from February 22 to March 04, 2016, The Galileo Galilei Institute for Theoretical Physics, Arcetri, Florence, Italy.

**2015**

4. *"The Modern Physics of Compact Stars and Relativistic Gravity"*,
   from September 30 to October 3, 2015, Yerevan, Armenia.

3. *NewCompStar School 2015 - "Dense Matter in Compact Stars: Experimental and Observational Signatures"*,
   September 21-25, 2015, Bucharest, Romania.

2. *"Annual NewCompStar Conference 2015"*,
   June 15-19, 2015, Budapest, Hungary.

1. *"Hadron physics at the Belle and BES experiments"*,
   May 18-22, 2015, Kloster Höchst, Germany.

**2013**

3. *Online course in QCD within the Regional Training Network in Theoretical Physics*,
   with the grade "excellent minus" during the winter term 2013, Bonn University, Germany.

2. *"First Autumn School of the Regional Training Network in Theoretical Physics"*,
   September 26-28, 2013, Bazaleti Lake, Georgia.

1. *"Third International Summer School on Symmetry in Integrable Systems and Nuclear Physics"*,
   July 3-13, 2013, Tsakhgadzor, Armenia.

## Scientific talks

**2018**

3. *"Electrical Resistivity and Hall effect in Binary Neutron-Star Mergers"*
   at Byurakan Astrophysical Observatory, 29 March, 2018, Armenia.

2. *"Transport coefficients of two-flavor quark matter from the Kubo formalism"*
   at University of Santiago de Compostela, 7 March, 2018, Spain.

1. *"Second-order fluid dynamics from a non-equilibrium statistical operator"*,
   at ITP, Goethe University, "Palaver" talk,
   5 February, 2018, Frankfurt am Main, Germany.

**2017**

5. *"Transport coefficients of two-flavor quark matter from the Kubo formalism"* at *"The Modern Physics of Compact Stars and Relativistic Gravity"*, 18 September, 2017, Yerevan, Armenia.

4. *"Bulk viscosity of two-flavor quark matter from the Kubo formalism"*, at ITP, Goethe University, "Palaver" talk, 19 June, 2017, Frankfurt am Main, Germany.

3. *"Electrical conductivity of a warm neutron star crust in magnetic fields"* at *"Annual NewCompStar Conference 2017"*, 28 March, 2017, Warsaw, Poland. (Received the 1st prize for the best student talk.)

2. *"Transport coefficients of two-flavor quark matter from Kubo formalism"* at ITP, Goethe University, "Palaver" talk, 6 February, 2017, Frankfurt am Main, Germany.

1. *"Electrical conductivity of a warm neutron star crust in magnetic fields"* at *"Neutron star mergers: From gravitational waves to nucleosynthesis"*, 20 January, 2017, Hirschegg, Austria.

**2016**

2. *"Electrical conductivity of warm neutron star crusts in magnetic fields"* at *"Pulsars and their environments"*, 19 May, 2016, Meudon, France.

1. *"Electrical conductivity of warm neutron star crust in magnetic fields"* at ITP, Goethe University, "Palaver" talk, 27 June, 2016, Frankfurt am Main, Germany.

**2015**

1. *"The electrical conductivity in the crust of neutron stars"* at ITP, Goethe University, "Palaver" talk, 14 December, 2015, Frankfurt am Main, Germany.

**2014**

1. *"Propagation and absorption of magnetohydrodynamic waves in the crust of a neutron star"* at University of Bonn, 12 February, 2014, Germany.

**2012**

1. *"Propagation and absorption of magnetosonic waves in the crust of a neutron star"* at Yerevan State University, Scientific seminar, December, 2012, Armenia.

## Teaching experience

Transport Theory, problem solutions, summer term 2016, ITP, Frankfurt am Main, Germany

## Skills

Computer skills: C programming, Wolfram Mathematica, Xmgrace, Matplotlib

Languages: English, Italian, Russian, German, Armenian (mother tongue)

## Referees

**Reference 1**

Name: Prof. Dr. Armen Sedrakian
Position: Fellow
Institution: FIAS, Goethe University
Address: Ruth Moufang str. 1, 60438 Frankfurt am Main, Germany
Email: sedrakian@fias.uni-frankfurt.de

**Reference 2**

Name: Prof. Dr. Luciano Rezzolla
Position: Professor
Institution: ITP, Goethe University
Address: Max-von-Laue str. 1, 60438 Frankfurt am Main, Germany
Email: rezzolla@th.physik.uni-frankfurt.de

**Reference 3**

Name: Prof. Dr. Dirk-Hermann Rischke
Position: Professor
Institution: ITP, Goethe University
Address: Max-von-Laue str. 1, 60438 Frankfurt am Main, Germany
Email: drischke@th.physik.uni-frankfurt.de